

Dissertation
submitted to the
Combined Faculty of Natural Sciences and Mathematics
of the Ruperto Carola University Heidelberg, Germany
for the degree of
Doctor of Natural Sciences

Presented by
M.Sc. Kerstin Ruoff
Born in: Backnang, Germany
Oral examination: 15.12.2020

Analysis of Synthetic Compounds and Natural Extracts
as Potential Antivirals
Against Human Noroviruses

Referees:

1st Examiner: apl. Prof. Dr. Martin Müller

2nd Examiner: Dr. Grant Hansman

Abstract

Human norovirus is the dominating+ cause of outbreaks of viral gastroenteritis across all age groups, with an estimated 684 million cases worldwide and 219,000 deaths per year. Outbreaks of human norovirus frequently occur in enclosed settings (e.g. cruise ships, hospitals, nursing homes). This is economically relevant, as it is estimated to cost 4.2 billion USD in direct health system and 60.3 billion USD in social costs. Although symptoms are self-limited to two to three days, the illness can be severe in young children, elderly, or immunocompromised people. The complete lack of treatment or vaccination limits counter measurements to easing symptoms. Additionally, spreading is limited by preventative measures, such as isolating infected individuals. An adequate treatment for patients as well as a possible early treatment (before symptoms appear) for people in the near environment of a beginning outbreak, including nurses and other staff, could prevent outbreaks from spreading. Therefore, inexpensive treatments with a minimum of side effects that can be delivered to patients and people in their surrounding are urgently needed. For more than four decades, antiviral research was hampered by the lack of cell culture systems for human norovirus propagation. Therefore, surrogate systems, such as murine norovirus and feline calicivirus, were used. Human noroviruses typically require histo-blood group antigens (HBGAs) as co-factors for viral infection. Thus, the HBGA pocket is the main target region on the viral capsid for the development of antivirals.

In this thesis, a panel of synthetic antivirals and natural extracts, including a set of 31 different honeys, were screened using various techniques (X-ray crystallography, ELISA, DLS, and EM) to identify potential norovirus capsid inhibitors. Several Nanobodies (Fab fragments of camelid derived heavy chain only antibodies) directed specifically against genotype GI.1 of human norovirus inhibited virus like particles (VLPs) in surrogate attachment inhibition ELISAs. However, inhibition by these Nanobodies was specifically directed against their respective genotype and showed limited cross-reactivity. The high specificity of the Nanobodies limits their use as broadly reactive antivirals. Of the Natural extracts, date syrup, wine, barley malt, coconut blossom syrup, apple sweetener, different types of honey and propolis inhibited the binding of VLPs to HBGAs. Treatment of VLPs with these compounds resulted in the disruption of VLP integrity and particle aggregation. Most natural extracts showed broad reactivity against VLPs of several genotypes. Preliminary structural analysis revealed the presence of small, unidentified ligand(s) for date syrup, coconut blossom

syrup, apple sweetener, and honey. The strongest inhibition was observed with date syrup, wine, and propolis. Three flavonols, common to these natural extracts, were identified as inhibiting compounds. To address if a combinatorial approach could improve the performance of the individual inhibitors, special combinatorial ELISAs were designed to assess the interaction between two inhibitors. These assays revealed combinations of Nanobodies with the HMO 2'FL or natural extracts to have additive or synergistic inhibition. This demonstrated a combinatorial approach with natural extracts and Nanobodies could be a comparatively easy, safe, and affordable treatment that could be administered to people suffering from norovirus disease and healthy people in the surrounding of a beginning outbreak.

Zusammenfassung

Humane Noroviren lösen häufig schwere Gastroenteritis Ausbrüche in beengten Umgebungen wie Kreuzfahrtschiffen, Krankenhäusern oder Altenheimen aus. Schätzungen der WHO gehen von weltweiten finanziellen Schäden in Höhe von 4,2 Milliarden USD an direkten Gesundheitskosten und 60,3 Milliarden USD an Sozialaufwendungen aus [4]. Obwohl Krankheitssymptome sich auf zwei bis drei Tage beschränken, kann es auch zu schweren Verläufen besonders bei Kindern, Älteren sowie immunsupprimierten Personen kommen. In Ermangelung spezifischer Medikamente oder Impfstoffe beschränkt sich die Behandlung auf Linderung der Symptome. Darüber hinaus wird die weitere Ausbreitung durch vorbeugende Maßnahmen, wie die Isolation Erkrankter, sowie adäquaten Desinfektionsmaßnahmen, verhindert. Die Ausbreitung lokaler Ausbrüche könnte durch eine passende medikamentöse Behandlung eingedämmt werden, welche neben Patienten auch die Behandlung von Personen in der unmittelbaren Umgebung eines Ausbruchs einschließt. Hierfür werden dringend günstige, nebenwirkungsarme Behandlungsmöglichkeiten benötigt, die an Patienten aber auch vorbeugend im Umfeld eines beginnenden Ausbruchs verabreicht werden können.

Humane Noroviren nutzen gewöhnlich Histo-Bluttgruppenantigene (HBGAs) als Kofaktoren zur Infektion von Körperzellen. Folglich wurde die HBGA-Bindestelle als vielversprechendes Ziel für die Entwicklung antiviraler Mittel identifiziert. Lange wurde die Erforschung antiviraler Mittel gegen humane Noroviren vom Mangel passender Zellkulturen geprägt. Daher musste auf verschiedene Zellkulturmodelle ausgewichen werden.

In der vorliegenden Dissertation wurden synthetische antivirale Stoffe sowie mehrere natürliche Extrakte einschließlich einer Auswahl verschiedener Honigsorten mit unterschiedlichen Techniken (Röntgenkristallographie, ELISA, DLS, und EM) auf ihre antiviralen Eigenschaften hin untersucht. Mehrere Nanokörper (Fab Fragmente der Schwereketten-Antikörper von Kameliden) spezifisch gegen humane Noroviren des Genotypen GI.1 gerichtet, zeigten Inhibition der Anhaftung virusartiger Partikel (VLPs) in einem Anheftungs-Inhibitions ELISA. Die beobachtete Inhibition dieser Nanokörper erwies sich jedoch als spezifisch für den jeweiligen Genotypen (wie bereits zuvor in unserem Labor beobachtet). Die hohe Spezifität der Nanokörper setzt ihrem Nutzen als breitwirksame Therapien Grenzen, da eine spezifische Medikation die präzise Identifikation des jeweiligen Norovirus-Stammes erfordern würde.

Unter den getesteten natürlichen Extrakten zeigten Dattelsirup, Wein, verschiedene Honigsorten und Propolis Inhibition der Anhaftung von VLPs an HBGAs. Das Inkubieren von VLPs mit diesen Extrakten führte zur Aggregation der einzelnen Partikel. Anders als die Nanokörper zeigten die meisten der genannten Extrakte Aktivität gegenüber VLPs verschiedener Genotypen. Nicht abgeschlossene Röntgenstrukturanalysen von Dattelsirup und Honig belegten zudem die Bindung kleiner, bisher nicht identifizierter Liganden. Ein Vergleich der Inhaltsstoffe der drei besten Inhibitoren (Dattelsirup, Wein, Propolis Extrakte) ergab, dass alle drei reich an Polyphenolen sind. Drei Flavonole wurden identifiziert, welche in allen drei Extrakten vorkommen. Inhibitionsexperimente zeigten, dass alle drei getesteten Flavonole (Quercetin, Kaempferol, Isorhamnetin) die Bindung von VLPs an HBGAs stören können.

Weitere Untersuchungen wandten sich der Frage zu, ob Kombinationen verschiedener Inhibitoren deren Wirkung noch verstärken könnten. Mit speziellen Kombinations-ELISAs wurden Wechselwirkungen der einzelnen Inhibitoren untereinander analysiert und additive, synergistische oder adverse Effekte quantifiziert. Diese Versuche zeigten, dass einige Kombinationen von Nanokörpern mit dem humanen Milchzucker 2'FL oder mit natürlichen Extrakten additive oder sogar synergistische Wechselwirkungen aufwiesen. Dies verdeutlicht, dass Mischungen breitwirksamer natürlicher Extrakte (ggf. mit spezifischen Nanokörpern) eine vergleichsweise einfache, sichere und günstige Lösung zur Behandlung humaner Noroviren bieten, welche sowohl als Therapie als auch vorbeugend zum Einsatz kommen könnten.

Table of Contents

Abstract	5
Zusammenfassung	7
Table of Contents	9
List of Figures	11
List of Tables	13
List of Abbreviations	14
1 Introduction	15
1.1 Impact of Norovirus and Historical Overview.....	15
1.2 Clinical Symptoms and Outbreak Locations	15
1.3 The <i>Caliciviridae</i> Family: Genome Organization and Classification.....	16
1.4 Norovirus Capsid.....	18
1.5 Norovirus Attachment Factors	19
1.6 Blood Groups and the HBGA-System.....	20
1.7 Norovirus and HBGAs	22
1.8 Vaccine Development.....	23
1.9 Synthetic Norovirus Inhibitors.....	24
1.10 Human Milk Oligosaccharides as Natural Norovirus Inhibitors.....	24
1.11 Natural Extracts as Antivirals	25
1.12 Aims and Objectives	28
2 Material and Methods	29
2.1 Preparation of Natural Extracts	33
2.2 Expression and Purification of P domains	35
2.2.1 Cloning and Expression of P domains.....	35
2.2.2 Purification of P domains	35
2.3 Expression and Purification of Nanobodies.....	37
2.3.1 Purchase of VHH Library and Cloning of Nanobodies	37
2.3.2 Expression of Nanobodies	38
2.3.3 Purification of Nanobodies.....	38
2.4 Expression and Purification of VLPs.....	39
2.4.1 Cloning of VLP Constructs and Production of Bacmid.....	39
2.4.2 Transfection of Sf9 Cells with Bacmid and Production of Seed Virus	40
2.4.3 Expression of VLPs.....	41
2.4.4 Purification of VLPs.....	41
2.5 Binding ELISAs.....	42
2.6 HBGA Attachment Inhibition Assay	44
2.6.1 Optimization of HBGA Inhibition ELISA for Screening.....	47
2.7 HBGA Attachment Inhibition ELISA – Combinatorial Inhibition	49
2.7.1 Analysis of Combinatorial Inhibition – Bliss Independence Evaluation	50
2.8 Dynamic Light Scattering (DLS).....	51
2.9 Electron Microscopy (EM)	51
2.10 X-ray Crystallography.....	52
2.10.1 Co-crystals with Natural Extracts	52
2.10.2 Data Collection, Structure Solution, and Refinement	53
2.11 Automated X-Ray Crystallography Screening.....	53
3 Results	55
3.1 Screening for Synthetic Antivirals.....	55
3.1.1 Screening of the NIH Collection	55
3.1.2 Synthetic Multivalent Fucose Oligomers.....	61

3.1.3	GI.1-specific Nanobodies – Initial Screening	67
3.1.4	GI.1-specific Nanobodies – Published Results.....	73
3.1.5	Binding of GI.1-specific Nanobodies to S Domain	82
3.2	Screening for Natural Extracts as Antivirals	83
3.2.1	HMO Screening.....	83
3.2.2	Plant Derived Syrups and Saps	88
3.2.3	Honey	102
3.2.4	Propolis.....	108
3.2.5	Polyphenolic Compounds Common to Natural Inhibitors	116
3.3	Combinatory Attachment Inhibition	119
3.3.1	Combinations of Nanobodies with 2'FL	119
3.3.2	Combinations of Nanobodies with Natural Extracts	125
3.3.3	Combinations of Natural Extracts	127
4	Discussion.....	128
4.1	Discussion – Screening for Synthetic Antivirals.....	128
4.1.1	Screening of the NIH Collection	128
4.1.2	Synthetic Multivalent Fucose Oligomers.....	130
4.1.3	GI.1-specific Nanobodies.....	131
4.2	Screening of Natural Extracts as Antivirals.....	133
4.2.1	HMO Screening.....	133
4.2.2	Plant Derived Syrups and Saps	134
4.2.3	Honey	138
4.2.4	Propolis.....	138
4.2.5	Polyphenolic Compounds Common to Natural Inhibitors	139
4.3	Combinatory Norovirus Attachment Inhibition.....	141
5	Conclusion	143
Appendix I	Amendments	144
Appendix I.1	Publications.....	144
Appendix I.2	Contributions	145
Appendix I.2.1	Screening of the NIH Collection	145
Appendix I.2.2	Synthetic Multivalent Fucose Oligomers	145
Appendix I.2.3	GI.1-specific Nanobodies.....	145
Appendix I.2.4	Binding of GI.1-specific Nanobodies to S Domain.....	146
Appendix I.2.5	HMO Screening	146
Appendix I.2.6	Plant Derived Syrups and Saps.....	147
Appendix I.2.7	Honey	147
Appendix I.2.8	Honey	147
Appendix I.2.9	Combinations of Nanobodies with 2'FL	147
Appendix I.2.10	Combinations of Nanobodies with Natural Extracts.....	148
Appendix I.2.11	Combinations of Natural Extracts	148
Appendix I.3	Supplemental Tables and Figures	149
Appendix I.3.1	Automated X-ray Crystallography Screening	149
Appendix I.3.2	HBGA-Mimetic Compounds /Synthetic Multivalent Fucose Oligomers	171
Appendix I.3.3	HMO Screening	173
Appendix I.3.4	Plant Derived Syrups and Saps.....	174
Appendix I.3.5	Honey	183
Appendix II	Acknowledgements	184
Appendix III	References	186

List of Figures

Figure 1-1:	Caliciviridae phylogenetic tree with eleven genera.	16
Figure 1-2:	Genome organization of norovirus.	17
Figure 1-3:	Norovirus family-tree and host range.	17
Figure 1-4:	X-ray crystallographic structure of norovirus capsid (left) and isolated VP1 dimer (right).	18
Figure 1-5:	Norovirus attachment and entry to host cells.	19
Figure 1-6:	Synthesis of antigens H, A, and B.	21
Figure 1-7:	A schematic of a Nanobody.	24
Figure 2-1:	Negative stain EM images of different batches of GII.10 026 VLPs.	48
Figure 2-2:	GII.10 Binding ELISA, detection with serially diluted Rabbit 1.	48
Figure 2-3:	GII.10 Binding ELISA, detection with serially diluted anti-rabbit.	49
Figure 3-1:	X-ray screening; density map of GII.10 P domain after automated processing.	56
Figure 3-2:	X-ray crystallography screening; density map of GII.10 P domain after manual processing.	57
Figure 3-3:	Inhibition ELISA of NIH collection at 18.75 μ M.	58
Figure 3-4:	Inhibition ELISA evaluating effect of DMSO.	59
Figure 3-5:	Inhibition ELISA of NIH collection compounds at 5 μ M.	60
Figure 3-6:	Schematic representation of HBGA-mimetic fucose oligomers.	61
Figure 3-7:	HBGA-binding site GII.10 P domain in complex with: left: KB 41A, right: KB 32A.	62
Figure 3-8:	Density map of GII.10 026 P domain in complex with KB 80A.	63
Figure 3-9:	X-ray crystallography structure analysis of GII.10 P domain with multivalent-fucose oligomer KB 80A. ...	64
Figure 3-10:	Inhibition ELISA of serial dilution of fucose-oligomers.	65
Figure 3-11:	Re-testing inhibition ELISA of serial dilution of fucose-oligomers.	66
Figure 3-12:	GI.1 Norwalk VLPs used in this chapter.	68
Figure 3-13:	Cross-reactivity of GI.1-specific Nanobodies, heat-map.	68
Figure 3-14:	Binding ELISA of serially diluted GI.1-specific Nanobodies to GI.1 VLPs.	69
Figure 3-15:	Binding ELISA of GI.1-specific Nanobodies (serially diluted) to #8 VLPs.	70
Figure 3-16:	Binding of GI.1-specific Nanobodies to GI.1 P domain and VLPs.	70
Figure 3-17:	Binding of GI.1-specific Nanobodies to VLP-coated plates at different concentrations of GI.1 VLPs.	71
Figure 3-18:	Heat-map of cross-reactivity inhibition ELISA with GI.1-specific Nanobodies against GI VLPs.	72
Figure 3-19:	X-ray crystal structures of GI.1 P domain in complex with Nano-7, -62, and -94.	73
Figure 3-20:	Close-up of the P domain dimer in complex with Nano-7.	74
Figure 3-21:	Close-up of the P domain dimer in complex with Nano-62.	75
Figure 3-22:	Close-up of the P domain dimer in complex with Nano-94.	76
Figure 3-23:	Binding of Nano-7, Nano-62, and Nano-94 to GI.1 P domain or GI.1 VLPs.	77
Figure 3-24:	Binding affinities of Nano-7, Nano-62, and Nano-94 to GI.1 P domain.	78
Figure 3-25:	Illustration of Nanobody binding sites based on an alignment of seven GI capsid sequences.	79
Figure 3-26:	Inhibition of VLP binding to PGM by Nanobodies.	80
Figure 3-27:	DLS measurements to evaluate hydrodynamic diameter of GI.1 VLPs after treatment.	80
Figure 3-28:	EM images of GI.1 VLPs untreated or treated with Nano-7, Nano-62, or Nano-94.	81
Figure 3-29:	Binding ELISA of GI.1-specific Nanobodies to GI.1 S domain.	82
Figure 3-30:	Binding ELISA (GII.10, GII.4, GII.17) detection by Nano-26.	83
Figure 3-31:	Binding events in the HMO screening at NCFG.	84
Figure 3-32:	HMO binding array Heat Map Part I fractions 1-110.	86
Figure 3-33:	HMO binding array Heat Map Part II fractions 111-220.	87
Figure 3-34:	Structure analysis of GII.10 026 P domain crystals in complex with apple sweetener.	89
Figure 3-35:	Example for large single crystals at the crystal tracker.	90
Figure 3-36:	Structural analysis of GII.10 P domain in complex with date syrup.	92
Figure 3-37:	Attachment inhibition of GI.1, GII.1, GII.4, GII.10, and GII.17 VLPs by natural extracts.	94
Figure 3-38:	Detection of GII.17 VLPs inhibition with date syrup using Nanobodies with/without biotinylation.	95
Figure 3-39:	Inhibition of GII.10 VLPs by different types of date syrup.	96
Figure 3-40:	Attachment inhibition of GII.10 VLPs by glycans identified in date syrup.	97
Figure 3-41:	Attachment inhibition of GII.10 VLPs with wines and juices.	98
Figure 3-42:	DLS measurements of different VLPs after treatment with natural extracts.	101
Figure 3-43:	Structure analysis of GII.10 026 P domain crystals in complex with honey.	102
Figure 3-44:	Attachment inhibition of GII.4 and GII.10 VLPs by different types of honey.	104

Figure 3-45: DLS measurements of different VLPs after treatment with different types of honey	106
Figure 3-46: Attachment inhibition ELISA of GII.4 VLPs by honey, aging effect	107
Figure 3-47: Attachment inhibition of GII.10 VLPs by eight different propolis extracts	108
Figure 3-48: Attachment inhibition ELISA, testing propolis without VLPs.....	109
Figure 3-49: Attachment inhibition ELISA GII.10 VLPs by propolis extracts, serial dilution in respective solvent	110
Figure 3-50: Attachment inhibition ELISA of GI.1 VLPs by propolis extracts, serial dilution	110
Figure 3-51: Attachment inhibition of GII.4 VLPs by different types of propolis	113
Figure 3-52: DLS measurements of different VLPs after treatment with propolis extract.....	115
Figure 3-53: Inhibition ELISA testing four tannic compounds against GII.10 VLPs	116
Figure 3-54: Structure formula of the three flavonols tested	117
Figure 3-55: Inhibition ELISA testing three flavonol compounds against GII.4 and GII.10 VLPs	118
Figure 3-56: Charts and heat map of combinatorial treatment of Nano-94 with 2'FL (example for synergy).....	120
Figure 3-57: Charts and heat map of combinatorial treatment of Nano-7 with 2'FL (example for additivity).	121
Figure 3-58: Charts and heat map of combinatorial treatment of Nano-85 with 2'FL (example for additivity).	123
Figure 3-59: Heat map of combinatorial treatment of Nano-32 and Nano-14 with 2'FL.....	124
Figure 3-60: Heat map of combinatorial treatment of Nano-26 with honey, propolis and date syrup	125
Figure 3-61: Heat map of combinatorial treatment of Nano-85 with honey, propolis and date syrup	126
Figure 3-62: Combinatorial treatment of date syrup/propolis with propolis/date syrup, heat maps	127
Figure A I.3-1:Chemical notation of HBGA-mimetic synthetic fucose oligomers A	171
Figure A I.3-2:Chemical notation of HBGA-mimetic synthetic fucose oligomers B	172
Figure A I-3: Attachment inhibition of GII.10 VLPs by 30 different types of honey.....	183

List of Tables

Table 2-1:	List of chemicals	29
Table 2-2:	List of equipment	30
Table 2-3:	List of cells	31
Table 2-4:	List of commercial kits.....	32
Table 2-5:	List of enzymes	32
Table 2-6:	List of antibodies	32
Table 2-7:	List of honeys and propolis	33
Table 2-8:	List of natural extracts.....	34
Table 2-9:	List of P domains used.....	35
Table 2-10:	Buffers used for P domain purification	36
Table 2-11:	List of primers.....	37
Table 2-12:	Buffers used for Nanobody purification.....	39
Table 2-13:	List of VLPs used for VLP expression	40
Table 2-14:	List of VLPs used in ELISA	42
Table 2-15:	Binding ELISA protocol GII.10 VLPs	43
Table 2-16:	Binding ELISA protocol GI.1 VLPs	43
Table 2-17:	Binding ELISA protocol GI.1 P domain.....	43
Table 2-18:	HBGA blocking ELISA protocol GII.10 026 VLPs, variant A	45
Table 2-19:	HBGA blocking ELISA protocol GII.10 026 VLPs, variant B.....	45
Table 2-20:	HBGA blocking ELISA protocol GII.4 Sydney VLPs	45
Table 2-21:	HBGA blocking ELISA protocol GI.1 Norwalk.....	46
Table 2-22:	HBGA blocking ELISA protocol GII.17 Kawasaki VLPs	46
Table 2-23:	HBGA blocking ELISA GII.1 Hawaii VLPs + bile	46
Table 2-24:	Mother solutions for GII.10 026 P domain and GII.10 026 P domain co-crystals	52
Table 3-1:	Summary of results of automated X-ray crystallography of GII.10 P domain vs. NIH collection	56
Table 3-2:	Results of X-ray crystallography screening with fucose-oligomers.....	62
Table 3-3:	Primary selected crystallization conditions for GII.10-P domain co crystals.....	91
Table 3-4:	Secondary selected crystallization conditions for GII.10-P domain co crystals	91
Table 3-5:	Inhibition ELISA protocols	93
Table 3-6:	Summary result of ELISA, EM, and DLS natural extracts using different types of VLPs	101
Table 3-7:	Structure analysis GII.10 P domain crystals soaked with natural extracts.....	103
Table 3-8:	Summary result of ELISA, EM, and DLS of GII.10 and GII.4 VLPs treated with honey	106
Table 3-9:	Summary result of ELISA, EM, and DLS of GII.10 and GII.4 VLPs treated with propolis	114
Table A I-1:	Summary of automated X-ray crystallography analysis results (Pipedream)	149
Table A I-2:	Summary of automated X-ray crystallography screening results (Pipedream).....	167
Table A I-3:	Top twenty binders of HMO screening against GII.10, GII.4, GII.17, and GII.17 VLPs.....	173
Table A I-4:	Summary table structure screening natural extracts, propolis and honey	174
Table A I-5:	Summary of JCSG-condition screening for co-crystals of GII.10 P domain + natural extract.....	176
Table A I-6:	Summary table structure screening natural extracts, optimized JCSG-crystallization conditions	182

List of Abbreviations

µm	Micro meter
2'FL	2-fucosyl-lactose, HMO
CHO	Chinese hamster ovary
d	Day
DLS	Dynamic light scattering
ELISA	Enzyme-linked immunosorbent assay
EM	Electron microscopy
ESRF	European Synchrotron Radiation Facility, Grenoble, France
FCV	Feline calicivirus
FUT2	α-1,2-fucosyltransferase gene
h	Hour
H5 cells	High Five cells
HBGA	Histo-blood group antigen
HMO	Human-milk oligosaccharide
HRP	Horseradish peroxidase
IPTG	Isopropyl β-D-1-thiogalactopyranoside
ITC	Isothermal titration calorimetry
kDa	Kilo Dalton
LB	Lysogeny (Luria) broth
mAb	Monoclonal antibody
min	Minute
MNV	Murine norovirus
Nano	Nanobody
NCFG	National Center for Functional Glycomics
NTPase	Nucleoside-triphosphatase
OD	Optical density
ON	Overnight
OPD	o-phenylenediamine dihydrochloride
ORF	Open reading frame
P domain	Protruding domain
PCR	Polymerase chain reaction
PDB	Protein data base
PGM	Porcine gastric mucin type III
RT	Room temperature
RT-qPCR	Reverse transcription qualitative real time PCR
s	Second
S domain	Shell domain
SDS-PAGE	Sodium dodecyl sulfate–polyacrylamide gel electrophoresis
Sf9 cells	Clonal isolate of <i>Spodoptera frugiperda</i> Sf21 cells
TB	Terrific broth
VHH	Camelid single domain Antibodies / Nanobodies
VLP	Virus-like particle
VP1	Major capsid protein
VP2	Minor capsid protein
VPg	Viral protein genome-linked

1 Introduction

1.1 Impact of Norovirus and Historical Overview

In 1968, an acute outbreak of non-bacterial gastroenteritis occurred in Norwalk, USA, Ohio [102]. The causative agent of this outbreak was identified four years later, in 1972, as a small, heat and acid stable non-enveloped agent that could be transmitted from human to human, suggesting reproductive capacity [23]. In the same year, the first electron microscopy images of viruses derived from the Norwalk outbreak were published by Albert Kapikian and his colleagues [55]. Since then human noroviruses have been identified as the leading cause of viral acute gastroenteritis among all age groups [110]. Today, noroviruses are assumed to cause approximately one-fifth of all diarrhea cases worldwide [79]. The estimated global annual costs of norovirus infections are about 4.2 billion USD in direct health system costs and 60.3 billion USD in social costs [4].

In 2015, WHO estimated norovirus to be responsible for 684 million illnesses [62]. This is by far the largest number of cases caused by a single pathogen. Furthermore, the WHO estimated that about 219,000 deaths annually are caused by norovirus infections [4, 62]. According to WHO, these numbers are likely to be underestimated. Correct attribution of actual cases is challenging regarding proper count of norovirus-related cases, costs and deaths. Often infections are regarded as non-norovirus due to limits in detection and improper sample storage. Also, the self-limiting nature of the disease is troublesome. Many patients simply stay at home without consulting medical aid. Therefore, such cases often remain undetected. On the other hand, detection of norovirus is based on highly sensitive RT-qPCR, which may also detect virus in stool of control individuals without gastroenteritis. Therefore, standardized testing and diagnostic tools discriminating between disease-causing and asymptomatic infections are needed [79].

1.2 Clinical Symptoms and Outbreak Locations

Norovirus infections are characterized by a short incubation period of only 24-48 h, followed by a sudden onset of symptoms such as diarrhea and/or projectile vomiting, sometimes accompanied by abdominal cramps, nausea, and fatigue [61]. Symptomatic infections, in

healthy individuals, typically resolve within 1-3 days without treatment. However, in some cases, especially in vulnerable populations, prolonged vomiting and diarrhea results in dehydration, and if left unattended, can lead to death. Norovirus-associated outbreaks commonly occur in enclosed settings, such as hospitals [34], nursing homes [74], cruise ships [119], and military bases [12]. Despite the discovery of the virus almost 50 years ago, there are still no vaccines or antivirals available [55].

1.3 The *Caliciviridae* Family: Genome Organization and Classification

Norovirus belongs to the *Caliciviridae* family, which further comprises; *Lagovirus*, *Vesivirus*, *Sapovirus*, *Nebovirus*, *Nacovirus*, *Bavovirus*, *Recovirus*, *Valvovirus*, *Minovirus* and *Salovirus* (Figure 1-1) [48, 60]. These viruses are non-enveloped single-stranded RNA virus with a broad host range including humans, non-human primates, pigs, cattle, dogs, cats, mice, sheep, bats, and sea lions [16].

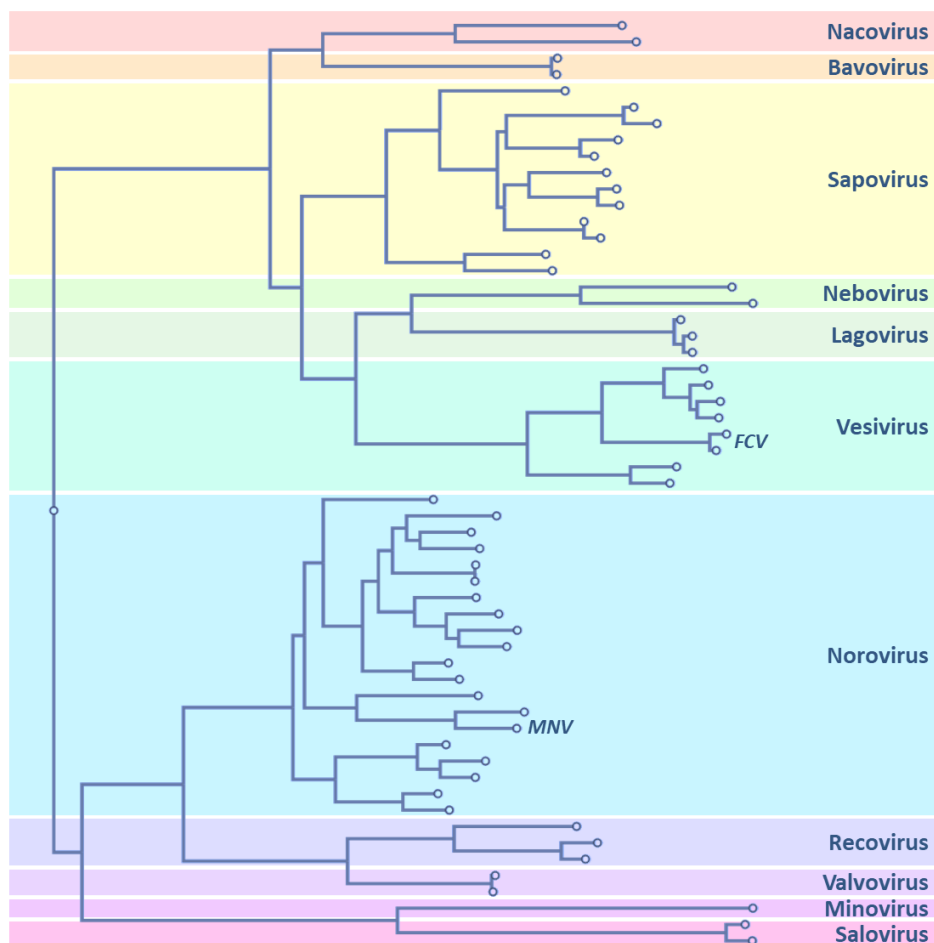


Figure 1-1: *Caliciviridae* phylogenetic tree with eleven genera. Phylogenetic tree of at least two representative full-length genomes of each genera. Genera are color-coded with the respective name of each genera given within the colored field. Typical surrogate viruses used for studies in cell culture like FCV (feline calici virus, Vesivirus), MNV (murine norovirus, Norovirus), and RHDV (rabbit haemorrhagic disease virus, Lagovirus) are indicated within the tree.

The genome of noroviruses is approximately 7.5 kb in length, with a viral protein (VPg) covalently attached at the 5'-end and polyadenylated at the 3'-end [16]. The norovirus genome is organized into three open reading frames (ORFs), where ORF1 encodes for six non-structural proteins, ORF2 encodes the major capsid protein (VP1), and ORF3 encodes the minor capsid protein (VP2) (Figure 1-2) [16, 63]. VP2 is located on the inside of the capsid and it has been speculated to play a role in capsid assembly, genome encapsidation, or host-cell entry [16].

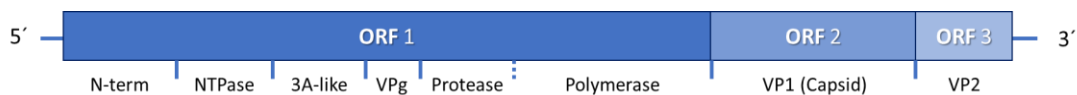


Figure 1-2: *Genome organization of norovirus.* Schematic representation of norovirus genome organization into three ORFs (ORF1-3). ORF1 encodes for non-structural proteins; including NTPase, 3A-like protein, VPg (covalently attached to the 5'-end of the genomic RNA), protease, and the RNA-dependent RNA polymerase. ORF2 and ORF3 encode for the major capsid protein VP1 and the minor capsid protein VP2, respectively.

Based on the full-length capsid amino acid sequences, norovirus can be divided into at least ten genogroups (GI-GX, Figure 1-3) and several variants within [16, 40]. Infections in humans are caused by GI, GII, and GIV, whereas the remaining genogroups cause infections in other animals. Each of the norovirus genogroups is further subdivided into numerous genotypes [40]

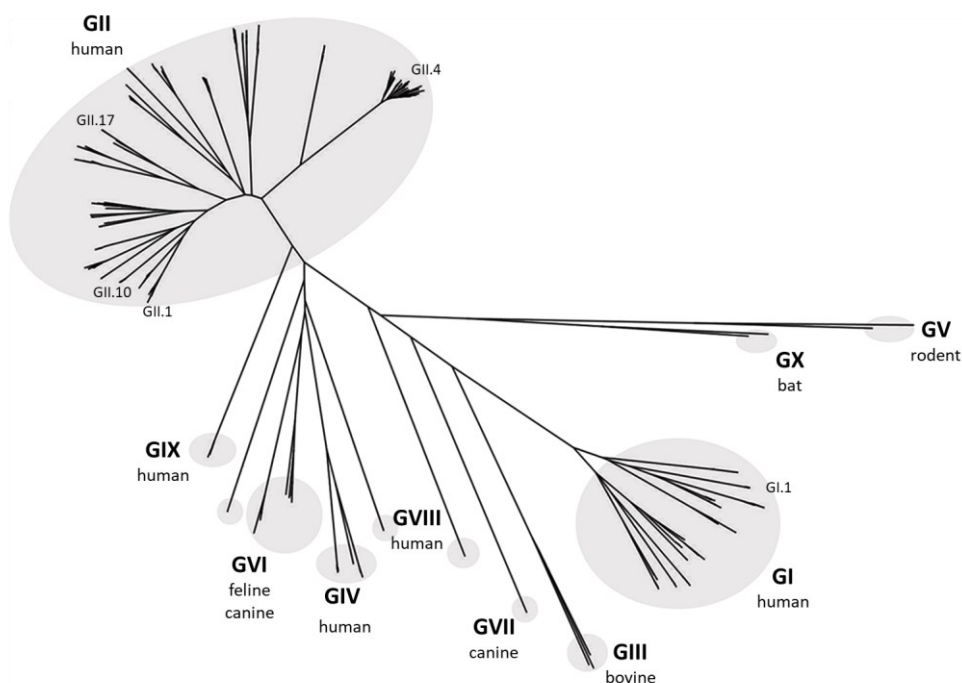


Figure 1-3: *Norovirus family-tree and host range.* Phylogenetic tree of noroviruses based on full-length VP1 sequences. Genogroups and their dominant host species are indicated. The five human genotypes (GI.1, GII.1, GII.4, GII.10, GII.17) used in this thesis are shown. Note: the diversity in genogroup GII and GI and the many variants indicated for GII.4, which was the dominant pathogenic strain worldwide in the past decade. Figure modified from Chhabra et al., 2019 [16].

1.4 Norovirus Capsid

The icosahedral particles of norovirus virions are formed by 90 copies of VP1 dimers, resulting in a particle of 35-45 nm in diameter exhibiting a T = 3 symmetry [55, 96]. The capsid protein VP1 can be expressed in insect cells, where it self-assembles into virus-like particles (VLPs) [55, 64, 96]. VLPs are assumed to be morphologically similar to native virions, hence their structure is thought to be unaltered whereas the particles lack the viral RNA genome. In 1999, the first X-ray crystal structure of the prototype genogroup I genotype 1 (GI.1) norovirus VLPs was published [96]. According to this structure, the capsid can be divided into two domains; a closed inner shell (S domain) and spikes protruding from the shell (P domain) [96]. Both domains are connected via a flexible hinge region [96]. The surface exposed P domains can be further subdivided into P1 and P2 subdomains. The P2 subdomain is the most surface exposed structure and thus contains the main determinants of antigenicity and host binding epitopes (Figure 1-4). Therefore, it is also the main target for neutralizing antibodies or antivirals [2]. P2 is an insertion into the P1 subdomain and is formed by six anti-parallel β -sheets forming a β -barrel-like structure [9, 17]. The P1 subdomain links the P2 subdomain and the S domain together, it consists of two twisted antiparallel β -sheets and one α -helix (Figure 1-4) [9, 17].

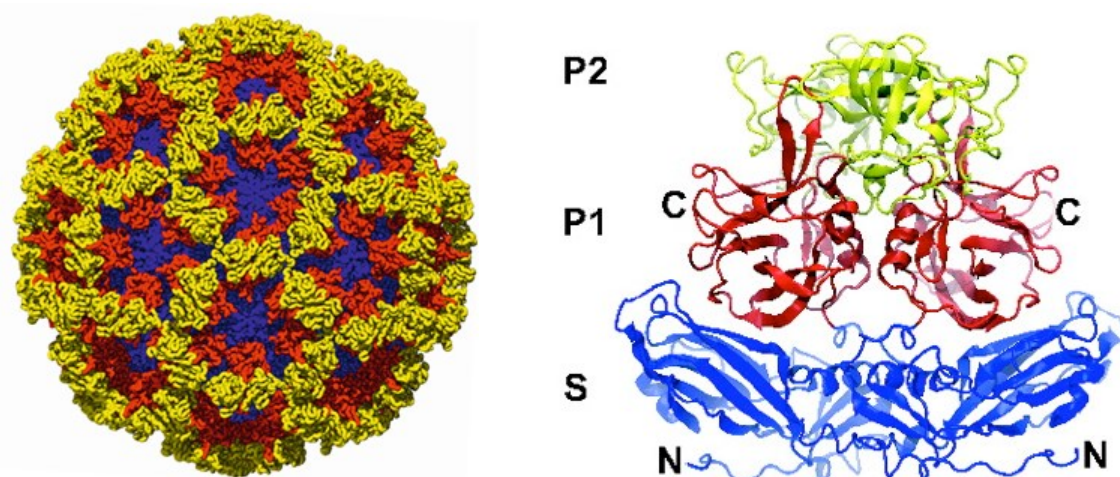


Figure 1-4: X-ray crystallographic structure of norovirus capsid (left) and isolated VP1 dimer (right). Scheme exhibiting shell domain (blue) and P domain comprising P1 (red) and P2 (yellow). The HBGA-binding site is located at the top of the P domain (P2). Image taken from [17].

1.5 Norovirus Attachment Factors

For non-enveloped viruses, cell entry is a complex process involving many coordinated steps. It starts with viral attachment to the target cells of the host, followed by receptor engagement, endocytosis, cell membrane penetration, uncoating, and finally the delivery of the viral genome into the cytoplasm (Figure 1-5) [37]. In this process, viral binding to the surface plays a critical, and often rate-limiting, role for infection. It determines cell tropism, host range and pathogenesis. Host cell binding is mediated by attachment factors and receptors on the host cell. Attachment factors are molecules on the surface of host cells that do not actively mediate viral cell entry [83]. They are not essential but increase the efficiency of a viral infection by concentrating the virus on the cell surface [83]. In contrast, viral receptors are essential for infections. They specifically bind to the virus, often induce conformational changes within the virus and actively promote cell entry [83].

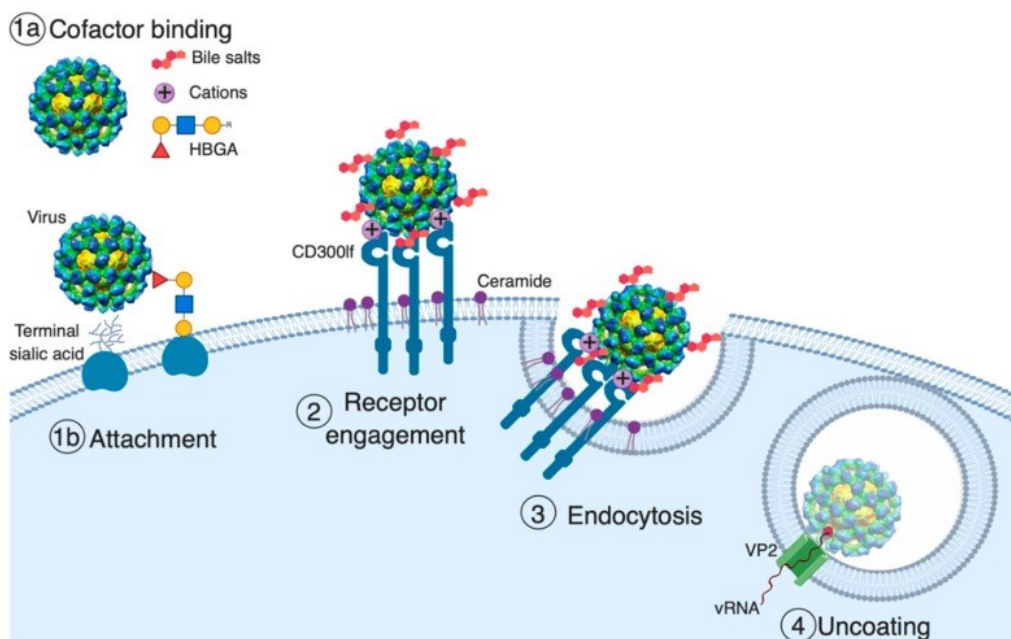


Figure 1-5: *Norovirus attachment and entry to host cells.*
Schematic of norovirus host-cell attachment and entry. Image taken from [37]

Despite the continual research of norovirus since its discovery, little is known about the norovirus attachment factors or receptors [37]. Challenge studies showed that certain strains predominantly infect people of specific blood-group type [47, 112, 127]. Also, it has been shown that interaction between human norovirus and histo-blood group antigens (HBGAs, also see 1.6) is important for infection (e.g., GI.1, GII.4, GII.10, and GII.17) [47, 82, 105, 111,

112, 127]. However, some genotypes bind poorly to HBGAs e.g. GII.1 which only binds to HBGAs in the presence of bile salts [47, 82, 111, 112]. HBGAs are expressed on epithelial cells and can be found as soluble antigens in saliva. Studies imply that norovirus interacts with HBGAs either prior to [50] and/ or during attachment to cell surfaces [27].

During the past four decades studies have mainly been hindered by lack of infectious clones and a reliable cell culture system [37]. Recently, three culture systems for human norovirus have been published (B cells, human intestinal enteroids (HIE) and zebra fish larvae [27, 50, 115]). However, during the absence of a reliable culture system for human noroviruses, a lot of research regarding attachment and entry mechanisms were performed with surrogate systems, such as the closely related murine norovirus (MNV) [56, 120, 125] and feline calicivirus (FCV) [106]. For both viruses, a system with susceptible cells and infectious molecular clones is available. For MNV, CDf300lf has been identified as a proteinaceous receptor during the past years [38, 89]. An X-ray crystal structure of the CDf300lf in complex with MNV P domain was recently published [59].

Unlike for MNV and FCV, no proteinaceous surface-receptor has been identified for human noroviral cell attachment so far. Apart from HBGAs, the only other interaction partner that could be identified are certain bile salts, and cations [27, 37, 58, 78]. Bile salts seem to play an important role in infection efficiency [27]. Specific binding sites for bile salts have been identified on the capsid surface [58].

1.6 Blood Groups and the HBGA-System

Blood groups defined by surface glycans are a double-edged sword: on one hand they may serve as false receptors preventing binding of pathogens to target tissues. On the other hand, several viruses, bacteria, and toxins use HBGAs as attachment factors to overcome host clearance or to facilitate internalization or colonialization [18]. HBGAs are polymorph glycans attached to cell membrane proteins or lipids of various tissues (e.g. epithelial cells of the intestine) as well as red blood cells but may also occur as soluble glycans in body fluids like saliva [20].

Blood Groups and the HBGA-System

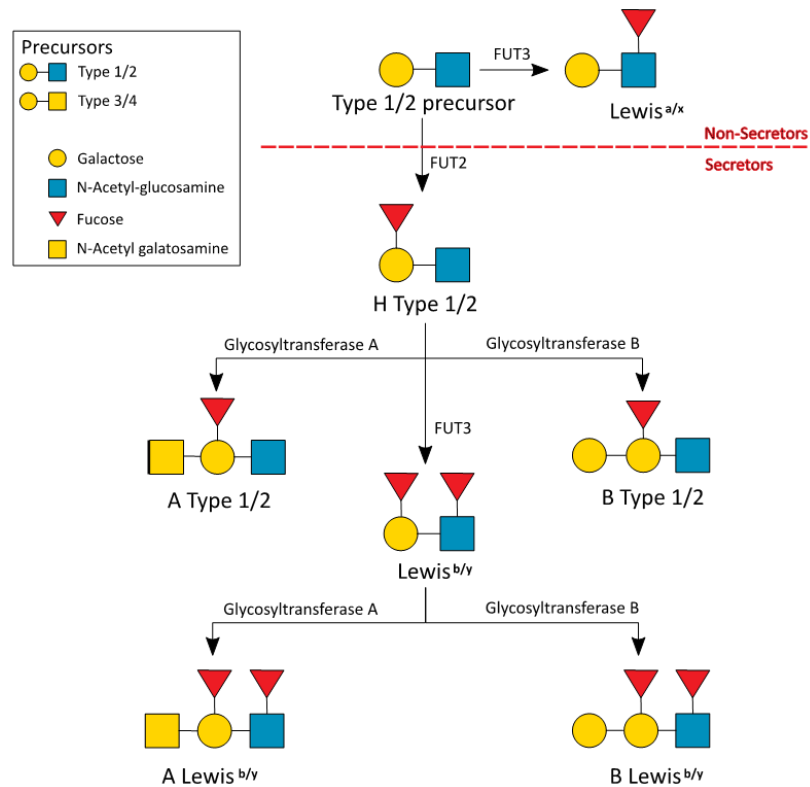


Figure 1-6: Synthesis of antigens H, A, and B.

FUT1 forms the H antigen by adding a 1-2 fucose. H antigen can also function as a precursor for ABO glycosyltransferase. Individuals of blood group type A express a 1-3N-acetylgalactosamine (GalNAc) whereas Group B individuals express a 1-3galactose (Gal). Individuals of group O have inactive *FUT2*. and therefore, only express the H-antigen.

The ABO-system comprises two antigens (A and B) both are the product of two autosomal co-dominant genes. This gene products are reflected in four blood-types (A, B, AB, and O). The blood-group O is the product of an autosomal recessive allele resulting in the expression of the H-antigen, a precursor to A and B antigens (Figure 1-6). Therefore, ABO describes the blood-group type, whereas A, B, and H refer to the antigens present [18].

Synthesis of ABO antigens occurs by addition of carbohydrates to an existing oligosaccharide [20]. H-antigen (Fuc α 1,2Gal β 1,4GlcNAc-R) is formed by addition of a terminal fucose to lactosamine by an α 1,2-fucosyltransferase (*FUT1*). In the absence of A or B glycosyltransferase activity only the H antigen or "O" is expressed. The H antigen can also function as a precursor for "A" antigen (addition of a N-acetylgalactosamine, GalNAc) of "B" antigen (addition of galactose (Gal)) [3]. The precursor oligosaccharide on which the antigens are synthesized are tissue- and species-specific. In red blood cells, for example, the ABO chains are mainly based on type 2 chains (lactosamine-type, Gal β 1,4GlcNAc-R). In contrast, the main precursor are usually type 1 chains (Gal β 1,3GlcNAc-R) in gastrointestinal epithelial tissues [18, 20]. Antigens

based on type 1 chains are also commonly found in saliva, mucus, and plasma [20]. Synthesis on type 2 chains requires FUT1 whereas synthesis on type 1 chains requires FUT2. Aside from this, chain type 1 FUT2 can also use chain type 3 and type 4 as a precursor, all of which are strictly tissue specific [18].

Similar to the ABO system, the Lewis blood group types are the result of the action of two distinct glycosyltransferases: FUT2 and FUT3. Lewis synthesis is tissue specific with expression pre-dominantly in respiratory, gastrointestinal and genitourinary tissues. Le^a and Le^b are the two Lewis antigens which can form four phenotypes: Le(a+b-), Le(a-b+), Le(a-b-), and Le(a+b+) although the later is seldom observed among adults. Le^a is synthesized by FUT3 by the addition of an α 1,4 fucose to the GlcNac of the type 1 chain. Le^b requires the synthesis of the H precursor from type 1 chains by FUT2, which is then used as a precursor for FUT3. After synthesis, Le^b can function as a precursor for ABO producing ALe^b and BLe^b [18, 20, 81]

1.7 Norovirus and HBGAs

The pathogenicity of human noroviruses is still poorly understood, and no viral receptor or entry mechanism have been identified yet. However, it has been discovered that susceptibility to different viruses is highly influenced by genetically defined HBGAs on the host cells [45, 47, 78]. One example for this genetically defined susceptibility is the *FUT2* gene. This gene enables synthesis of terminal α -1,2-linked fucose residues. Carriers of the *FUT2* allele are termed secretor-positive (or secretors) and can express HBGAs A, B, H-type 1, and Lewis b. Individuals lacking *FUT2* are termed secretor-negative (or non-secretors), a condition linked to insusceptibility to certain norovirus genotypes including GII.4 and GI.1 [86, 113].

In 2002, a study showed that GI.1 VLPs bind to cells in all tissue sections from secretors but not to non-secretors [82]. In this study, norovirus recognized cells expressing H types 1 or 3 antigens. To further examine this, tissue sections of secretors were treated with a fucosidase specifically cleaving off α -1,2-linked fucose residues [82]. In these tissue sections, which are now mimicking non-secretor status, the binding of norovirus VLPs to the cells was abolished, demonstrating the importance of a fucose residue in alpha1,2 linkage [82]. Furthermore, the ability of serum antibodies to block HBGA binding was reported to correlate with protection against infection [2, 101]. Therefore, attachment to HBGAs plays a major role in viral

attachment and infectivity [47, 78]. Nevertheless, there are norovirus genotypes that do not require HBGAs for attachment [47, 82, 111, 112]. HBGAs are complex glycan structures either exposed on cellular surfaces or secreted as soluble antigens into saliva. So, HBGAs could either work as cell attachment factors or virions might interact with the soluble HBGAs in saliva prior to cell attachment [27, 50].

Marionneau and colleagues further showed that human norovirus was internalized after binding to Chinese hamster ovary (CHO) cells transfected with the α -1,2-fucosyltransferase gene (FUT2) [82]. Internalization did not occur when cells were not transfected with FUT2 [82]. Expression of the carbohydrate ligand was required for internalization of the viral particles. Since CHO cells are derived from hamster ovary cells, the process of internalization appears to be independent of the species of cells [82].

These findings suggest that only individuals of secretor type can be infected by the virus, because non-secretors lack the HBGA H oligosaccharide on epithelial cells of the gut. Serum antibodies blocking the attachment of human norovirus VLPs from attaching to HBGAs is one of the most promising candidates for antiviral development [78]. Nonetheless, there are examples of human norovirus genotypes infecting hosts disregarding secretor status and Lewis or ABO phenotypes [86]. Despite the importance of the fucosylated carbohydrate as attachment factors these findings hint towards an unknown attachment factor.

1.8 Vaccine Development

Noroviruses are antigenically and genetically a highly diverse group of viruses. Therefore, the development of vaccines is a challenging task. The norovirus strains infecting humans are spanned over three different genogroups, each divided into numerous genotypes. Immunity induced from previous infection seems to be genotype, or even strain, specific, with limited cross-protection from other genotypes [6, 79, 121]. Additionally, the duration of protective immunity is not lifelong [49, 91]. This high diversity, limited cross-protection and continual emergence of new variants suggest that a vaccine for norovirus will have to be polyvalent comprised of different variants [79]. Similar to influenza, the norovirus vaccine will need to be constantly updated with newly emerged strains [79].

1.9 Synthetic Norovirus Inhibitors

In 2016, a study described a monoclonal antibody targeted for the GI.1 HBGA binding site that was capable of preventing norovirus VLPs from attaching to HBGAs by steric hindrance [101]. Similar to that, our lab identified several norovirus-specific camelid-derived heavychain-only variable domains (termed Nanobodies) that could block VLP attachment to HBGAs by sterically blocking the HBGA binding site [65]. Nanobodies are the variable domain of heavychain-only antibodies found in members of the camelid family (Figure 1-7) [57]. They display the typical immunoglobulin folding but lack the disulfide bridges because they only consist of a single domain (Figure 1-7). Therefore Nanobodies can be easily produced in *Escherichia coli* (*E.coli*) and do not require complex production in eukaryotic cells.

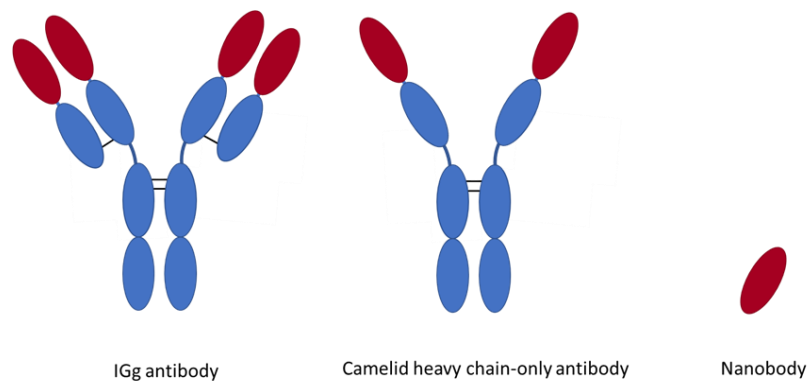


Figure 1-7: A schematic of a Nanobody.

From left to right a normal IgG antibody, a heavy chain-only antibody derived from members of the camelid family and a Nanobody (antigen-binding immunoglobulin domain of a camelid heavy chain-only antibody) are displayed.

Nanobodies are small in size (~15 kDa), highly specific and comparatively stable [85]. Nanobodies have been shown to inhibit VLP attachment through different mechanisms like particle disassembly or aggregation [66, 67].

1.10 Human Milk Oligosaccharides as Natural Norovirus Inhibitors

Another highly interesting group of potential inhibitors are human milk oligosaccharides (HMOs). HMOs are the third most abundant substance class of human mothers milk and were shown to protect against various pathogens [28, 72]. HMOs closely resemble HBGAs, both being complex glycans consisting of differently linked monosaccharaides. It has therefore been speculated that HMOs act as a sort of cofactor decoy for pathogens, mimicking HBGAs and thus blocking cell attachment [123]. Our study group identified one HMO,

2-fucosyllactose (2'FL), capable of blocking HBGA attachment of GI.1, GII.10 and GII.17 norovirus VLPs [65].

Unlike 2'FL, cross-reactivity among diverse human norovirus genotypes is a highly limiting factor for many antivirals. One possibility to improve cross-reactivity and overall performance of antivirals is the joint administration of multiple compounds. Indeed several state-of-the-art therapies take advantage of combinatorial treatments [30]. The combination of two or more drugs can remarkably enhance the effectiveness of treatment [29, 92, 95].

Since no effective antiviral drugs or vaccines are currently available, testing of non-toxic natural extracts is an interesting starting point for the discovery or development of novel and efficient antivirals. Insufficient cross-reactivity among the diverse norovirus genotypes is a limiting factor and a major challenge for development of broad-range therapy [65, 101].

1.11 Natural Extracts as Antivirals

A good inhibitor for human noroviruses has to meet three typical antiviral requirements; it should be (a) affordable, (b) safe and (c) highly efficient against their target. In order to meet these three goals, natural extracts have been screened for their potential antiviral activities (in this study and by other groups) against human norovirus [77, 98]. Most of these natural extracts have been consumed by humans as part of nutrition or traditional medicine for thousands of years. Therefore, they are regarded as safe [77]. Their natural origin, as well as the fact that humans already consumed these extracts for a long time, also increases their acceptance in the population. Thus, studies have tested various natural extracts as antivirals against human norovirus, and some interesting results were observed [77, 98].

However both reviewers point out problems with comparing the results between the different studies due to usage of different surrogate systems, concentrations of natural extracts, incubation times and viral titers [77, 98]. A comparison regarding stability of different surrogates raises the question how comparable results obtained in different systems might be and if observations are transferable to human norovirus [19]. Another drawback in testing natural extracts for their use as antivirals is the chemical complexity of the saps and extracts derived from plants, often making it difficult to identify the active compound within the highly diverse mixture.

Before the recent discovery of a cell culture system for human norovirus [27], most of the antiviral testing against human norovirus were performed in surrogate cell culture systems with related but culturable caliciviruses such as murine norovirus (MNV) or feline calicivirus (FCV). One typical study examined the norovirus inhibition caused by grape seed extract, using standard plaque assays with MNV, FCV and hepatitis A. Grape seed extract (5 mg/ml) was shown to reduce MNV infection below the detection limit after an incubation time of 105 min. In the same study, FCV was reduced by 0.59 log₁₀ plaque forming units (PFU)/ml after incubation with grape seed extract (0.5 mg/ml for 15 min) [52]. In another study, a set of 29 herbal extracts were tested for their ability to inhibit MNV and FCV. *Camellia sinensis* and *Ficus carica* (100 µg/ml) inhibited FCV by 87 % and 49 % respectively. Ribavirin (100 µg/ml) inhibited FCV by 78 % and MNV by 59 %. *Inonotus obliquus* (150 µg/ml) and *Crataegus pinnatifida* (50 µg/ml) also inhibited MNV by 92 % and 58 %, respectively [100]. Infectivity of MNV and FCV was also greatly reduced by red ginseng and components of the extract [76]. Incubation of FCV with cranberry juice proanthocyanin (0.15 mg/mL) reduced the infectivity by 5 log₁₀ PFU/mL within 30 min of exposure, while incubation of MNV with cranberry juice for 1 h reduced viral titers by 1 log₁₀ PFU/mL [108]. The same group also studied the effects of pomegranate juice and polyphenols on MNV and FCV. FCV and MNV titers were reduced by 2.56 and 1.32 log₁₀ upon 1 h of incubation with pomegranate juice. However, the antiviral effects observed with cranberry on FCV and MNV most likely arose from inhibiting adsorption [107, 108]. Antiviral activity exhibited by pomegranate-derived polyphenols was even greater: plaque formation of MNV was reduced by 1.30–3.61 log₁₀ PFU/mL [109]. Black raspberry juice also showed antiviral capacity against MNV and FCV. It decreased infectivity by 75.3 % and 92.7 % at concentrations of 3 % and 6 %, respectively [88]. Mulberry (*Morus alba* 0.005 %) juice inhibited MNV to 0.25 % and FCV to 50 % [75]. MNV and FCV were also inhibited by essential oils of clove, oregano and zataria [25]. Ueda et al., tested the antiviral effect of persimmon extracts in MNV culture assays. MNV was pre-treated with of persimmon extract (0.25 % for 3 min) and the mixture was added to the cells for 1 h. This led to a reduction of up to 4.3 log₁₀ PFU/ml [114]. The polymer chitosan which is created from the exoskeleton of crustaceans by deacetylation, more specifically reduced infectivity of FCV but showed no effect on MNV [22]. Oregano essential oil (4.0 %) and its primary component carvacrol reduced MNV by 0.95 log₁₀ after treatment for 15 min [36].

Methanolic extracts of green tea also exhibited reduction of FCV infectivity [87]. A further study tested the inhibition caused by blueberry juice and blueberry proanthocyanidins against FCV and hepatitis A virus using plaque assays. PFU of both viruses were reduced to undetectable levels by treatment with blueberry proanthocyanidins (0.5 mg/ml for 1 h or 1 mg/ml blueberry juice for 3 h). However, the authors stated that the commercial blueberry juice used in their studies also contained sodium citrate as a preservative agent. This raises the question if inhibition might have arisen from citrate [51].

Only few natural inhibitors have been tested in a setting with human norovirus. Whilst no reliable cell culture system was available, few groups, including ours, utilized surrogate ELISAs to investigate the effects of potential antivirals on VLP attachment to a HBGA-scaffold. We discovered the binding of citric acid to the HBGA-binding site of human norovirus using X-ray crystallography [41]. ELISA experiments with human norovirus VLPs were also conducted to confirm HBGA-attachment inhibition. Another study by Zhang et al., tested 50 clinically effective Chinese medical herbs traditionally used for treatment of intestinal diseases [126]. It was examined in ELISAs if the herbal extracts could disrupt attachment of human norovirus P domain to HBGAs. Chinese gall and pomegranate juice were identified as extracts able to disrupt VLP attachment. The group suspected tannic acid as the main active compound, as it is present in both Chinese gall and pomegranate juice [126]. Further, the influence of persimmon extract and its tannins on human norovirus (GII.4 strain) replication, by qPCR, was examined. Human norovirus GII.4 was pretreated with persimmon extract or its tannins. The group found that extracts containing more than 0.11 mg/ml of persimmon tannin reduced viral replication by more than 70 % [54].

1.12 Aims and Objectives

Human noroviruses constitute a massive burden both socially and economically. The lack of treatment or vaccination raises an increasing demand for an effective, affordable, and safe medication that exhibits broad reactivity against the various genotypes and variants circulating worldwide. Therefore, the overall aim of this thesis was to identify potential natural and synthetic inhibitors of human norovirus. The thesis was organized into five main aims:

1. ***Testing of synthetic inhibitors.***
Synthetic fucose oligomers and compounds of the National Institute of Health (NIH) collection were screened.
2. ***Testing of synthetically produced Nanobodies.***
Nanobodies raised against GI.1 were tested.
3. ***Testing of natural saps and extracts.***
A panel of 24 natural extracts, 31 types of honey and different propolis extracts were tested for their attachment inhibition.
4. ***Testing combinations of different inhibitors to evaluate how development of a therapy could benefit from combinatorial approaches.***
Previously identified inhibitors as well as inhibitors identified through the first part of this thesis were tested in combinations to identify how individual inhibitors might benefit from mutual activity.
5. ***Assessing the mode of action by examining the integrity of VLPs after treatment.***
Dynamic light scattering electron microscopy and X-ray crystallography were utilized to assess the possible mode of inhibition.

2 Material and Methods

Table 2-1: List of chemicals

Chemical Names	Company
1.2-Propanediol	Sigma-Aldrich
2' Fucosyl-lactose	Jennewein Biotechnologie GmbH
Acetic acid	Sigma-Aldrich
Agarose	Carl Roth
Ampicillin	Sigma-Aldrich
Bis-tris propane	Sigma-Aldrich
Blue White Select Screening Reagent	Sigma-Aldrich
Bromphenol blue	Alfa Aesar
Calcium chloride	Sigma-Aldrich
Cesium chloride	Sigma-Aldrich
DMSO (Dimethyl sulfoxide)	Sigma-Aldrich
DNA Gel loading dye purple (6x)	New England BioLabs
Effectene [®] Transfection Reagent	Qiagen
Ethanol	Carl Roth
Ethidium bromide	Bio-Rad
Ethylene glycol (EDO)	AppliChem
Ex-Cell 405 Serum-Free Medium	Sigma- Aldrich
EZ-Link [™] Sulfo-NHS-LC-Biotin	Thermo Fisher Scientific
GCDCA (glycocheno-deoxycholic acid)	Sigma-Aldrich
GelCode Blue protein stain	Thermo Fisher Scientific
Gentamycin	Biowest
Glucose	Sigma-Aldrich
Glycerol	MP Biomedicals
H ₂ O ₂ (hydrogen peroxide)	Sigma-Aldrich
Hydrochloric acid, 37%, fuming	Fisher Chemical
Imidazole	Sigma-Aldrich
Isopropyl alcohol	Sigma-Aldrich
Kanamycin	Carl Roth
LB agar (Miller) plates	VWR Chemicals
LB broth (Luria/Miller), granulated	Carl Roth
Lipofectamine 2000	Invitrogen
Magnesium-Chloride solution, 1M	Serva
Mini-Protean TGX Precast Gels (4-15%)	Bio-Rad
Ni-NTA agarose	Qiagen
O-phenylenediamine dihydrochloride	Sigma-Aldrich
PAGE ruler [™] Plus prestained protein ladder	Thermo Fisher Scientific
PBS 10x powder	Genaxxon
PEG 200	Sigma-Aldrich

Aims and Objectives

Chemical Names	Company
PEG 3350	Qiagen
Phosphate-citrate buffer tablets	Sigma-Aldrich
Porcine gastric mucin (PGM) type III	Sigma-Aldrich
Puromycin	Gibco
S.O.C medium	Invitrogen
Sf900II SFM (1X)	Gibco
Skim milk powder	Sigma-Aldrich
Sodium chloride	Carl Roth
Sodium fluoride	Sigma-Aldrich
Sodium hydroxide	Grüssing GmbH
Sodium nitrate	Sigma-Aldrich
Sodium thiocyanate	Sigma-Aldrich
Sucrose	Sigma-Aldrich
Terrific Broth (TB-) medium powder	Carl Roth
Tetracycline	VWR International
Tris-acetate EDTA (TAE) 50x	Carl Roth
Tris-Glycine-SDS 10x	Fisher BioReagents
Trizma hydrochloride solution	Sigma-Aldrich
Trypan Blue Dye 0.40%	Bio-Rad
Tween-20	Sigma-Aldrich
Uranyl acetate	Serva
Water, sterile filtered, for cell culture	Sigma-Aldrich

Table 2-2: List of equipment

Equipment	Company
96-well maxisorp plates Nunc	Thermo Fisher Scientific
Accu-jet pro pipet boy	Brand
Äkta prime plus	GE Healthcare
Analysenwaage ABS-N ABJ-NM ACS ACJ	KERN
AVANTI J-26 XP centrifuge	Beckman Coulter
Beckman Optima LE 80K Ultracentrifuge	Beckman Coulter
Beckman Optima MaxE Ultracentrifuge	Beckman Coulter
Centrifuge 5418	Eppendorf
Centrifuge 5430R	Eppendorf
ChemiDoc™ MP	Bio-Rad
Concentrators	Sartorius
Counting Slides, Dual Chamber Cell Counter	Bio-Rad
Dialysis Cassettes (slide-a-lyzer)	Thermo Fisher Scientific
DMi1 Light Microscope	Leica
Ecotron incubator	Infors HT

Aims and Objectives

Equipment	Company
Erlenmeyer Flasks	Corning
Filter Paper No.1	Whatman
GloMax Explorer	Promega
HiLoad™ 26/600 Superdex™ 200 pg	GE Healthcare
HiLoad™ 26/600 Superdex™ 75 pg	GE Healthcare
iMark™ Microplate Reader	Bio-Rad
ImmunoWash 1575 Microplate Washer	Bio-Rad
Microcal ITC 200	Malvern
Multitron Incubator	Infors HT
Nanodrop Lite Spectrophotometer	Thermo Fisher Scientific
Nikon SMZ 1500	Nikon
OD600 DiluPhotometer	Implen
Rotor JA 25.5	Beckman Coulter
Rotor JLA 8.1	Beckman Coulter
Rotor SW 40	Beckman Coulter
Rotor SW 56	Beckman Coulter
Rotor Ti45	Beckman Coulter
Rotor TLA 55	Beckman Coulter
Shaker DRS-12	NeoLab
Stirred Water Bath WB-4MS	Kisker Biotech GmbH & Co KG
Stirrer C-MAG HS10	IKA
Syringe Filters Millex®-HA	Merck Millipore
TC20™ Automated Cell Counter	Bio-Rad
Thermomixer Comfort	Eppendorf
Tissue Culture Flask 175 cm ²	Falcon
Tissue Culture Flask 25 cm ²	Falcon
UP200HT Ultrasonic processor	Hielscher Ultrasonics
Vortex Genie 2	Scientific Industries
Xplorer plus multipipettes	Eppendorf
Zetasizer Nano ZS	Malvern

Table 2-3: List of cells

Cell Type	Company
E. coli BL21 (chemically competent)	Invitrogen
E. coli DH5α (chemically competent)	Invitrogen
E. coli WK6 (chemically competent)	Invitrogen
HIGH FIVE™	Thermo Fisher Scientific
MAX efficiency DH10Bac Competent cells	Invitrogen
Sf9	Gibco

Aims and Objectives

Table 2-4: List of commercial kits

Kit	Company
QIAprep Spin miniprep Kit	Qiagen
QIAquick Gel Extraction Kit	Qiagen
QIAquick PCR purification Kit	Qiagen

Table 2-5: List of enzymes

Enzyme	Company
Gateway LR Clonase Enzyme Mix	Thermo Fisher Scientific
HRV 3C Protease	Novagen
Phusion High-Fidelity PCR Master Mix	New England BioLabs
Restriction enzyme BstEII	New England BioLabs
Restriction enzyme PstI	New England BioLabs
T4 DNA Ligase	New England BioLabs

Table 2-6: List of antibodies

Antibody for Detection	Company
Monoclonal HRP-conjugated goat α -His antibody	Sigma-Aldrich
Monoclonal HRP-conjugated goat α -mouse antibody	Thermo Fisher Scientific
Monoclonal HRP-conjugated goat α -rabbit antibody	Sigma-Aldrich
Polyclonal rabbit α -GII.10 VLP antibodies	In-house production at DKFZ
Polyclonal rabbit α -GII.4 VLP antibodies	In-house production at DKFZ
Nano-26 (cross-reactive used to detect GII.4, GII.10, GII.17)	In-house production Hansman lab
Nano-26 biotinylated	In-house production Hansman lab
Nano-4 (used to detect GII.17)	In-house production Hansman lab
Nano-4 biotinylated	In-house production Hansman lab
Nano-60 biotinylated (GI.1-specific)	In-house production Hansman lab

2.1 Preparation of Natural Extracts

Natural extracts and different types of honey (Table 2-7 and Table 2-8) were purchased and pre-diluted in PBS, at a concentration of 25 % (50 % for honeys) of original matter. After pre-dilution, all natural extracts and honeys were filtered (0.45 µm) and stored at 4°C in the dark. Propolis of three different origins (all from local beekeepers in south-west Germany) were extracted. Propolis is a mixture of resinous substances collected by bees in the surrounding of their hive. Therefore, composition of propolis is highly dependent on the region in which the hives are located. For the three propolis samples (Table 2-7), 100 % DMSO, 20 % PEG 200, 90 % ethanol, 70 % ethanol, 15 % ethanol, 100 % Propan-2-diol, 95 % Glycerol, and 100 % H₂O extracts were prepared. One gram of grinded propolis was incubated with 10 ml of the respective solvent (PEG and ethanol were diluted in water) for 3 or 30 days (d) with occasional shaking in the dark at room temperature (RT). Extracts were centrifuged and supernatants were filtered (pore size 0.45 µm).

Table 2-7: List of honeys and propolis

	Honey/Propolis	Company/Origin
1	Honey – Fir I	RU 0762880
2	Honey - Blossom	XNN0972100
3	Honey – Blossom Maile	AXIX0656071 Local beekeeper (Maile, Kernen)
4	Honey – Rape blossom	Imkerei Bunsen, Germany
5	Honey - Cornflower	BioGourmet GmbH, Brandenburg, Germany
6	Honey - Raspberry	Imkerei Bernhard Niepalla, Germany
7	Honey - Coriander	Atrium Import GmbH, Ukraine
8	Honey - Lavender	Atrium Import GmbH, France
9	Honey – Wild lavender	Atrium Import GmbH, EU
10	Honey – Acahual blossom	GEPA, Mexico
11	Honey – Eucalyptus	GEPA, Uruguay
12	Honey – Orange blossom	GEPA, Mexico
13	Honey – Acacia	Imkerei Bunsen, Germany
14	Honey – Linden tree blossom	Allos, Rumania
15	Honey – Fir II	Imkerei Bunsen, Black Forrest, Germany
16	Honey – Alpine forest	Breitsamer Honig, Italy, Austria
17	Honey – Mountain blossom	Bienenwirtschaft, EU/non EU alpine region
18	Honey – Alpine blossom	Breitsamer Honig, Italy, Austria
19	Honey – Tuscany	Breitsamer Honig, Italy
20	Honey – Andalusia	Breitsamer Honig, Spain
21	Honey – Mexico blossom	GEPA, Mexico
22	Honey – Latin America blossom	Langnese Honig, Latin America

Preparation of Natural Extracts

Honey/Propolis	Company/Origin
23 Honey – Acacia	Langnese Honig, EU
24 Honey – Medlar	Miel Company S.C., Spain
25 Honey – Rosemary	Miel Company S.C., Spain
26 Honey – Thyme	Miel Company S.C., Spain
27 Honey – Oak tree	Imkerei Ullrich, Odenwald, Germany
28 Honey – Chestnut tree	Imkerei Ullrich, Pfälzer Wald, Germany
29 Honey – Sweet clover	Himstedt, Italy
30 Honey – Sunflower	Allos, Germany
31 Honey – Robinia	Wabenschatz, Germany
Propolis tincture 96 % EtOH	Miel Company S.C., Spain
Propolis	Local beekeeper
Propolis ME (Kernen)	Local beekeeper (Maile, Kernen)
Propolis MF (Fellbach)	Local beekeeper (Maile, Fellbach)

Table 2-8: List of natural extracts

Extract	Company/Origin
Barley malt extract	Lindenmeyer, Germany
Maple syrup	Naturata, Canada
Erythritol	Gesund & Leben, Germany
Stevia Glycosides	Govinda Natur GmbH, Germany
Stevia	Borchers, Germany
Apple sweetener	Rigoni di Asiago, Italy
Agave syrup	BioTropic GmbH, Germany
Agave syrup II	REWE Markt GmbH, Mexico
Coconut flower syrup	Rapunzel Naturkost, Germany
Date syrup 1	Rapunzel Naturkost, Germany
Date syrup 2	Aldi Bio, Germany
Date syrup 3	Sample provided by Dr. Charles Sabin
Xylit	Dr. Groß GmbH, Germany
Merlot juice	REWE Feine Welt, Germany
New Red wine	REWE, Germany
New White wine	REWE, Germany
Prickly pear	Fresh fruit, local
Royal jelly	Cum Natura GmbH, Germany

2.2 Expression and Purification of P domains

2.2.1 Cloning and Expression of P domains

The production and expression of the norovirus P domain (GII.10, PDB-ID: 3ONU) was performed as previously described [66]. In brief, the codon-optimized GII.10 P domain sequence (residues 224 to 538) was cloned into a modified expression vector (pMal-c2X, performed by Dr. Grant Hansman) and transformed into chemically competent *E. coli* BL21 cells for expression [66]. One μl (150 ng/ μl – 400 ng/ μl) of the pMal-c2X vector containing the MBP-His-P domain construct was mixed with 50 μl of competent *E. coli* BL21 cells and incubated on ice for 10 min, followed by 45 s at 42°C in a water bath. After 2 min of incubation on ice, 600 μl of S.O.C. medium was added, and the cells were incubated for 1 h at 37°C. The cells were sub-cultured into 120 ml of lysogeny broth (LB) medium containing 100 $\mu\text{g/ml}$ of ampicillin overnight at 37°C, shaking at 160 rpm. Nine liters (l) of LB medium with 100 $\mu\text{g/ml}$ ampicillin were inoculated with the subculture (1:100). The cells were grown for about 1.5 h at 37°C shaking until the optical density (OD) reached 0.4 – 0.6. The temperature was lowered to 22°C for 1 h before expression was induced with 0.66 mM of IPTG. The expression was performed overnight (about 18 h) at 22°C. Cells were harvested by centrifugation at $10,543 \times g$ for 15 min at 4°C. Cell pellets were frozen at -20°C until purification.

Table 2-9: List of P domains used

Genotype	Strain	Accession Number	Capsid Protein ID
GI.1	Norwalk	M87661	AAB50466
GII.10	Vietnam 026	AF504671	AAT12445

2.2.2 Purification of P domains

All buffers (Table 2-10) were produced from stock solutions using deionized water and filtered (pore size 0.45 μm) before use. The cell pellet was thawed and resuspended in 150 ml of PBS at 4°C. The cell suspension was sonicated for 2 min (power 130 W, amplitude 20 %, pulse frequency 50 %) on ice. The lysate was centrifuged at $43,667 \times g$ for 30 min at 4°C to remove cell debris. The clarified lysate was incubated for at least 40 min with 20 ml of Nickel (Ni)-NTA agarose beads pre-equilibrated with 10 mM Imidazole buffer (Table 2-10). The mixture of Ni-NTA agarose beads and lysate was added to a chromatography column and slowly washed with 5 column volumes of 10 mM, 20 mM, and 50 mM Imidazole buffer (Table 2-10). The MBP-

Expression and Purification of P domains

His-P domain fusion protein was eluted from the Ni-NTA-agarose beads by incubation with small volumes of 250 mM Imidazole buffer (Table 2-10). During elution, the OD₂₈₀ of the eluate was checked on a Nanodrop spectrophotometer to evaluate the presence of protein. After elution, Ni-NTA agarose beads were washed with 250 mM Imidazole buffer to remove any remaining bound protein.

Table 2-10: Buffers used for P domain purification

Buffer	Tris-HCl pH 7.6	NaCl	Imidazole pH 8.0
250 mM Imidazole buffer	20 mM	200 mM	250 mM
50 mM Imidazole buffer	20 mM	200 mM	50 mM
20 mM Imidazole buffer	20 mM	200 mM	20 mM
10 mM Imidazole buffer	20 mM	200 mM	10 mM
Gel filtration buffer (GFB)	25 mM	300 mM	-

The presence of the MPB-His-P domain fusion protein was verified by sodium dodecyl sulfate–polyacrylamide gel electrophoresis (SDS-PAGE) (45 A, 20 V, 45 min). After confirmation, the MBP-His-P domain fusion protein was concentrated to about 3 mg/ml using commercial concentrators (50 kDa cut-off). The fusion protein was then cleaved, into MPB-His and P domain, by incubating it with HRV-3C protease (1 U for 100 µg of protein) during dialysis against 10 mM Imidazole buffer (~1:100) overnight at 4°C.

The Ni-NTA agarose beads were equilibrated with 10 mM Imidazole buffer and incubated with the cleaved and dialyzed P domain for 30 min at 4°C with slow rotation. The mixture of Ni-NTA agarose beads and P domain was applied to a chromatography column and the flow-through was collected. Similarly, the OD₂₈₀ of the flow-through was evaluated using a Nanodrop. The presence of the cleaved P domain without MBP-His was evaluated on an SDS-PAGE gel as described above. The cleaved P domain was concentrated in commercial concentrators (30 kDa cut-off) to a concentration of 3 mg/ml and dialyzed against GFB (~1:100, Table 2-10) overnight at 4°C.

Size exclusion chromatography (using a Superdex-200 or Superdex-75 column) was used to further purify the P domain. The fractions were checked on an SDS-PAGE gel and only the purest fractions were pooled and concentrated with commercial concentrators (30 kDa cut-off) to about 2.5 - 2.8 mg/ml. The P domain was then stored in GFB at 4°C. Other P domains

(GI.1, Table 2-9) were purified following the same protocol, only the final concentration to which each P domain was concentrated after purification varied slightly (~3 mg/ml) according to optimal concentrations for later storage or setting up of crystals.

2.3 Expression and Purification of Nanobodies

2.3.1 Purchase of VHH Library and Cloning of Nanobodies

Nanobodies were produced at the ‘VIB Nanobody Service Facility’ with the approval of the Ethical Commission of Vrije Universiteit, Brussels, Belgium [67]. For production of Nanobodies, a single alpaca was injected subcutaneously with the respective purified VLPs (GI.1 or GII.10). For each VLP, a VHH library was constructed and screened by phage display for the presence of antigen-specific Nanobodies. The VIB provided a library of glycerol stocks with the Nanobody sequence in a pMECs vector. The constructs were subcloned into pHEN6 for expression of the Nanobody. The glycerol stocks were grown in LB medium overnight and the plasmid was purified from the cell pellet using a miniprep Kit and following manufacturer’s instructions. The Nanobody construct in pMECs was amplified by PCR using the primers PMCF and AGE (Table 2-11).

Table 2-11: List of primers

Name	Sequence (5' - 3')	Purpose
AGE	GATGTGCAGCTGCAGGAGTCTGGAGGAGG	PCR Nanobody
PMCF	GTAGTGCGGCCGCTGAGGAGACGGTGACCT	PCR Nanobody
Universal Forward	CGC CAG GGT TTT CCC AGT CAC GAC	Sequencing
Universal Reverse	TCACACAGGAAACAGCTATGAC	Sequencing

Constructs were purified using the QIAquick PCR purification kit following the manufacturer’s instructions. The purified plasmid DNA were digested with restriction enzymes PstI-Hf and BstEII-Hf for 1.5 h at 37°C. After digestion, fragments were purified with the QIAquick PCR purification kit. For ligation, the digested fragments were ligated with the pHEN6 vector (pre-cut with the same restriction enzymes) using T4 Ligase for 10 min at RT. The ligated product was transformed into competent DH5α *E. coli* cells with a heat shock protocol. The cells were plated onto LB (ampicillin) agar plates for selection and grown overnight. On the next day, colonies were picked and transferred into LB (ampicillin) and grown overnight at 37°C. The plasmids were extracted from the overnight liquid cultures with a miniprep kit and sequenced

at GATC (Primers: Invitrogen universal forward; universal reverse, Table 2-11). To verify the Nanobody construct in the sequence the program Sequencer was used.

2.3.2 Expression of Nanobodies

The subcloned construct in pHEN6c was transformed into WK6 *E. coli* cells by a heat shock protocol. Cells were thawed and 2 μ l of the construct was added. The cells were incubated on ice for 10 min followed by a heat-shock for 45 s at 42°C, followed by another 2 min on ice. S.O.C. medium (600 μ l) was added, and the cells were incubated 1 h at 37°C shaking. The cells were sub-cultured in 100 ml of LB with 100 μ g/ml ampicillin at 37°C shaking at 160 rpm overnight. The overnight culture was used to inoculate two flasks of 1.5 l of TB medium each supplemented with 1 g/l of glucose, 2 mM MgCl₂ and 100 μ g/ml ampicillin. Cells were grown at 37°C, 160 rpm shaking, until the OD₆₀₀ reached 0.6 – 0.9, then the temperature was lowered to 28°C, and overnight expression was induced with 1 mM of IPTG. The cell pellet was collected by centrifugation at 10,543 \times g for 15 min at 4°C. Cell pellets were frozen (-20°C) until purification.

2.3.3 Purification of Nanobodies

To extract the Nanobodies from the periplasm, the frozen pellet was re-suspended in 12 ml of TES buffer per liter of cell culture (Table 2-12) at 4°C. After the frozen pellet was fully suspended in TES, 18 ml per liter of TES/4 (Table 2-12) was added, and incubated on a shaker at 4°C for 40 min. The suspended cells were centrifuged for 30 min at 39,191 \times g at 4°C. Ni-NTA agarose beads were pre-equilibrated in 10 mM Imidazole buffer (Table 2-12). The supernatant containing the Nanobodies was incubated with pre-equilibrated Ni-NTA agarose beads for 40 min under agitation at 4°C. The supernatant/Ni-NTA agarose beads mixture was transferred to a chromatography column and washed with at least one column volume of 10 mM, 20 mM, and 50 mM Imidazole buffer (Table 2-12). The Nanobodies were eluted from the column by stepwise addition of 250 mM Imidazole buffer. Presence of the protein was monitored during elution via the OD₂₈₀ on a Nanodrop. The protein was concentrated using commercial concentrators (5 kDa cut-off), the presence of Nanobodies was verified on an SDS-PAGE gel and dialyzed against GFB overnight at 4°C. Finally, the Nanobodies were purified by size exclusion chromatography using a Superdex-200 or Superdex-75 column. The peak fractions were pooled and the purified Nanobodies were concentrated with commercial concentrators to a concentration of 3 – 5 mg/ml and stored in GFB at 4°C.

Expression and Purification of VLPs

Table 2-12: Buffers used for Nanobody purification

Buffer	EDTA	Sucrose	Tris-HCl pH 7.6	NaCl	Imidazole pH 8.0
TES buffer	0.5 mM	0.5 mM	0.2 M	-	-
TES/4 buffer	0.125 mM	0.125 mM	50 mM	-	-
250 mM Imidazole buffer			20 mM	200 mM	250 mM
50 mM Imidazole buffer			20 mM	200 mM	50 mM
20 mM Imidazole buffer			20 mM	200 mM	20 mM
10 mM Imidazole buffer			20 mM	200 mM	10 mM
Gel filtration buffer (GFB)			25 mM	300 mM	-

2.4 Expression and Purification of VLPs

2.4.1 Cloning of VLP Constructs and Production of Bacmid

For the production of norovirus VLPs (Table 2-13), a plasmid (pDONR221) containing the complete ORF2 sequence was purchased from Invitrogen. The ORF2 fragment was cloned into pDEST8 using the Gateway cloning system (Invitrogen). One μl of pDONR221 containing the construct (100 ng/ μl), 1 μl of pDEST8 plasmid, 6 μl of water and 1.5 μl of LR clonase II mix (Invitrogen) were incubated for 1 h at 25°C. The reaction was terminated by adding 1 μl of Proteinase K and incubation for 10 min at 37°C.

For the transformation of competent *E. coli* DH5 α cells, 50 μl of cells were mixed with 2 μl of reaction mix, followed by incubation on ice for 10 min, heat shocked for 45 s at 42°C and transferred back to ice for 1 min. The cells were then re-suspended in 600 μl S.O.C. medium and incubated for 1 h at 37°C, shaking. The cells were plated onto LB agar plates with ampicillin spread on the surface (10 μl of 100 mg/ml) and grown overnight at 37°C. Three colonies were selected and cultured in 4 ml of LB supplemented with ampicillin (100 $\mu\text{g}/\text{ml}$) overnight at 37°C.

Table 2-13: List of VLPs used for VLP expression

Genotype	Strain	Accession number
GI.1	Norwalk virus	Q83884
GI.1	West Chester	AY502016
GI.2	Funabashi 258	AB078335
GI.2	Southampton	L07418
GI.3	Kashiwa 645	BD011871
GI.4	Chiba	AB042808
GI.11	#8	AB058547

From the liquid cultures, plasmids were purified with a miniprep purification kit and the presence of the insert in pDEST8 was verified on an 1 % agarose gel using gel electrophoresis and stained with ethidium bromide. *E. coli* DH10 BAC cells (60 µl) were transformed with 1 µl of the construct with a heat shock protocol. Cells and plasmid were incubated on ice for 10 min, followed by a heat shock for 45 s at 42°C. After 1 min of incubation on ice, the cells were re-suspended in 700 µl of S.O.C. medium and incubated for 4 h at 37°C, shaking. The cells were plated onto LB agar plates on which 20 µl of kanamycin (50 mg/ml), 20 µl of tetracycline (10 mg/ml), 3 µl of gentamycin (50 mg/ml), and 40 µl of blue/white reagent were spread. Plates were incubated at 37°C for 48 h.

Four colonies per plate were selected and grown in LB medium supplemented with 50 µg/ml kanamycin, 10 µg/ml tetracycline, 7 µg/ml gentamycin, at 37°C overnight. Glycerol stocks of the overnight cultures were prepared. The rest of the overnight cultures were used for plasmid purification using a miniprep kit, and plasmid DNA was subsequently used for transfection of Sf9 cells.

2.4.2 Transfection of Sf9 Cells with Bacmid and Production of Seed Virus

Two days before transfection, cells were split in suspension culture. On the day of transfection, cells were seeded to 6-well plates with $1.5 - 2 \times 10^6$ cells per well. Cells were left to settle in the plates. Then medium was removed and replaced by 1 ml of fresh medium per well. In a separate tube, 90 µl of EC buffer were mixed with 3.2 µl of Enhancer and 8 µl of the purified plasmid (150–200 ng/µl) and incubated for 2–5 min at RT. Effectene (10 µl) was then added to each tube, mixed and incubated for 5–10 min at RT. Medium (900 µl) was added to each of the tubes and the complete content of each tube was added dropwise to one well each. The cells were left to grow for 7 days at 28°C in the transfection mixture. The supernatant and cells of each well were added to a T75 flask of Sf9 cells to expand the

baculovirus. After 5–7 days, the supernatant containing the baculovirus was centrifuged at $1,057 \times g$ for 10 min to remove cells, sterile filtered (Stericup®), and stored at 4°C (termed seed virus).

2.4.3 Expression of VLPs

The seed virus was either used to inoculate Sf9 cells to produce more baculovirus or High Five cells (H5) for production of VLPs. Before infection, cells were grown in 200 ml of liquid culture in their respective medium (Sf9 in Sf900 medium, H5 in Ex-Cell 405 serum-free medium) for three days. Three h prior inoculation, cells were transferred to fresh medium. For inoculation of H5 cells, 300 ml of medium were inoculated with 60 ml of cells and 15–20 ml of seed virus (depending on the quality of the seed virus). Sf9 cells were infected in a similar manner. 250 ml of medium were inoculated with cells and 15–20 ml of seed virus was added. The expanded seed virus was harvested as described previously for the initial production of seed virus (2.4.2).

2.4.4 Purification of VLPs

To harvest VLPs from H5 cells, the culture was first centrifuged at $1,057 \times g$ for 10 min followed by $4,960 \times g$ for 1 h at 4°C. The supernatant was transferred to ultracentrifuge tubes and centrifuged at $142,032.1 \times g$ for 2 h at 4°C to pellet VLPs. PBS (1 ml) was added to the VLP pellets overnight at 4°C to allow resuspension.

VLPs were further purified on a caesium chloride (CsCl) gradient (0.36 g of CsCl per 1 ml of VLP suspension). The VLPs in CsCl were centrifuged at $121,780.9 \times g$ for 18-24 h at 4°C in a swing-out Rotor (SW56) to allow the gradient to form and the VLPs to accumulate according to their density. VLPs were taken from the gradient by piercing the centrifugation vials horizontally with a needle to suck out the blueish white band containing concentrated VLPs. The VLPs were diluted with PBS and centrifuged at $71,680 \times g$ for 2 h at 4°C to pellet the VLPs. The VLP pellets were resuspended in fresh PBS overnight at 4°C to remove the CsCl and to concentrate the sample.

H5 and Sf9 cells were either grown by Dr. Grant Hansman or Dr. Jessica Devant and splits of cells were handed for VLP or seed virus production. Most VLPs used during this thesis were kindly provided by Dr. Grant Hansman and Dr. Jessica Devant.

2.5 Binding ELISAs

Binding ELISAs were used to test the binding ability of Nanobodies or antibodies to their respective VLPs or P domains (Table 2-14, Table 2-9). For binding ELISAs, 96-well microtiter plates (MaxiSorp, Thermo Scientific) were coated with VLPs or P domain to provide a scaffold for Nanobodies to bind to.

Table 2-14: List of VLPs used in ELISA

Genotype	Strain	Accession number
GI.1	Norwalk Virus	Q83884
GI.1	West Chester	AY502016
GI.2	Funabashi 258	AB078335
GI.2	Southampton	L07418
GI.3	Kashiwa 645	BD011871
GI.8	WUG1	AB081723
GI.11	#8	AB058547
GII.1	Hawaii	U07611
GII.4	Sydney	K4LM89
GII.4	Chiba Virus (CV)	AB042808
GII.10	Vietnam 026	AF504671
GII.17	Kawasaki	LC037415
GII.17	Saitama	KJ196286.1

For a binding ELISA with GI.1 VLPs, microtiter plates were coated with 10 µg/ml of GI.1 VLPs for 1 h at 37°C. The plates were washed with phosphate-buffered saline (PBS, pH 7.4) containing 0.1 % of Tween 20 (PBS-T) using a plate washer (ImmunoWash 1575 Microplate Washer, Bio-Rad). The plates were then blocked with 5 % skimmed milk in PBS for 1 h at RT, followed by another washing step. As a primary antibody, the GI.1 Nanobodies to be tested were serially diluted (starting at a concentration of 100 µg/ml,) and added to the plate before incubation at 37°C for 1 h. Following another wash step, HRP-conjugated polyclonal anti-His antibody was added 1:4,000 to the wells for 1 h at 37°C to detect the His-tag of attached Nanobodies. Plates were washed and *o*-phenylenediamine dihydrochloride (OPD) and H₂O₂ were added and incubated for 30 min at RT in the dark. After adding 3 N HCl to the plates to stop the reaction and enhance the signal, the OD₄₉₀ of the wells was read with an iMark™ Microplate Reader. Wells without primary antibody were added in each experiment as negative controls.

Binding ELISAs

The binding ELISA assay slightly varied, depending on the VLPs or P domains used for coating. Below are short descriptions of the different variations of the assay in tabular format (Table 2-15 - Table 2-17). The last two steps after removal of secondary antibody (adding of 100 µl/well of OPD buffer for 30 min at RT followed by addition of 50 µl/well of 3 N HCL) were the same in all assays.

Table 2-15: Binding ELISA protocol GII.10 VLPs

Step	Reagent	Concentration	Incubation time	Incubation temperature
Coating	GII.10 026 VLP	10 µg/ml	1h	37°C
Blocking	Skim milk	5 %	1h	RT
1st Ab	Nanobodies/Rabbit 1	Serial dilution/1:20,000	1h	37°C
2nd Ab	Anti-His/anti-Rabbit	1:4,000/1:40,000	1h	37°C

Table 2-16: Binding ELISA protocol GI.1 VLPs

Step	Reagent	Concentration	Incubation time	Incubation temperature
Coating	GI.1 VLPs	5 µg/ml	1h	37°C
Blocking	Skim milk	5 %	1h	RT
1st Ab	Nanobodies for testing	Serial dilution; starting at 100 µg/ml	1h	37°C
2nd Ab	Anti-His	1:4,000	1h	37°C

Table 2-17: Binding ELISA protocol GI.1 P domain

Step	Reagent	Concentration	Incubation time	Incubation temperature
Coating	GI.1 P domain	10 µg/ml	1h	37°C
Blocking	Skim milk	5 %	1h	RT
1st Ab	Nanobodies for testing	Serial dilution; starting at 100 µg/ml	1h	37°C
2nd Ab	Anti-His	1:4,000	1h	37°C

2.6 HBGA Attachment Inhibition Assay

The HBGA blocking assay was used to screen different compounds; natural extracts, Nanobodies and antibodies, for their ability to disrupt attachment of VLPs to an HBGA scaffold provided by porcine gastric mucin type III (PGM, containing HBGAs). The binding of GI.1, GII.1, GII.4, GII.10 and GII.17 VLPs to PGM was previously determined [65]. The blocking assay with GII.10 VLPs is as described; first, microtiter plates were coated with 100 μ l/well of PGM (10 μ g/ml) for 4 h at RT. Plates were then washed and blocked with 5 % skimmed milk overnight at 4°C. In a separate deep well plate, compounds such as natural extracts, Nanobodies or antibodies were serially diluted in PBS (unless specifically mentioned otherwise) and 10 μ g/ml of GII.10 026 VLPs were added, mixed, and incubated for 3 h at RT. Microtiter plates were washed and 100 μ l of the respective inhibitor/VLP mixture was added to triplicate wells, the plate was incubated for 2 h at RT to allow attachment of the VLPs to the PGM-coated plates. After another washing step, GII.10-specific polyclonal rabbit antibody (Rabbit1, raised against GII.10 VLPs, 1:40,000 in PBS-T plus 0.5 % skimmed milk) was added to the plates and incubated for 1 h at RT. After washing, horseradish peroxidase (HRP)-conjugated polyclonal anti-rabbit antibody (anti-rabbit, 1:40,000 in PBS-T with 0.5 % skimmed milk) was added for 1 h at RT. Plates were washed before OPD and H₂O₂ were added and further incubated in the dark for 30 min at RT. The reaction was stopped by adding 50 μ l of 3 N HCl per well. The absorbance was measured at 490 nm (OD₄₉₀). In all plates, VLPs without inhibitor and wells without VLPs were included as positive and negative controls, respectively. The OD₄₉₀ value of untreated VLPs was set as a reference corresponding to 0 % of inhibition, the OD₄₉₀ value of wells without VLPs corresponded to 100 % of inhibition. Finally, the percentage of inhibition was computed as $[1 - (\text{treated VLP mean OD}_{490} / \text{mean positive reference OD}_{490})] \times 100$. The half-maximal inhibitory concentration (IC₅₀) was determined using Prism software (version 8.0) [117]. All experiments with PGM binding were performed in triplicate wells and standard deviation was calculated. Major experiments were performed as three independent experiments and standard deviation was calculated.

The usage of different VLPs in the HBGA binding ELISA makes it necessary to optimize each assay individually for the respective VLP. The following tables give a brief summary of the protocols followed for the different VLPs (Table 2-18 - Table 2-23). The last two steps

HBGA Attachment Inhibition Assay

performed after removal of secondary antibody were the same in all assays; addition of 100 µl/well of OPD buffer for 30 min at RT, followed by addition of 50 µl/well of 3 N HCL. For GII.10 VLPs, two variants of the HBGA blocking assay are given. Initially variant A (Table 2-18) was used. Usage of different aliquots of detection antibody and the discovery of prolonged reaction time with some antibodies/natural extracts in DLS forced the introduction of variant B (Table 2-19).

Table 2-18: HBGA blocking ELISA protocol GII.10 026 VLPs, variant A

Step	Reagent	Concentration	Incubation time	Incubation temperature
Coating	PGM	10 µg/ml	4h	RT
Blocking	Skim milk	5 %	ON	4°C
Pre-incubation	GII.10 026 VLP + Inhibitor	10 µg/ml	1h	RT
Incubation in plate			2h	RT
1st Ab	GII.10-specific polyclonal rabbit antibody (Rabbit 1)	1:20,000	1h	RT
2nd Ab	HRP-conjugated polyclonal anti-rabbit antibody	1:40,000	1h	RT

Table 2-19: HBGA blocking ELISA protocol GII.10 026 VLPs, variant B

Step	Reagent	Concentration	Incubation time	Incubation temperature
Coating	PGM	10 µg/ml	4h	RT
Blocking	Skim milk	5 %	ON	4°C
Pre-incubation	GII.10 026 VLP + Inhibitor	10 µg/ml	3h	RT
Incubation in plate			2h	RT
1st Ab	GII.10-specific polyclonal rabbit antibody (Rabbit 1)	1:40,000	1h	RT
2nd Ab	HRP-conjugated polyclonal anti-rabbit antibody	1:20,000	1h	RT

Table 2-20: HBGA blocking ELISA protocol GII.4 Sydney VLPs

Step	Reagent	Concentration	Incubation time	Incubation temperature
Coating	PGM	10 µg/ml	1h	37°C
Blocking	Skim milk	5 %	1h	RT
Pre-incubation	GII.4 VLP + Inhibitor	1 µg/ml	2h	RT
Incubation in plate			1h	37°C
1st Ab	GII.4-specific polyclonal rabbit antibody	1:1,000	1h	37°C
2nd Ab	HRP-conjugated polyclonal anti-rabbit antibody	1:5,000	1h	37°C

HBGA Attachment Inhibition Assay

Table 2-21: HBGA blocking ELISA protocol GI.1 Norwalk

Step	Reagent	Concentration	Incubation time	Incubation temperature
Coating	PGM	10 µg/ml	1h	37°C
Blocking	Skim milk	5 %	1h	RT
Pre-incubation	GI.1 VLP + Inhibitor	1.5 µg/ml	2h	RT
Incubation in plate			1h	37°C
1st Ab	GI.1-specific biotinylated Nanobody 60 (Nano-60)	1:2,500	1h	37°C
2nd Ab	HRP-conjugated streptavidin	1:5,000	1h	37°C

Table 2-22: HBGA blocking ELISA protocol GII.17 Kawasaki VLPs

Step	Reagent	Concentration	Incubation time	Incubation temperature
Coating	PGM	10 µg/ml	1h	37°C
Blocking	Skim milk	5 %	1h	RT
Pre-incubation	GII.17 Kawasaki VLP + Inhibitor	1.5 µg/ml	2h	RT
Incubation in plate			1h	37°C
1st Ab	GII.17 specific biotinylated Nanobody 26 (Nano-26)	5 µg/ml	1h	37°C
2nd Ab	HRP-conjugated streptavidin	1:5,000	1h	37°C

Table 2-23: HBGA blocking ELISA GII.1 Hawaii VLPs + bile

Step	Reagent	Concentration	Incubation time	Incubation temperature
Coating	PGM	10 µg/ml	ON	4°C
Blocking	Skim milk	5 %	2h	RT
Preincubation VLP + bile	GII.1 VLPs + GCDCA +	10 µg/ml 0.4µM	1h	RT
Pre-incubation VLP + bile + inhibitor	GII.1 VLPs + GCDCA + Inhibitor		2h	RT
Incubation in plate			1h	RT
1st Ab	GII.1-specific polyclonal rabbit antibody HV-1068	1:5,000	1h	RT
2nd Ab	HRP-conjugated polyclonal anti-rabbit antibody	1:20,000	1h	RT

2.6.1 Optimization of HBGA Inhibition ELISA for Screening

Initial ELISA-based screenings for inhibition by either natural or synthetic compounds were performed with GII.10 026 VLPs. The GII.10 026 P domain crystallizes quickly, making it ideal to screen structures using X-ray crystallography to find bound inhibitors. Therefore, this strain was chosen so potential inhibitors identified in ELISA screens could also rapidly be tested for ligands in the crystal structure of the P domain.

The performance of ELISAs for testing the inhibitory potential of various extracts and synthetic compounds required the establishment of a reliable ELISA to perform standardized testing of possible candidates. This included testing different GII.10 VLP production batches because detection levels achieved with a given protocol can vary slightly depending on the batch. The standard ELISA protocol was published [105], however, it was optimized for different VLPs and P-domains (Table 2-18). To compare different VLP batches, samples were examined with negative stain by EM (Figure 2-1). The difference between small and native sized VLPs was clearly visible (Figure 2-1). Despite the difference in VLP sizes, the ELISA maximum detection level did not depend on VLP size.

HBGA Attachment Inhibition Assay

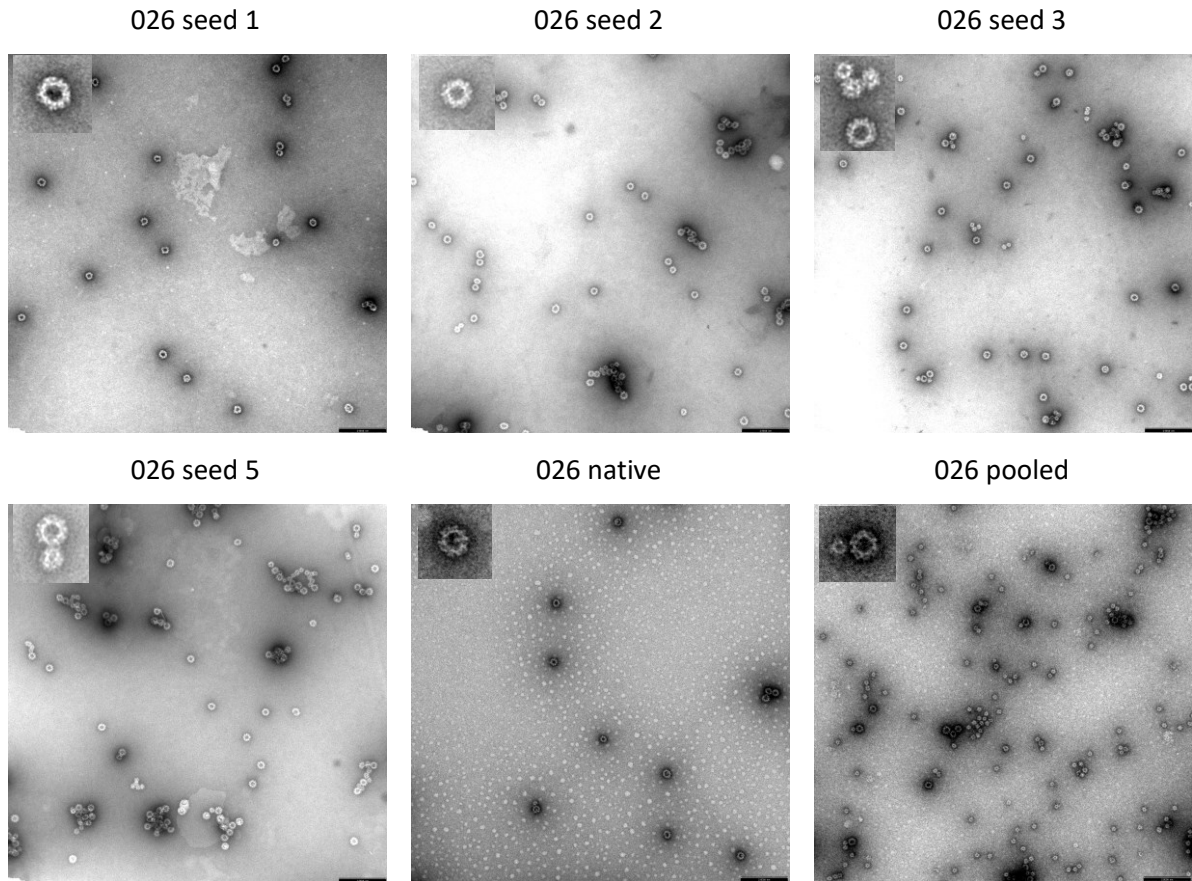


Figure 2-1: Negative stain EM images of different batches of GII.10 026 VLPs. 026 seed 1 – 3 and 5: VLP-batches prepared with different seed virus batches; 026 native: native sized 026 VLPs; 026 pooled: older VLP-batches that were pooled together. Batches seed 1, seed 2, and native comprise of mainly native sized VLPs whereas seed 3, seed 5 and pooled also contain a high number of small-sized VLPs. Scale bar 250 nm:

During optimization different concentrations of primary and secondary antibodies were tested (Figure 2-2 and Figure 2-3), following the protocol of a binding ELISA (plates coated with VLPs as described in Table 2-15, with rabbit 1 1:20,000 as the primary antibody and a serial dilution of anti-rabbit as the secondary antibody). As expected, variations of the Rabbit 1 or anti-rabbit concentration exhibited a direct impact on the detection levels achieved.

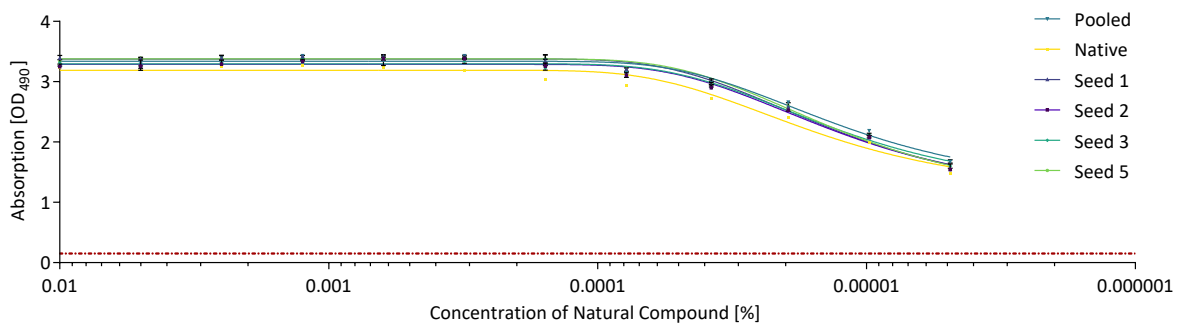


Figure 2-2: GII.10 Binding ELISA, detection with serially diluted Rabbit 1. Rabbit 1 was used as primary antibody (concentration as indicated) and anti-rabbit was used as a secondary antibody (1:40,000). Detection levels of different VLP production batches (pooled, native, seed 5, new seed 3, new seed 2, new seed 1) were compared and the concentration of rabbit 1 was optimized (protocol Table 2-15)

HBGA Attachment Inhibition ELISA – Combinatorial Inhibition

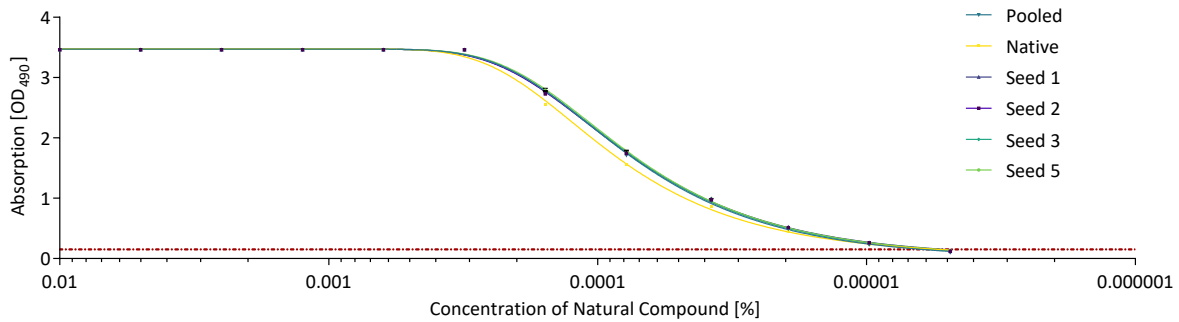


Figure 2-3: *GII.10 Binding ELISA, detection with serially diluted anti-rabbit*
Rabbit 1 was used as primary antibody (1:20,000) and anti-rabbit was used as a secondary antibody
(concentration as indicated; protocol Table 2-15).

The binding ELISAs also established that the antibodies were able to detect GII.10 026 VLP. At 37°C, the detection system of Rabbit1 and anti-rabbit could detect the VLPs at high OD₄₉₀ if the plates were directly coated with GII.10 026 VLPs. The problematic step in the GII.10 HBGA attachment ELISA is the attachment of GII.10 026 VLPs to PGM, which seems to be rather weak and requires the entire ELISA after the attachment step to be performed at RT in order not to abolish this interaction. With a new aliquot of detection antibody, the protocol as shown in Table 2-18 was established and used for all other testing with GII.10 VLPs.

2.7 HBGA Attachment Inhibition ELISA – Combinatorial Inhibition

Combinatorial inhibition experiments (2.6) were carried out to evaluate how a combination of two inhibitors performs in comparison to the use of each inhibitor separately. This enabled the evaluation of potential additive, synergistic or adverse effects when two or more inhibitors were used in combination. The HBGA blocking ELISA for combinatorial inhibition has already been described [97]. In this study a natural compound, 2`FL, at a given concentration was added to serially diluted VLP-specific Nanobody.

In general, microtiter plates were coated with PGM, washed three times with PBS-T and blocked with skimmed milk as described in 2.6. Inhibitor A was serially diluted in PBS and added to Inhibitor B, which was diluted to a given constant concentration. If inhibitor B causes full inhibition on its own, no additional inhibition provided by inhibitor A can be detected. If the concentration of B is too low, then only the serial inhibition curve of inhibitor A will be detectable. Therefore, the concentration of inhibitor B had to be chosen and optimized carefully. It had to be in a close interval around the IC₅₀ value.

After mixing of the two different inhibitors, VLPs were added and incubated for 2 h at RT. Blocking was removed from the plates by washing and 100 µl of the VLP-inhibitor mixture was added to triplicate wells of the plates and incubated (according to the respective protocol depending on the VLPs used) to allow VLP attachment. Plates were further washed, detected, and developed according to their respective protocol as described in 2.6. Each combinatorial experiment required inclusion of wells in which each of the two inhibitors was added separately. This was needed to determine the inhibition each inhibitor caused on its own.

2.7.1 Analysis of Combinatorial Inhibition – Bliss Independence Evaluation

To evaluate the interaction between two different inhibitors, the Bliss model for independent inhibition was used [5, 94]. The model assumes a stochastic process in which each inhibitor causes an independent amount of inhibition. An independent stochastic inhibition process in this model would be inhibition through different mechanisms or inhibition at different target sites. Following this assumption, an assumed expected additive inhibition (E_{A+B}) caused by the combination of the two inhibitors is calculated based on the probability of the individual inhibition events (E_A and E_B), where $0 \leq E_A \leq 1$ and $0 \leq E_B \leq 1$:

$$E_{A+B} = E_A + E_B - (E_A \times E_B)$$

Comparison between the observed effect of a combination and the calculated expected effect (E_{A+B}) of the same combination allows evaluation of the nature of the interaction, which might be additive, synergistic, adverse, or antagonistic. If the two inhibitors act independently, the observed inhibition will be close to the calculated expected effect and the interaction of the two can be regarded as additive. If the observed effect of the combination is $\geq 20\%$ above the expected effect of the combination, then the combination is regarded as synergistic (criterion of relevance [94]). If the observed effect of the combination is $\leq 20\%$ below the expected additive effect, the combination of the two inhibitors is considered antagonistic. The effects between additive and antagonistic are regarded as adverse effects. Since both are negative results for a given combination, all effects below additivity will be regarded 'adverse' regardless of the 20 % criterion. To address the combinatory effect, several charts displaying both calculated and observed effect at varying concentrations were evaluated. As an example of this, the charts of combinations of serially diluted Nanobody and 2'FL at given concentrations are shown (Figure 3-56 - Figure 3-58, left sides). The library of GII.10 Nanobodies was subcloned and screened by Dr. Anna Koromyslova, therefore, Nanobodies

suitable for experiments were selected based on her results. For simplified visualization and overview, only the differences between the actual observed effect of a combination and the calculated expected additive effect are displayed as heat maps (Figure 3-56 - Figure 3-58, right sides).

2.8 Dynamic Light Scattering (DLS)

To evaluate particle swelling, disruption, or aggregation upon treatment with natural extracts or Nanobodies, the hydrodynamic sizes of VLPs were analyzed with dynamic light scattering (DLS) using a Zetasizer Nano S (Malvern). VLPs (1 mg/ml) and natural extracts/propolis (25 %) or Nanobodies (1 mg/ml) were mixed at equal volumes and incubated for 10, 60, and 120 min at RT (all Nanobodies were only incubated for 30 min). For examination in the Zetasizer, the samples were diluted in 1 ml of distilled water, filled into a cuvette and instantly measured. The measurements were performed at 25°C in three runs with 15 measurement cycles. Propolis samples were prepared differently due to the wax-precipitation upon dilution in water. Samples were pre-diluted from 100 % to 25 % 1 d before measurement and stored in the fridge. Before the experiment, the pre-diluted propolis samples were centrifuged at $16,873 \times g$ for 10 min to remove precipitated beeswax from the solution. The samples were then treated like other natural extract samples. To make sure measurements reflected VLP aggregation caused by propolis and not the respective solvent of propolis, all measurements were repeated with 25 % of the respective solvent.

2.9 Electron Microscopy (EM)

Negative stain electron microscopy was used to evaluate the morphology of the VLPs before and after treatment with natural extracts or Nanobodies as previously described [67]. Natural extracts at a concentration of 25 % or Nanobodies at a concentration of 1 mg/ml were mixed with equal volumes of VLPs (1 mg/ml) and incubated for 1 h at RT. The mixtures were diluted 1:40 with distilled water just before loading them on carbon coated EM grids. Each sample (6 μ l) was placed on a grid and incubated for 30 s. Excess liquid was removed and the grid washed 2 times with distilled water. After removing the water, one drop of 0.75 % uranyl acetate was placed on the grid for 9 s, then the excess uranyl acetate was removed, and the grid was left to dry. The grids were examined on a Zeiss 900 electron microscope at a magnification range between $7,000 \times$ and $50,000 \times$ at the Core Facility unit Electron Microscopy, DKFZ, Heidelberg.

2.10 X-ray Crystallography

2.10.1 Co-crystals with Natural Extracts

Co-crystals of GII.10 P domain and apple sweetener were obtained by mixing GII.10 P domain (2.5 mg/ml) with apple sweetener (25 %) followed by a 2 h incubation. The complex crystals were grown using the hanging-drop vapor diffusion method for 3 days at 18°C. The mother solution contained 0.2 M sodium nitrate, 0.1 M bis-tris propane (pH 7.5) and 20 % (w/v) PEG3350. Initially, this condition was tested for the other natural extracts as well. For date syrup and coconut blossom syrup, however, co-crystallization or soaking in the regular mother solution for GII.10 P domain, as mentioned above, was not sufficient and did not show any ligand in the P domain crystal. Therefore, GII.10 P domain (2.5 mg/ml) and compound (25 %) were mixed 1:1 and sent to the protein crystallization platform at the excellence cluster Cell Networks of the University of Heidelberg for crystal screening against a JCSG crystallization screen. The screening conditions were manually screened for crystal formation and the best conditions (large single crystals) were reproduced. Co-crystals of GII.10 P domain with date syrup or coconut blossom syrup, were grown in mother solution containing 0.2 M sodium fluoride and 20 % w/v PEG3350. Prior to flash freezing in liquid nitrogen, single crystals were transferred to a cryo-protectant containing the mother liquor with 30 % ethylene glycol.

Table 2-24: Mother solutions for GII.10 026 P domain and GII.10 026 P domain co-crystals

For crystallization of:	Concentration		Compounds
GII.10 P dom/ GII.10 P dom + apple sweetener (G5)	0,1	M	Bis-tris propane
	0,2	M	Sodium nitrate
	20	% (w/v)	PEG3350
GII.10 P dom + date /+ coconut blossom syrup	0,2	M	Sodium fluoride
	20	% (w/v)	PEG3350

2.10.2 Data Collection, Structure Solution, and Refinement

X-ray crystallography diffraction data were collected at the European Synchrotron Radiation Facility (ESRF, Grenoble, France) at beamlines ID23-1, ID29, and ID30B and processed with XDS [53]. The GII.10 P domains in complex with apple sweetener, date syrup and coconut blossom syrup were solved using molecular replacement with GII.10 P domain (3ONU) as a search model in PHASER [84]. The complex structures were refined and improved by multiple runs of manual model building in COOT [26] and refined with PHENIX [1].

2.11 Automated X-Ray Crystallography Screening

INEXT is a crystallographic screening approach and was performed by Jose A. Marquez and his team at ESRF, Grenoble, France. For a screening against a given panel of compounds, GII.10 026 P domain and crystallization solution (G5) were sent to the ESRF, and data were collected for evaluation after screening. In this case, the screening was performed against the clinical compound library of FDA approved drugs collected by the national institutes of health (NIH collection). The screening was performed as follows:

Automated crystallization experiments utilized the sitting drop vapor-diffusion method and were carried out in re-designed 96-well vapor-diffusion crystallization microplates (CrystalDirect plates). The crystallization conditions were provided by the users (18°C, G5). Set up was 100 nl sample and 100 nl crystallization solution on the inner surface of a thin, low X-ray-background film within the CrystalDirect plates (with 45 µl of crystallization solution in the reservoir). A laser beam was used to puncture the film and one drop of 50 nl ligand solution (500 mM in 100 % DMSO) was deposited on top of the laser generated aperture to allow direct contact with the crystallization drop. Thereby the ligands can be delivered to the crystals by diffusion. After incubation, the mix of crystallization solution and ligand solution was removed by aspiration through the same hole. Crystals were harvested and mounted by cutting the film around the crystal, gluing the piece of film to the top of an X-ray crystallography data-collection pin and frozen by transferring the pin to a cryocooling jet. Each ligand was soaked to at least two independent crystallization drops, and two or more crystals were harvested and analyzed by X-ray diffraction. Scaling was performed with the XDS software [53], initial phasing was done with molecular replacement method using MOLREP and a search model of the protein from the protein Data Base (PDB).

Ligands were detected by monitoring differences in the electron density map relative to the structure of the protein without ligand. This enables the direct visualization of the bound ligand in interaction with the protein. Therefore, this screen also provided valuable information on where and how the ligand interacts with the target protein. This information allows early decisions whether or not a ligand candidate is suitable and if structure directed optimization of the ligand can be applied.

3 Results

Contributions to chapters of the Results part are listed in the Appendix I.2, Contributions.

3.1 Screening for Synthetic Antivirals

3.1.1 Screening of the NIH Collection

Automated X-ray Crystallography Screening of the NIH Collection

Before the actual GII.10 026 P domain screening at the ESRF, the condition for crystallization had to be optimized. For crystallization in this screening the standard mother solution of our lab was used (Table 2-24, G5). The optimal protein concentration to obtain large single crystals varies slightly with each batch of P domain produced. To optimize the condition, two batches of purified P domain were tested at various concentrations (1.9, 2.0, 2.1 and 2.3 / 2.5 mg/ml) with different drop ratios (drop ratio: 1:1, 1:1.25, 1:1.5, 1:2). Formation of large single crystals was observable at concentrations of 1.9, 2.0 and 2.1 mg/ml. Higher concentrations of P-domain formed many but tiny crystals and were therefore not optimal for screening. Also, a drop ratio of 1:1.25 or 1:1.5 gave better (large, single, thick plates instead of thin platelets) crystals but results were not highly consistent. Therefore, a ratio of 1:1.5 and a concentration of 2.0 mg/ml was used in the final screening.

One batch of purified GII.10 026 P domain and 500 ml of G5 mother solution were sent to ESRF, in Grenoble, for the screening of the GII.10 026 P domain crystals with the NIH collection. The datasets were processed through Pipedream, a software for automated analysis of the data produced in the automated screening. Additionally, data sets were evaluated manually. A total of 478 datasets were acquired, Pipedream was not able to fully auto process 224 datasets (complete table see Appendix Table A I-1). A total of 252 datasets showed possible hits according to pipedream. Manual screening of these successfully auto-processed and evaluated hits left about 77 data sets where a ligand seemed to be present (Table 3-1).

Screening for Synthetic Antivirals

Table 3-1: Summary of results of automated X-ray crystallography of GII.10 P domain vs. NIH collection

Count	Results of X-ray crystallography screening and automated/manual post processing
478	Datasets acquired in total
254	Auto processed
252	Pipedream placed a ligand
77	Possible hits manually verified in auto processed data sets
22	Manually verified ligands
5	Ligands found in locations different from Pipedream analysis
94	Datasets manually processed and evaluated
1	Possible ligand identified after manual processing

A manual check of all successfully auto-processed data sets of Pipedream yielded some interesting observations. The side chain of ARG287A was flipped in almost all pipedream data sets compared to the model (3ONU). Close to TRY452, in almost all maps the density of DMSO could be found. Between GLU472A and B there were additional densities in many maps, most likely these were specially coordinated waters.

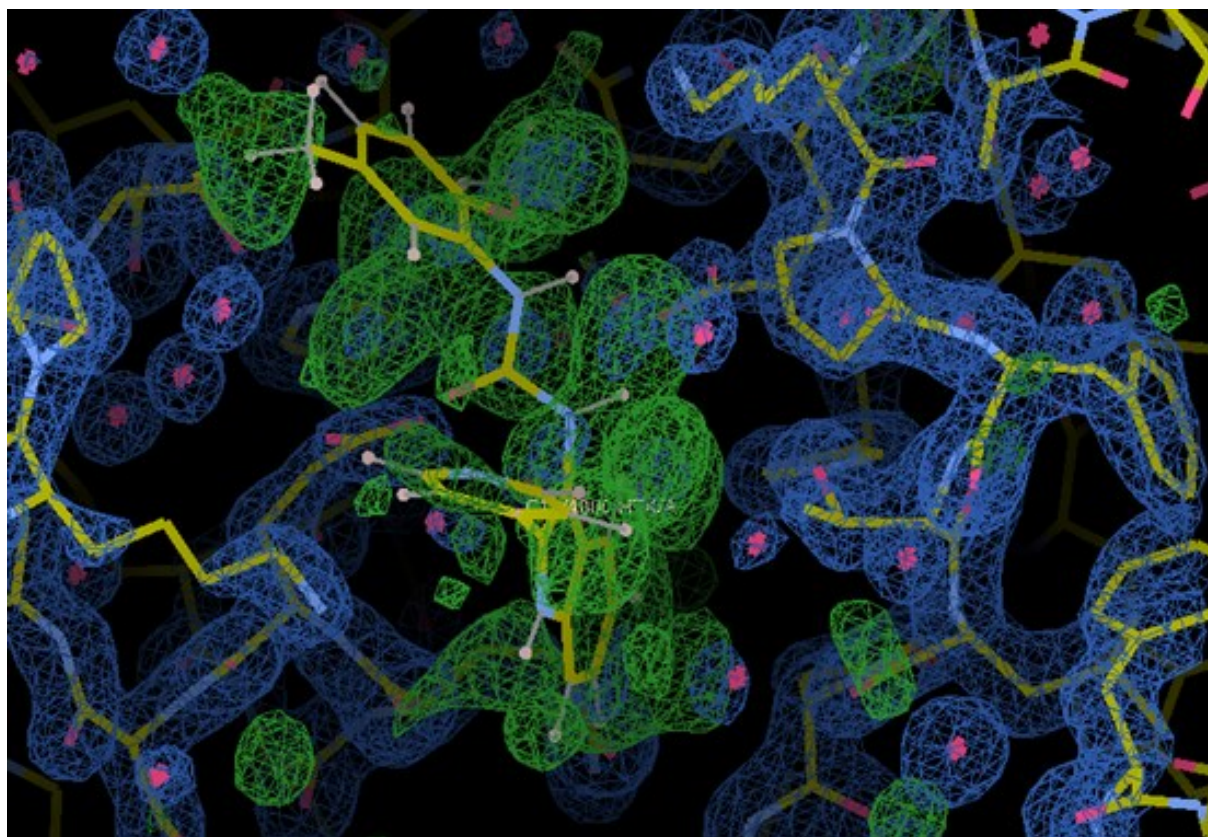


Figure 3-1: X-ray screening; density map of GII.10 P domain after automated processing
Density for apo-structure of P GII.10 026 P domain (blue), P domain model fitted into the density (yellow sticks), additional densities interpreted as water molecules (blue spheres with red cross), unexplained density presumably ligand (green). Example of 'blobby' density of a ligand after automated processing and placement by pipedream (dataset: PDMN-CD022192_B08-3_pipedream)

Upon evaluation of the automatically processed data sets, it became apparent that the Pipedream software fitted the expected ligand into any unexplained density within the structure of the P domain. Often the density of the ligand seemed to be an accumulation of single round spheres as expected for water molecules. Apparently, one large ligand was fitted into densities that clearly belonged to single water molecules within the crystal. Also, the density of many ligands looked strangely segmented as if it was composed of many single spheres (Figure 3-1). Pipedream identified ligands in a surprisingly high amount of processable datasets (ligand according to pipedream in 252 of 254 sets). Additionally, many of the ligands identified were found at places where the structure of empty P domain usually contains a lot of waters. In some cases, we were able to identify an unexplained density in the map large enough to hold a ligand but not where Pipedream had placed the model of the ligand. According to Pipedream, a surprisingly high number of datasets had a ligand bound within the structure of the crystal.

Therefore, we decided to manually process all datasets in which we could manually verify the presence of a ligand or where we could find an unexplained density greater than water (94 sets). To avoid potential mistakes made by pipedream, we restarted with the raw images and processed them manually with XDS, Phaser and Phenix.refine. After this step of re-processing, parts of a ligand could only be found in a single dataset (PDMN-CD022192_E09-3, see Figure 3-2 and appendix Table A I-2). However, the density of this ligand is incomplete as the density map shows only parts of a ring (Figure 3-2).

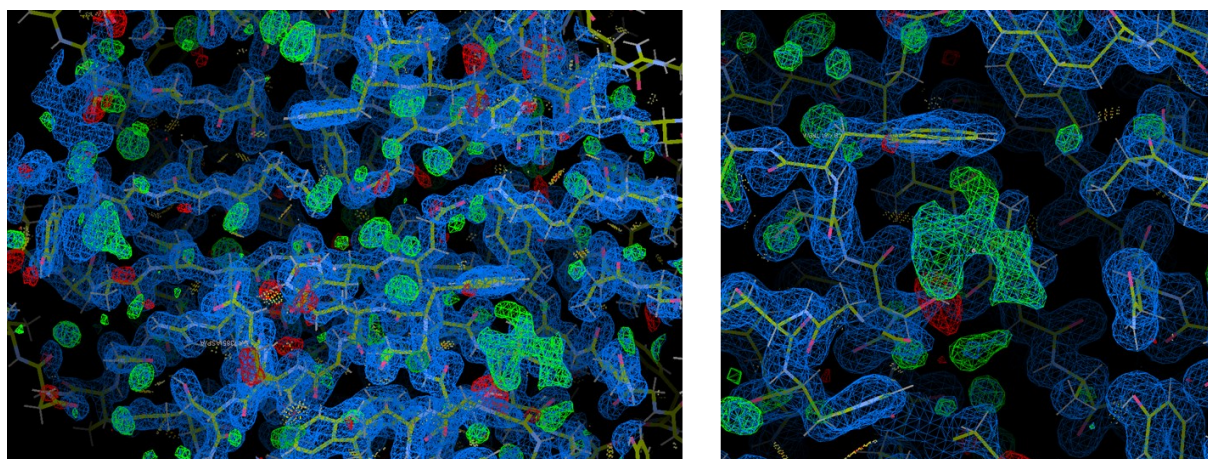


Figure 3-2: X-ray crystallography screening; density map of GII.10 P domain after manual processing
Density map (blue) with model of GII.10 026 P domain dimer (yellow sticks). This is the only dataset with unexplained density (green, probably ligand) that could be verified after manual processing and refining of the structures. Right: Overview of top of the P domain with both HBGA binding sites (one with unknown ligand one with DMSO). Left zoomed in on HBGA binding site with ligand (green) (Dataset: PDMN-CD022192_E09-3_pipedream)

ELISA Screening of the NIH Collection

The NIH collection was additionally screened in attachment inhibition ELISAs to identify potential inhibitors against human noroviruses. The collection was assessed using a surrogate inhibition ELISA in which inhibitors were tested against GII.10 026 VLPs (protocol Table 2-18). HBGAs for VLP-attachment were presented by coating plates with porcine gastric mucin (PGM). Instead of infectious virions, non-infectious VLPs were used. For the screening ten compounds were pooled. The numbering of the sample corresponds to the row and plate of samples that were combined for the test-mix. Samples were tested at a concentration of 18.75 μM (1.8 % of DMSO) in triplicate wells. For most cases, inhibition ranged between -15 and +24.2 %, which cannot be regarded as true inhibitory capacity. Especially for low inhibition, the standard deviation of readout was high because low inhibition values correspond to high signal (high amount of VLP detected with a strong signal caused by HRP). Most striking were several cases where the inhibition showed high negative values corresponding with more signal than was detected in the positive control with VLP alone, 06A (-38 % inhibition), 04E (-71 %), and 05H (-19 %). This ‘negative’ inhibition or enhancement of binding seemed concentration-dependent in a second assay where small dilution series were tested (serial dilution, 1:4; 10 - 0.01 μM ; data not shown). Due to the limited supply of NIH compounds, this screen could only be performed at a concentration of 18.75 μM and without repeats. A concentration of 18.75 μM might be sufficient to detect good inhibitors, but nonetheless it is a very low concentration to identify moderate inhibition.

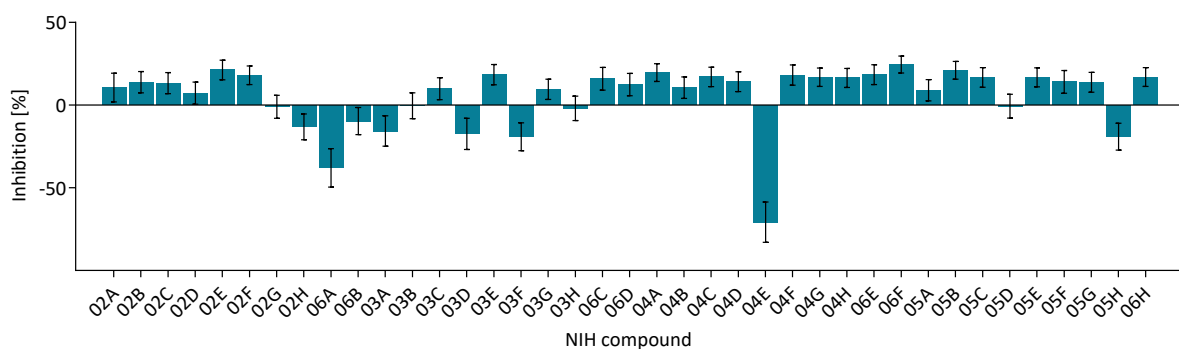


Figure 3-3: Inhibition ELISA of NIH collection at 18.75 μM HBGA blocking assay of pooled NIH collection with GII.10 VLPs. Ten different compounds were pooled and the inhibition of 18.75 μM of each compound was tested in a PGM attachment inhibition assay. All values are based on single measurements, no replicates. Single experiment; measurements were performed in triplicate wells, error bars shown.

Screening for Synthetic Antivirals

Our experiments indicated that DMSO had an influence on our assay. Therefore, the influence of DMSO on the assay/on VLP inhibition was evaluated. DMSO at different concentrations was added like a regular compound for testing. 2'FL was used as a positive control inhibitor. DMSO in high concentrations showed a strong influence on the assay. At a concentration of 5 % DMSO, enhanced binding (the detection) of VLPs was observed, resulting in a signal increase that corresponded to a 20 % increase in VLP binding/detection. This effect was concentration dependent and even occurred when an inhibitor was added. This resulted in a 'shielding' of the actual inhibition that the respective inhibitor (2'FL) is known to cause. Therefore, high DMSO concentrations might shield the actual inhibition caused by a compound by the enhancing effect.

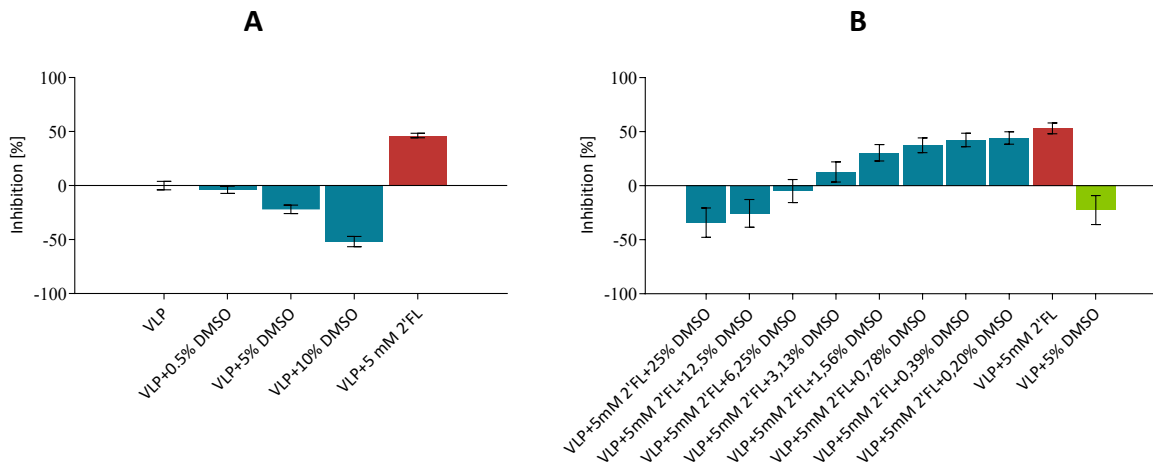


Figure 3-4: Inhibition ELISA evaluating effect of DMSO

A: 2 µg/ml of GII.10 026 VLPs were combined with either 0.5, 5, and 10 % of DMSO resulting in 'negative' inhibition (-4 %, -22 %, -52 %), or 5 mM 2'FL (red, 46 % inhibition). B: Serial dilution of DMSO (25 % -0.2 %) was added to 2 µg/ml of GII.10 026 VLP + 5 mM 2'FL; Inhibition of 2'FL without DMSO (red, 53 % inhibition), VLP + 5 % DMSO (green, -22 % inhibition). Single experiment; measurements were performed in triplicate wells, error bars shown.

Screening for Synthetic Antivirals

The DMSO concentration in the first NIH collection testing was 3.75 % (Figure 3-3). Therefore, a shielding effect of a possible (weak) inhibition cannot be excluded. The NIH collection was screened again at a lower concentration (5 μ M, protocol Table 2-18, Figure 3-5), to minimize the effect of DMSO (DMSO concentration 0.5 %). However, this caused also the testing of the actual compounds to be shifted to a lower concentration. Also, this time 0.5 % DMSO (same concentration as in compounds tested) was added to the controls. In this assay, a concentration of 2 μ g/ml of VLPs was used. Once more, no inhibitor could be identified. In general, the Inhibition varied between -12 % and 12 %. Exceptions were 02H (-25 %), 05H (-28%), and 04E (-76 %), which showed enhanced inhibition values as described earlier.

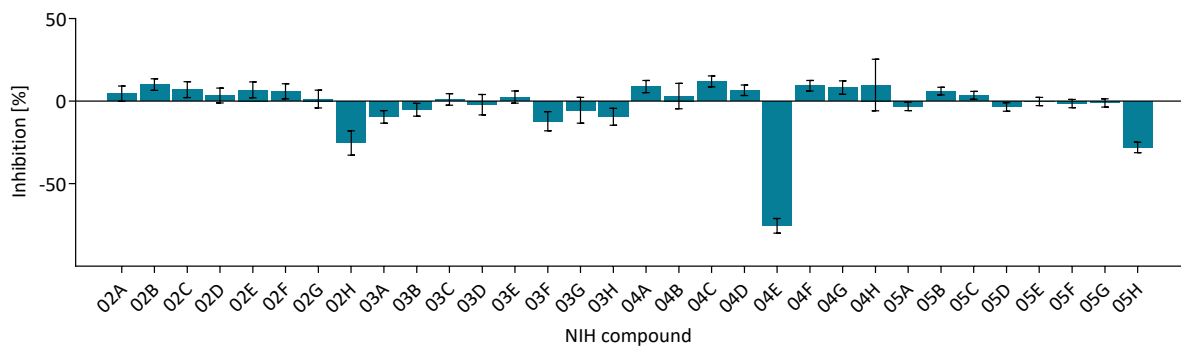


Figure 3-5: Inhibition ELISA of NIH collection compounds at 5 μ M

HBGA blocking assay of pooled NIH collection compounds with GII.10 VLPs. Ten different compounds were pooled and the inhibition of 5 μ M of each compound was tested in a PGM attachment inhibition assay. Inhibition varied between -12 % and +12 % except 02H (-25 %), 05H (-28 %), and 04E (-76 %). Single experiment; measurements were performed in triplicate wells, error bars shown.

3.1.2 Synthetic Multivalent Fucose Oligomers

In collaboration with Katharina Bücher (Heinrich-Heine-University Düsseldorf, Institute for Organic Chemistry and Macromolecular Chemistry, Düsseldorf, Germany), we analyzed the potential of synthetic compounds to act as norovirus inhibitors. Katharina Bücher designed and produced 15 synthetic fucose-oligomers. The idea for the multivalent-fucose oligomers was based on the previous finding that the P domain of noroviruses has multiple binding sites for fucose [68]. Although the functional role of these multiple binding sites remains unclear, the possibility of a multivalent mechanism seems plausible. Therefore, the multivalent-fucose oligomers were designed and synthesized to find a model and perhaps a good inhibitor suitable to bind to the multivalent fucose binding sites.

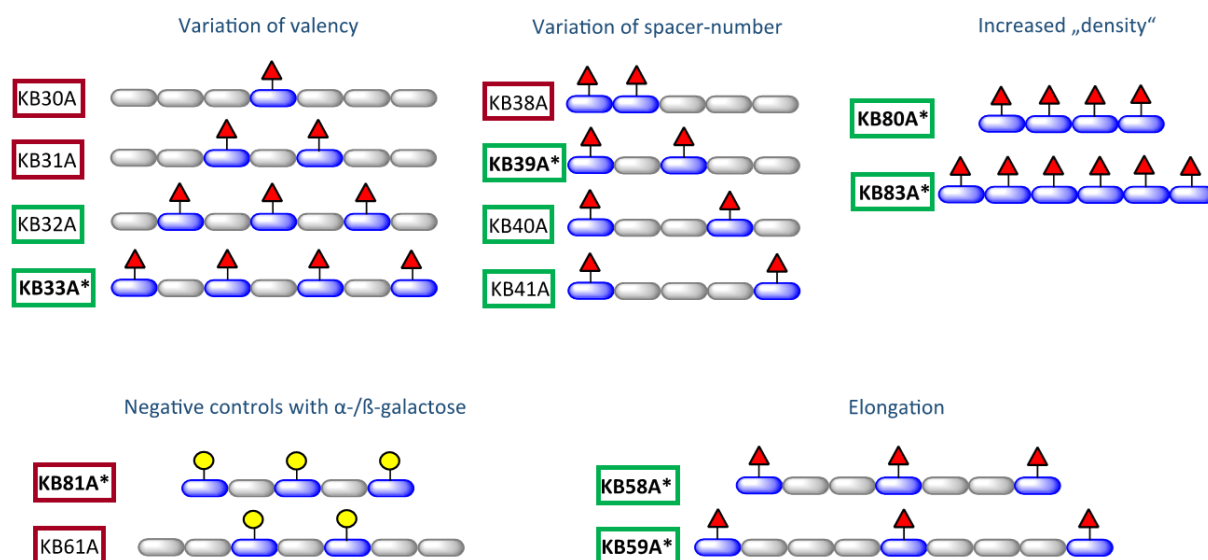


Figure 3-6: Schematic representation of HBGA-mimetic fucose oligomers. Units of oligomer backbone (blue/gray), fucose moieties (red triangles), galactose moieties (yellow circles). Red boxes: no ligand in GII.10 P domain crystal observed, green boxes: ligand or traces of ligand detected at the HBGA binding site. For chemical notation of fucose oligomers, please see appendix Figure A I.3-1 and Figure A I.3-2. Figure was provided by Katharina Bücher.

Synthetic Multivalent Fucose Oligomers X-ray Crystallography

GII.10 026 P domain crystals were grown in a 1:1 mixture of protein sample and mother solution (G5) at 18°C for 2 days. A single crystal was soaked briefly with multivalent fucose-oligomer in a cryoprotectant containing mother solution with 30 % of ethylene glycol and flash frozen in liquid nitrogen before data collection. X-ray crystallography diffraction data were collected at the ESRF, France, at beamlines ID23-1 and ID29. Structural data were analyzed using XDS, PHASER, COOT, and PHENIX as described (0). Data were validated using Molprobit [13]. Atomic coordinates and structure factors of 3 (KB 80A) in complex with GII.10 P domain were deposited in the Protein Data Bank (PDB) with accession code 6GY9.

Oligomers 3 (KB 80A), 7 (KB 41A), and 12 (KB 32A) (Figure 3-7 and Figure 3-8) showed binding of complete fucose rings at the HBGA-binding site of the P domain (Table 3-2). For oligomers 1 (KB 40A), 5 (KB 58A), 8 (KB 59 A), 10 (KB 39A), 13 (KB 33A), and 14 (KB 83A), fragments of the fucose ring were found at the HBGA-binding site of the P domain (Table 3-2, Figure 3-6). Fucose oligomer KB 80A even displayed parts of the linker structure attached to the fucose ring in the X-ray crystallography structure. KB 80A was therefore selected for further refinement and publication of the structure (Figure 3-9).

Table 3-2: Results of X-ray crystallography screening with fucose-oligomers

No	Original Name	Comment	Data Collection	Binding	Description
1	KB 40A		done	yes	fragment
2	KB 30A		done	-	-
3	KB 80A		done	yes	ring + tail
4	KB 88A		done	-	-
5	KB 58A		done	yes	fragment
6	KB 31A		-	-	-
7	KB 41A		done	yes	ring
8	KB 59A		done	yes	fragment
9	KB 38A		-	-	-
10	KB 39A		done	yes	fragment
11	KB 81A	neg. control	done	-	-
12	KB 32A		done	yes	ring
13	KB 33A		done	yes	fragment
14	KB 83A		done	yes	fragment
15	KB 61A	neg. control	done	-	-

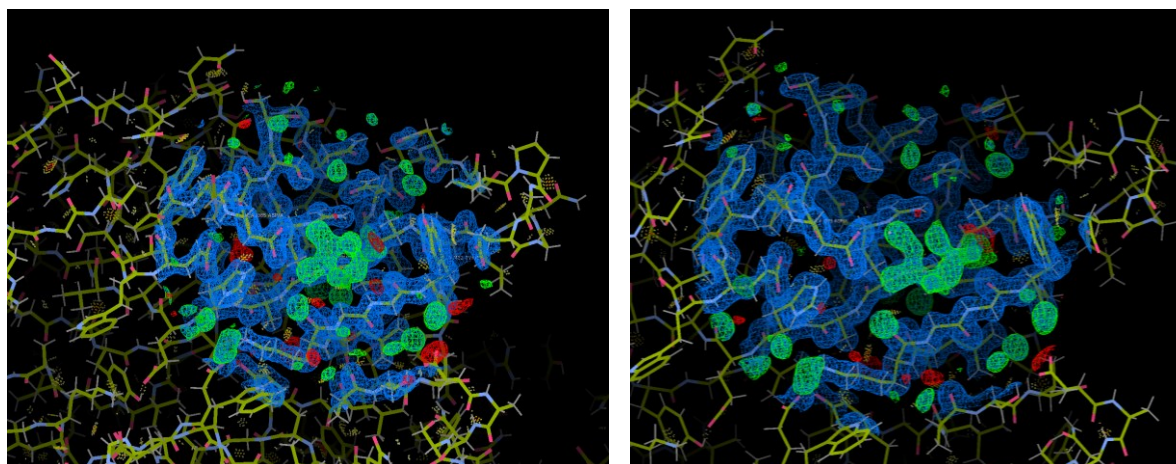


Figure 3-7: HBGA-binding site GII.10 P domain in complex with: left: KB 41A, right: KB 32A

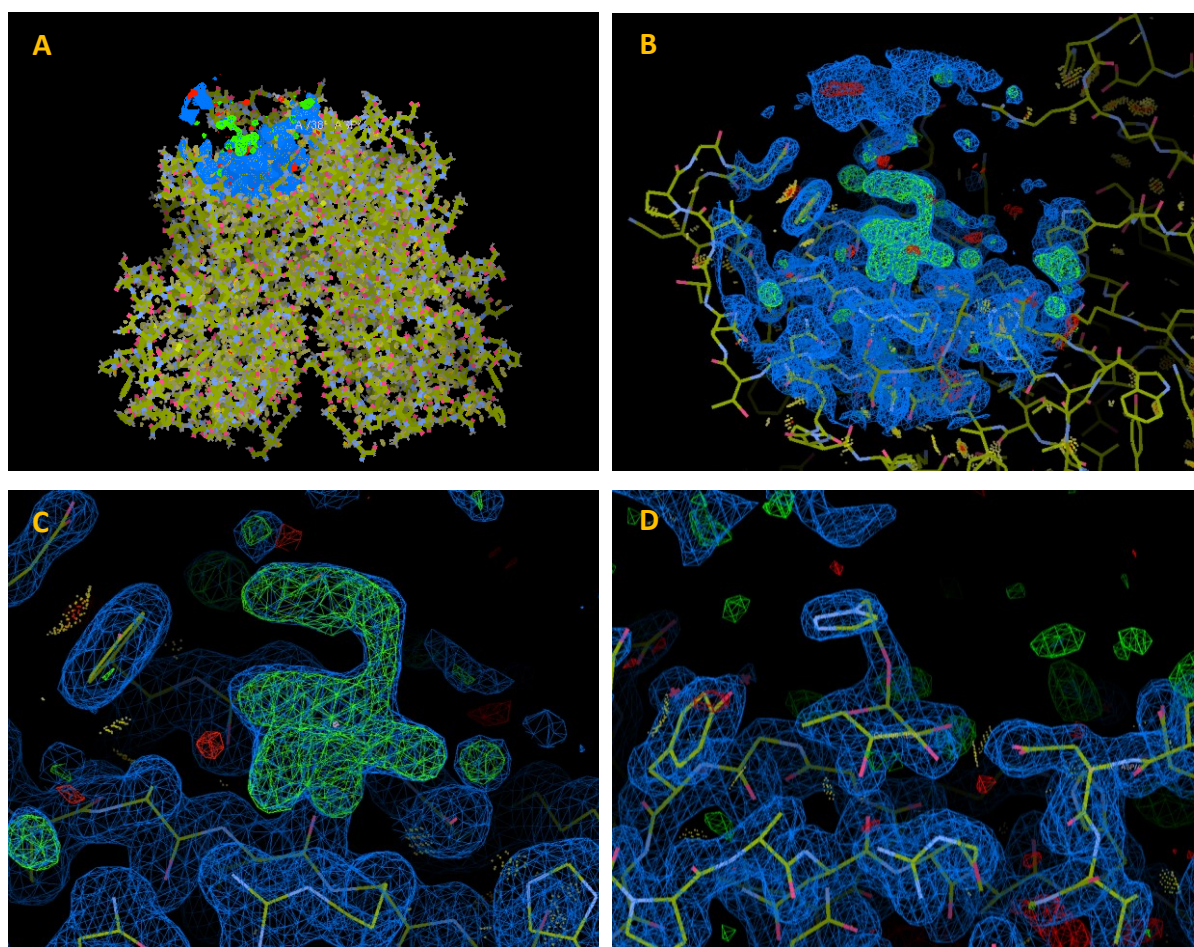


Figure 3-8: Density map of GII.10 026 P domain in complex with KB 80A
A: overview complete P domain dimer (yellow sticks, partially with blue density map) with KB 80A (green density map), B: medium close up of the region of the HBGA binding site with KB 80A, C: Close up of the ligand KB 80A, D: Close up of the bound ligand with model for compound placed in the density map.

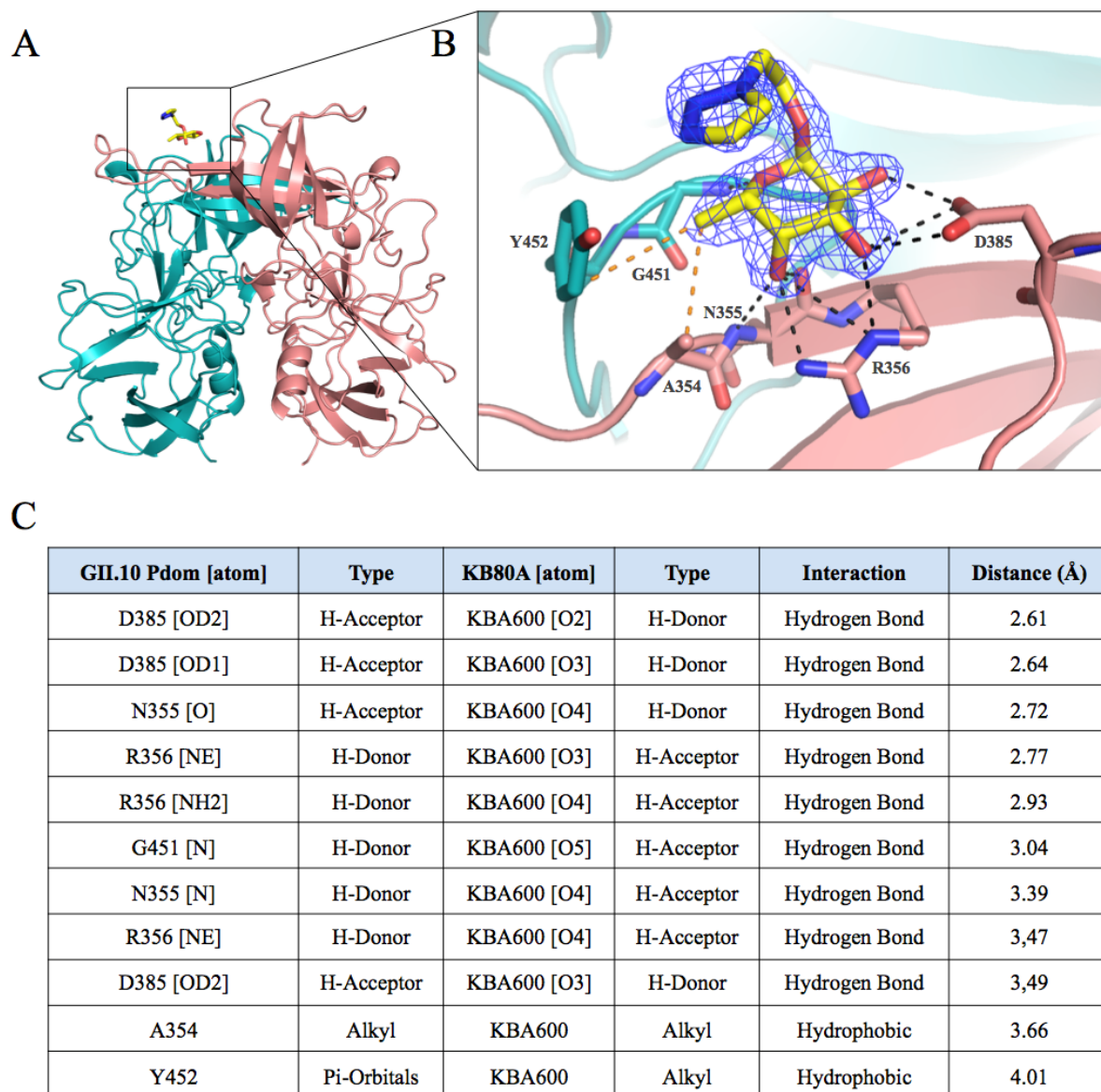


Figure 3-9: X-ray crystallography structure analysis of GII.10 P domain with multivalent-fucose oligomer KB 80A. A: The GII.10 P domain is represented by its two monomeric chains A (salmon) and B (teal). The fucose-oligomer is shown as yellow sticks. B: Close-up of the HBGA binding pocket of the GII.10 P domain with the bound fucose ring and part of the linker structure of the fucose-oligomer KB 80A. Dashed black lines: hydrogen bonds, dashed orange lines hydrophobic interactions. Figure taken from published results [10]

Synthetic Multivalent Fucose Oligomers Attachment Inhibition ELISA

The inhibition of the fucose oligomers was evaluated in a HBGA attachment inhibition ELISA (31,25 μM starting concentration) using GII.10 VLPs (protocol Table 2-18). Unfortunately, none of the compounds showed relevant inhibition whereas the standard deviations were high. The lowest observed inhibition value was with 4 (KB 88A, -20 %), whereas 11 (KB 81A), a negative control without fucose moieties, showed the highest inhibition of 18 %. The inhibition mean across all fucose-oligomers was 9 % (Figure 3-10).

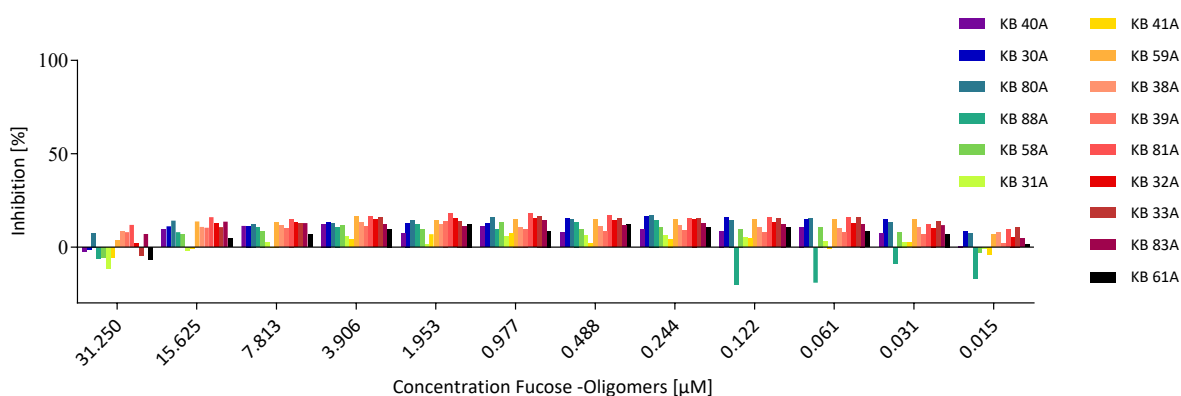


Figure 3-10: Inhibition ELISA of serial dilution of fucose-oligomers

All 15 multivalent fucose oligomers were tested for inhibitory capacities (GII.10 026 VLPs). No relevant inhibition was observed. Lowest inhibition: KB 88A (-20.46 %), highest inhibition KB 81 (18.19 % negative control, no fucose). Single experiment; measurements were performed in triplicate wells, error bars shown.

The fucose-oligomers, 11 (KB 80A), 8 (KB 59A), 7 (KB 41A), and 12 (KB 32A), which showed binding of complete fucose rings in X-ray crystallography analysis were re-tested in ELISA (2 repeats, protocol Table 2-19, but anti-rabbit 1:5000, 250 and 500 μM starting concentration), with 2'FL (250 mM) as a positive control and for comparison of inhibition. Once again, no inhibition was observed with the fucose-oligomers (Figure 3-11). However, the concentration at which the fucose-oligomers were tested was low (250 μM max vs. 250 mM max for 2'FL). Therefore, detection of inhibition was only possible if inhibition by the oligomers was at least one magnitude higher than with 2'FL.

Screening for Synthetic Antivirals

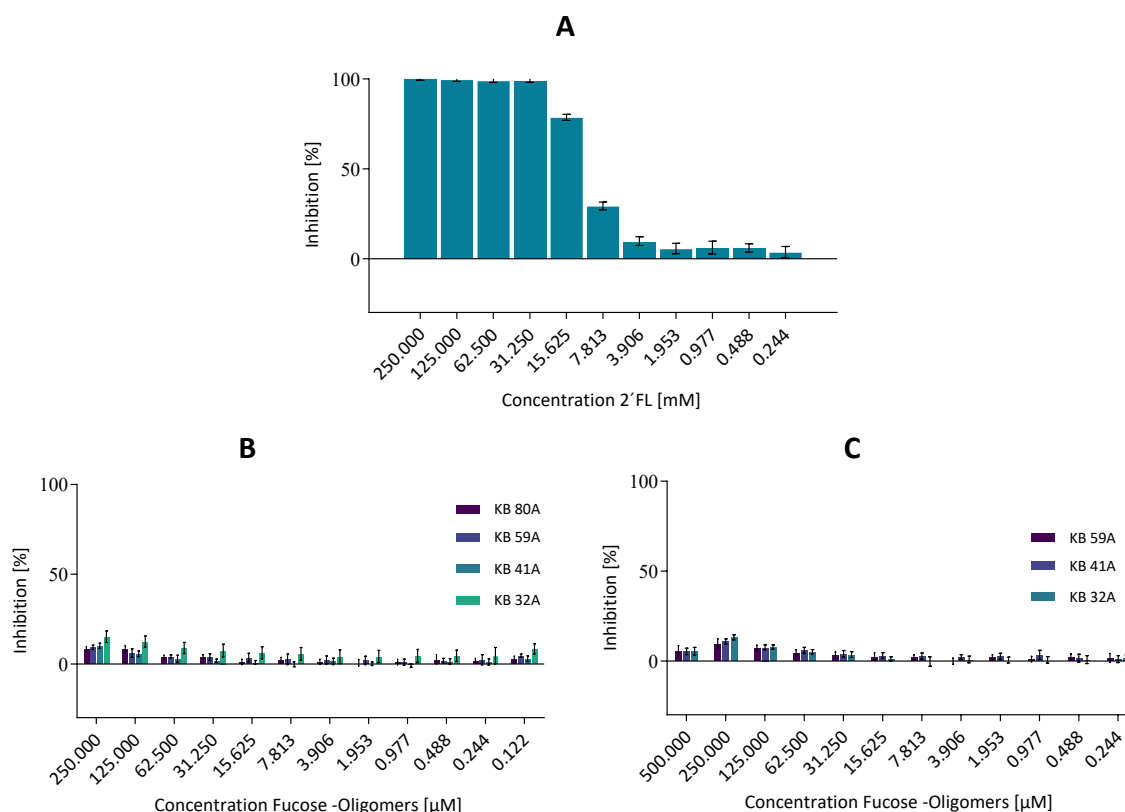


Figure 3-11: Re-testing inhibition ELISA of serial dilution of fucose-oligomers

A: Inhibition by serial dilution of 2'FL for comparison. B: Inhibition by selected multivalent fucose oligomers 11 (KB 80A), 8 (KB 59A), 7 (KB 41A), and 12 (KB 32A). C: Repeat of oligomers: 8 (KB 59A), 7 (KB 41A), and 12 (KB 32A). Similar to previous assays, no relevant inhibition could be detected at these higher concentrations. Single experiment; measurements were performed in triplicate wells, error bars shown

From the same group, a second set of heteromultivalent compounds (KB 96A, KB 97A, KB 98A, KB 14B, KB 15B) was received. In this set, the backbone of the oligomers remained the same, but instead of fucose moieties with different spacing, these oligomers comprised different moieties. Crystals soaked with the new heteromultivalent compounds were screened at the ERSF at beamlines ID30B and ID23.2. To evaluate the influence of fucose oligomers on VLP integrity, the hydrodynamic size of VLPs after treatment with fucose oligomers was measured in DLS. GII.10 VLPs (10 μl at 1 mg/ml) were mixed with 1 μl of the respective fucose oligomers and incubated for 10 min at RT. None of the fucose oligomers caused any changes to the VLP diameter when compared to untreated VLPs (data not shown).

3.1.3 GI.1-specific Nanobodies – Initial Screening

Chapters: 3.1.3 and 0 are product of collaborative work:

Expression and purification of the GI.1-specific Nanobodies was performed by Alexander Hempelmann, Celina Geiss, Juliane Graf, Michelle Haas, and Imme Roggenbach in the norovirus study group of Dr. Grant Hansman. Expression of GI VLPs was performed by Dr. Jessica Devant, Alessa Riengel and myself. For X-ray crystallography of Nano-7, I set up crystals, collected the data sets and started the analysis of the data files. The structures were refined and finalized by Dr. Turgay Kilic. The screening of the panel of GI.1 specific Nanobodies was performed by myself. Further ELISA experiments and their analysis were the result of the joint efforts between Dr. Jessica Devant, Alessa Ringel and myself. EM and DLS analyses were performed by Dr. Jessica Devant and myself. ITC analysis were performed by Dr. Anna Koromyslova and myself. The manuscript was written by Dr. Grant Hansman, Dr. Jessica Devant, Alessa Ringel, Dr. Anna Koromyslova, and myself. The manuscript was published in Journal of Virology:

Structural Basis of Nanobodies Targeting the Prototype Norovirus

Kerstin Ruoff, Turgay Kilic, Jessica Devant, Anna Koromyslova, Alessa Ringel, Alexander Hempelmann, Celina Geiss, Juliane Graf, Michelle Haas, Imme Roggenbach, Grant Hansman

Journal of Virology Mar 2019, 93 (6) e02005-18; DOI: 10.1128/JVI.02005-18

Several figures in chapter 0 were adapted from this publication and are labeled accordingly.

Production of GI VLPs

Different GI genotype VLPs were expressed and purified (2.4) to assess the cross-reactivity of GI.1-specific Nanobodies. The panel consisted of GI.1 Norwalk, GI.2 Southampton, GI.2 Fusabashi258, GI.3 Kashiwa 645, GI.4 Chiba, GI.8 WUG1, and GI.11 #8 VLPs. All purified VLPs were checked in negative stain EM (as described in 2.9), and consisted mostly of a mixture of small and native-sized VLPs (e.g. GI.1 VLPs Figure 3-12) with the typical norovirus morphology. However, the proportion of native/small-sized differed between the different types.

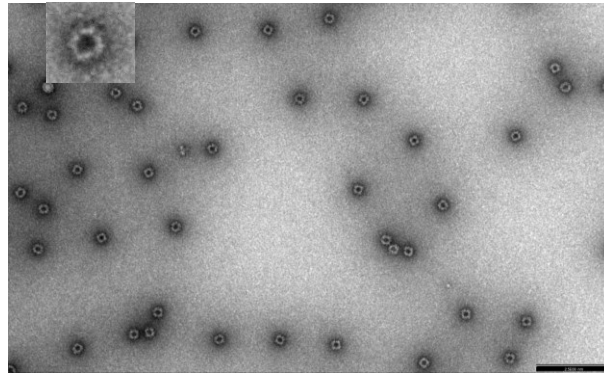


Figure 3-12: GI.1 Norwalk VLPs used in this chapter
 As an example, the VLPs of GI.1 Norwalk are displayed. Negative stain EM image, scale bar 250 nm. Close up of a single particle in upper left corner. Mainly native sized VLPs.

Binding of GI.1-specific Nanobodies

The panel of GI.1-specific Nanobodies was screened for their ability to bind to different GI VLPs using binding ELISAs (protocol see Table 2-16). Testing was performed with 100 µg/ml of Nanobody in triplicate wells; plates were coated with 5 µg/ml of the respective VLPs. This was a pre-test to identify candidates, binding to their target (GI.1 Norwalk) and exhibiting cross-reactivity. The experiment was performed once.

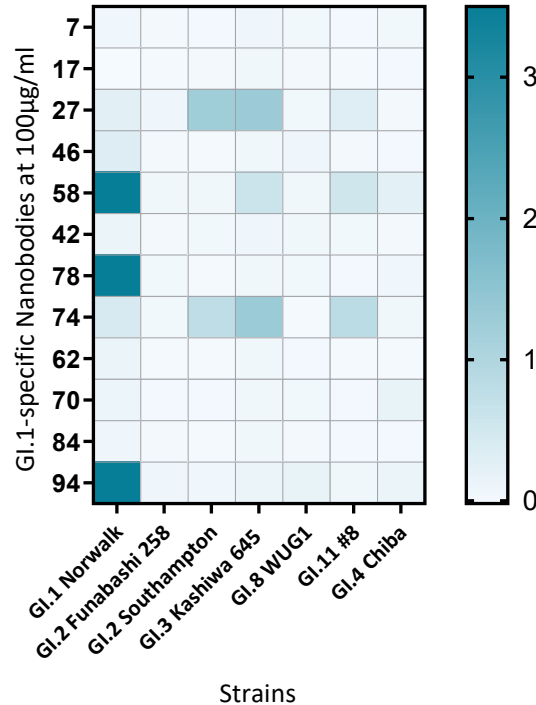


Figure 3-13: Cross-reactivity of GI.1-specific Nanobodies, heat-map
 Binding of GI.1-specific Nanobodies to VLPs of different genotypes were tested in an ELISA. OD₄₉₀ detectable for each VLP-Nanobody pair is displayed in a heat map. Only a single experiment with triplicate wells was performed. For additional information on norovirus strains see Table 2-14.

Of all 12 GI.1 Nanobodies tested, Nano-58, Nano-78, and Nano-94 showed the best binding to GI.1 Norwalk VLPs (Figure 3-13). Nano-58 showed limited cross-reactivity with GI.11 #8 and GI.3 Kashiwa 645 VLPs but not with GI.2 Southampton, GI.8 WUG1, GI.4 Chiba, or GI.2 Funabashi 258 (Table 2-14). The other two interesting candidates (Nano-78 and Nano-94) showed no cross-reactivity with the given strains. However, Nano-74, which showed limited binding to GI.1 VLPs, displayed comparatively high binding to GI.11 #8, GI.2 Southampton, and GI.3 Kashiwa 645. Similarly, Nano-27 showed a higher signal with GI.2 Southampton and GI.3 Kashiwa 645 when compared to GI.1 VLPs. None of the Nanobodies showed binding to GI.8 WUG1, GI.4 Chiba, and GI.2 Funabashi 258 VLPs.

GI.1-specific Nanobodies identified during initial experiments (Figure 3-13) were tested for their ability to bind to GI.1 and GI.11 #8 VLPs in a serial dilution to determine their binding limits (protocol Table 2-16, but 10 µg/ml VLP). The best binders in the novel GI.1 binding experiment were Nano-94, Nano-78, and Nano-58 (maximal OD₄₉₀ detection levels: 3.12, 3.12, and 3.14 respectively, Figure 3-14). Nano-74 exhibited the best binding to GI.11 #8 VLPs, followed by Nano-27 and Nano-58 (maximal OD₄₉₀ detection levels: 0.93, 0.65, and 0.54 respectively Figure 3-15). However, the maximum OD₄₉₀ observed when Nanobodies bound to GI.11 #8 VLPs was about 1, whereas binding to GI.1 Norwalk VLPs was about three times higher.

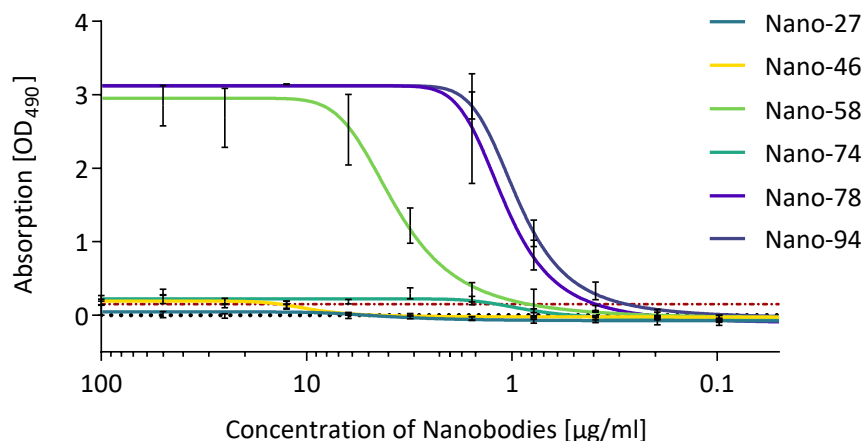


Figure 3-14: Binding ELISA of serially diluted GI.1-specific Nanobodies to GI.1 VLPs. The binding limits of six GI.1-specific Nanobodies (numbers are given in the chart legend) against GI.1 Norwalk VLPs were tested. Best binding was observed for Nano-94 and Nano-78, followed by Nano-58 (maximal OD₄₉₀ detection levels: 3.12, 3.12, and 3.14 respectively). Single experiment; measurements were performed in triplicate wells, error bars shown

Screening for Synthetic Antivirals

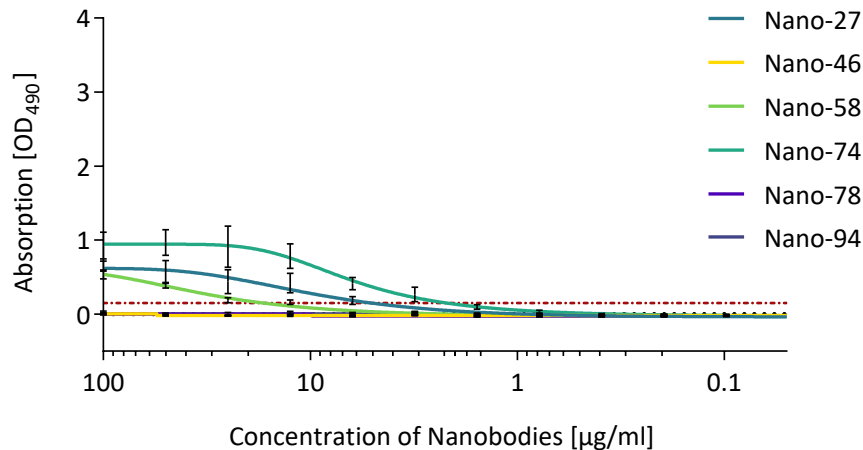


Figure 3-15: Binding ELISA of Gl.1-specific Nanobodies (serially diluted) to #8 VLPs
The binding limits of six Gl.1-specific Nanobodies (numbers are given in the chart legend) against Gl.11 #8 VLPs were tested. Best binding was observed for Nano-74 and Nano-27 followed by Nano-58 (maximal OD₄₉₀ detection levels: 0.93, 0.65, and 0.54 respectively). Single experiment; measurements were performed in triplicate wells, error bars shown.

A binding ELISA of the entire panel of Gl.1 specific Nanobodies was performed with Gl.1 P domain (10 µg/ml) or Gl.1 VLPs (10 µg/ml), to compare binding to VLPs and to P domain. With VLPs (10 µg/ml) all tested Nanobodies showed an OD₄₉₀ at or above the detection limit of the plate reader (OD₄₉₀ 3.50). Since this did not allow distinction between the binding properties of the Nanobodies, the assay was repeated with a lower concentration of VLPs (5 µg/ml). Binding of Gl.1-specific Nanobodies to VLPs or to P domain showed great similarities, where Nanobodies that detected VLPs at a high OD₄₉₀ level also showed high signals on P domain (Figure 3-16). The highest ratio in detectable OD₄₉₀ levels (VLP (5 µg/ml)/P domain (10 µg/ml)) was observed with Nano-84 (4.8), followed by Nano-46 (2.5). The lowest ratio was observed with Nano-17 (0.38) the other nanobodies ranged between 1.3 and 0.7.

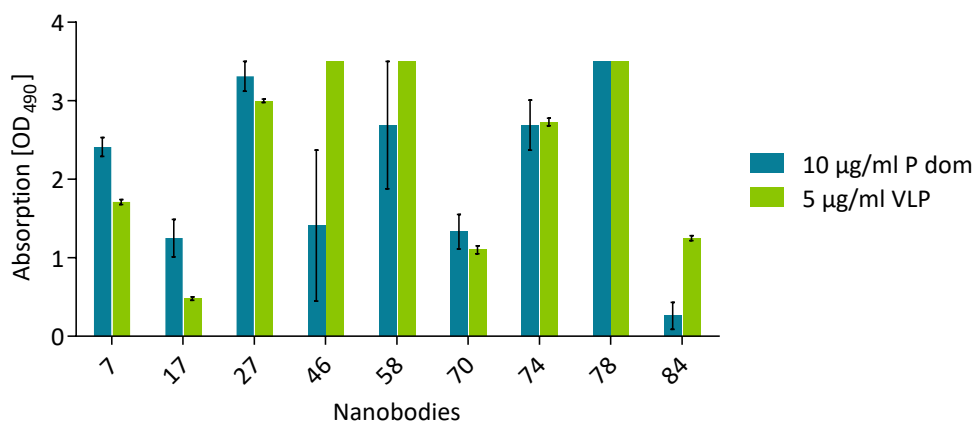


Figure 3-16: Binding of Gl.1-specific Nanobodies to Gl.1 P domain and VLPs
All tested Nanobodies exhibited binding to Gl.1 VLPs and P domain. Best binders were Nano-27, Nano-58 and Nano-78. Single experiment; measurements were performed in triplicate wells, error bars shown. For signals reaching the detection limit of the assay (OD₄₉₀ 3.5) no error can be displayed (three equal values).

For direct comparison, a binding ELISA was performed with three different concentrations of VLP to evaluate the effect of VLP concentrations on Nanobody binding and detection (OD_{490}). Interestingly, the decrease in signal levels between 10, 5 and 1 $\mu\text{g}/\text{ml}$ of GI.1 VLPs was not the same for all Nanobodies (Figure 3-17). From 5 $\mu\text{g}/\text{ml}$ to 1 $\mu\text{g}/\text{ml}$, some showed stronger proportional reduction in signal [24.56 (Nano-84), 4.42 (Nano-17)] compared to other Nanobodies [2.97 (Nano-7), 3.09 (Nano-27), 3.26 (Nano-42), 3.20 (Nano-70), and 2.93 (Nano-74), Figure 3-17]. For two Nanobodies (Nano-58 and Nano-78), the signal never decreased below the upper detection limit, suggesting they have a higher binding capacity.

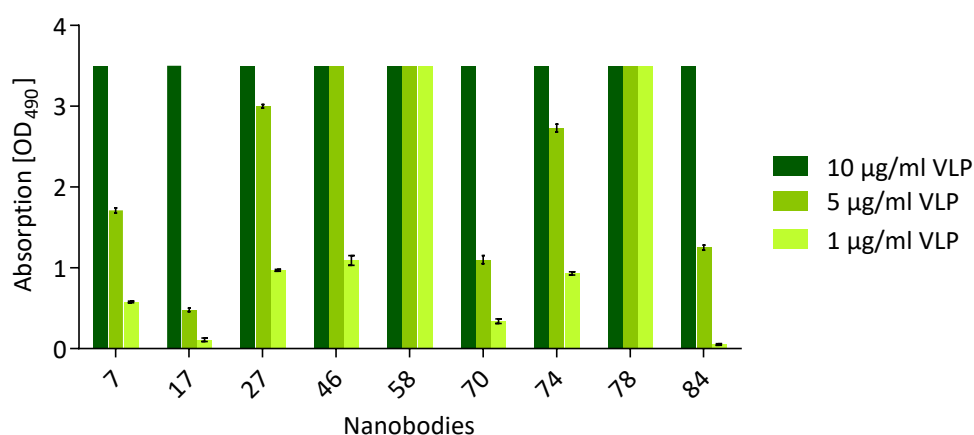


Figure 3-17: Binding of GI.1-specific Nanobodies to VLP-coated plates at different concentrations of GI.1 VLPs. Proportional signal reduction between 5 $\mu\text{g}/\text{ml}$ and 1 $\mu\text{g}/\text{ml}$ varied; strong decrease observed (Nano-84 reduction by: 24.56, Nano-17 reduction by: 4.42) and lower decrease observed (Nano-7 reduction by: 2.97, Nano-27 reduction by: 3.09, Nano-42 reduction by: 3.26, Nano-70 reduction by: 3.20, Nano-74 reduction by: 2.93). Proportional signal reduction is not given for values against the upper signal limit. No signal reduction was observed for Nano-58 and Nano-78. Single experiment; measurements were performed in triplicate wells, error bars shown. For signals reaching the detection limit of the assay (OD_{490} 3.5) no error can be displayed (three equal values).

Inhibition of GI.1-specific Nanobodies

Interesting candidates identified in the ELISA binding assays described above (Nanobodies 7, 27, 46, 58, 74, 78, 94) were tested for their ability to inhibit the attachment of various GI strains in an HBGA attachment inhibition ELISA (Table 2-21). GI.11 #8 VLPs were excluded from this experiment due to its inability to bind to PGM. GI.8 WUG1 was also excluded because the VLPs did not express well and therefore not enough VLPs were available to include this genotype in the inhibition assay. GI.2 Funabashi 258, GI.2 Southampton and GI.4 Chiba were detected with mAb 19-4 (1:100, mouse anti-GI.1, in house production by DKFZ). An HRP-conjugated polyclonal anti-mouse (1:1000) was used as a secondary antibody. Inhibition of GI.2 Funabashi 258, GI.2 Southampton and GI.4 Chiba by all of the tested Nanobodies was

very low (highest inhibition was 21 % by Nano-46 against GI.4 Chiba). Five of the Nanobodies (7, 27, 74, 78, and 94) showed good inhibition values (maximal inhibition observed 98 %, 85 %, 55 %, 74 %, 95 %) with GI.1 Norwalk. In a later setup all Nanobodies regardless of binding capacities were tested for their inhibiting potential.

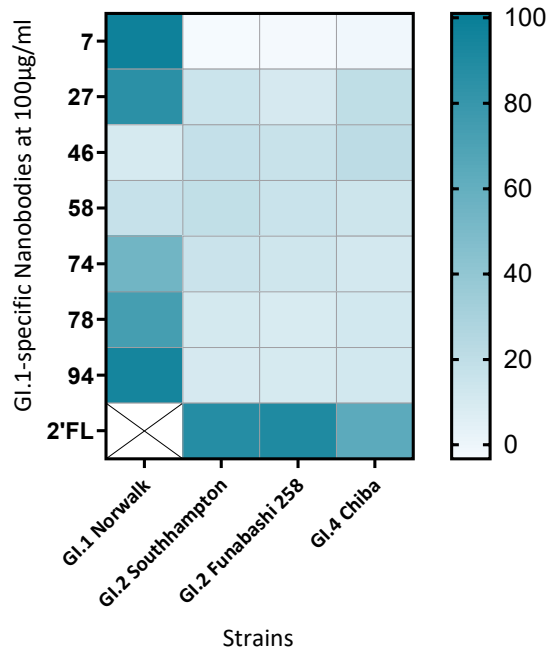


Figure 3-18: Heat-map of cross-reactivity inhibition ELISA with GI.1-specific Nanobodies against GI VLPs
Inhibition of different GI genotypes by GI.1-specific Nanobodies was tested. Results were based on a single experiment with triplicate wells. Highest inhibition of GI.1 Norwalk was observed for Nano-7 (98 %), Nano-94 (95 %), Nano-27 (85 %), Nano-78 (74%), and Nano-74 (55 %). Candidates for cross-reactivity testing were primarily selected based on their performance in binding assays. Inhibition by the highly cross-reactive HMO 2'FL was added as an inhibition control.

For Nanobodies 7, 27, 46, 58, 74, 78, and 94, cross-reactivity in inhibition ELISAs was tested. None of the tested Nanobodies showed cross-reactive inhibition (Figure 3-18). The HMO 2'FL was included in this assay to test its cross-reactivity among GI strains. 2'FL showed inhibition with GI.2 Southampton (88 %), GI.2 Funabashi 258 (90 %), and GI.4 Chiba (64 %). In spite of its high inhibition with GI.1 VLPs (98 %), Nano-7 showed no inhibition with other GI strains.

3.1.4 GI.1-specific Nanobodies – Published Results

Based on X-ray crystallography analysis, binding and inhibition performance, Nano-7, Nano-62 and Nano-94 were selected as the most interesting Nanobody-candidates for further experiments and results were published [97].

Structure Analysis of GI.1-specific Nano-7, Nano-62, Nano-94 with GI.1 P domain

X-ray crystallography was used to determine the binding sites of the three Nanobodies. Structures of P domain in complex with Nano-62 and Nano-94 were analyzed by Dr. Turgay Kilic. The structure of GI.1 P domain comprised residues 226 to 278 and 406 to 520. The structure of the P domain in complex with the Nanobodies was in general similar to the apo structure. The Nanobodies were well resolved and showed the typical immunoglobulin fold (Figure 3-19). Nano-7 and Nano-62 bound at similar positions on the side of the P domain (Figure 3-19 A and B), whereas Nano-94 bound to the top of the P domain (Figure 3-19 C).

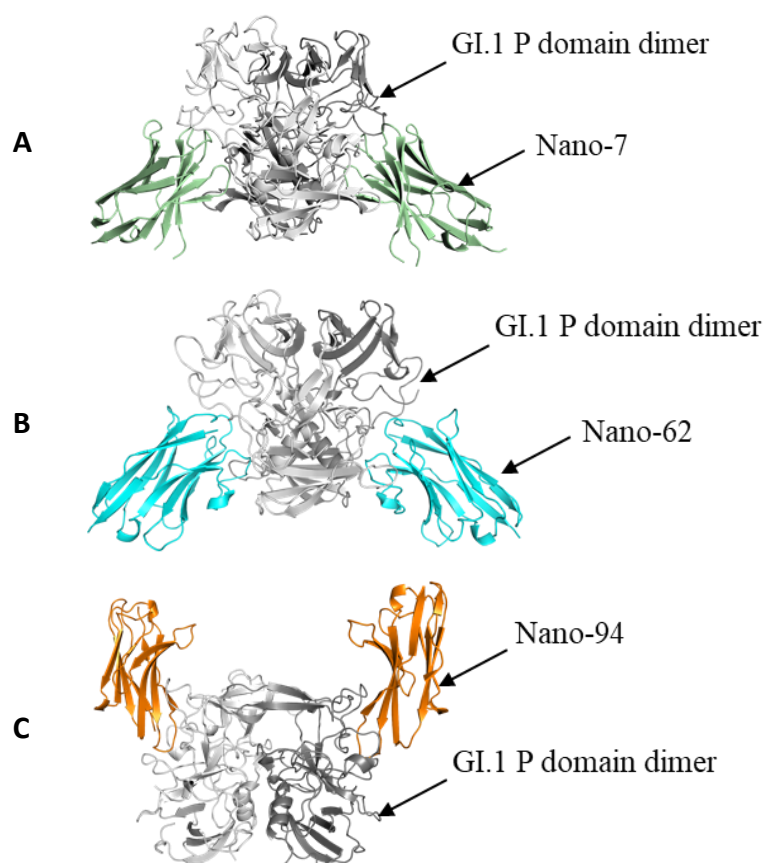


Figure 3-19: X-ray crystal structures of GI.1 P domain in complex with Nano-7, -62, and -94.

For all P domain-Nanobody complexes the asymmetric unit contained one P domain dimer (gray) and two Nanobody molecules (Nano-7: green (A), Nano-62: cyan (B), Nano-94: orange (C)). Nano-7 and Nano-62 bound to the side of the P domain. In contrast Nano-94 bound to the top of the P domain). For Nano-7 in complex with P domain only finalization was done by Dr. Turgay Kilic, Structures with Nano-62 and Nano-94 were entirely processed by Dr. Turgay Kilic. Figures were taken from published results [97].

The structure of the Gl.1 P domain-Nano-7 complex was solved at a resolution of 1.58 Å. Nano-7 bound to a groove on the side of the P domain (Figure 3-19 A). It bound to P1 and P2 subdomains and to the chains of both monomers. In total, the interaction between Nano-7 and P domain comprised of 21 P domain residues and 33 interactions (Figure 3-20). So far, this is the most interactions observed between a P domain and a Nanobody. Of the 21 interacting residues, 11 were located on the P1 subdomain, whereas 9 were from the P2 subdomain. The orientation and location of the bound Nanobody suggested that the side of the Nanobody, opposite of the complementary-determining region (CDR), might clash or be in contact with the S domain and/or neighboring P domains. Therefore, superposition of the Nano-7-P domain complex with the structure of a Gl.1 VLP was performed (by Dr. Jessica Devant, [97]) and revealed clashes of Nano-7 with S domain as well as neighboring P domains. The ability of Nano-7 to bind to VLPs, as verified in ELISA, implied the neighboring P domains and/or S domain would need to move to allow the attachment of Nano-7 to the P domains of the particle.

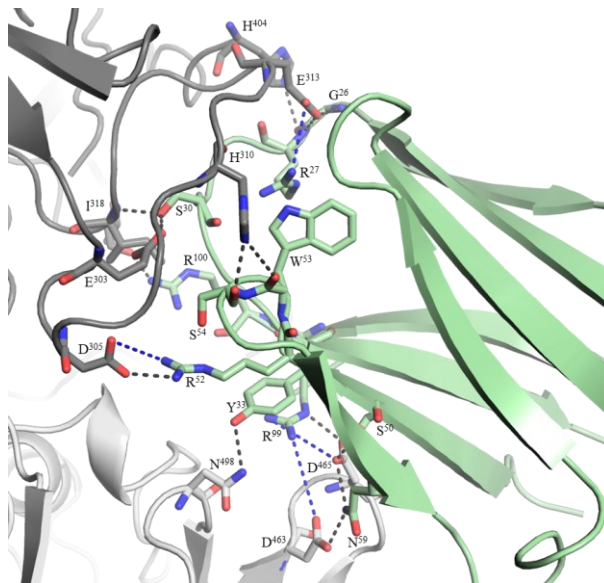


Figure 3-20: Close-up of the P domain dimer in complex with Nano-7.

The interaction between Nano-7 and P domain was formed by hydrogen bond interactions and involved sidechain and mainchain interactions from both monomers. Direct hydrogen bonds were formed with P domain chain A-Nano-7, H310-S54, E313-R27, D305-R52, I318-S30, D305-R52, E303-S30, T280-R100, Q449-D105, H404-G26, Q449-T103, E313-G26, and H310-W53; and chain B, D465-S50, D463-N59, N498-Y33, D465-R99, and D465-N59. Electrostatic interactions formed between P domain chain A-Nano-7, F312-R27, D305-R52, R275-D105, E313-R27, R275-D105; and chain B, D463-R99 and D465-R99. Hydrophobic interactions involved P domain chain A-Nano-7, V282-L101, L276-R100, A446-L101, L276-L101, and F312-R27; and chain B, P237-A102, P464-A102, V500-A102, and P237-L101. Figure was taken from published results [97].

The X-ray crystallography structure of the GI.1 P domain Nano-62 complex was solved at a resolution of 2.09 Å (Figure 3-21). Similar to Nano-7, Nano-62 also bound to the side of the P domain, in a groove between the two monomers. Compared to the interaction between Nano-7 and the P domain, however, fewer (10) hydrogen bonds were observed for Nano-62. Also, most interactions were located between the P1 subdomain and the Nanobody. Ten residues interacting with the Nanobody were located on the P1 subdomain whereas only 3 interacting residues of the P2 subdomain were involved. Like Nano-7, Nano-62 was bound and oriented in a way that suggested Nanobody clashing with the S domain and neighboring P domains. This was verified in a superposition of the complex on a GI.1 VLP structure [97].

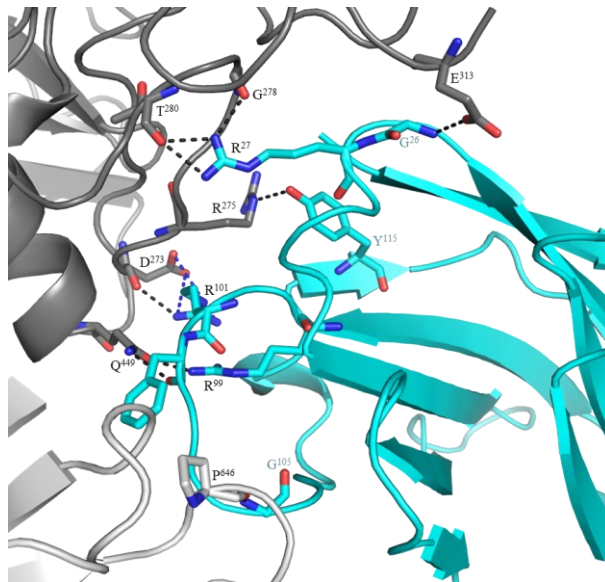


Figure 3-21: Close-up of the P domain dimer in complex with Nano-62.

The interaction between Nano-62 and P domain was formed by hydrogen bond interactions and involved sidechain and mainchain interactions from both monomers. Direct hydrogen bonds were formed with P domain chain A-Nano-62, P464-G105 and D465-R52; and chain B, Q449-R99, E313-G26, G278-R27, T280-R27, R275-Y115, T280-R27, D273-R101, and Q449-F102. Electrostatic interactions formed between P domain chain A-Nano-62, D465-R52; and chain B, D273-R101. Hydrophobic interactions involved P domain chain A-Nano-62, P237-F102 V500-F102, V462-V104, P464-F102, and P464-V104; and chain B, H404-S25 and R275-R101. Figure taken from published results [97].

The structure of the GI.1 P domain Nano-94 complex was solved to 2.31 Å resolution (Figure 3-22). In contrast to the other two Nanobodies, Nano-94 was found to bind to the top of the P domain and only interacted with one P domain monomer. All but one residue involved in binding were located on the P2 subdomain. The binding site of Nano-94 was close to the HBGA-binding site but both did not share any common residues.

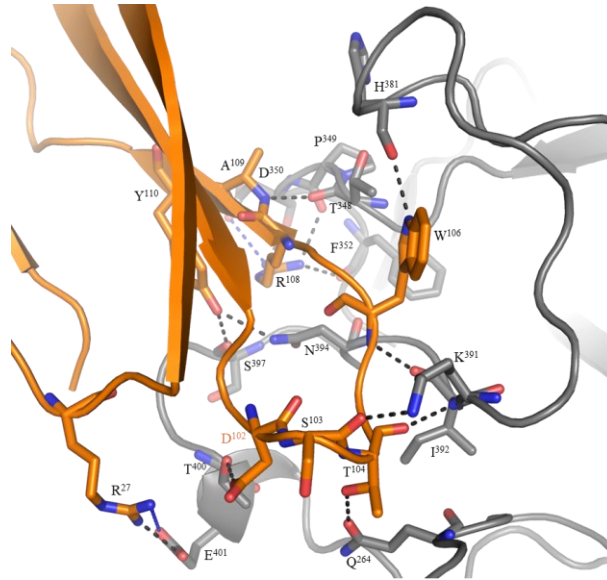


Figure 3-22: Close-up of the P domain dimer in complex with Nano-94.

The interaction between Nano-7 and P domain was formed by hydrogen bond interactions and involved sidechain and mainchain interactions from both monomers. Direct hydrogen bonds were formed with P domain chain A-Nano-94, Q264- T104, K391-S103, S397-Y110, I392-W106, T348-A109, T400-D102, F352-R108, I392-T104, E401-R27, N394-Y110, H381-T106, P349-R108, and D350-R108. Electrostatic interactions formed between P domain chain A-Nano-94, D350-R108 and E401-R27. Hydrophobic interactions involved P domain chain A-Nano-94, P382-F107, H381-Y98, P379-W106, and I392-I105. Figure was taken from published results [97].

Binding ELISAs of Nano-7, Nano-62, and Nano-94 to GI.1 VLPs and P Domain

Binding properties of the three Nanobodies selected for further investigation were analyzed in binding ELISAs on GI.1 P domain and GI.1 VLPs (protocols Table 2-17, Table 2-16). All Nanobodies were tested in serial dilutions. Binding curves are shown in Figure 3-23.

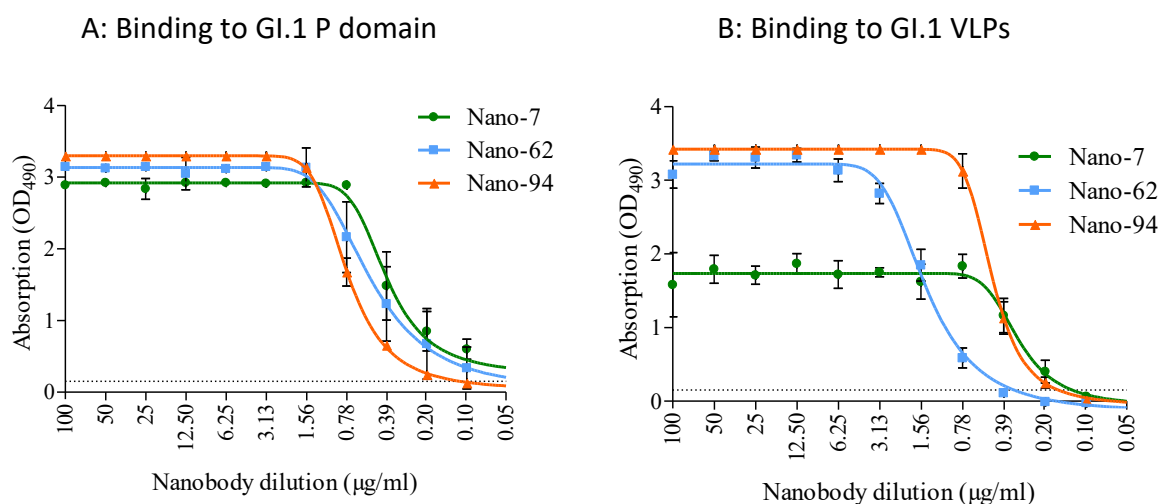


Figure 3-23: Binding of Nano-7, Nano-62, and Nano-94 to GI.1 P domain or GI.1 VLPs

A: All three nanobodies detected 10 µg/ml of GI.1 P domain in a dose-dependent manner. Detection levels were: Nano-7 0.2 µg/ml, Nano-62 0.1 µg/ml, and Nano-94 0.1 µg/ml. B: All three Nanobodies bound to GI.1 VLPs (5 µg/ml), for Nano-7 the maximal detection level was about half the signal observed with Nano-62 and Nano-94. Still the cut-off levels of the three Nanobodies were comparable. Experiments were performed in triplicate (error bars shown), cut-off for OD₄₉₀ at 0.15 as dashed line. Charts were taken from published results [97].

All three Nanobodies bound to GI.1 P domain in a dose dependent manner with cut-off values within a close range (0.1 µg/ml for Nano-7 and Nano-62, and 0.2 µg/ml for Nano-94). Nano-62 and Nano-94 also bound to GI.1 VLPs in a similar manner, both showed a comparable maximal OD₄₉₀ level (3.3 and 3.4 respectively). Nano-7 had a lower maximal OD₄₉₀ level (1.6) which was half of the levels observed with to other two Nanobodies (Nano-62 and Nano-94). Nonetheless, all three Nanobodies showed similar cut-off dilutions upon binding to GI.1 VLPs (0.2 µg/ml (Nano-7), 0.39 µg/ml (Nano-62), and 0.2 µg/ml (Nano-94)). All three Nanobodies interacted with the P domain and were also able to attach to intact VLPs.

Thermodynamic Properties of GI.1-specific Nano-7, Nano-62, Nano-94 Binding to GI.1 P Domain

The thermodynamic properties of the binding between Nanobodies and P domain were analyzed by isothermal titration calorimetry (ITC) and are summarized in Figure 3-24. Nano-62 and Nano-94 both exhibited nanomolar affinities where the dissociation constant K_d of Nano-62 was 4.58 nM and the K_d of Nano-94 was 43.4 nM. Binding of Nano-62 to the P domain

was an exothermic reaction, the large enthalpy change was coupled with a with a favorable entropy change. In contrast, the binding reaction of Nano-94 was endothermic, but characterized by a positive enthalpy change and a large positive entropy (experiments performed by Dr. Anna Koromyslova). Nano-7 exhibited a sub nanomolar K_d of 0.163 nM. The high affinity of the Nanobody might reflect the high number of interactions observed between Nanobody and P domain in X-ray crystallography. Binding of Nano-7 to the P domain was an exothermic reaction driven by a very large enthalpy change. The change in entropy was not favorable but also less significant. Overall, the stoichiometry of the reactions indicted the binding of one Nanobody per P domain dimer.

A

	ΔK_d (M)	ΔH (cal/mole)	ΔS (cal/mole/deg)	ΔG (cal/mole)
Nano-7	1.63E-10 (5.8E-11)	-63633 (1803)	-18.68 (7.8)	-5.79E+04 (954)
Nano-62	4.58E-09 (2.8E-09)	-7120 (269)	13.87 (2.6)	-1.13E+04 (565)
Nano-94	4.34E-08 (2.0E-08)	4550 (199)	49.16 (0.6)	-1.01E+04 (347)

B

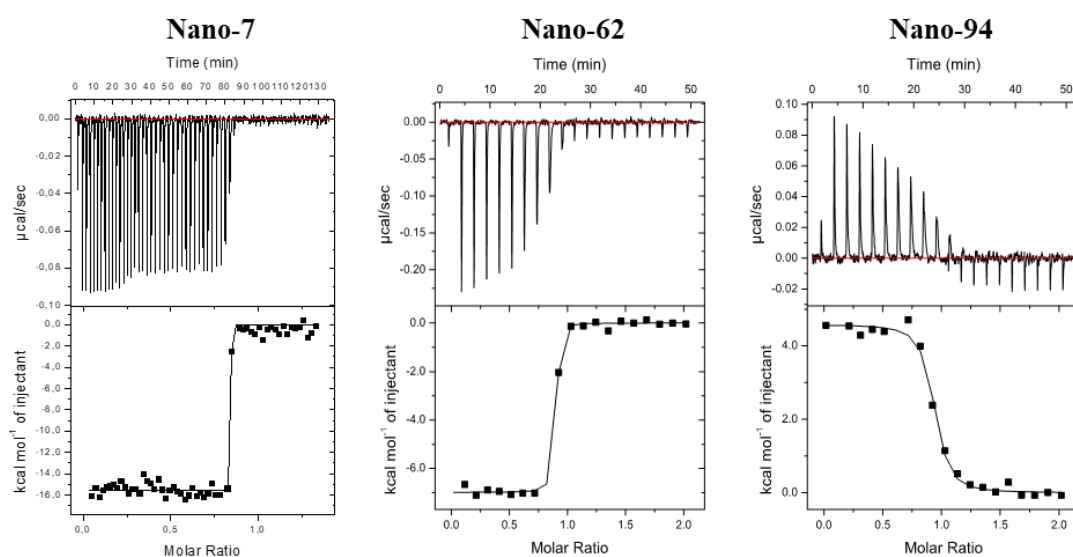


Figure 3-24: Binding affinities of Nano-7, Nano-62, and Nano-94 to Gl.1 P domain
 (A) Thermodynamic constants of the binding reaction between Nanobodies and Gl.1 P domain (ΔH , enthalpy change; ΔS entropy change; K_d , binding affinity, ΔG Gibb's energy change) are summarized in the table. (B) Thermodynamic properties of the binding interaction between Gl.1 P domain and Nanobodies was evaluated using ITC measurement. Upper graphs display examples of the titrations. After subtracting the heat of dilution binding isotherms were calculated using the model of single binding sites (lower graphs). Binding of Nano-94 was an endothermic process whereas binding of Nano-7 and Nano-62 was exothermic. All three Nanobodies bound with 1:1 stoichiometry and showed nanomolar binding affinities (Nano-7 even sub-nanomolar). Experiments with Nano-7 were performed with supervision by Dr. Anna Koromyslova, Nano-62 and Nano-94 were performed by Dr. Anna Koromyslova. Table and charts were taken from published results [97]

Comparison of Binding Sites of Nano-7, Nano-62, Nano-94

An alignment of seven different capsid sequences of GI genotypes was performed to better understand the high genotype specificity of the GI.1 Nanobodies (Figure 3-25). The sequences used for the alignment were GI.1 Norwalk virus, GI.1 West Chester, GI.2 Funabashi 258, GI.3 Kashiwa 645, GI.4 Chiba, GI.8 WUG1, and GI.11 #8 (accession numbers see Table 2-14). The sequence of GI.1 West Chester was used like a consensus sequence for simplified representation. In general, the GI genogroup seems less homogenic than the GII genogroup [11, 40]. The binding sites of the Nanobodies are not limited to conserved regions. They seem to be located in areas that are a mixture of conserved and non-conserved residues. Therefore, the lack of cross-reactivity among other genotypes is a result of the non-conserved sites of binding. Moreover, this lack of capsid conservation might explain the limited ability to identify cross-reactive GI Nanobodies or antibodies as observed previously (Figure 3-13 and Figure 3-18).

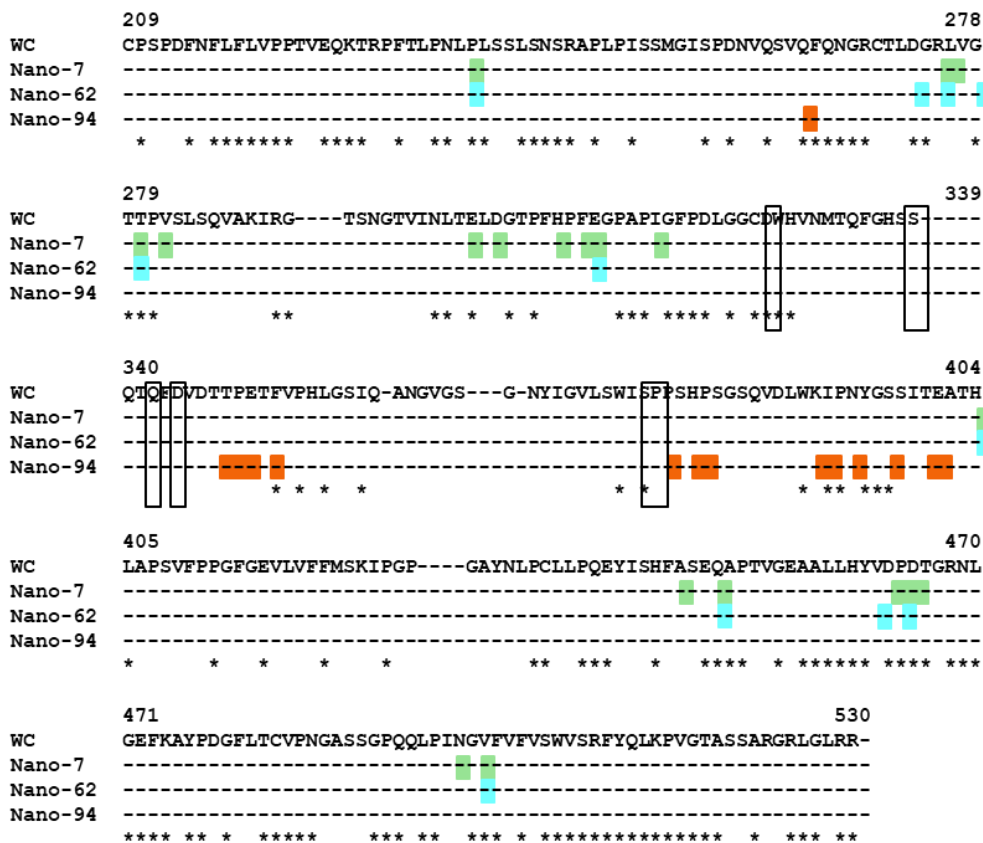


Figure 3-25: Illustration of Nanobody binding sites based on an alignment of seven GI capsid sequences. To simplify the figure only the residues of the GI.1 West Chester (GenBank accession no. AY502016.1) capsid sequence are displayed; other sequences GI.1 Norwalk virus (GenBank accession no. Q83884), GI.2 258 (GenBank accession no. AB078335), GI.3 645 strain (GenBank accession no. BD011871), GI.4 Chiba strain (GenBank accession no. AB042808), GI.8 WUG1 strain (GenBank accession no. AB081723), and GI.11 #8 strain (GenBank accession no. AB058547) were deleted. The residues interacting with either of the Nanobodies are color-coded: Nano-7 (green), Nano-62 (cyan), and Nano-94 (orange). Residues interacting with HBGAs are boxed. Residues conserved in the alignment of the seven sequences are marked by an asterisk. Figure was taken from published results [97]

Inhibition ELISAs of Nano-7, Nano-62, Nano-94

In a separate set of ELISAs, the PGM binding abilities of the three selected Nanobodies was evaluated. All three Nanobodies displayed dose dependent PGM attachment inhibition (Figure 3-26). Nano-62 showed lower inhibition (maximal inhibition of 15 %) compared to Nano-7 and Nano-94, which had 90 to 100 % inhibition with half-maximal inhibitory concentrations (IC_{50}) of 0.4 $\mu\text{g}/\text{ml}$ and 9.2 $\mu\text{g}/\text{ml}$, respectively (Figure 3-26).

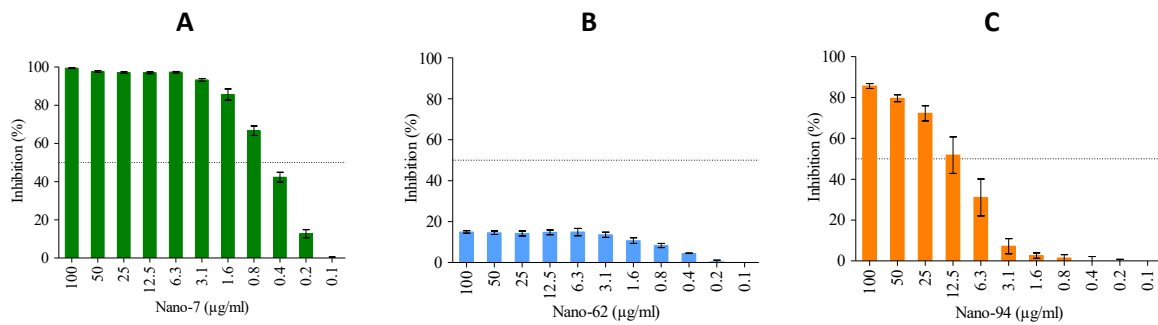


Figure 3-26: Inhibition of VLP binding to PGM by Nanobodies.

In an HBGA blocking assay, serially diluted Nano-7, Nano-62 or Nano-94 were added to GI.1 VLPs, pre-incubated at RT and added to PGM-coated plates. Nano-7 and Nano-94 inhibited PGM attachment of VLPs in a dose dependent manner, with IC_{50} values of 0.43 $\mu\text{g}/\text{ml}$ and 9.23 $\mu\text{g}/\text{ml}$, respectively. Nano-62 showed weak inhibition with a maximum inhibition of 15 %. All experiments were performed in triplicate (error bars shown). Charts were taken from published results [97].

Since previous studies with GII Nanobodies [66] showed alteration of the VLPs upon Nanobody binding, we were also interested in evaluating the VLP integrity. Firstly, the diameters of the untreated VLPs were measured, using DLS. These VLPs exhibited a single symmetrical peak, indicating a homogeneous sample with a VLP diameter of 42 nm (Figure 3-27). Treatment with Nano-7 or Nano-62 did not alter the shape of the peak, indicating no alteration of VLP diameter (Figure 3-27). On the other hand, treatment with Nano-94 resulted in a peak-shift to ~ 1000 nm and an increased heterogeneity of the sample, indicating the formation of massive aggregates (Figure 3-27).

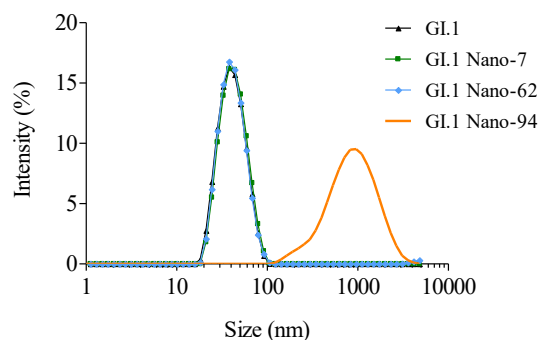


Figure 3-27: DLS measurements to evaluate hydrodynamic diameter of GI.1 VLPs after treatment.

VLPs were either untreated or treated with Nano-7, Nano-62, or Nano-94. Treatment with Nano-7 or Nano-62 resulted in the same peak as untreated VLPs. Treatment with Nano-94 caused a massive peak shift indicating formation of aggregates. Experiments were performed with $T=3$ native sized-VLPs in triplicates. Figure was taken from published results [97].

VLP Integrity After Treatment with GI.1-specific Nanobodies

The integrity of VLP particles, treated with and without Nanobodies, was examined by negative stain EM. Treatment with Nano-7 or Nano-62 did not have any influence on the morphology of the VLPs, as suggested by DLS measurements. However, after treatment with Nano-94, massive aggregates were observed in the specimen, confirming the results obtained with DLS (Figure 3-28).

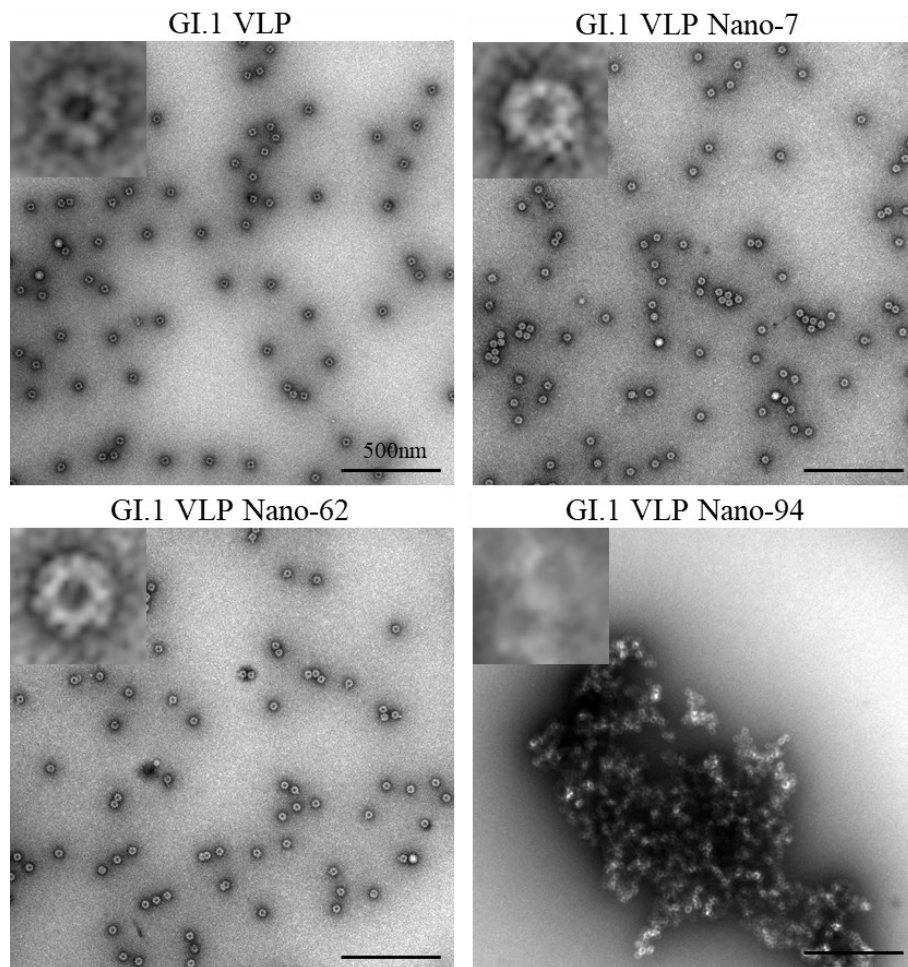


Figure 3-28: EM images of GI.1 VLPs untreated or treated with Nano-7, Nano-62, or Nano-94. Untreated VLPs exhibit the typical norovirus morphology (GI.1 VLP). Treatment with Nano-7 or Nano-62 did not alter this morphology. Upon treatment with Nano-94, large aggregates of intact native-sized VLPs were observed. Experiments were performed with T=3 native-sized VLPs. Images were taken from published results [97].

3.1.5 Binding of GI.1-specific Nanobodies to S Domain

Several Nanobodies showed comparatively weak binding to P domains while exhibiting better binding to VLPs, therefore a separate set of ELISAs were conducted to determine if the GI.1-specific Nanobodies were able to bind to the GI.1 S domain. Three GI.1 S domain constructs (215, 220 and 225) were designed, and the S domains were expressed as described in the P domain expression protocol (2.2). The protocol for the S domain binding assay was the same as for P domain binding (Table 2-17). Experiments were performed in duplicates.

All Nanobodies of the panel showed binding to the GI.1 S domain 215 construct but at detection levels considerably lower ($OD_{490 \text{ max}} 0.78$, Figure 3-29) than with P domain or VLP ($OD_{490 \text{ max}} \geq 3.5$, Figure 3-16 and Figure 3-17). Most Nanobodies were also able to bind to the 220 S domain construct, but at even lower detection levels ($OD_{490 \text{ max}} 0.35$, Figure 3-29). None of the Nanobodies were able to bind the S domain construct 225. Our attempts to crystallize S domain protein only yielded salt crystals or crystals that showed no diffraction.

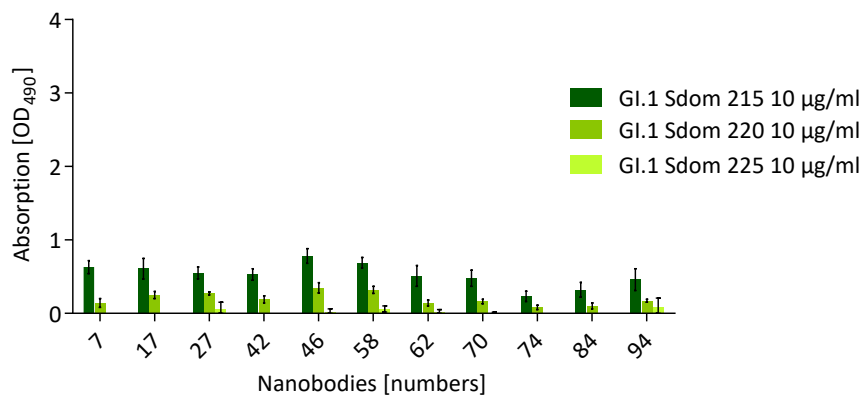


Figure 3-29: Binding ELISA of GI.1-specific Nanobodies to GI.1 S domain

Three different constructs of GI.1 S domain (GI.1 Sdom215, GI.1 Sdom220, and GI.1 Sdom225) were expressed and purified. Binding of the panel of GI.1-specific Nanobodies to plates coated with the S domain constructs were tested. All Nanobodies showed binding to the 215 construct but at very low detection levels ($OD_{490 \text{ max}} 0.78$). Most Nanobodies were also able to bind to the 220 construct but at even lower detection levels ($OD_{490 \text{ max}} 0.35$). Range of Y-axis identical to binding ELISAs with GI.1-specific Nanobodies binding to GI.1 P domain and VLPs (Figure 3-16 and Figure 3-17). Single experiment; measurements were performed in triplicate wells, error bars shown.

3.2 Screening for Natural Extracts as Antivirals

Although the previous chapter already identified some promising inhibitors, the major disadvantage of Nanobodies is their highly specific nature. In practice an antiviral needs broader reactivity among the various genotypes and variants (as observed with the natural inhibitors citrate and the HMO 2'FL). The natural extract screening presented here included sugary extracts and a specific external screening of HMOs [124].

3.2.1 HMO Screening

For the HMO-screening provided by the National Center of Functional Glycomics (NCFG) service [124] GII.10 (026), GII.4 (Sydney), GII.17 (Kawasaki), and GII.17 (Saitama) VLPs were selected. As a suitable detection system, Nano-26 was chosen after binding ELISAs (protocol Table 2-16, but 5 $\mu\text{g}/\text{ml}$ of the respective VLPs) confirmed detection of all four VLPs (Figure 3-30). Anti-His HRP was used to detect the His-tag of the bound Nanobodies.

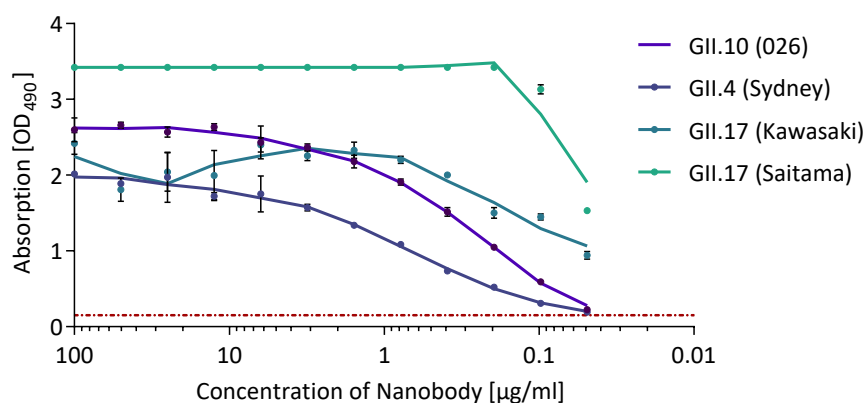


Figure 3-30: Binding ELISA (GII.10, GII.4, GII.17) detection by Nano-26. All tested VLPs were detected by Nano-26. Maximal OD₄₉₀ levels varied slightly depending on the VLPs used (2 for GII.17 Kawasaki to 3.5 for GII.17 Saitama). Cut-off 0.15 as dashed/dotted line (red). Single experiment; measurements were performed in triplicate wells, error bars shown.

Screening for Natural Extracts as Antivirals

The HMO screening analyzed which VLPs were able to bind to an array of printed HMOs from one donor sample [124]. Results were received from the external screening, and are summarized in Figure 3-31 - Figure 3-33. All VLP samples exhibited binding to several HMOs. A second screen run with a lower VLP concentration showed that binding-signal in most cases was concentration dependent. Figure 3-31 shows the original figures displaying the results as they were provided by the NCFG.

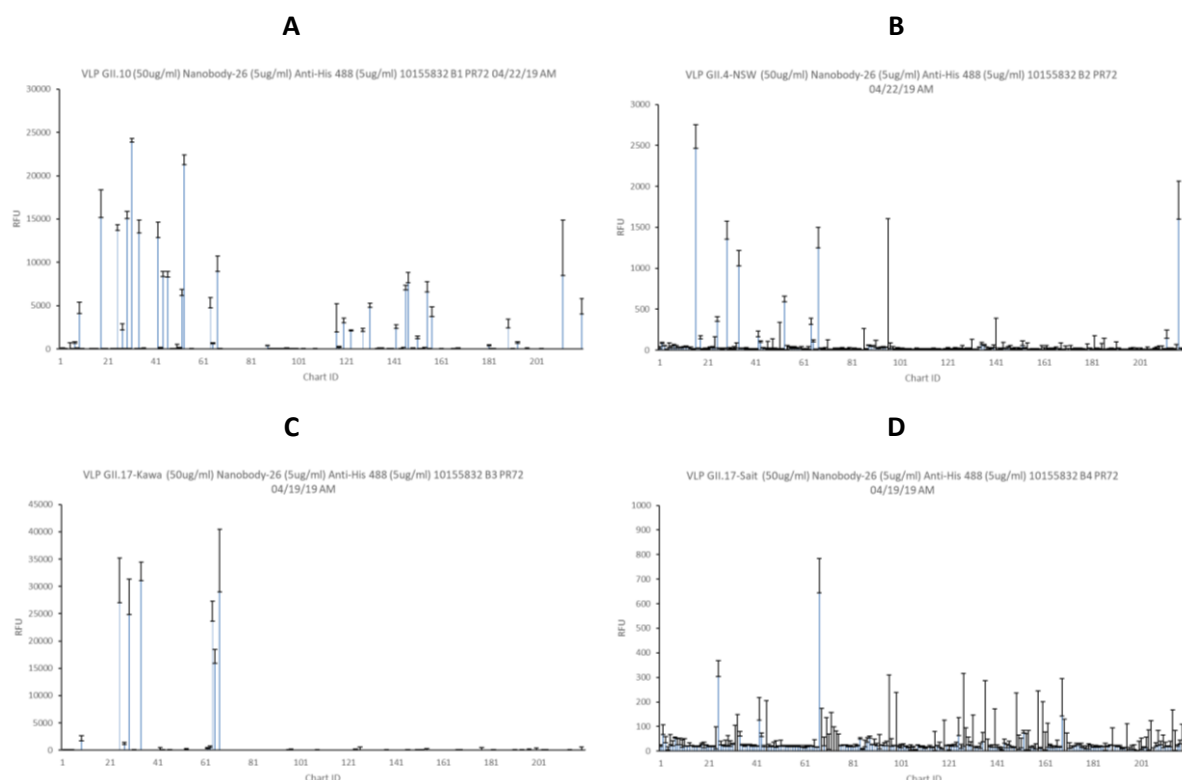


Figure 3-31: Binding events in the HMO screening at NCFG

Original presentation of result data of the HMO screening as analyzed and provided by NCFG. A: GII.10 026 VLP, B GII.4 Sydney, C: GII.17 Kawasaki, D. GII.17 Saitama. All VLPs were tested at a concentration of 50 $\mu\text{g}/\text{ml}$ and detected with 5 $\mu\text{g}/\text{ml}$ of Nano-26 and 5 $\mu\text{g}/\text{ml}$ of Anti-His 488. All experiments were repeated with 5 $\mu\text{g}/\text{ml}$ of VLPs (data not shown).

For enhanced overview and to better compare the binding between the different norovirus VLP variants, heat maps of the binding events were constructed (Figure 3-32 and Figure 3-33). Signal intensity of the detected binding was measured in relative fluorescence units (RFU). The lowest detected signal was 1 RFU, and this was interpreted as no binding. The maximal signals varied depending on the VLPs in the assay; 24,074 RFU for GII.10 026, 2,608 RFU for GII.4 Sydney, 34,706 RFU for GII.17 Kawasaki and 715 RFU for GII.17 Saitama VLPs.

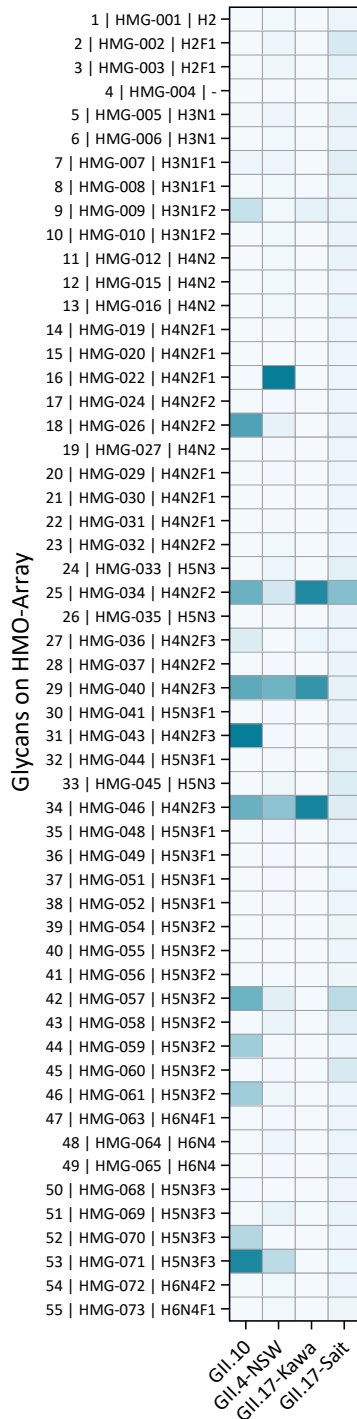
Of all (220) tested, samples fraction 67 showed the highest overall binding signal with all tested VLPs; GII.10 026 (9,853 RFU), GII.4 Sydney (1,375 RFU), GII.17 Kawasaki (34,706 RFU), and GII.17 Saitama (715 RFU). Since the maximal detection signal varied greatly depending on the VLP genotype, comparison of the absolute RFU values is not practical. For interpretation of results and the generation of heat maps, RFU values were normalized to percentage relative to maximal detection level of the respective VLP (Table A I-3). For fraction 67 normalized detection levels are 40.93 % (GII.10 026), 52.70 % (GII.4 Sydney), 100 % (GII.17 Kawasaki), and 100 % (GII.17 Saitama). Fraction 25 showed very strong binding to GII.10 026 VLPs (58 %), GII.17 Kawasaki (90 %) and GII.17 Saitama (47 %), but weaker binding to GII.4 Sydney VLPs (15 %). Fractions 29 and 34 exhibited strong binding for GII.10 026 VLPs (64 % and 59 % respectively and GII.4 Sydney (56 %, 43 %, respectively) and GII.17 Kawasaki (81 %, 94 %). It also bound to GII.17 Saitama VLPs, albeit comparatively weaker (6 % and 10 % respectively). Fraction 31 exhibited the highest binding (100 %) observed with GII.10 026, whereas fraction 16 displayed the highest binding observed with GII.4 Sydney VLPs (100 %). A list of the top twenty binders was attached in the appendix (Table A I-3).

Several other fractions (Figure 3-32 and Figure 3-33) also showed strong binding but only to a single VLP-type. The strongest of these more specifically binding fractions were: 16 and 217 (binding to GII.4), 31, 53, and 18 (binding to GII.10), 64 (binding to GII.17, Kawasaki), and weaker 168 (binding to GII.17, Saitama).

Unfortunately, the NCFG made a mistake in matching the numbers of the fractions in the screen with the HMOs that were identified by the group. Therefore, the only result from this screen was that the four genotypes bind to various HMOs. But the interpretation what exact HMOs remains unclear.

Screening for Natural Extracts as Antivirals

**HMO Binding Array Heat Map
fractions 1-55**



**HMO Binding Array Heat Map
fractions 56-110**

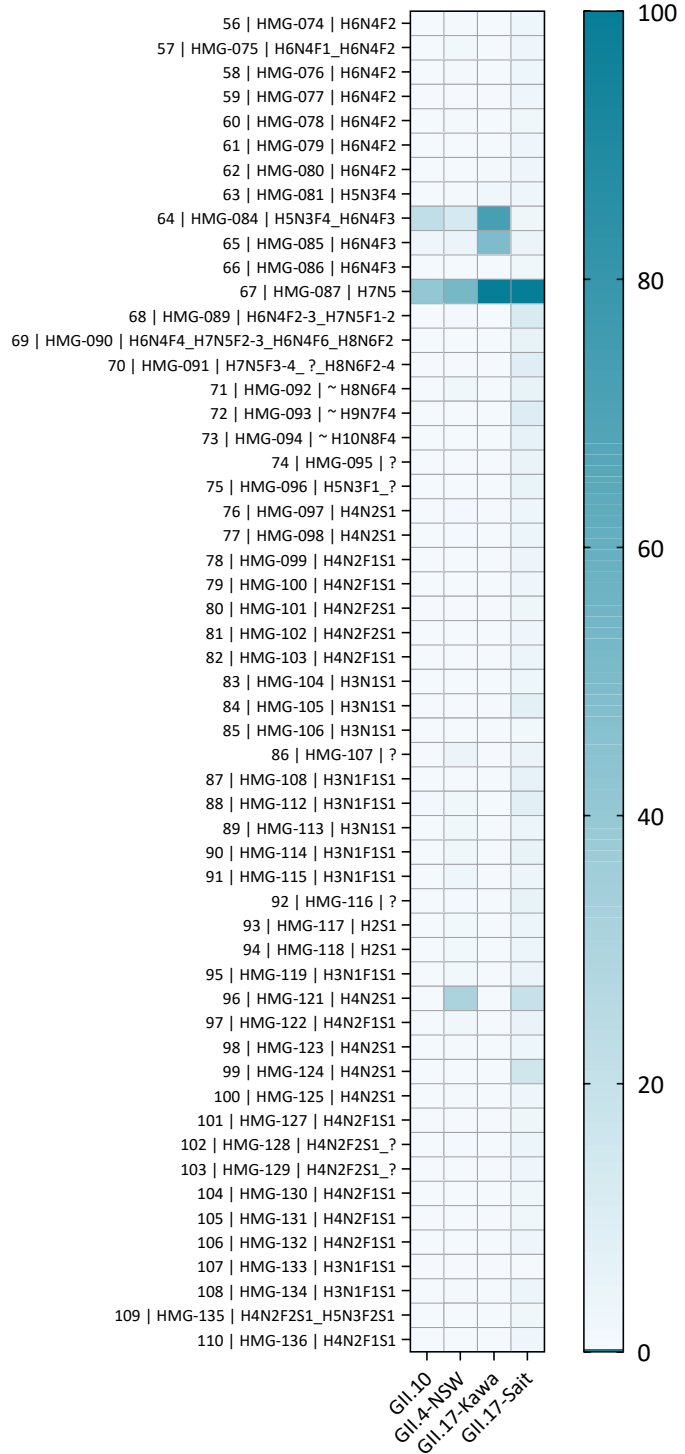


Figure 3-32: HMO binding array Heat Map Part I fractions 1-110

RFU-results were calculated in percentage relative to maximal detection of respective VLP at 50 µg/ml (GII.10 026, GII.4 Sydney (NSW), GII.17 Kawasaki (Kawa), and GII.17 Saitama (Sait)). Color-coding according to respective calculated value (0-100 % see scale at the right).

Screening for Natural Extracts as Antivirals

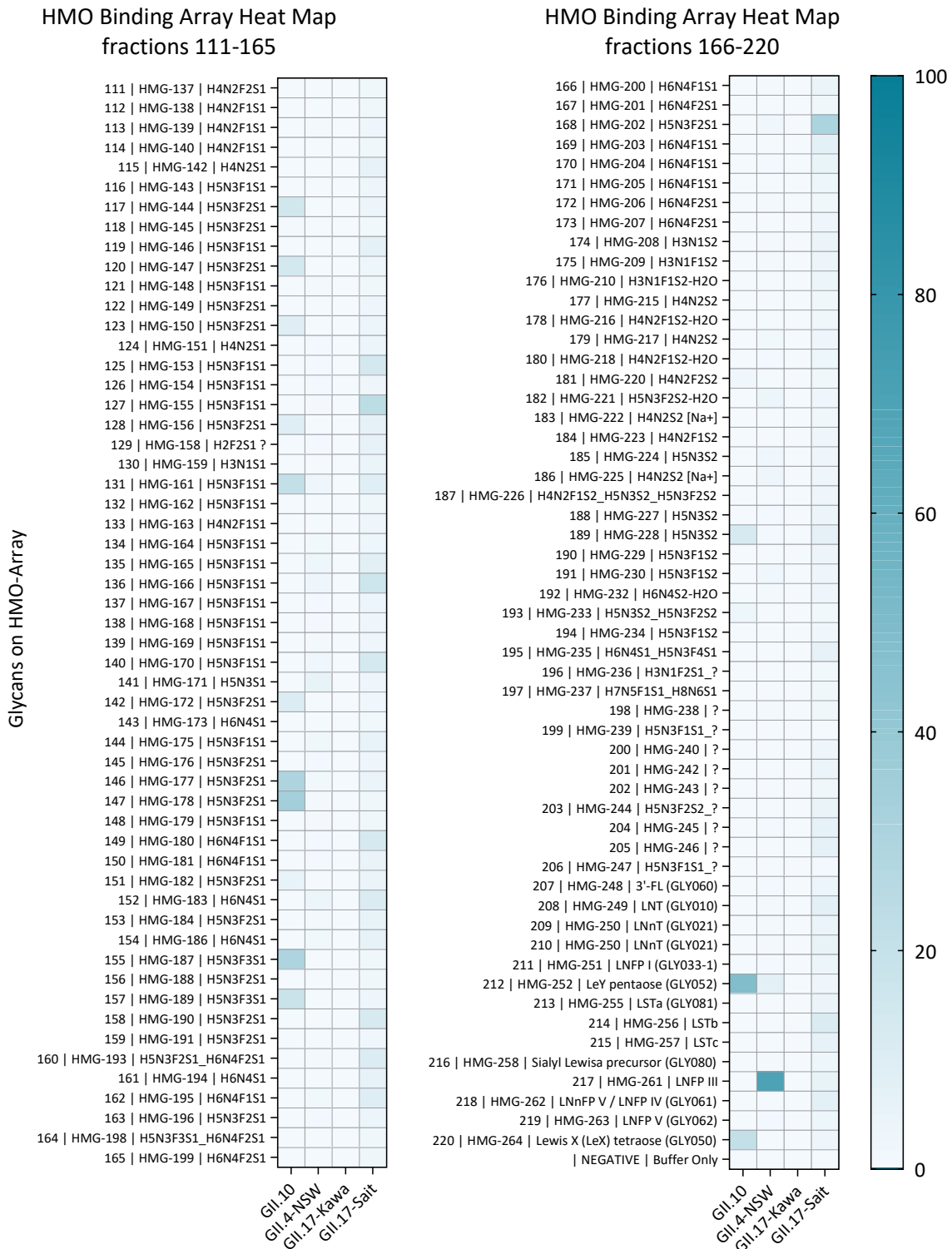


Figure 3-33: HMO binding array Heat Map Part II fractions 111-220
 RFU-results were calculated in percentage relative to maximal detection of the respective VLP at 50 µg/ml (GII.10 026, GII.4 Sydney, GII.17 Kawasaki (Kawa), and GII.17 Saitama (Sait)). Color-coding according to respective calculated value (0-100 % see scale at the right).

3.2.2 Plant Derived Syrups and Saps

Natural extracts were screened in a surrogate HBGA inhibition ELISA (2.6). Extracts rich in glycans were included in the screen, as glycans are the substance class HBGAs belong to and are hypothesized to comprise of compounds that are able to block HBGA binding, due to their structural similarities. The aim was to identify potential inhibitors in a panel of extracts which are rich in glycans, non-toxic, and approved as parts of regular human nutrition. In these assays, many natural extracts were screened on their ability to inhibit HBGA attachment of VLPs. In the first trial ELISA to test the inhibition, a panel of various natural extracts was used at a concentration of 12.5 % of original matter.

Plant Derived Syrups and Saps – Structure Analysis: GII.10 026 P domain Co-Crystals

An X-ray crystallography screen with the natural extracts identified in the initial experiments was performed. GII.10 026 P domain crystals were co-crystallized or soaked with the respective extract. The aim was to identify the compound of the respective extract causing inhibition. Therefore, crystal structures of P domain were screened for the presence of a ligand bound to the P domain.

A total of 86 GII.10 026 P domain co-crystals with natural extracts were screened. Of those, 56 crystals were obtained in co-crystallization with propolis extracts, date syrup, coconut blossom syrup, and apple sweetener further 30 crystals were obtained by soaking with date syrup, coconut blossom syrup, apple sweetener, or honey. All 86 crystals were analyzed at the ESRF, France. Data sets were collected for 80 of the crystals. For six crystals no data were obtainable. Some of the natural extracts (including some propolis extracts) hindered formation of co-crystals. Regardless of the technique (co-crystallization or soaking) no ligand was observable in structure analysis of all processed crystals except apple sweetener.

In all crystals with apple sweetener (co-crystallization or soaking) two different ligands were found (Figure 3-34). One ligand was at the HBGA-binding (between Asp385 and Tyr452) site. It showed a ring-like structure similar to previously observed and published fucose rings. Unlike the fucose ring the structure appeared to be an open (not fully closed) ring. The second ligand also exhibited a ring-like structure and was found between His468A/B at the bottom of the P domain between the two dimers.

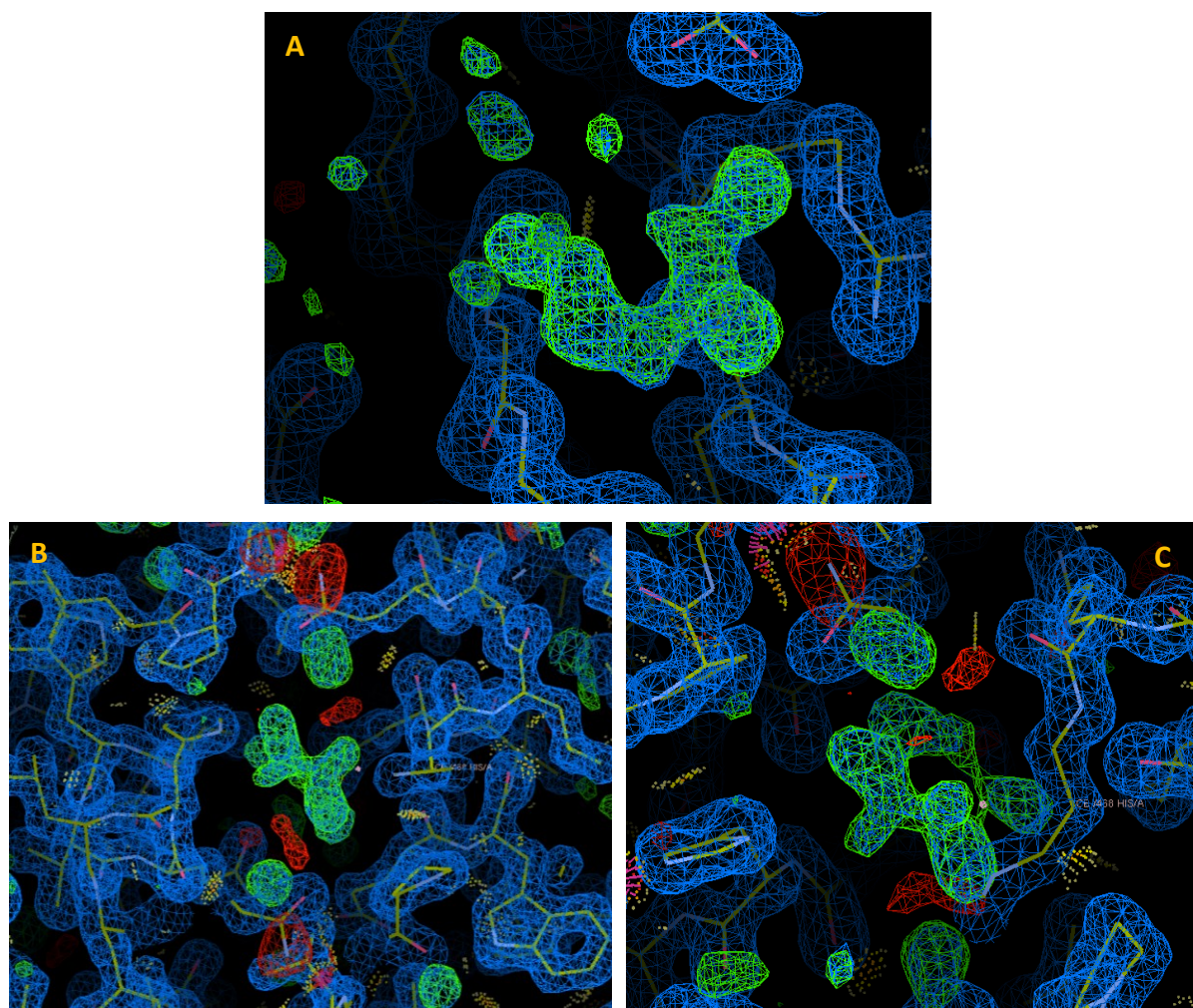


Figure 3-34: Structure analysis of GII.10 026 P domain crystals in complex with apple sweetener
 A: Open ring-like structure in the HBGA binding site at the top of the P domain
 B: Ring between His468A/B at the bottom of the P domain between the dimers
 C: Magnification of B with slight rotation to show ring.
 Co-crystals were grown in regular GII.10 026 P domain mother solution (G5). All X-ray crystallography data were collected at ERSF, ID29,

In crystals with other natural extracts (soaked or co-crystallized) no ligands could be observed (Appendix Table A I-4). This could either be the result of less restrictive binding between P domain and ligand enabling movement, rotation, or different steric orientations. As a result, the averaging nature of X-ray crystallization data acquisition and processing would remove the ligand from the structure. Another possibility is that the crystal packing excludes the ligands of other extracts that could bind without the context of a crystal. Either because the ligand in itself is too large or because it causes massive alterations in protein folding, disabling the protein to form crystals in this condition. To address this question, all data sets were thoroughly evaluated (Appendix Table A I-4) for disordered/missing loops and comparatively small, unexplained densities to find structural deviations from the model (pdbID: 3ONU).

Further, the co-crystallization conditions of the individual mixtures of GII.10 026 P domain and the respective natural extract were optimized.

Plant Derived Syrups and Saps – Structural Analysis: Optimization of Co-Crystals

To optimize crystallization conditions of the individual co-crystals, mixtures of GII.10 026 P domain and the four most promising natural extracts (based on performance in ELISA and DLS) were sent to the Crystallization platform at the excellence cluster, University of Heidelberg:

GII.10 026 P domain + coconut blossom syrup

GII.10 026 P domain + date syrup

GII.10 026 P domain + 95 % Ethanol propolis extract

GII.10 026 P domain + 100 % DMSO propolis extract

The evidence of inhibition (assessed by ELISA) made interaction between these extracts and the P domain likely, but so far, no ligand was present in any of the crystals screened (co-crystals or soaking). In many of the conditions tested by the crystal-tracker, crystals formed (Table A I-5). The majority of observed crystals were large single crystals (e.g. Figure 3-35). If the P domain was mixed with date syrup noticeably often more but smaller crystals formed.

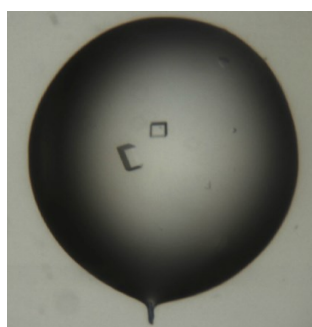


*Figure 3-35: Example for large single crystals at the crystal tracker
Co-crystals of GII.10 026 P domain with coconut blossom syrup in JSCG-1 A8 mother solution*

15 conditions were chosen to set up in the lab to grow larger crystals for data collection (supported by Dr. Turgay Kilic, Appendix Table A I-5). Co-crystals of GII.10 026 P domain with coconut blossom syrup, date syrup and propolis extract (95 % ethanol and DMSO) were set up. Crystals were observed in all conditions. Single crystals from six of these conditions (Table 3-3) were selected, covering all four extracts. Data of all crystals were collected at the ESRF, France (resolution 1.37 - 2.04 Å) and processed as described (2.10):

Screening for Natural Extracts as Antivirals

Table 3-3: Primary selected crystallization conditions for GII.10-P domain co crystals

Screen-No	Composition
JCSG-1 B1	0,2M sodium chloride, 20m/v PEG 3000, 0,1M HEPES
JCSG-1 B5	20 w/v PEG 4000, 0,1 M HEPES, 10 v/v 2 propanol
JCSG-1 F1	10 w/v PEG 6000, 0,1 M MES
JCSG-1 G4	20 w/v PEG 6000, 0,1 M citric acid
JCSG-2 D11	12 w/v PEG 20,000, 0,1 M MES
JCSG-1 F1	10 w/v PEG 6000, 0,1 M MES

Because no ligands bound within the P domain could be found within this selection of crystallization conditions, a second set of co-crystals in different crystallization condition was selected for data acquisition (Table 3-4).

Table 3-4: Secondary selected crystallization conditions for GII.10-P domain co crystals

Screen-No	Composition
JCSG-1 A8	0,2M sodium citrate, 20 m/v PEG3350
JCSG-1 B7	0,2 M di-sodium tartrate, 20 w/v propylene glycol 3350
JCSG-1 C12	0,2 M sodium thiocyanate, 20 w/v PEG 3350
JCSG-1 G3	1 M lithium chloride, 10 w/v PEG 6000, 0,1 M citric acid
JCSG-2 C5	0,2 M sodium fluoride, 20 w/v PEG 3350
JCSG-1 F2	0,2 M magnesium formate, 20 w/v PEG 3350
JCSG-1 A8	0,2M sodium citrate, 20 m/v PEG3350
JCSG-1 B5	20 w/v PEG 4000, 0,1 M HEPES,10 v/v 2 propanol
JCSG-1 F1	10 w/v PEG 6000, 0,1 M MES

Within this set of crystals (Appendix Table A I-6) four interesting datasets were identified:

Date syrup JCSG2 C5; resolution 1.73 Å

Date syrup JCSG1 F2; resolution 2.04 Å

Coconut blossom syrup JCSG2; resolution C5 1.59 Å

Coconut blossom syrup JCSG1 F2; resolution 1.83 Å

These structures all displayed a ligand at the HBGA binding site and additional densities in the central channel of the P domain (between 468 A/B). After refining and adding waters to the model of the P domain, a third ligand became visible (due to the overall improvement of the model by adding waters): between W381 A/B, located in the channel between the two HBGA binding sites (summarized in Figure 3-36). Unfortunately, no ligands were observed in any of the propolis data sets.

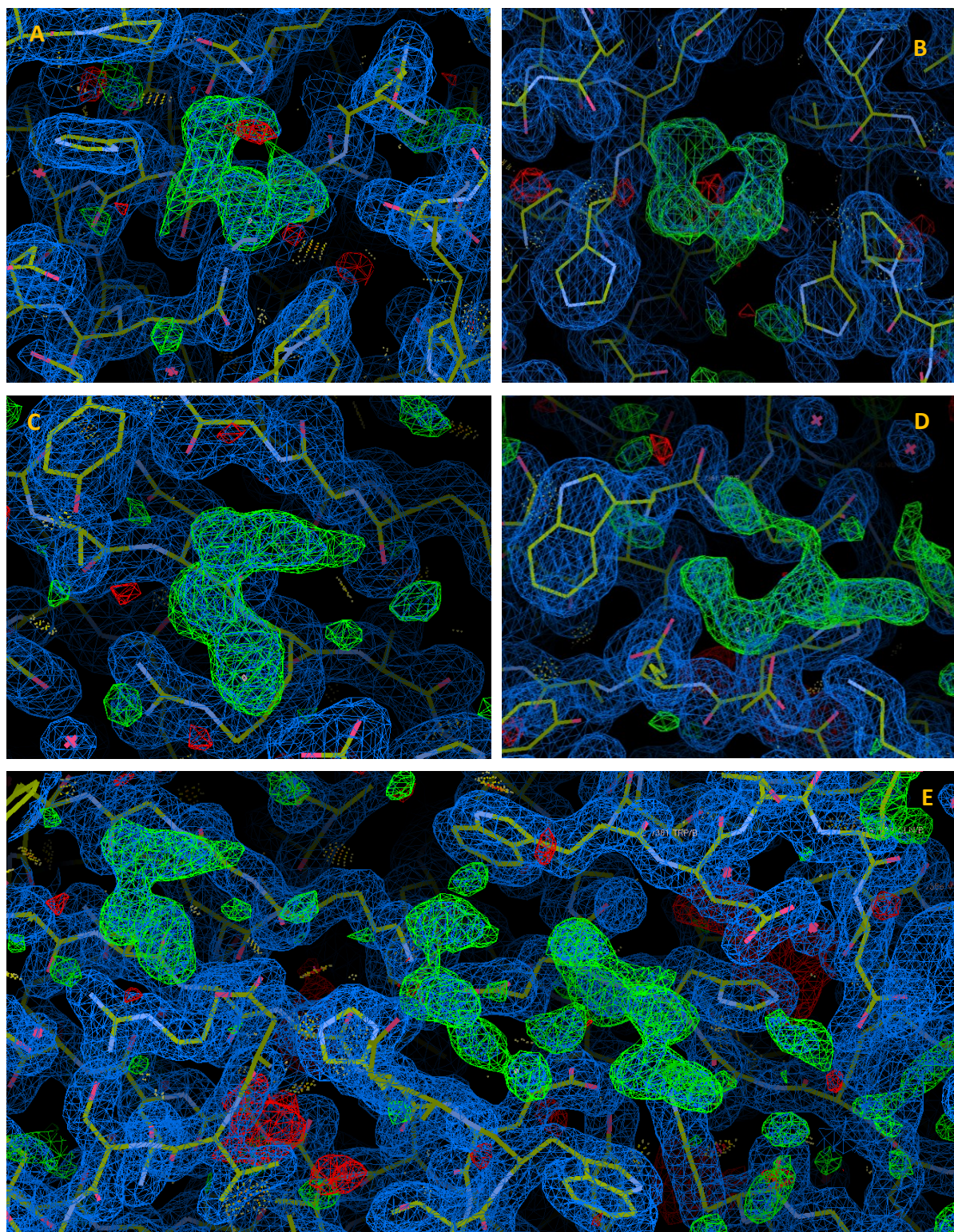


Figure 3-36: Structural analysis of GII.10 P domain in complex with date syrup
 Several additional densities were identified within the crystal:
 A and B: ring-like structure between HIS468 A/B in the central channel displayed in two different angles
 C: HBGA binding site, 385 A with a half-ring,
 D: One of the densities between residues 381 A/B, this density increased and became clearer during refinement,
 E: Comprises additional densities shown in C and D on the left the HBGA binding site with ligand (C). All images taken from JCSG2 C5 date syrup.

Plant Derived Syrups and Saps - ELISA: Inhibition in a Surrogate HBGA Attachment Assay

To determine if the natural extracts exhibiting inhibition are cross-reactive with other genotypes, VLPs of different genotypes were used in an inhibition ELISA. The ELISA protocols varied slightly according to the VLPs tested (overview in Table 3-5).

Table 3-5: Inhibition ELISA protocols

VLP	Protocol
GII.10	Table 2-19
GII.4	Table 2-20
GII.17	Table 2-22
GI.1	Table 2-21
GII.1	Table 2-23

Date syrup exhibited the highest inhibition across all genotypes, with low IC₅₀ values in all tested genotypes: GII.10 (Figure 3-37 A; IC₅₀=0.11 %), GII.4 (Figure 3-37 B; IC₅₀=0.06 %), GII17 (Figure 3-37 C; IC₅₀=0.14 %), GI.1 (Figure 3-37 D; IC₅₀=0.15 %), and GII.1 (Figure 3-37 E; IC₅₀=0.49 %). In contrast, barley malt showed more specific inhibition towards GII.4 (Figure 3-37 B; IC₅₀=0.90 %), whereas inhibition was much lower in other genotypes (GII.10, GII.17, GI.1, Figure 3-37 A, C, D; IC₅₀ values not calculable). Coconut blossom syrup and apple sweetener showed inhibition (ranging from 15 to 75 % across different tested VLPs) at high concentrations (12.5 – 3.1 %) but this inhibition pattern was consistent with different genotypes (GII.4, GII.17, GI.1, less with GII.10 Figure 3-37 B, C, D, A) except GII.1. Agave nectar, royal jelly and maple syrup showed low inhibition (0 – 50 % at a concentration 12.5 %) but were included as examples for little to no inhibition (GII.10, GII.4, GII.17, GI.1 Figure 3-37 A, B, C, D). GII.1 was included in this set of experiments because it has a different type of antigenicity. GII.1 VLPs are only able to bind to HBGAs in the presence of bile salts [58]. In spite of the difference in HBGA binding, GII.1 VLPs could be inhibited by the natural extracts presented. All inhibitors, except date syrup, showed higher inhibition with GII.1 VLPs (Figure 3-37 and Table 3-6).

Screening for Natural Extracts as Antivirals

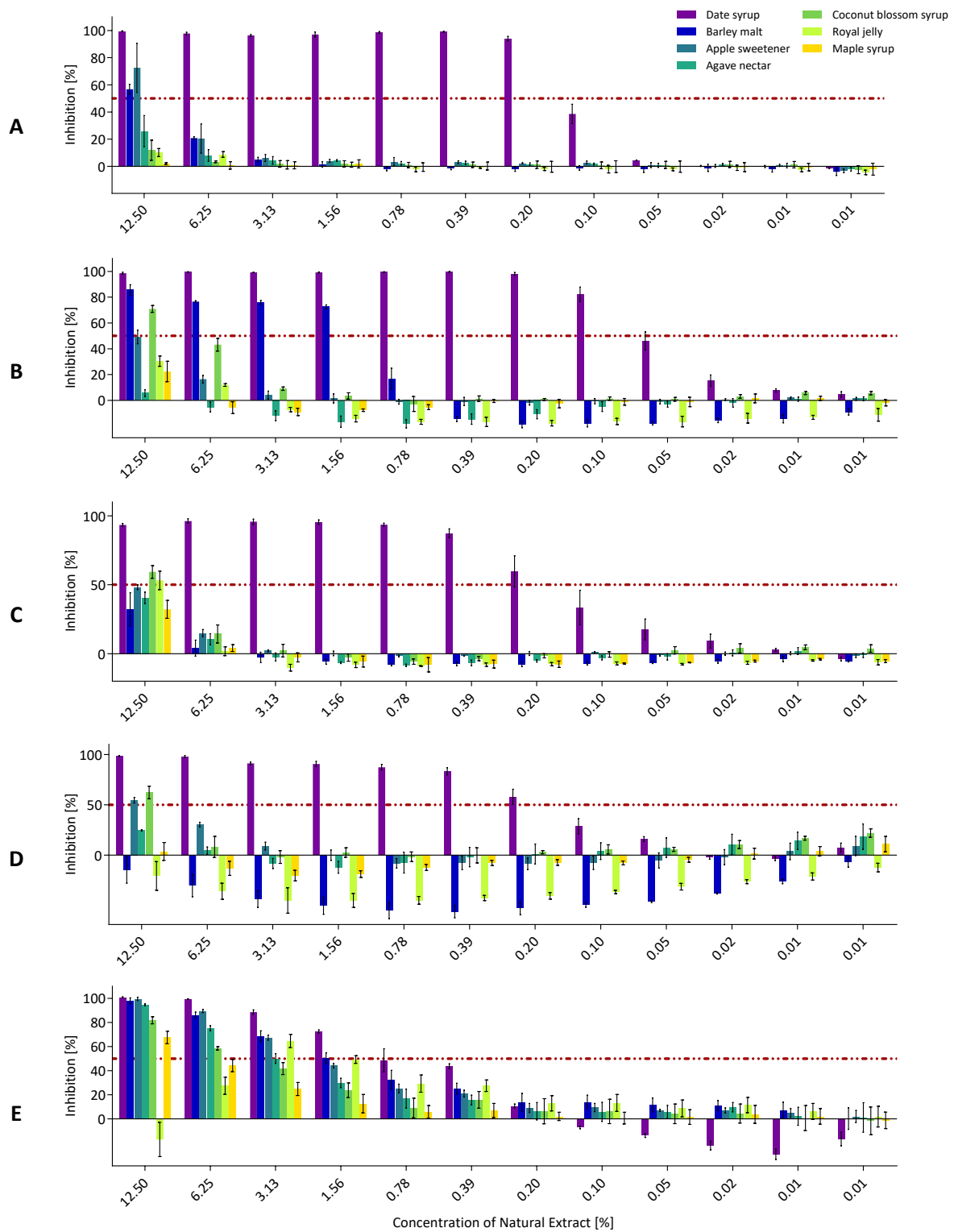


Figure 3-37: Attachment inhibition of GII.1, GII.1, GII.4, GII.10, and GII.17 VLPs by natural extracts
Attachment inhibition of GII.10 (A), GII.4 (B), GII.17 (C), GII.1 (D), and GII.1 (E) VLPs. Highest inhibition with all genotypes was observed with date syrup (GII.10: IC₅₀=0.11 %, GII.4: IC₅₀=0.06%, GII.1, IC₅₀=0.14%, GII.1; IC₅₀=0.15%, and GII.1; IC₅₀=0.49%). Barley malt more specifically inhibited GII.4 (IC₅₀=0.90%). Coconut blossom syrup and apple sweetener showed 15 – 75 % of inhibition at high concentrations (12.5 – 3.1 %) but this pattern was consistent with different genotypes. Agave nectar, royal jelly and maple showed low inhibition (0 – 50 % at a concentration of 12.5 %). GII.1 VLPs could be inhibited by natural extracts presented, all inhibitors, except date syrup, showed higher inhibition with GII.1 VLPs (E). IC₅₀ is indicated as dashed/dotted line (red). Measurements were performed in triplicates. Error bars show SD.

Of all natural extracts tested, the most efficient compound was date syrup. It completely abolished the interaction between the HBGA scaffold and VLPs of different genotype. Barley malt also displayed inhibition, whereas coconut blossom syrup and apple sweetener only reduced detectable VLPs to about 50 %. A comparatively low level of inhibition was also observed with two agave nectars, stevia glycosides, royal jelly, and a honey sample. This showed that the assays were able to discriminate between extracts inhibiting attachment of VLP to HBGAs and extracts that were not able to inhibit like aloe vera, maple, erythritol, and stevia extract.

To ensure that the strong inhibition observed with date syrup with various different genotypes was not the result of a detection issue within the ELISA setup, the inhibition experiment with GII.17 was repeated with two Nanobodies (detection Nanobodies Nano-26 and Nano-4, Table 2-6). In the initial GII.17 experiments, the OD₄₉₀ reading of the negative control was unusually high, which resulted in negative values of the calculated inhibition. And, in the control wells (VLPs without inhibitor), lower OD₄₉₀ were observed than with low concentrations of inhibitor resulting in bars displaying negative inhibition (same in three repeats, data not shown). To test if this could result from a detection issue, the detection of VLPs by Nano-26 with Nano-4, with and without biotinylation was compared (protocol Table 2-22). For detection Nano-26, Nano-26-biotinylated, Nano-4, and biotinylated-Nano-4, as a secondary antibody HRP-anti-His (1:4000, for non-biotinylated Nanobodies) or HRP-conjugated streptavidin (1:5000, for biotinylated Nanobodies) were used.

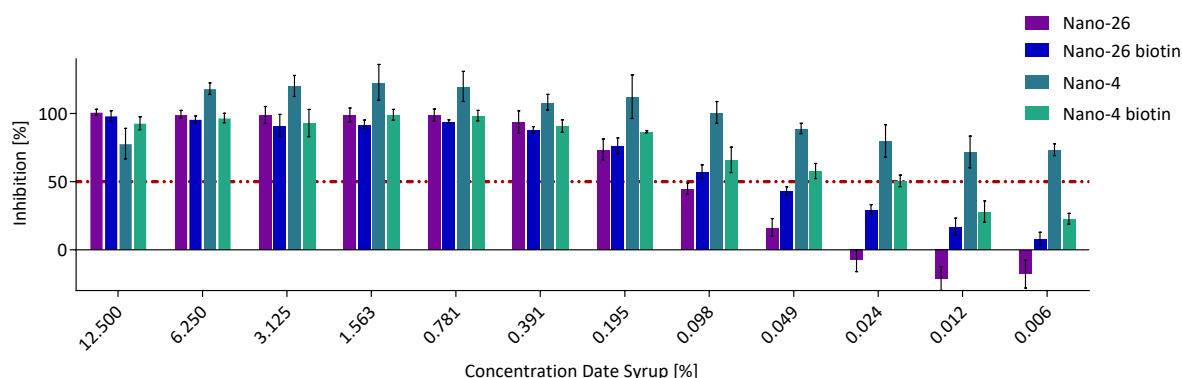


Figure 3-38: Detection of GII.17 VLPs inhibition with date syrup using Nanobodies with/without biotinylation. Both Nanobodies (Nano-26 and Nano-4) were able to detect the inhibition curve of GII.17 VLPs incubated with date syrup at comparable levels (IC_{50} 0.04 – 0.08 % for all four detection Nanobodies). Biotinylated Nano-26 showed negative inhibition whereas the percentage of inhibition detected by Nano-26 is not below 0. Nano-4 showed higher inhibition even at low concentrations of date syrup. IC_{50} is indicated as dashed/double dotted line (red). Single experiment; measurements were performed in triplicate wells, error bars shown.

The result showed that the detection Nanobody had no influence on the inhibition observed (IC_{50} values 0.04 - 0.08 %). However, the negative inhibition was reduced when biotinylated Nanobody and streptavidin-HRP were used for detection, instead of detecting the His-tag of the Nanobodies (Figure 3-38). Further, implementation of an additional wash step before adding the secondary antibody was able to reduce this phenomenon even further. Some of the natural compounds seem to interfere with the detection of the His-tag.

Date Syrup: Inhibition of GII.10 VLPs by Three Different Date Syrups

The inhibition of three different types of date syrups was compared (protocol Table 2-19, but anti-rabbit 1: 5000). Of the three (Date syrup 1 – 3), only two showed complete inhibition (1 and 2) whereas the last (3) showed a considerably lower inhibition (Figure 3-39). The maximal inhibition of date syrup 3 at a concentration of 12.5 % was 20 %, whereas both other syrups exhibited about 100 % of inhibition at same the dilution. Date syrup 1 exhibited the highest inhibition with an IC_{50} of 0.07 %, closely followed by date syrup 2 (IC_{50} at 0.3 %).

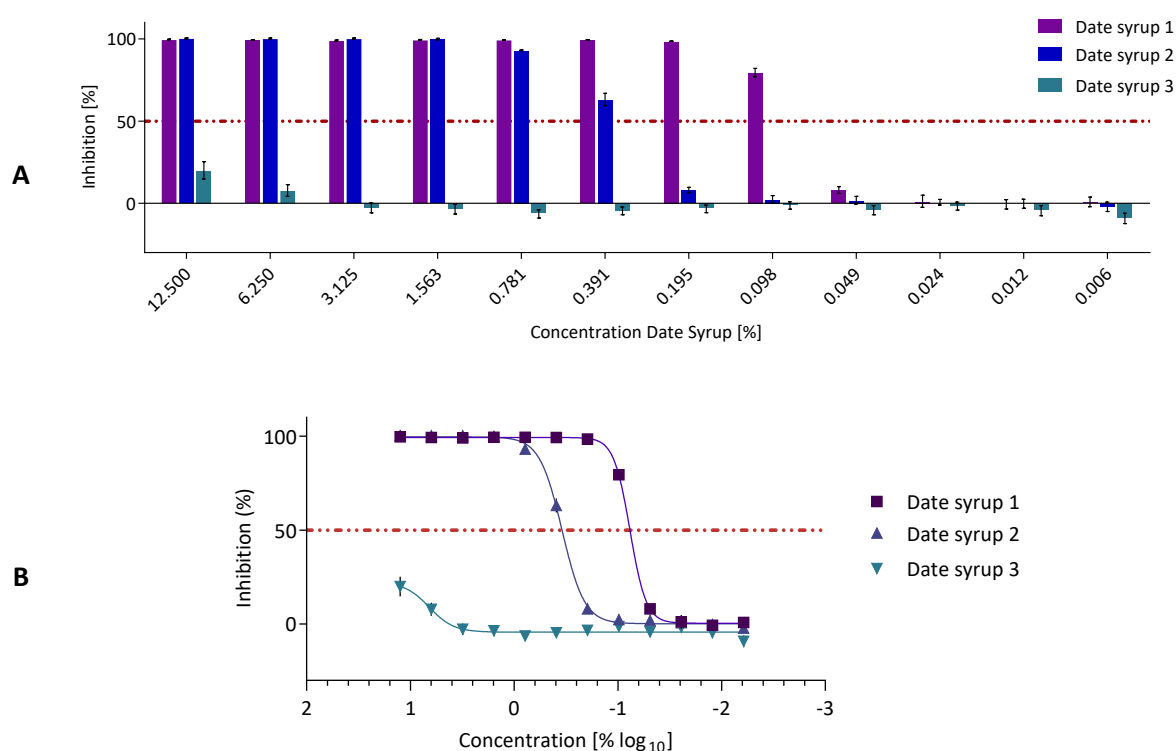


Figure 3-39: Inhibition of GII.10 VLPs by different types of date syrup. Date syrups 1 and 2 showed good inhibition (IC_{50} 0.07 %, 0.3 %). Date syrup 3 showed very little inhibition (maximal inhibition observed 20 %) A: Bar chart of inhibition by date syrups. Single experiment; measurements were performed in triplicate wells, error bars shown. B: Line chart of regression fit to calculate IC_{50} values for date syrup inhibition by Graphpad Prism (log₁₀ of concentrations). In both charts, IC_{50} values are marked as dashed/double dotted line (red).

Date Syrup: Inhibition by Sugars Identified in Date Syrup

Gas chromatography analysis performed by the Metabolomics Core Technology Platform University Heidelberg (Gernot Poschet) was used to identify compounds within the natural extracts. Three samples (date syrup, coconut blossom syrup and apple sweetener) that showed inhibition, as well as two further samples (aloe vera and maple) that didn't show inhibition were analyzed at the core facility. Eight glycans (inositol, mannitol, sorbitol, galactose, glucose, mannose, sucrose) of high concentration were identified in date syrup. All of these eight sugars were tested in inhibition ELISAs (maximal concentration 250 mM) with GII.10 VLPs (protocol Table 2-19, in duplicates, Figure 3-40). None of the eight glycans appeared to be the compound in date syrup causing the strong inhibition (maximal inhibition values observed with the eight glycans 10 – 44 %).

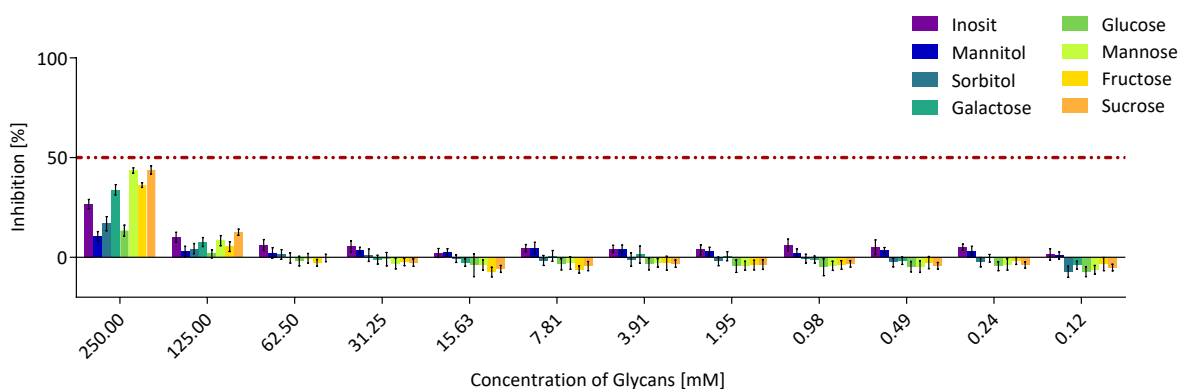


Figure 3-40: Attachment inhibition of GII.10 VLPs by glycans identified in date syrup. Maximal inhibition observed varied between 10 and 44 % at concentrations of 250 mM. IC_{50} marked as dashed/double dotted line (red). Measurements were performed in triplicates. Error bars show SD.

Wine: Inhibition by Wine and Grape Juices

Since tannic acid was shown to inhibit noroviruses [21] and red wine is high in tannins, some wine samples were tested. All red wines and grape juices exhibited high inhibition (maximal inhibition of all ~100 %). Best inhibition showed red wines Syrah (IC_{50} = 0.26 %), Tempranillo (0.31 %), Merlot (0.34 %), and red Burgunder (0.43 %, Figure 3-41). Closely followed by red grape juices where the IC_{50} values were about twice the values observed with red wines: red grape juice Krämer (IC_{50} = 0.86 %), Merlot grape juice (0.92 %), and red grape juice REWE (1.02 %). White wine and juice displayed a maximal inhibition of ~50 % and also showed higher IC_{50} values of ~31 % for white grape juice Kumpf and white Burgunder. Freshly produced (largely unfermented) red and white wine (namely new red wine and new white wine), as well as Merlot juice from another batch were screened. All three samples showed attachment inhibition (Figure 3-41) but displayed lower inhibition compared to date syrup or wines. Still

Screening for Natural Extracts as Antivirals

inhibition was higher than observed with most other natural extracts. Interestingly, the IC_{50} values for new red wine (1.65 %) and merlot juice (1.20 %) were higher than new white wine (9.58 %).

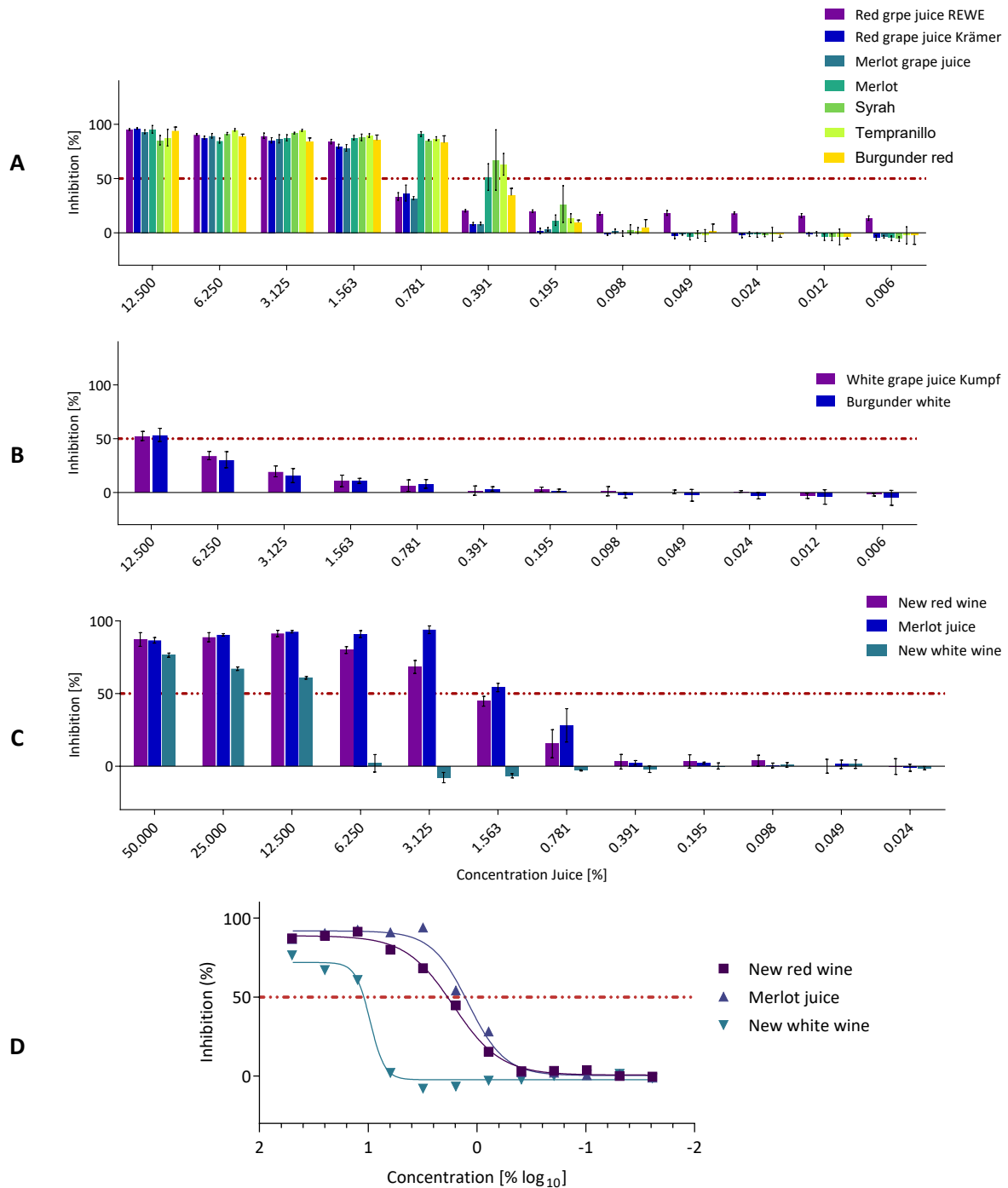


Figure 3-41: Attachment inhibition of GII.10 VLPs with wines and juices

A: All red wines and grape juices exhibited high inhibition (maximal inhibition of all ~100 %, IC_{50} values: 1.02 % for red grape juice REWE, 0.86 % for red grape juice Krämer, 0.92 % for Merlot grape juice, 0.34 % for Merlot, 0.26 % for Syrah, 0.31 % for Tempranillo, and 0.43 % for red Burgunder). B: White wine and juice displayed a maximal inhibition of ~50 % and also showed lower IC_{50} values (31 % for white grape juice Kumpf and white Burgunder). All grape juices in A and C showed good inhibition. C: Bar chart of Inhibition by grape juices (IC_{50} 1.65% for new red wine, 1.20 % for Merlot juice, and 9.58 % for new white wine). D: Line chart of regression fit to calculate IC_{50} values for grape juice inhibition by Graphpad Prism (\log_{10} of concentrations). In both charts, the IC_{50} is indicated by the red dashed/dotted line. Measurements were performed in triplicates. Error bars show SD.

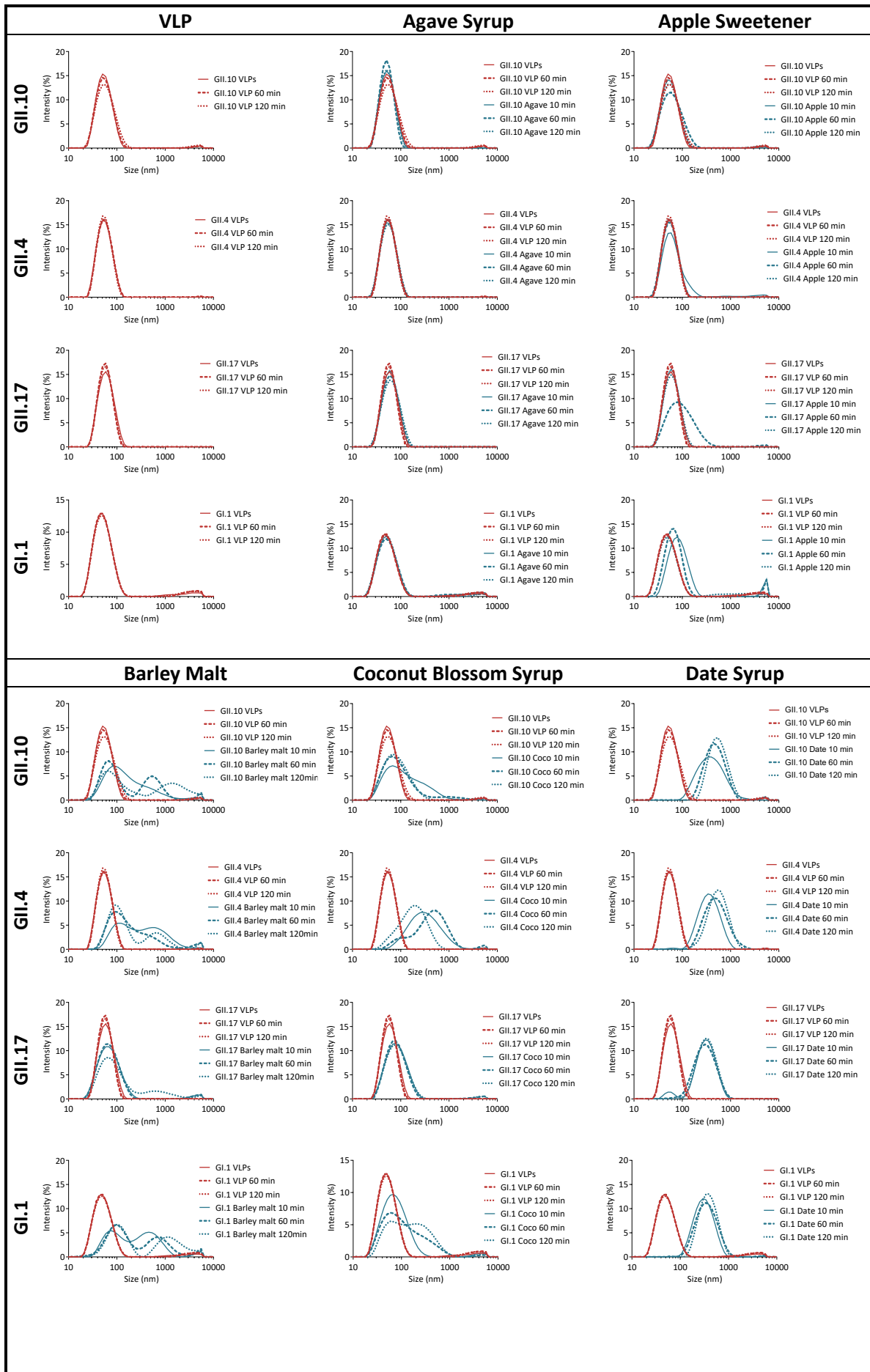
Plant Derived Syrups and Saps – DLS and EM: Assessing VLP integrity upon Treatment

To analyze the influence of the natural extracts on VLP integrity, the hydrodynamic diameters of VLPs (GII.10, GII.4, GII.17, GI.1) were evaluated. All DLS analyses were performed in triplicates at 10, 60, and 120 min. Untreated VLPs were included in the measurements for comparison.

Agave syrup, apple sweetener and maple did not cause peak shifts at the given concentrations with any of the given VLPs (Figure 3-42). Treatment with coconut blossom syrup showed slight peak shifts with GII.10, GI.1 and GII.17 VLPs (Figure 3-42) indicating formation of small aggregates while many single particles were still present. For GII.4 VLPs, the peak shifts were more prominent (Figure 3-42), indicating more severe aggregation. With date syrup, a large peak shifting towards increased diameters for all genotypes tested was measured (Figure 3-42). This suggests the formation of massive aggregates with only a minor proportion of single particles.

To validate DLS results structural integrity of VLPs after treatment with natural extracts was also assessed in EM. Results of electron microscopy are summarized in Table 3-6 along with results obtained in DLS and ELISA. EM analysis showed that date syrup and barley malt caused formation of compact aggregates with GII.10, GII.4 and GII.17 VLPs. With barley malt single particles were still frequent whereas with date syrup only occasional single particles were observed. Incubation of GII.10, GII.4 and GII.17 VLPs with apple sweetener was indistinguishable from untreated VLPs. This was also observed with GII.10 VLPs after treatment with coconut blossom syrup and GII.4 VLPs after treatment with maple syrup. In all other cases treatment with natural extracts caused formation of large aggregates while still many single VLPs were observed. A very special observation was made upon treatment of any of the tested VLPs with royal jelly. Presence of royal jelly was marked by long rods in the specimen of approximately the same diameter as the VLPs. Due to these rods only very few VLPs could be observed. Therefore, VLP integrity was not evaluated with this treatment.

Screening for Natural Extracts as Antivirals



Screening for Natural Extracts as Antivirals

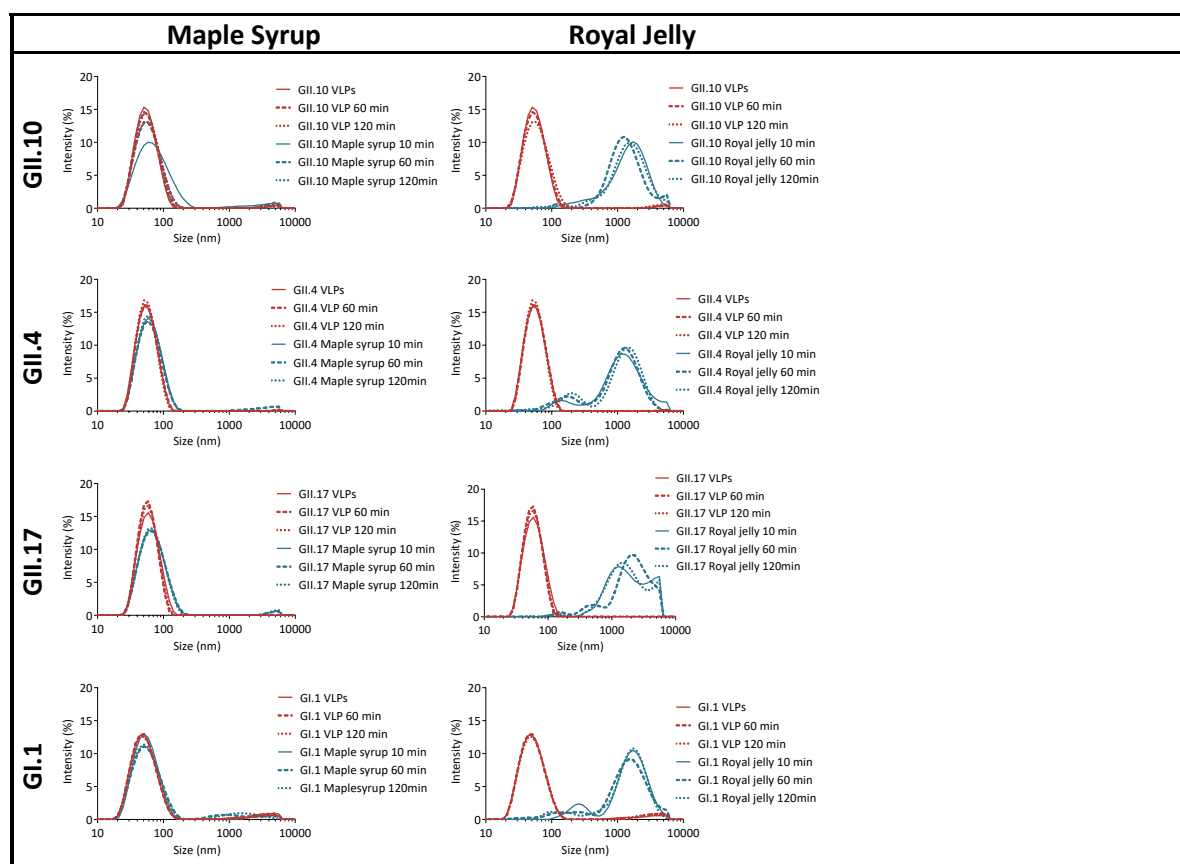


Figure 3-42: DLS measurements of different VLPs after treatment with natural extracts GII.10, GII.4, GII.17, and GI.1 VLPs as indicated on the left. VLPs were treated with natural extracts for 10 min, 60 min, or 120 min as indicated in each graph. All graphs contain untreated VLPs (red) for comparison. Date syrup and royal jelly induced a strong peak shift indicating formation of aggregates. Coconut blossom syrup and barley malt caused milder peak shifts indicating the presence of smaller aggregates and single particles. Agave syrup, apple sweetener, and maple syrup showed no shifting towards larger particle sizes.

Table 3-6: Summary result of ELISA, EM, and DLS natural extracts using different types of VLPs

Extract	IC ₅₀ Values					EM			DLS			
	GII.10	GII.4	GII.17	GI.1	GII.1	GII.10	GII.4	GII.17	GII.10	GII.4	GII.17	GI.1
Coco	n.a.	5.84	9.69	7.88	n.a.	SP	LA + SP	LA + SP	Slight shift	Shift	Slight shift	Slight shift
Date	0.11	0.056	0.14	0.15	0.49	Big CA + few SP	Big CA + few SP	Big CA + few SP	Strong shift	Strong shift	Strong shift	Strong shift
Agave	n.a.	n.a.	n.a.	n.a.	4.96	LA + SP	LA + SP	LA + few SP	No shift	No shift	No shift	No shift
Apple	n.a.	14.96	10.07	n.a.	2.53	SP	SP	SP	No shift	No shift	No shift	No shift
Royal jelly	n.a.	n.a.	n.a.	n.a.	n.a.	Rods, few SP + agg.	Rods, few SP + agg.	Rods, few SP + agg.	Very strong shift	Very strong shift	Very strong shift	Very strong shift
Barley malt	n.a.	0.90	n.a.	n.a.	2.71	CA + SP	CA + SP	CA + SP	2 peaks	2 peaks	No shift	2 peaks
Maple	n.a.	n.a.	n.a.	n.a.	10.17	LA + SP	SP	LA + SP	No shift	No shift	No shift	No shift

Note: IC₅₀ values in % of original extracts, SP (single particle), LA (large aggregates), CA (compact aggregates), n.a. (not applicable – usually because of too low maximal inhibition). Intensity of colors indicates strong or weak effects, background (white) indicates unclear result.

3.2.3 Honey

Honey - Structural Analysis: GII.10 026 P domain Co-Crystals

In addition to the X-ray crystallography screening of various natural extracts (0), three GII.10 026 P domain crystals were soaked with a honey (provided by Dr. Grant Hansman). Unidentified densities within the structure of P domain crystals soaked with honey were observed (Figure 3-43 and Table 3-7).

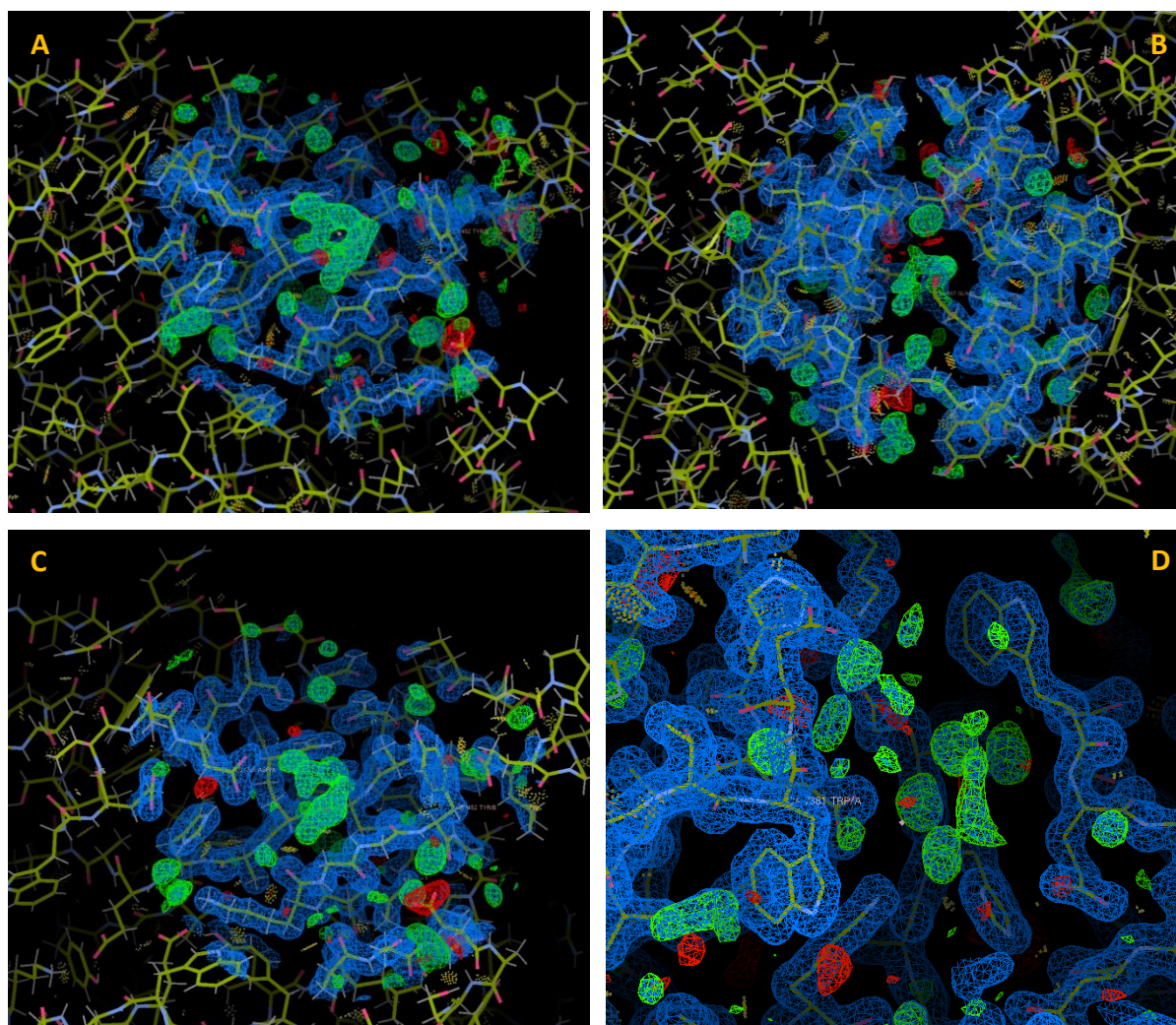


Figure 3-43: Structure analysis of GII.10 026 P domain crystals in complex with honey
 A: Honey crystal 1, ring in the HBGA binding site at the top of the P domain and
 B: ring between His468A/B at the bottom of the P domain between the dimers
 C: Honey crystal 2, ring fragment in the HBGA binding site at the top of the P domain
 D: Honey crystal 3, weaker density of a ring between 381A/B in the channel at the top of the P domain.
 All X-ray crystallography data were collected at ERSF, ID29. Honey sample was provided by Dr. Grant Hansman

Screening for Natural Extracts as Antivirals

Table 3-7: Structure analysis GII.10 P domain crystals soaked with natural extracts

Natural Extract	No of crystals	Comments
Honey	1	Ring A385 2 symmetric blobs between 381A/B Blob between 468A/B
Honey	3	Ring site 1 2 symmetric blobs between 381A/B Ring between 468A/B
Honey	5	2 symmetric blobs between 381A/B

Two additional densities were identified in P domain crystals soaked with honey. One was located in the regular HBGA binding site of the P domain, whilst the other was found in the central channel between the two dimers of the P domain. The shape of both densities resembled a glycan ring. However, identification of the ligands with no other information about the molecule than locked parts of the shape in X-ray crystallography is nearly impossible. Many ‘rings’ are known in chemistry that might fit into the density. Moreover, determination of the compound was obstructed by possible movement or differential sterical states within the crystal.

Honey - ELISA: Inhibition in a Surrogate HBGA Attachment Inhibition Assay

A set of 31 different types of honey (Table 2-7) was tested for their inhibition against norovirus using ELISA. Moreover, it was analyzed how different regional and consequently herbal origins might influence the inhibition caused by honey. The different types of honey were screened for their ability to inhibit attachment of GII.10 VLPs to PGM (Appendix Figure A I-3). Of these 31 different types of honey, ten (alpine forest honey, coriander honey, eucalyptus honey, fir honey I, fir honey II, Mexico honey, oak honey, orange blossom honey, raspberry honey, robinia honey) were selected and are presented in this chapter (GII.10-protocol Table 2-19, GII.4 protocol Table 2-20, but for both new anti-rabbit 1:40,000). All ten of the selected honeys showed inhibition of GII.10 VLPs (Figure 3-44 A). Inhibition with both genotypes (GII.10 and GII.4) could only be observed at comparatively high concentrations, with IC₅₀ values ranging from 3.38 % to 24.77 % depending on the respective honey and VLP (Table 3-8). The highest inhibition was observed with alpine forest honey (IC₅₀=3.38 % with GII.10 and IC₅₀=4.78 % with GII.4), raspberry honey (IC₅₀=5.60 % with GII.10 and IC₅₀=4.72 % with GII.4), oak honey (IC₅₀=6.11 % with GII.10 and IC₅₀=5.85 % with GII.4), and eucalyptus honey (IC₅₀=5.96 % with GII.10 and IC₅₀=6.22 % with GII.4) (Figure 3-44 A and B). The broad reactivity of different types of honey and the additional densities observed in crystallography experiments attracted my

interest. Could there be some compound common to the inhibiting types of honey (mainly collected from trees) that might cause the inhibition. This resulted in the idea of additionally testing propolis for its inhibitory potential.

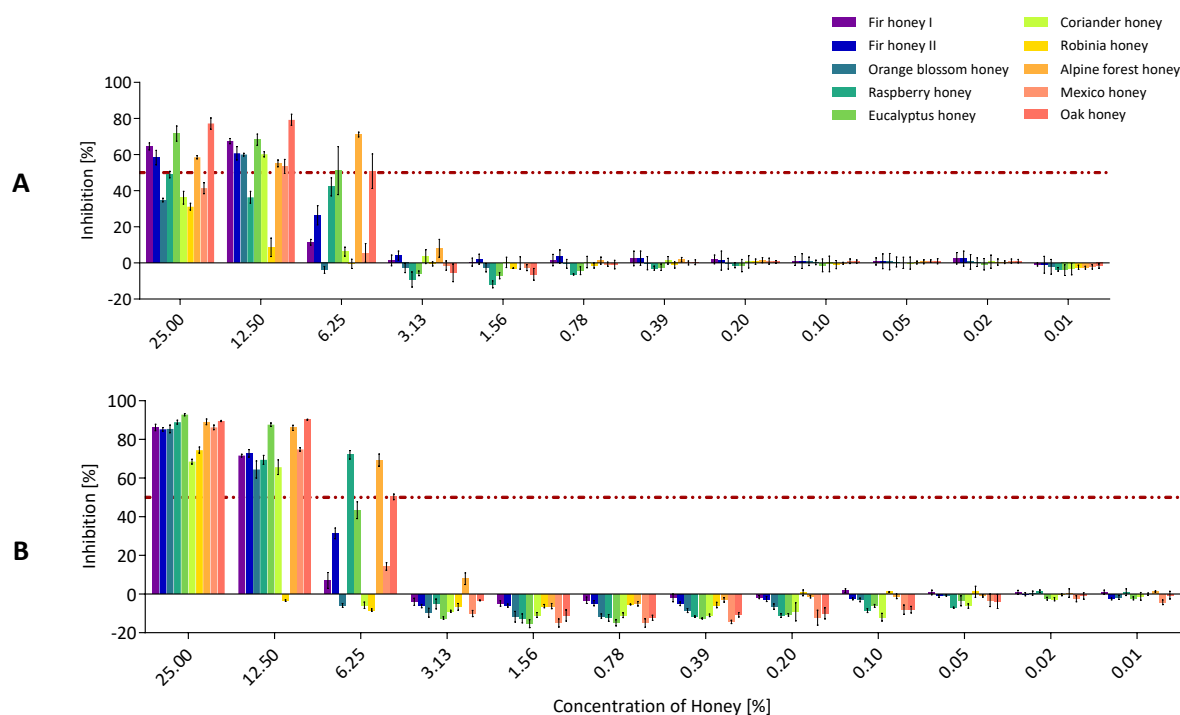


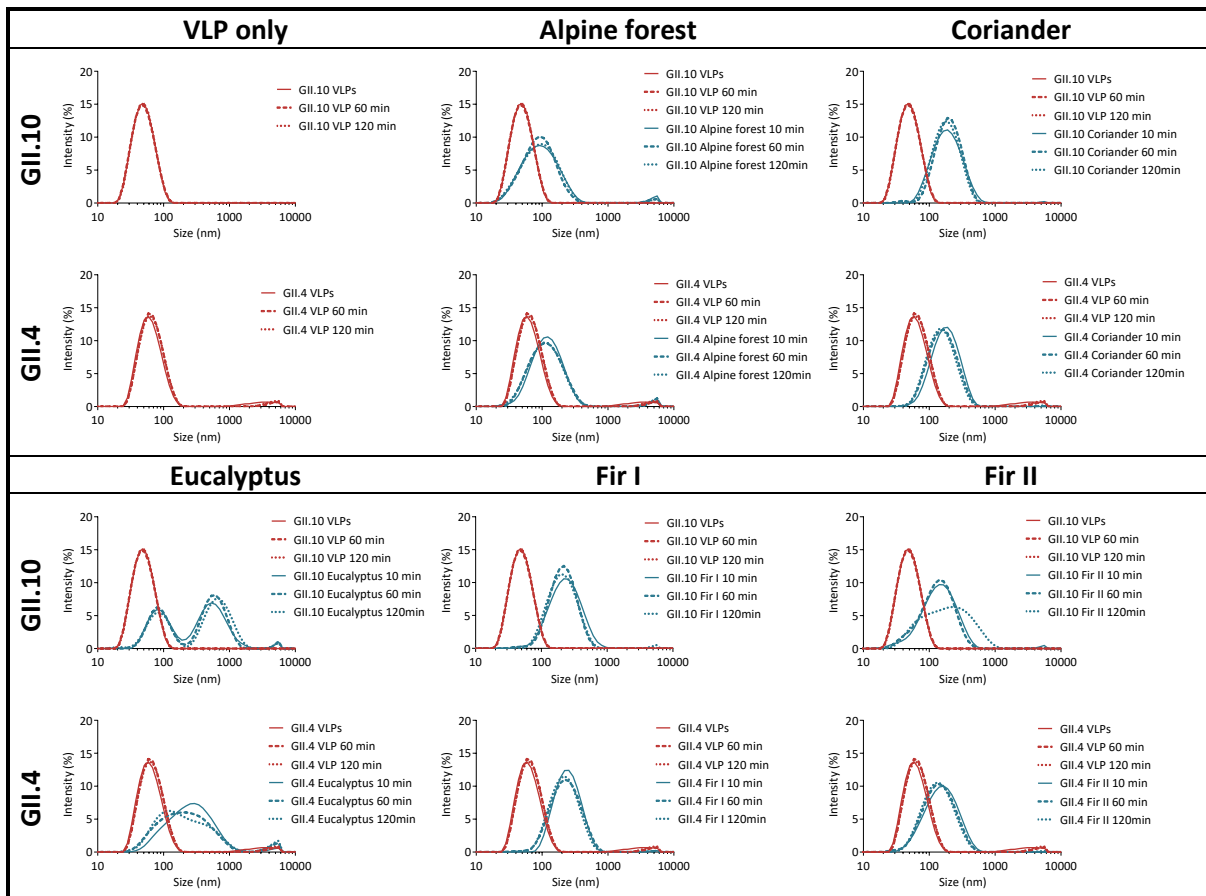
Figure 3-44: Attachment inhibition of GII.4 and GII.10 VLPs by different types of honey
 A: Inhibition with GII.10 VLPs. Highest inhibition was observed with alpine forest honey ($IC_{50}=3.38\%$), raspberry honey ($IC_{50}=5.60\%$), eucalyptus honey ($IC_{50}=5.96\%$), and oak honey ($IC_{50}=6.11\%$). B: Inhibition with GII.4 VLPs. Highest inhibition was observed with raspberry honey ($IC_{50}=4.72\%$), alpine forest honey ($IC_{50}=4.78\%$), oak honey ($IC_{50}=5.85\%$), and eucalyptus honey ($IC_{50}=6.22\%$). IC_{50} is indicated as dashed/dotted line (red) Measurements were performed in triplicates. Error bars show SD.

Honey - DLS and EM: Aggregation of VLPs upon Treatment

Similar to other potential inhibitors (including natural extracts), DLS measurements were performed to assess changes in VLP particle size upon treatment such as aggregation, disintegration or swelling.

In DLS, all 10 types of honeys showed peak shifts indicating formation of aggregates (Figure 3-45, Table 3-8). Peak shifts observed with GII.10 and GII.4 VLPs were comparable, except for eucalyptus, raspberry, and robinia honey. Eucalyptus honey caused the formation of two prominent peaks with GII.10 VLPs (Figure 3-45, eucalyptus). The first and smaller peak contained most likely many single particles whereas the second peak presumably comprised of aggregates. With GII.4 VLPs, a single peak was observed but with a massive shoulder towards larger particle sizes (Figure 3-45, eucalyptus B). This indicated the formation of small aggregates while many single particles were present. The second exception, Raspberry honey

also led to formation of two peaks with GII.10 VLPs in DLS, one indicated the presence of single particles, while the other smaller peak indicated aggregates (Figure 3-45, raspberry). With GII.4 VLPs on the other hand, only a minor peak shift could be observed (Figure 3-45, raspberry B). Formation of a shoulder facing towards larger particle sizes indicated formation of small aggregates while still mainly single particles were present. The third exception was robinia honey, which showed remarkable differences with GII.10 and GII.4 VLPs. The peak shift observed with GII.10 VLPs was the strongest among the different types of honey, indicating formation of large aggregates (Figure 3-45, robinia). Upon treatment of GII.4 VLPs, the shift was considerably smaller (Figure 3-45, robinia) indicating formation of small aggregates. VLP integrity upon treatment with different types of honey was also analyzed in EM experiments (Table 3-8). Treatment of GII.10 and GII.4 VLPs with raspberry honey was indistinguishable from untreated VLPs. Treatment of GII.10 VLPs also showed no effect on VLP integrity in EM. After treatment with all other types of honey formation of aggregates was observed in EM. Fir honey I and oak honey showed formation of larger aggregates with fewer single particles visible than the other honeys.



Screening for Natural Extracts as Antivirals

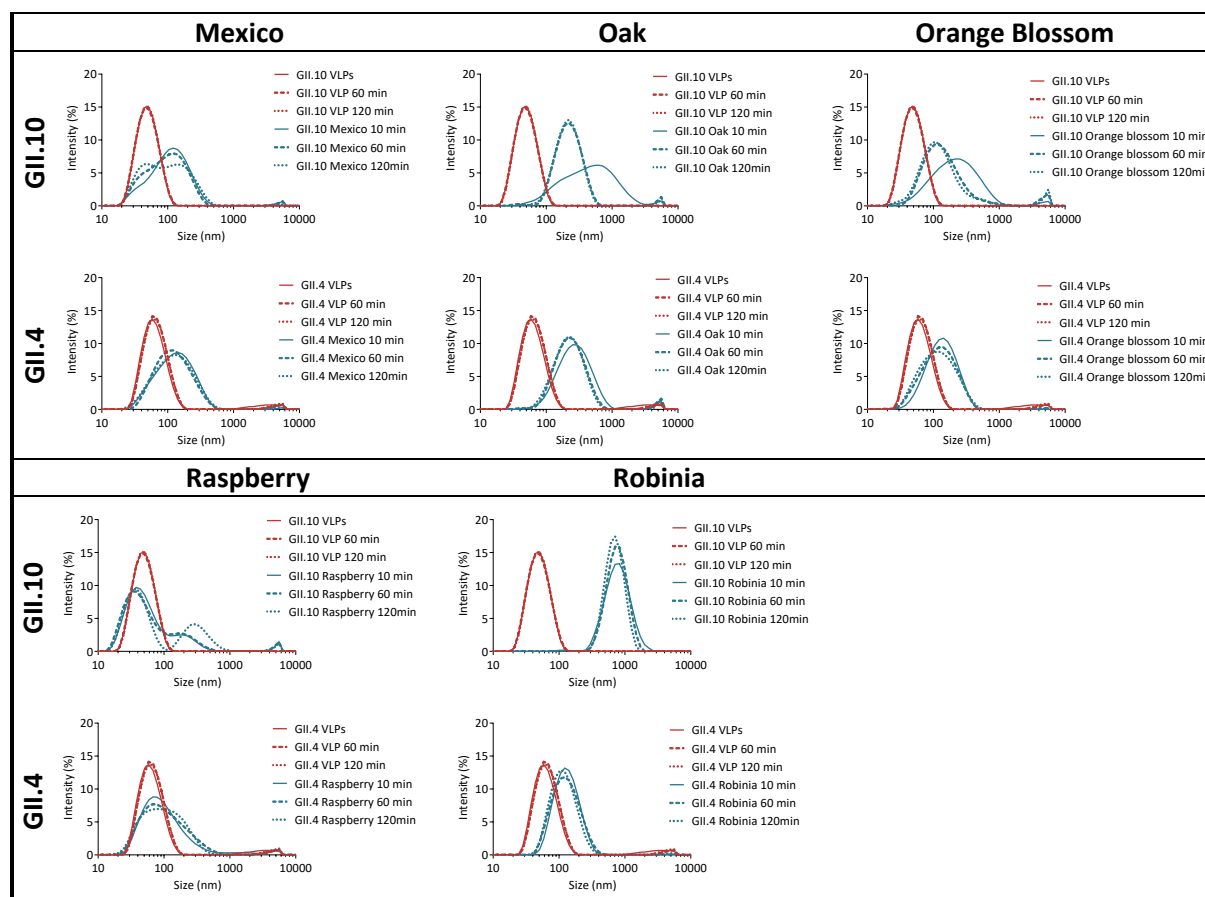


Figure 3-45: DLS measurements of different VLPs after treatment with different types of honey. GII.10 and GII.4 VLPs were either untreated as a control or treated with different types of honey as indicated. Treatment for 10 min, 60 min, or 120 min as indicated in each graph. All graphs contain untreated VLPs (red) for comparison.

Table 3-8: Summary result of ELISA, EM, and DLS of GII.10 and GII.4 VLPs treated with honey

Types of honey	IC ₅₀ Values		EM		DLS	
	GI.10	GI.4	GI.10	GI.4	GI.10	GI.4
Raspberry honey	5.60	4.72	SP	SP	2 peaks	Slight shift
Fir honey I	6.74	9.39	LA + few SP	Big CA + few SP	Shift	Shift
Orange blossom honey	9.55	11.75	LA + SP	LA + SP	Shift	Slight shift
Fir honey II	6.39	7.05	LA + SP	LA + SP	Shift	Slight shift
Eucalyptus honey	5.96	6.22	LA + SP	LA + SP	2 peaks	Slight shift
Coriander honey	6.82	8.95	LA + SP	LA + SP	Shift	Slight shift
Robinia honey	15.26	24.77	LA	LA + SP	Very strong shift	Slight shift
Alpine forest. honey	3.38	4.78	SP	LA + few SP	Slight shift	Slight shift
Mexico honey	6.69	8.02	LA + SP	LA + SP	Slight shift	Slight shift
Oak honey	6.11	5.85	Big LA + few SP	Big LA + few SP	Shift	Shift

Note: IC₅₀ values in % of original matter, SP (single particle), LA (large aggregates), CA (compact aggregates)

Honey - Analysis of Aging in Attachment Inhibition ELISA

The inhibiting compound in honey seems to be temperature sensitive and can be degraded over time. Honey samples kept at 4°C performed better than the same samples kept at RT. Three different honeys that showed high inhibition in previous experiments were tested. Of each, a pre-dilution kept at 4°C (old) and a new pre-dilution (new) of pure honey samples that were stored at RT were used. Pre-dilutions kept at 4°C showed comparable inhibition observed one year prior, whereas the new pre-dilutions (from stocks kept at RT) showed no inhibition at the same concentrations (protocol Table 2-20, Figure 3-46), suggesting temperature sensitivity or aging of the active compound.

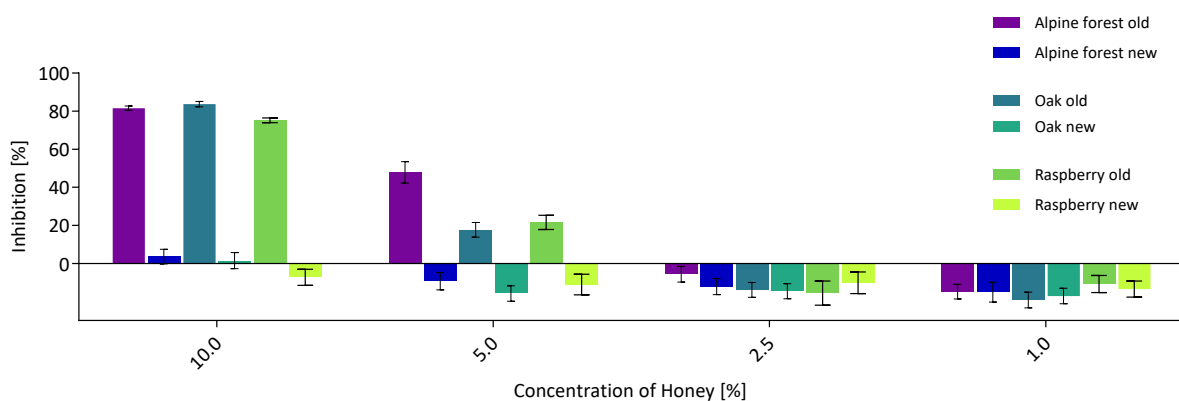


Figure 3-46: Attachment inhibition ELISA of GII.4 VLPs by honey, aging effect
 Re-testing of previously examined honey samples. Pre-dilution kept at 4°C (old) and a new pre-dilution (new) of honey samples that were stored at RT. Honey kept at RT showed no inhibition compared to equal concentrations of honey samples stored at 4°C.

3.2.4 Propolis

Propolis - Evaluation in Preliminary Attachment Inhibition ELISA

Eight different extracts of a single propolis sample were prepared (2.1). As described, the same propolis/solvent ratio and protocol was used for all extracts, the only parameter varied was the solvent used for extraction. In a first attachment inhibition ELISA, all propolis samples (3-day extraction) exhibited inhibition (Figure 3-47, protocol Table 2-19, but anti-rabbit 1:5000). Among the better inhibitors were 95 % ethanol ($IC_{50} = 5.7$ %), 70 % ethanol ($IC_{50} = 2.9$ %), propanediol ($IC_{50} = 2.3$ %), and DMSO ($IC_{50} = 2.1$ %) whereas glycerol ($IC_{50} = 14.3$ %), 15 % ethanol (not applicable) or H₂O ($IC_{50} = 11.6$ %) were considerably higher.

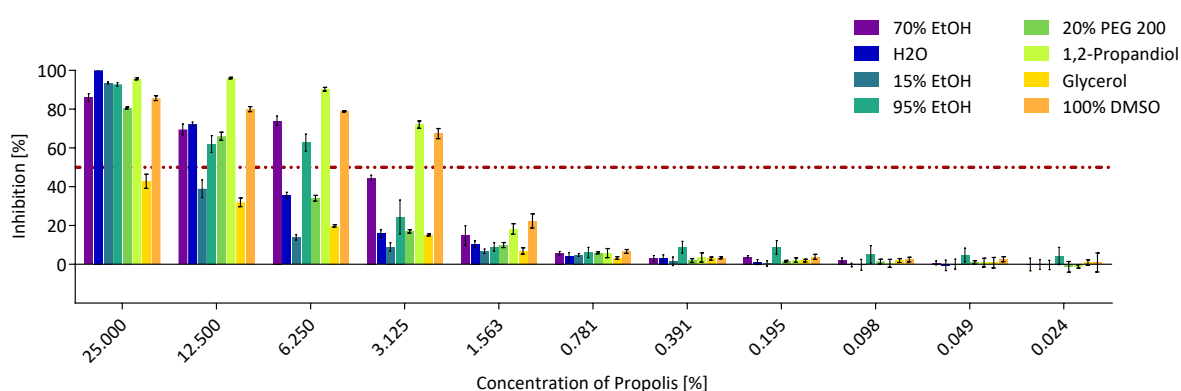


Figure 3-47: Attachment inhibition of GII.10 VLPs by eight different propolis extracts

All Propolis extracts showed attachment inhibition of GII.10 VLPs: 70 % ethanol ($IC_{50} = 2.9$ %), H₂O ($IC_{50} = 11.6$ %), 15 % ethanol (n. a.), 95 % ethanol ($IC_{50} = 5.7$ %), 20 % PEG200 ($IC_{50} = 8.6$ %), propanediol ($IC_{50} = 2.3$ %), glycerol ($IC_{50} = 14.3$ %), and DMSO ($IC_{50} = 2.1$ %). IC_{50} is indicated as dashed/double dotted line (red). Single experiment; measurements were performed in triplicate wells, error bars shown.

For some of the propolis samples (95 % ethanol, 70 % ethanol, 1,2-propandiol, and 100 % DMSO) precipitation of beeswax in the wells of the ELISA-plates (for high concentrations of propolis) were observed after pre-incubation of propolis samples and VLPs in the coated wells (extracts are diluted 1:1 with VLPs in PBS). To determine if this interfered with the assay, an assay without VLPs was performed (protocol Table 2-19, but anti-rabbit 1:5000). In this assay only a serial dilution of the respective propolis was added to the wells. Consequently, the wells were blank, equaling to an inhibition of 96.8-100 % (Figure 3-48). The propolis-precipitates in the wells did not cause detectable signal or unspecific retention of detection antibodies, which would cause a signal.

Screening for Natural Extracts as Antivirals

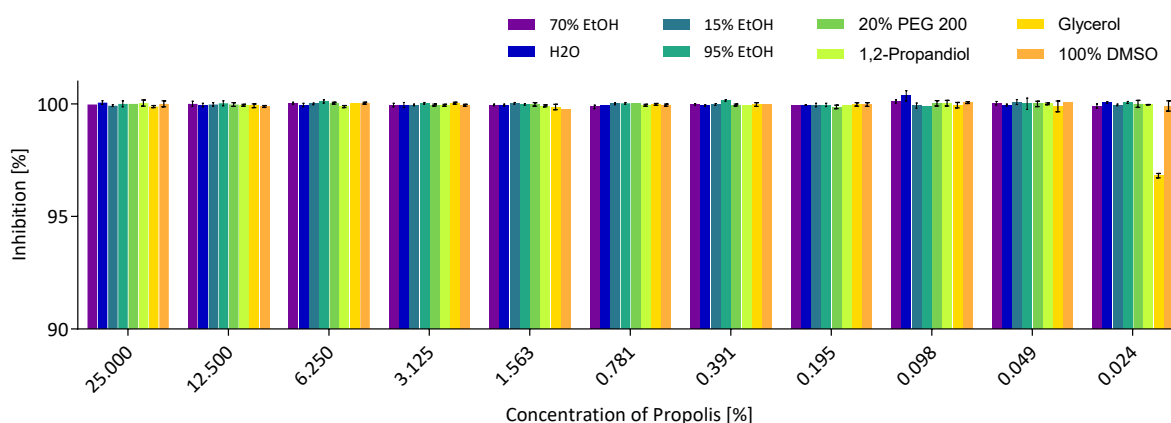


Figure 3-48: Attachment inhibition ELISA, testing propolis without VLPs

To determine if precipitated beeswax might interfere with the assay, an assay without VLPs was performed. Only serial dilution of the respective propolis was added, no VLPs in the wells. In absence of VLPs consequently 'inhibition' of 96.81-100 % was observed. No detectable signal or unspecifically retention of detection antibodies was observed. Y-axis range 90–100 % to make small differences at high inhibition levels visible.

In another experiment, VLPs were incubated with a serial dilution of the respective solvent (used for preparation of respective propolis extract) to test inhibition caused by solvent without propolis. This yielded a very high detection level (>95 % inhibition), suggesting that the solvents did not interfere with the assay.

In another ELISA, propolis was serially diluted in the respective solvent instead of PBS. Therefore, the attachment inhibition assay was repeated with propolis, but extracts and VLPs were diluted in their respective solvent. The high concentration of some of the solvents made this assay highly artificial but eliminated the possibility that the inhibition was based on the precipitation of beeswax. VLP signals were much lower with 95 % ethanol and 100 % DMSO, resulting in a low inhibition throughout the assay (similar to influence of DMSO in Figure 3-4). Both extracts were removed from the graph (Figure 3-49) because the OD₄₉₀ in all wells (including positive control) were below 0.5. Also, glycerol was removed as a solvent in this assay because the high viscosity made precise pipetting of the serial and transfer of the dilution row into ELISA wells impossible. In other assays, the propolis extracts were serially diluted in PBS (thereby stepwise reducing viscosity) making usage of 98 % glycerol propolis extract applicable.

Screening for Natural Extracts as Antivirals

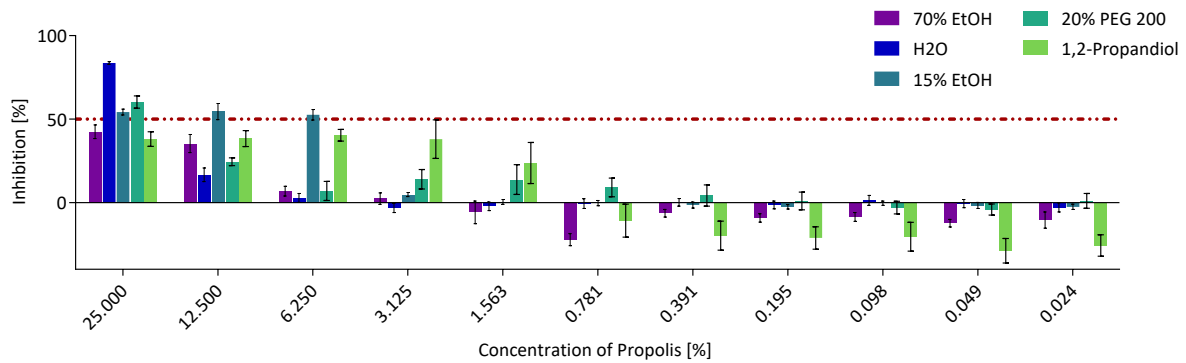


Figure 3-49: Attachment inhibition ELISA GII.10 VLPs by propolis extracts, serial dilution in respective solvent
Propolis extracts were serially diluted in the respective solvent instead of PBS to monitor the effect of the high concentrations of the solvents on the assay/on inhibition. 95 % ethanol and 100 % DMSO were excluded because of very low OD_{490} in all wells (including positive control, below 0.5). Glycerol extract was also excluded because the high viscosity led to pipetting errors in the serial dilution. IC_{50} values ranged between 8 – 1.1 %. IC_{50} is indicated as dashed/double dotted line (red). Single experiment; measurements were performed in triplicate wells, error bars shown

Inhibition of GI.1 VLPs by eight different propolis extracts was analyzed to evaluate potential cross-reactive inhibition (protocol Table 2-21, but Nano-60 1:50,000). All extracts showed inhibition of GI.1 VLPs (70 % ethanol IC_{50} = 2.3 %, H₂O IC_{50} = 2.4 %, 15 % ethanol IC_{50} = 3.0 %, 95 % ethanol IC_{50} = 1.8%, 20 % PEG IC_{50} = 1.8 %, propanediol IC_{50} = 2.9 %, glycerol IC_{50} = 2.0 %, DMSO IC_{50} = n.a., Figure 3-50). DMSO and glycerol showed reduced inhibition at high concentrations compared to the remaining solvents. Both solvents exhibited problems with the assay at high concentration as described in the previous experiment. Aside from these two, other propolis extracts performed better with GI.1 VLPs than with other VLPs tested.

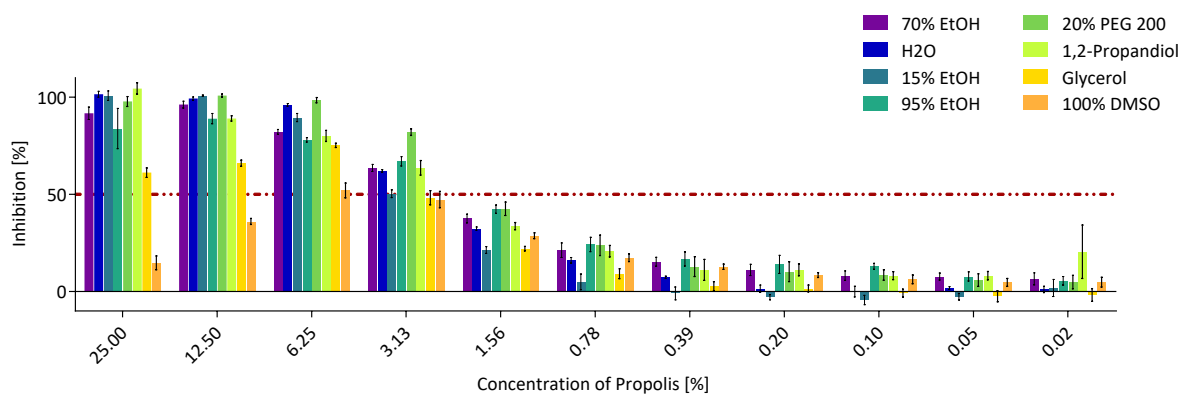


Figure 3-50: Attachment inhibition ELISA of GI.1 VLPs by propolis extracts, serial dilution
All extracts showed inhibition 70 % ethanol IC_{50} = 2.3 %, H₂O IC_{50} = 2.4 %, 15 % ethanol IC_{50} = 3.0 %, 95 % ethanol IC_{50} = 1.8 %, 20 % PEG IC_{50} = 1.8 %, propanediol IC_{50} = 2.9 %, glycerol IC_{50} = 2.0 %, DMSO IC_{50} = n.a. IC_{50} is indicated as dashed/double dotted line (red). Single experiment; measurements were performed in triplicate wells, error bars shown

The propolis matter used for extraction was incubated with fresh 10 ml of (respective) solvent after the first extraction. The aim was to see how much of the inhibiting compound was left after the first extraction and to evaluate if the extraction was complete. In a single attachment inhibition ELISA with GII.10 VLPs (protocol Table 2-19, but anti-rabbit 1:5000), the inhibition by first and second extract were compared (data not shown). The second extracts of 95 % ethanol, 70 % ethanol DMSO and 1,2-propanediol showed greatly reduced inhibition (e.g. at a concentration of 12.5 %, a reduction of 76 %, 87 %, 83 %, 75 % for the respective solvents). On the other hand, for extracts in 15 % ethanol, water, 20 % PEG200, and glycerol less reduction in inhibition was observed (at a concentration of 12.5 %, reduction by 58 %, 24 %, 20 % for the respective solvents).

After discovering that some propolis still contained active compound for GII.10 VLPs inhibition after the first extraction, the extraction process was prolonged in attempt to improve performance of the extracts. The idea was to improve the performance of 'less cell toxic' extracts, such as water or low concentrations of ethanol, because so far only extracts with high DMSO or ethanol concentrations showed high inhibition, both of which are not suitable for testing in cell culture. Performance of 3-day and 30-day propolis extracts of eight different solvents were tested in an attachment inhibition ELISA with GII.10 VLPs (protocol Table 2-19, but anti-rabbit 1:5000). The inhibitory capability of 3-day extracts and 30-day extracts were compared (data not shown), but only little differences were observed when 95 % ethanol, DMSO, and water were used for extraction. The first two seemed to rapidly extract the inhibiting compound leaving nothing to extract any further in the additional time, while water might simply reach its limited maximal extraction capacity within a short time. The 30-day extraction performed slightly better than the 3-day extraction in four cases: 70 % ethanol, 15 % ethanol, 20 % PEG200, and 1,2-propanediol (at a concentration of 12.5 % inhibition improvement by 14 %, 13 %, 19 %, 8 %). These solvents could slightly benefit from the extended extraction time. The only extract performing substantially better after 30 days compared to 3 days was glycerol (at a concentration of 12.5 %, inhibition was improved by 54 %).

Especially the hydrophobic organic solvents dissolve beeswax when preparing the extracts. When the concentration of the respective solvent is lowered (adding PBS during dilution or when adding VLPs) some wax precipitates in the wells (as described previously). Apparently, this has only minor influence on the ELISA experiment. The amount of beeswax was reduced by stepwise lowering the temperature to 4°C during centrifugation to gradually precipitate the wax from the solvent. In some of the extracts, wax precipitated and was removed by filtration. With this method a lot of wax could be removed from the extracts. Still a considerable amount of precipitation occurred during ELISA and only a minor difference in inhibition was observed between wax and no wax removal. This suggests that wax is not the main causative for the inhibition and does not influence the OD₄₉₀ measurement. Of note, the presence of Tween20 in the washing buffer usually completely removed the precipitated wax from the wells before the final measurement.

Since propolis is a mixture of resins collected by bees in the surrounding of their hive, the composition of propolis is highly dependent on location of the hives. Propolis from three different origins were extracted and inhibition was compared in attachment inhibition ELISAs with GII.10 VLPs (protocol Table 2-19, but anti-rabbit 1:5000). The overall performance was comparable with slight differences only observable in water, 20 % PEG200 and 15 % ethanol extracts (data not shown). However, all propolis samples were from the south west of Germany and therefore most likely comprised similar compounds collected from similar plants.

Propolis - ELISA: Inhibition in a Surrogate HBGA Attachment Inhibition Assay

Eight different extracts of propolis were prepared, three of which were selected and presented here. Solvents used were 20 % PEG200, 70 % ethanol, 100 % DMSO, and one propolis extract was purchased as a ready-to-use tincture of 96 % ethanol. All were tested in inhibition ELISAs with VLP + solvent and PBS + solvent as controls (4 wells each). As these values represent the maximum and minimum OD₄₉₀ levels obtained upon the addition of propolis extracts, they were used to calculate the percentage of inhibition. All propolis extracts showed attachment inhibition with both GII.10 (Figure 3-51 A) and GII.4 (Figure 3-51 B) VLPs with IC₅₀ values ranging between 0.44 % and 5.38 % (Table 3-8). The highest inhibition was observed with the propolis extract in 96 % ethanol. The IC₅₀-values of observed attachment inhibition were 0.57 % and 0.44 %, for GII.10 (Figure 3-51 A) and GII.4 (Figure 3-51

B) VLPs, respectively. However, it is possible that for production of this tincture more propolis was added to the solvent than for the other propolis extracts (produced in-house), resulting in a higher concentration of the compound causing the inhibitory effect. The second-highest inhibition observed was for DMSO extract with GII.4 VLPs (Figure 3-51 B; IC_{50} =1.74%) Interestingly, DMSO also had the lowest IC_{50} observed among the propolis extracts for GII.10 (Figure 3-51 A; IC_{50} =5.38%). The 20 % PEG200 extract and the 70 % ethanol extract showed similar inhibition with GII.10 and GII.4 VLPs (Figure 3-51 A and B; IC_{50} values 3.16 % - 5.20%). In direct comparison, the PEG200 extract performed slightly better. In the pre-testing, propolis extracts in water (data not shown) were also examined. However, inhibition of this extracts was very low, suggesting that the inhibiting compound of propolis was practically insoluble in water whereas ethanol, DMSO and PEG solutions were able to solubilize the active compound.

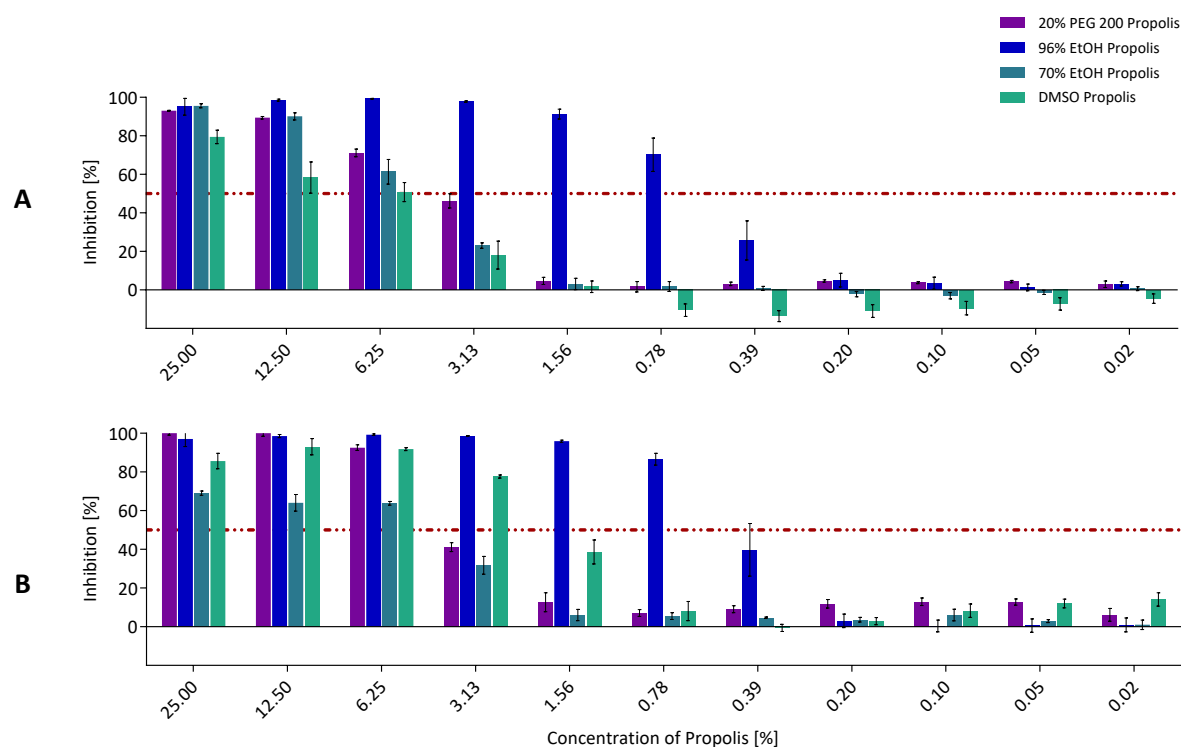


Figure 3-51: Attachment inhibition of GII.4 VLPs by different types of propolis
A: Inhibition of GII.10 VLPs by four propolis extracts. Best inhibition was observed with 96 % ethanol (IC_{50} = 0.57 %). All other extracts also showed attachment inhibition with comparable IC_{50} values of 3.47 % (20 % PEG200), 5.00 % (70 % ethanol), and 4.63 % (DMSO). B: Inhibition of GII.4 VLPs by four propolis extracts. Best inhibitors were 96 % ethanol (IC_{50} = 0.44 %) and DMSO (IC_{50} = 1.82) the other two extracts also showed attachment inhibition with IC_{50} values of 3.66 % (20 % PEG200), 3.29 % (70 % ethanol). **Positive control (0 % inhibition, maximal VLP binding signal):** VLP + Solvent at the respective concentration (a specific control for each dilution step of the serial dilution). **Negative control (100 % inhibition, minimal VLP binding value):** PBS + Propolis at the respective concentration (a specific control for each dilution step of the serial dilution). IC_{50} is indicated as dashed/double dotted line (red). Measurements were performed in triplicates. Error bars show SD.

Propolis - DLS and EM: Aggregation of VLPs upon Treatment

All propolis extracts except 20 % PEG200 caused formation of aggregates with GII.10 VLPs (Figure 3-52, Table 3-8). The largest peak shift indicating the largest aggregates could be observed upon treatment of GII.10 VLPs with 70 % ethanol extract (Figure 3-52, 70 % EtOH). DMSO and 96 % ethanol extracts caused less shifting of peaks indicating formation of smaller aggregates while more single particles were present (Figure 3-52, DMSO and 96 % EtOH). 70 % ethanol extract causing a stronger effect than 96 % ethanol extract is explainable since the extracts were produced from different propolis sources. The large peak shifts observable with GII.4 VLPs were similar between DMSO, 70 % ethanol and 96 % ethanol extracts (Figure 3-52, DMSO, 70 % or 96 % EtOH). Similar to results obtained with GII.10 VLPs, 20 % PEG 200 extract caused only a slight peak shift with GII.4 VLPs (Figure 3-52, 20 % PEG 200).

Aggregation caused by propolis extracts was also assessed in EM experiments. Upon treatment with any of the four propolis extracts (DMSO, 20 % PEG200, 70 % ethanol, 96 % ethanol) formation of aggregates was observed (Table 3-9). After treatment of GII.10 and GII.4 VLPs with 20 % PEG200 propolis extract besides large aggregates still many single particles were observed. Treatment of GII.4 VLPs with all other propolis extracts showed formation of larger aggregates and fewer single particles than observed with GII.10 VLPs. DLS and EM results were largely confirming with each other.

Table 3-9: Summary result of ELISA, EM, and DLS of GII.10 and GII.4 VLPs treated with propolis

Propolis extract	IC ₅₀ Values		EM		DLS	
	GI.10	GI.4	GI.10	GI.4	GI.10	GI.4
DMSO propolis	5.38	1.74	LA + SP	Big CA + few SP	Shift	Strong shift
20 % PEG200 propolis	3.23	3.16	LA + SP	LA + SP	No shift	Slight shift
70 % EtOH propolis	5.20	3.86	LA + SP	Big CA + few SP	Strong shift	Strong shift
96 % EtOH propolis	0.57	0.44	LA + few SP	Big CA + few SP	Shift	Strong shift

Note: IC₅₀ values in % of original matter, SP (single particle), LA (large aggregates), CA (compact aggregates)

Screening for Natural Extracts as Antivirals

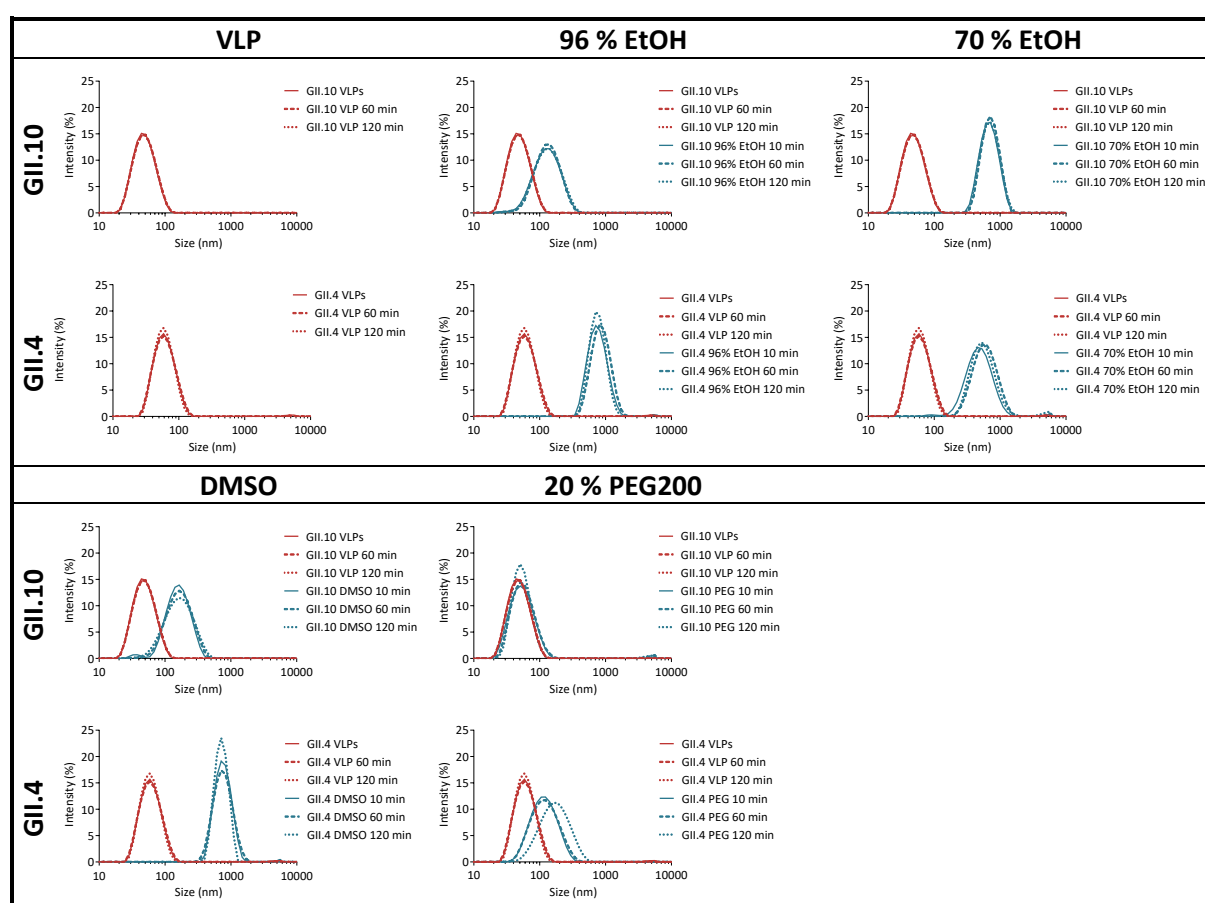


Figure 3-52: DLS measurements of different VLPs after treatment with propolis extract *GII.10*, *GII.4*, *GII.17*, and *GI.1* VLPs. VLPs were either untreated as a control or treated with natural extracts as indicated. Treatment for 10 min, 60 min, or 120 min as indicated in each graph. All graphs contain untreated VLPs (red) for comparison.

3.2.5 Polyphenolic Compounds Common to Natural Inhibitors

In search of compounds common to all natural inhibitors first a set of sugars identified as composites in date syrup were tested (Figure 3-40). The negative results obtained with these sugars as well as results of other groups suspecting different polyphenols as active antiviral components in other natural inhibitors resulted in the identification and testing of seven polyphenolic compounds common to date syrup, wines and propolis [7, 14, 39].

First a set of four tannins was tested (catechin, epicatechin, procyanidin B1, and procyanidin B2). All tannins were dissolved in 100 % DMSO and exhibited no inhibition at the tested concentrations (Figure 3-53). The highest inhibition value observed was with procyanidin B2 at a concentration of 500 $\mu\text{g/ml}$ where it exhibited 17 % inhibition. Also, pooling of all compounds did not result in inhibition.

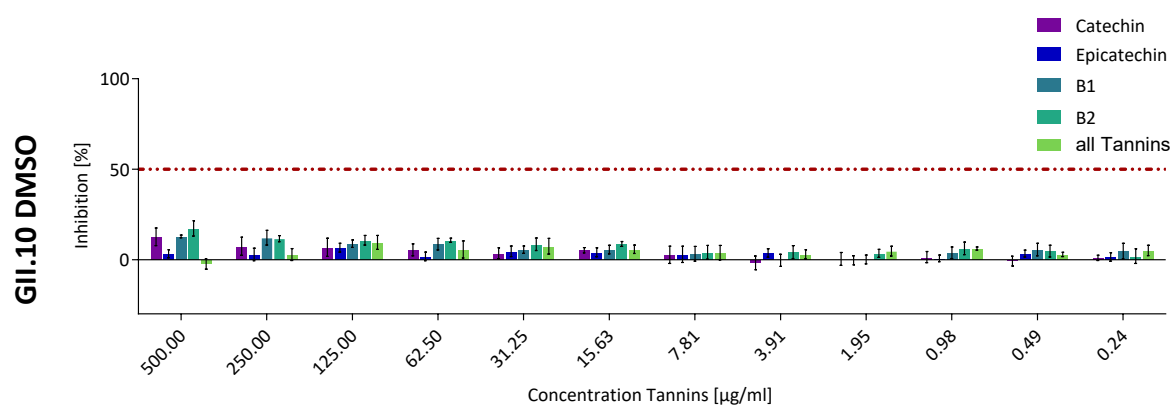


Figure 3-53: Inhibition ELISA testing four tannic compounds against GII.10 VLPs. Inhibition caused by catechin, epicatechin, procyanidin B1, and procyanidin B2 was examined with GII.10 VLPs. No high inhibition was identified. Maximal inhibition values with 500 $\mu\text{g/ml}$ of tannic compound were: 13 % (catechin), 3 % (epicatechin), 13 % (B1), 17 % (B2). Result of a single experiment is displayed; error bars show variation in triplicate wells.

Secondly a set of three flavonols was examined (quercetin, kaempferol, isorhamnetin, Figure 3-54). All flavonols were dissolved in DMSO or in 95 % ethanol for comparison. The inhibition observed with either of the flavonols highly depended on the solvent used (Figure 3-55). The most striking example for this is the maximal inhibition observed with GII.4 VLPs upon treatment with isorhamnetin dissolved in ethanol or DMSO: when isorhamnetin was dissolved in DMSO an inhibition of 98 % was observed whereas when isorhamnetin was dissolved in ethanol the inhibition decreased to 6 %. With GII.4 VLPs the lowest IC_{50} was observed for isorhamnetin dissolved in DMSO (25.8 $\mu\text{g/ml}$), followed by quercetin and kaempferol both dissolved in DMSO (80.4 $\mu\text{g/ml}$ and 136.4 $\mu\text{g/ml}$, respectively). Only quercetin showed a

similar IC_{50} value when dissolved in ethanol (60.24 $\mu\text{g}/\text{ml}$). The highest inhibition observed with GII.10 VLPs was also with isorhamnetin dissolved in DMSO (107.5 $\mu\text{g}/\text{ml}$). The maximal inhibition observed by the flavonols dissolved in DMSO was generally lower with GII.10 VLPs (43 %, 54 %, 68 % for quercetin, kaempferol, and isorhamnetin, respectively, pooled samples exhibited no inhibition) compared to GII.4 VLPs (96 %, 86 %, 98 %, 50 % for quercetin, kaempferol, and isorhamnetin, and pooled, respectively). Quercetin showed lower inhibitory potential with GII.10 VLPs (43 %, 80 % dissolved in DMSO or ethanol) than with GII.4 VLPs (96 %, 96 % in DMSO or ethanol). In general pooling of the three flavonols did not improve the inhibition obtained. With GII.4 VLPs the IC_{50} values observed for the pooled samples were: 206 $\mu\text{g}/\text{ml}$ (dissolved in DMSO, single experiment) and 227 $\mu\text{g}/\text{ml}$ (dissolved in ethanol, single experiment). Whereas with GII10 VLPs the IC_{50} values of pooled samples could not be obtained due to low maximal inhibition values.

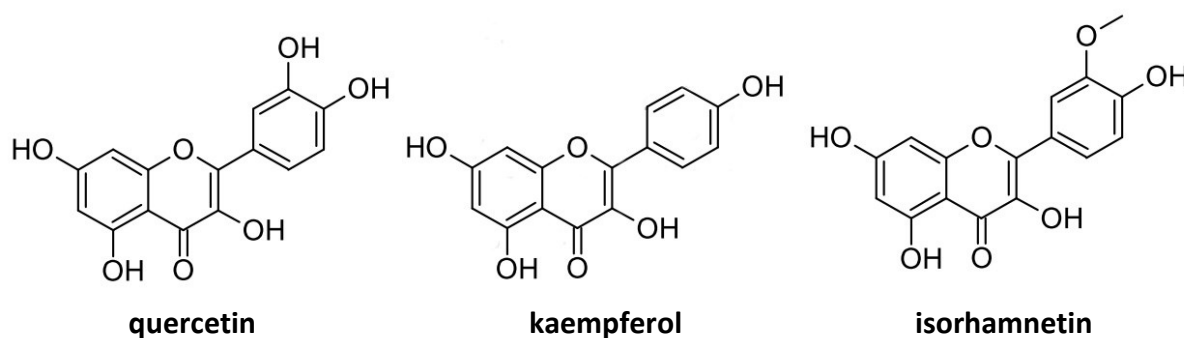


Figure 3-54: Structure formula of the three flavonols tested

Chemical notation of the three flavonols quercetin, kaempferol, and isorhamnetin. All three were identified in inhibiting natural extracts (date syrup, wine, honey, and propolis[7, 31, 39, 43, 122]). Figure modified from [31].

Screening for Natural Extracts as Antivirals

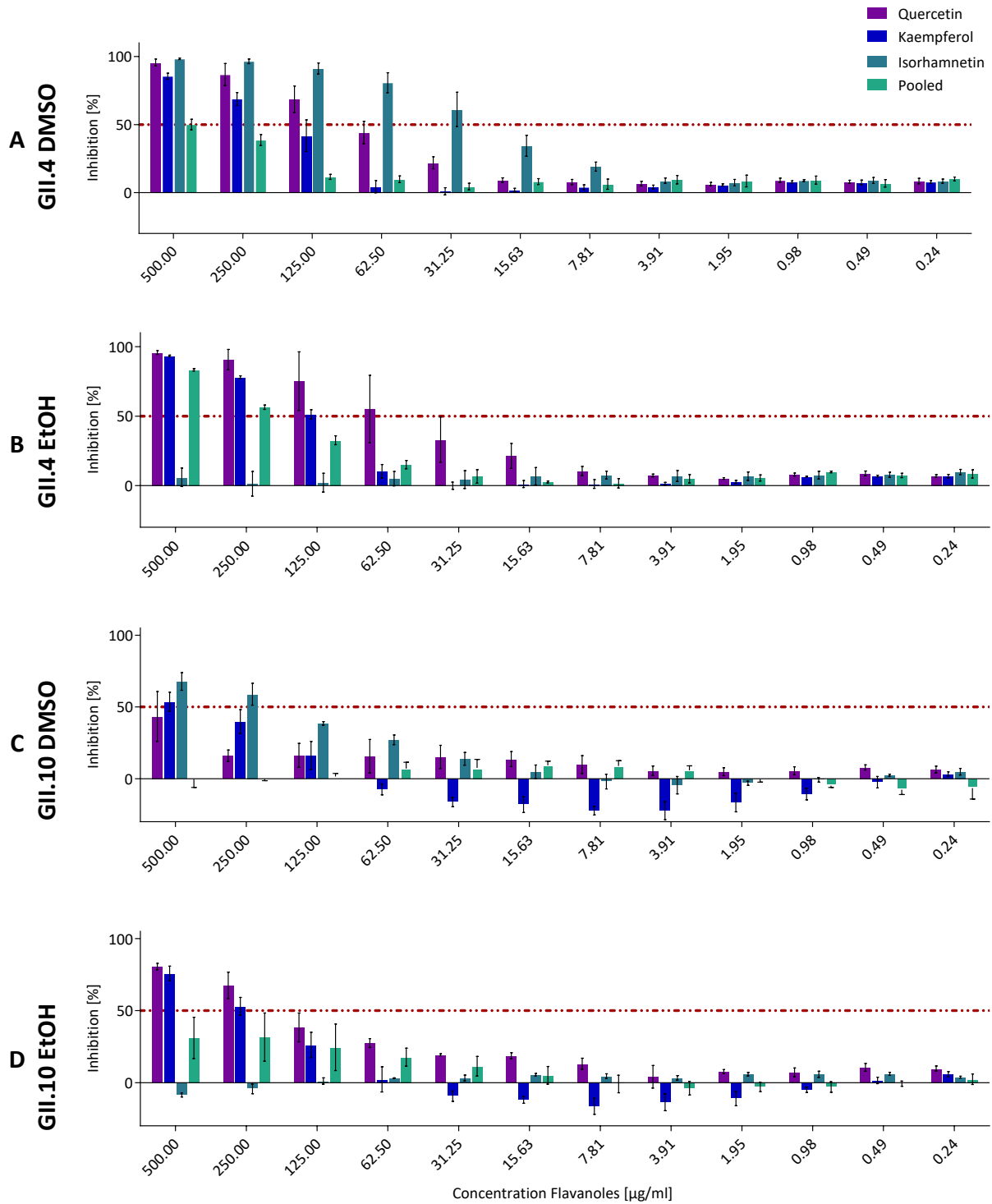


Figure 3-55: Inhibition ELISA testing three flavonol compounds against GII.4 and GII.10 VLPs
 Inhibition caused by three flavonols (quercetin, kaempferol, isorhamnetin, and pooled flavonols) was highly dependent on the solvent of the respective flavonol. Maximal inhibition values (quercetin, kaempferol, isorhamnetin, and pooled) and IC_{50} values as observed:
 A: GII.4 VLPs and flavonols in DMSO: 96 %, 86 %, 98 %, 50 %; 80 $\mu\text{g/ml}$, 136 $\mu\text{g/ml}$, 26 $\mu\text{g/ml}$, 206 $\mu\text{g/ml}$
 B: GII.4 VLPs and flavonols in ethanol: 96 %, 93 %, 6 %, 83 %; 60 $\mu\text{g/ml}$, 122 $\mu\text{g/ml}$, na, 227 $\mu\text{g/ml}$
 C: GII.10 VLPs and flavonols in DMSO: 43 %, 54 %, 68 %, 0 %; na, 144 $\mu\text{g/ml}$, 108 $\mu\text{g/ml}$, na
 D: GII.10 VLPs and flavonols in ethanol: 81 %, 76 %, 0 %, 31 %; 248 $\mu\text{g/ml}$, 168 $\mu\text{g/ml}$, na, na
 na: not applicable because of low inhibition. All assays were performed as triplicates with the exception of the pooled samples dissolved in DMSO or ethanol tested with GII.4 VLPs. IC_{50} is indicated by the red dashed/dotted line.

3.3 Combinatory Attachment Inhibition

To determine if a combinatorial approach could improve the overall inhibition and if this might be a possibility to address the challenge of cross-reactivity. It was analyzed if the inhibition of a cross-reactive inhibitor, such as 2'FL or a natural extract could be improved by the addition of a second, specific inhibitor, e.g. a Nanobody. Therefore, quantification of improvement of one inhibitor through addition of another was needed, thereby addressing the question if an interaction was adverse, additive, or synergistic.

3.3.1 Combinations of Nanobodies with 2'FL

Previous experiments showed that 2'FL inhibited GI.1 VLPs from binding to PGM, with an IC_{50} value of 50 mM [65]. Therefore, it was examined if a combination of Nanobody and 2'FL showed enhanced HBGA-blocking potential. In this variant of the HBGA-attachment inhibition assay, VLPs were preincubated with serially diluted Nano-7 or Nano-94 combined with 2'FL (10, 20, 30, 40, and 50 mM) (Figure 3-56, Figure 3-57). The combination of Nano-7 or Nano-94 with 2'FL led to improved inhibition, the enhancement correlated with increasing 2'FL concentrations, suggesting a synergistic effect (Figure 3-56). The Bliss independence model [5, 94] was used to determine if the interaction of Nanobodies and 2'FL was additive or synergistic (2.7.1). Combinations of Nano-94 with 40 mM or 50 mM 2'FL could not be synergistic, since such high concentrations of 2'FL alone already showed high inhibition, and the calculated values for expected additive effects already exceeded full (100 %) inhibition (Figure 3-56 D and E). The strongest synergistic effect was observed for combinations with 20 mM 2'FL. According to the 20 % criterion for synergistic effects, synergism was indicated at various Nano-94 and 2'FL combinations, for example, at 10 mM 2'FL combined with 25, 12.5, and 6.3 mg/ml of Nano-94 or at 20 and 30 mM 2'FL combined with 12.5 to 3.1 mg/ml of Nano-94. The differences between expected additivity and the observed synergistic values were statistically significant ($P = 0.05$), as determined by paired t test and two-way analysis of variance (ANOVA). Since evaluation and discussion of additivity, synergism, or adverse effects as performed is rather complex and hard to retrace in regular line charts and combinations of different compounds at specific concentrations, results of the combinatorial experiments are summed up in heat maps (e.g. A-E summed up in Figure 3-56 F). Coloring of all heat maps reflects values obtained by subtraction of calculated expected additivity from observed inhibition caused by the combination.

Combinatorial Attachment Inhibition

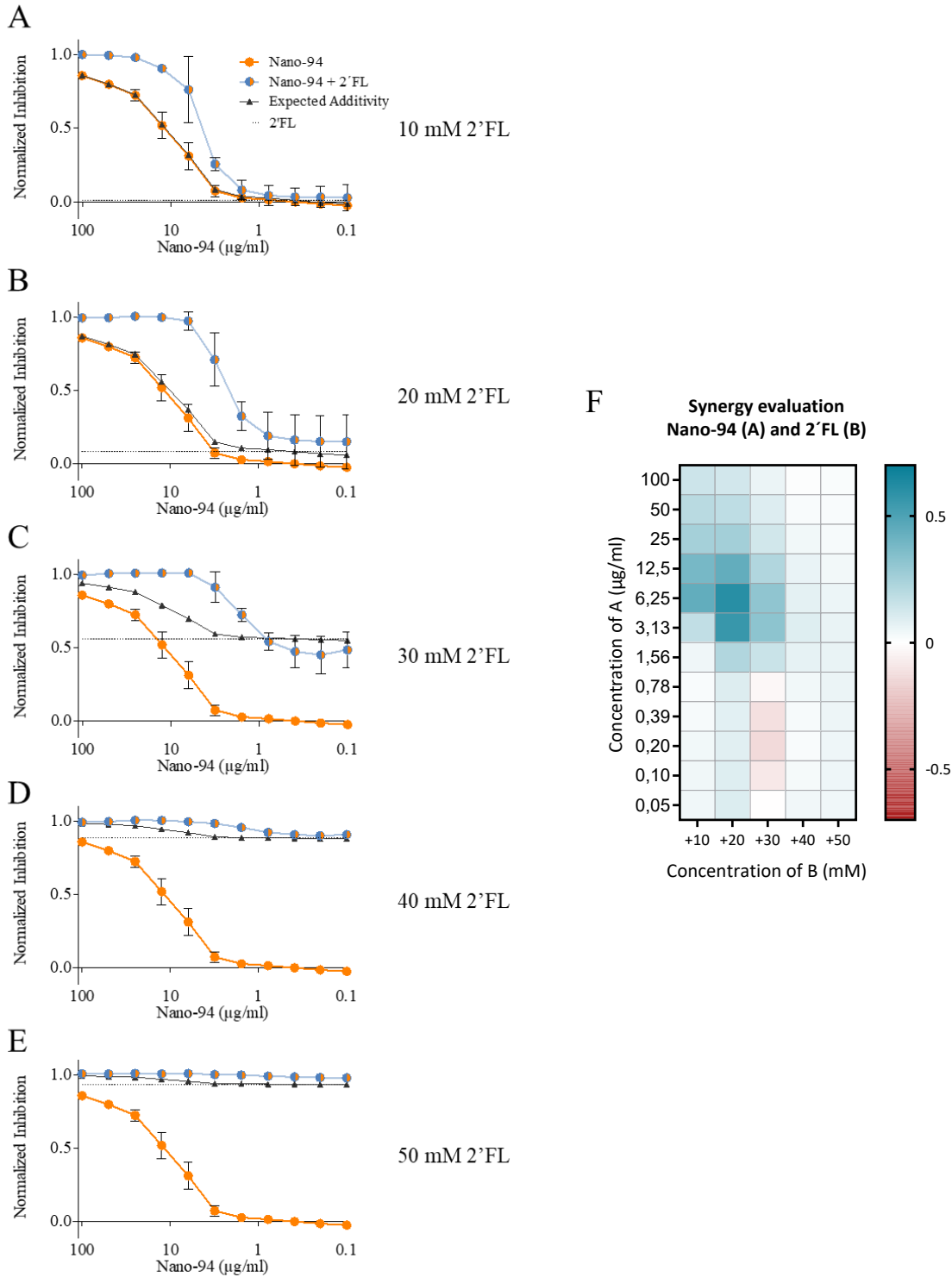


Figure 3-56: Charts and heat map of combinatorial treatment of Nano-94 with 2'FL (example for synergy). Serially diluted Nano-94 combined with constant concentrations of 2'FL, as indicated. Each graph (A-E) shows normalized inhibition of Gl.1 binding to PGM. Graphs show inhibition by Nano-94 alone (orange line), by 2'FL alone (dashed black line), inhibition observed for a combination of Nano-94 and 2'FL (blue line) and calculated expected values for additivity according to the Bliss model (black line). Nano-94–2'FL treatment shows synergistic effects, (blue line above black line) for combinations of 10, 20, and 30 mM 2'FL combined with 12.5–3.13 µg/ml of Nano-94. F: heat map summarizing combinatorial attachment inhibition by Nano-94 and 2'FL. Coloring of heat map reflects value obtained by subtraction of calculated expected additivity (black line) from observed (blue line). Charts A - E on the left were taken from published results [97]

Combinatory Attachment Inhibition

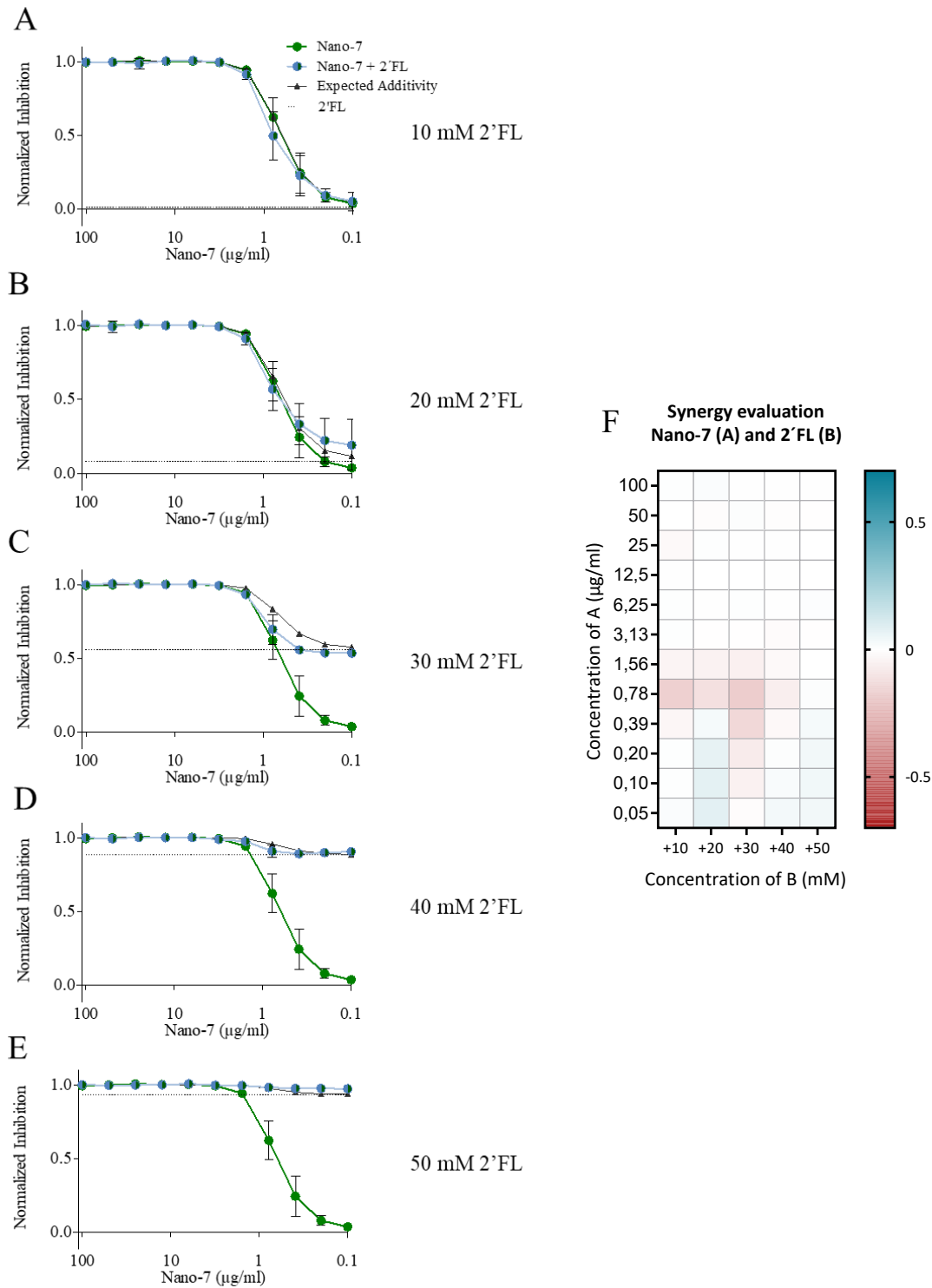


Figure 3-57: Charts and heat map of combinatorial treatment of Nano-7 with 2'FL (example for additivity). Serially diluted Nano-7 combined with constant concentrations of 2'FL, as indicated. Each graph (A-E) shows normalized inhibition of Gl.1 binding to PGM. Graphs show inhibition by Nano-7 alone (green line), by 2'FL alone (dashed black line), inhibition observed for a combination of Nano-7 and 2'FL (blue line) and calculated expected values for additivity according to the Bliss model (black line). Nano-7-2'FL treatment shows additive effects, (blue line matches black line). F: heat map summarizing combinatorial attachment inhibition by Nano-7 and 2'FL. Coloring of heat map reflects value obtained by subtraction of calculated expected additivity (black line) from observed (blue line). Charts A - E on the left were taken from published results [97]

Combinations of Nano-7 with 2'FL were also examined and analyzed. Combinations ranging from 100 to 1.6 µg/ml of Nano-7 were combined with 10 to 50 mM of 2'FL. For all examined combinations the observed inhibition closely followed the expected value for additive inhibition, as calculated by the Bliss model (Figure 3-57 A-E and F). This is reflected by a largely blank heat map (neither adverse nor synergistic effects).

To assess, whether the positive combinatorial effects observed with a Nanobody and 2'FL were genogroup dependent, the combination inhibition assay was repeated with GII.10 VLPs. Here a combination of a GII.10-specific Nanobody (Nano-85) and 2'FL was examined. The results obtained with this combination were similar to the observations obtained from the combination of Nano-7 and 2'FL (Figure 3-58, A-D). In this assay, the concentration of 2'FL had to be lowered to 1.0, 2.5, 5.0, and 10 mM of 2'FL because the IC₅₀ value of 2'FL for GII.10 VLPs was 5.5 mM [117]. Combining diluted Nano-85 with 1.0 mM of 2'FL did not improve inhibition, suggesting that this concentration was too low to support inhibition (Figure 3-58, A). With 2.5, 5.0, and 10 mM 2'FL, additive improvement of inhibition could be observed, and the observed inhibition closely followed the calculated expected inhibition (Figure 3-58, B-D) and therefore showed a 'blank' heat map (Figure 3-58, F). According to the Bliss independence criterion, the effects were determined to be additive (reflected in a slight blue staining especially of the upper part of the heat map (Figure 3-58, F)).

Combinatory Attachment Inhibition

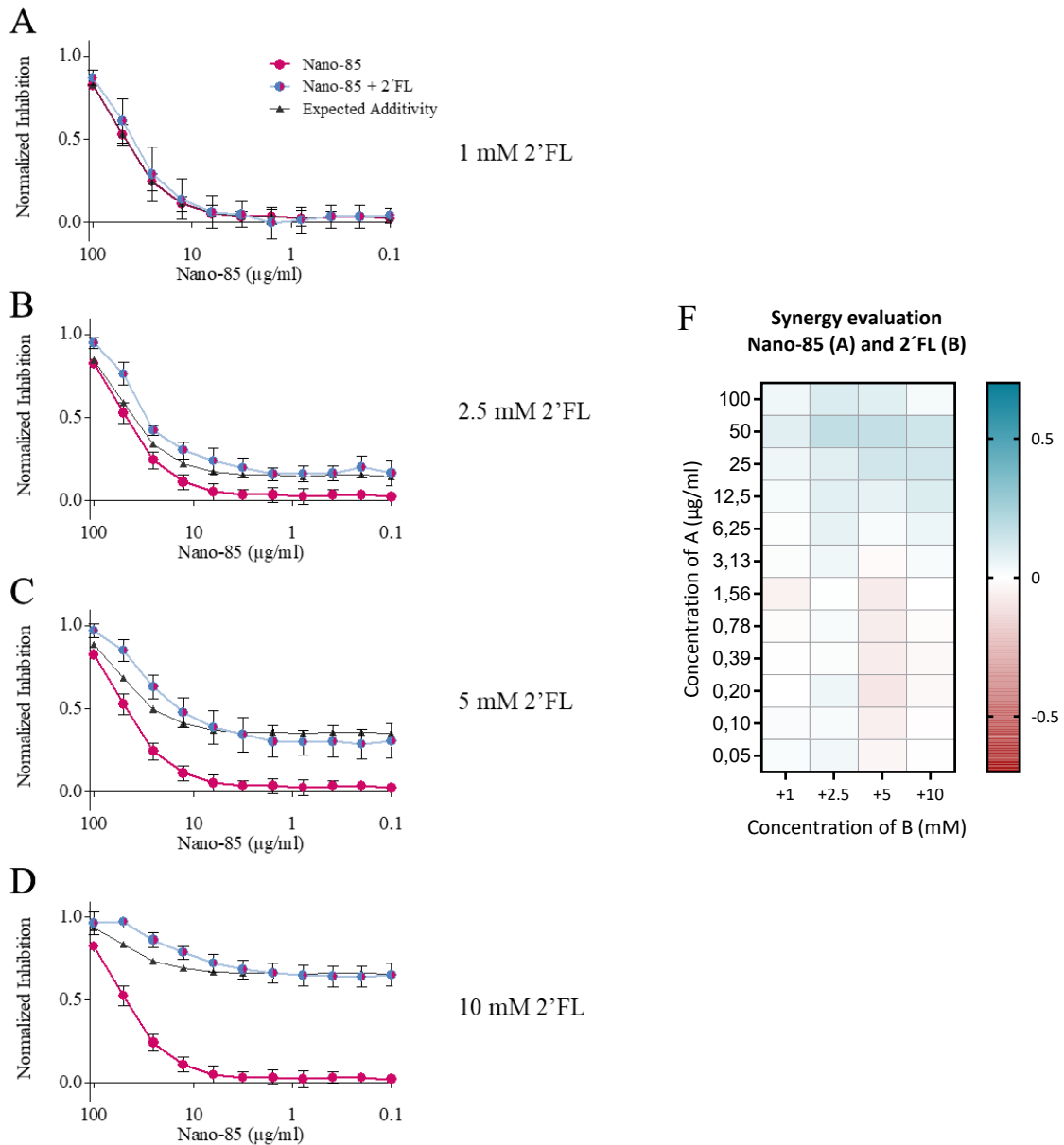


Figure 3-58: Charts and heat map of combinatory treatment of Nano-85 with 2'FL (example for additivity). Serially diluted Nano-85 was combined with constant concentrations of 2'FL. Each graph (A-F) shows normalized inhibition of GII.10 binding to PGM. Graphs show inhibition by Nano-85 alone (purple line), inhibition observed for a combination of Nano-85 and 2'FL (blue line) and calculated expected values for additivity according to the Bliss model (black line). Nano-85–2'FL treatment shows additive effects, (blue line matches black line). F: heat map summarizing combinatory attachment inhibition by Nano-85 and 2'FL. Coloring of heat map reflects value obtained by subtraction of calculated expected additivity (black line) from observed (blue line). Charts A - D on the left were taken from published results [97]

Combinatory Attachment Inhibition

The combinatorial attachment inhibition assay was repeated with GII.10 VLPs. Moreover, GII.10-specific Nano-32 or Nano-14 were combined with 2'FL. No adverse effects were observed (Figure 3-59). Especially Nano-32, but also Nano-14 showed additive effects with tendencies of synergy. However, the maximum difference between calculated and observed just reached the borderline of 20 %. The highest differences of 27 % were observed for 3.13 $\mu\text{g}/\text{ml}$ Nano-32 with 2.5 mM 2'FL and 21 % at 0.05 $\mu\text{g}/\text{ml}$ of Nano-14 with 2.5 mM 2'FL.

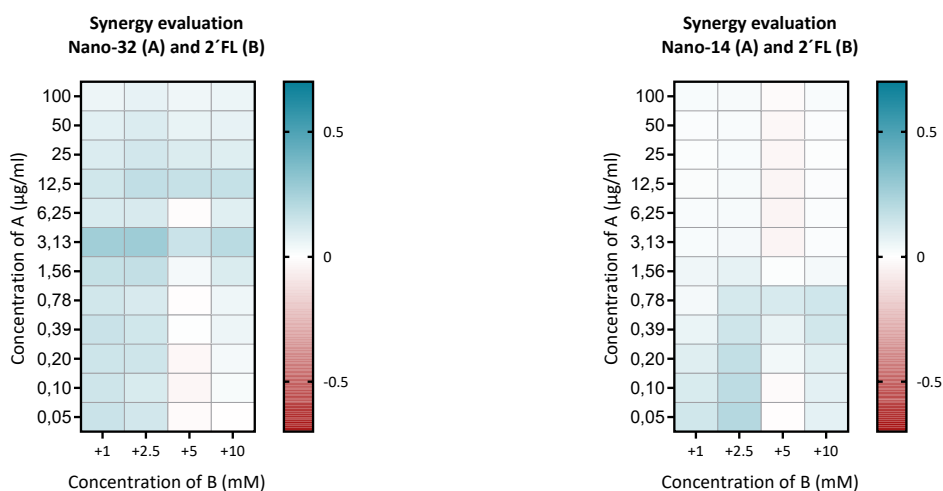


Figure 3-59: Heat map of combinatorial treatment of Nano-32 and Nano-14 with 2'FL. Heat maps summarizing combinatorial attachment inhibition by Nano-32 (left) or Nano-14 (right) and 2'FL. Coloring of heat map reflects value obtained by subtraction of calculated expected additivity from observed. Slight synergistic effects are reflected by faint blue coloring.

3.3.2 Combinations of Nanobodies with Natural Extracts

In further combinatorial attachment inhibition assays with GII.10 VLPs, combinations of Nanobodies and natural extracts were examined.

Serially diluted Nano-26 in combination with date syrup or honey showed adverse effects, especially at high concentrations of Nanobody (e.g. maximal reduction of 44 % (date syrup) 69 % (honey) compared to expected additive effect with date syrup or honey respectively Figure 3-60). Combinations of low concentrations of Nano-26 with date syrup or honey showed slightly additive effects (highest difference of 5 % at 0.78 $\mu\text{g}/\text{ml}$ Nano-26 with 2.5 % honey and 13 % at 1.56 $\mu\text{g}/\text{ml}$ of Nano-26 with 0.1 % date syrup). When Nano-26 was combined with propolis at high concentrations severe adverse effects occurred (strongest reduction of 85 % was observed at 50 $\mu\text{g}/\text{ml}$ Nano-26 with 0.5 % propolis compared to the calculated additive effect). At lower concentrations of Nano-26 adverse effects were milder. Between 3.31 and 0.05 $\mu\text{g}/\text{ml}$ of Nano-26 a reduction of 1 – 17 % of inhibition compared to expected additive effect was observed. (Figure 3-60).

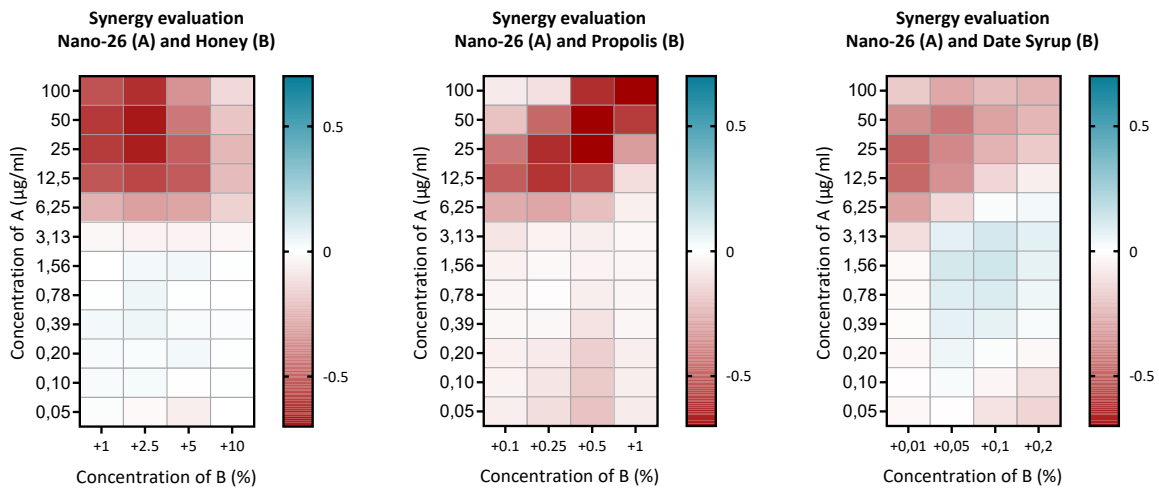


Figure 3-60: Heat map of combinatorial treatment of Nano-26 with honey, propolis and date syrup
Heat maps summarizing combinatorial attachment inhibition by Nano-26 (A, serial dilution) and honey, propolis or date syrup (B, given concentrations). Coloring of the heat map reflects value obtained by subtraction of calculated expected additivity from observed. Severe adverse effect are indicated by red coloring of parts of the heat map. Line graphs not displayed.

With GII.10 VLPs, combinatorial attachment inhibition of Nano-85 with natural extracts were also examined (Figure 3-61). Results closely followed observations obtained with Nano-26.

Combinatory Attachment Inhibition

A combination of Nano-85 with date syrup showed adverse effects with high concentrations of Nano-85 (12.5 – 100 µg/ml a reduction of inhibition compared to expected additivity of 4 – 28 %), whereas lower concentrations of Nano-85 with date syrup showed weak additive effects. A combination of 1.56 µg/ml of Nano-85 with 0.1 % of date syrup exhibited an increase of 8 % of inhibition over the expected additive effect (Figure 3-61). Results observed with a combination of Nano-85 with honey were similar. The highest positive effect was a 10 % increase observed for the combination of 0.78 µg/ml Nano-85 with 2.5 % honey. The strongest reduction (adverse effect) of 51 % was observed for the combination of 100 µg/ml of Nano-85 with 2.5 % of honey. Combinations of high concentrations of Nano-85 with propolis yielded in severe adverse effects (highest reduction in inhibition compared to expected additive effect was 73 % at 100 µg/ml Nano-85 with 0.5 mM propolis).

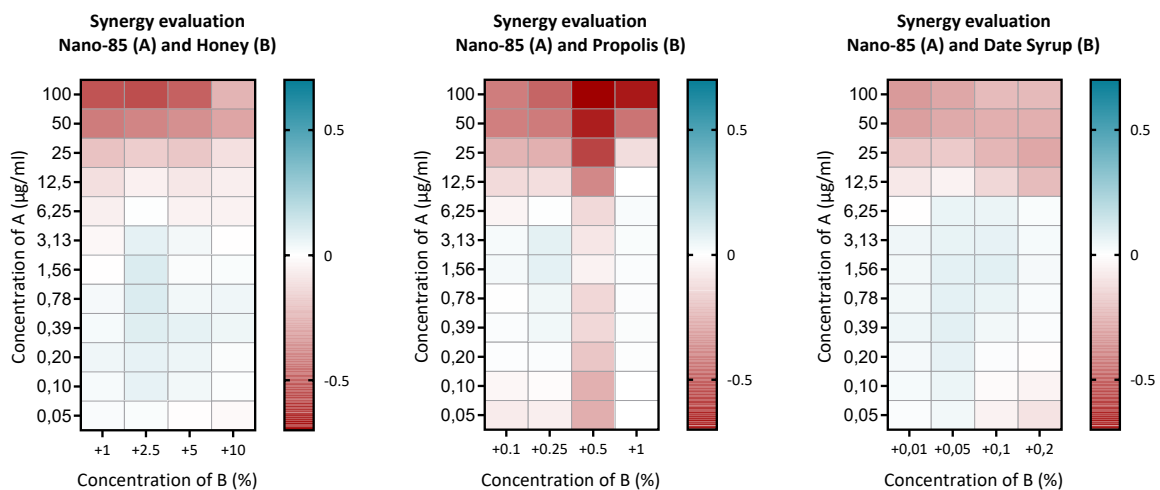


Figure 3-61: Heat map of combinatorial treatment of Nano-85 with honey, propolis and date syrup. Heat maps summarizing combinatorial attachment inhibition by Nano-85 and honey, propolis or date syrup. Coloring of heat map reflects value obtained by subtraction of calculated expected additivity from observed. Severe adverse effect. Line graphs not displayed.

3.3.3 Combinations of Natural Extracts

Similar to the previous assay, GII.4 VLPs were used to assess combinatorial attachment inhibition with date syrup and propolis (96 %-ethanol tincture) and vice versa. The combination of date syrup and propolis showed synergistic improvement of inhibition (Figure 3-62). Highest improvement was observed for 0.01 - 0.05 % of date syrup combined with 0.25 % of propolis (inhibition improved by 36 - 39 % over expected additive effect). In the vice versa experiment, the optimum was 0.39-0.01 % of propolis with 0.05 - 0.1 % of date syrup (inhibition improved by 30 - 56 % over expected additive effect). The optimal concentration range of both natural extracts was 0.01 - 0.05 % of date syrup with 0.2 - 0.01 % of propolis.

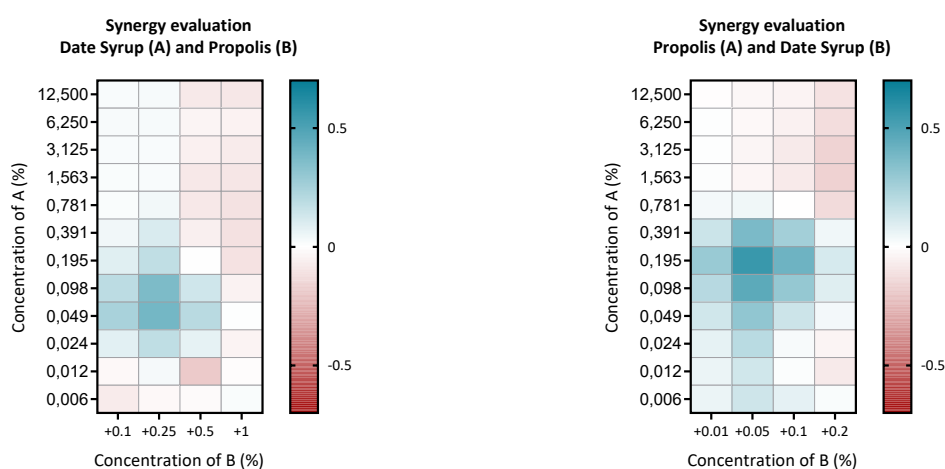


Figure 3-62: Combinatorial treatment of date syrup/propolis with propolis/date syrup, heat maps
Heat maps summarizing combinatorial attachment inhibition by syrup/propolis and propolis/date syrup. Coloring of heat map reflects value obtained by subtraction of calculated expected additivity from observed. Synergistic effect. Line graphs not displayed.

Overall, results obtained with GI.1, GII.4 and GII.10 VLPs indicated that positive effects of combinations of different inhibitors, were not genotype specific and that positive effects can be obtained by combination of a wide range of compounds and extracts. Positive combinations may be found between 2'FL and Nanobodies, or between date syrup and propolis. However, combinations between natural extracts and Nanobodies also caused severe adverse effects. Therefore, each combination should be examined carefully and no rash generalization of positive combinatorial results should be made.

4 Discussion

The large genetic and antigenic diversity of human norovirus remains a major challenge in the development of both vaccines and antivirals [79]. The protective immune response against one genotype seems to be specific, with little or no cross-protection from infections with related strains [6, 79, 121]. Thus, for sufficient protection a polyvalent vaccine will most likely be required, with updates to newly emerging strains [79]. A situation similar to the current influenza vaccination [79]. Consequently, the development of cross-reactive antivirals is of importance.

4.1 Discussion – Screening for Synthetic Antivirals

4.1.1 Screening of the NIH Collection

In search of new antivirals against human norovirus, the collection of the NIH was screened in both a novel automated X-ray crystallography screening method and an inhibition ELISA to identify a potential ligand/inhibitor among the collection of compounds approved by the FDA. As these compounds are already approved, the benefit of discovering an inhibiting molecule within this collection would be a shortened development and approval process.

With the automated X-ray crystallography screening, some interesting observations were obtained. Close to the amino acid Tyr452, a DMSO molecule was found in almost all data sets. Between Glu472 of the A and B chain, there were additional densities in numerous datasets. Notably, these coordinated additional densities were observed in a number of data sets, where usually only a limited number of structural data sets are available for analysis. These findings might be of interest for further drug design and development of synthetic antivirals, because they highlight sites on the P domain where binding of certain molecules is preferred. These positions might be promising sites for the design of specialized small molecule inhibitors.

Unfortunately, Pipedream was unable to completely auto-process almost half of the data sets (224 of 478). The numbers of the data sets that failed to be auto-processed suggested that an entire crystallization plate could not be accessed. The reason for the high number of unfinished data processing was not communicated from the co-operation partners of the

external screening, however the automated system is still under development. The placement of ligands into densities that clearly showed single water molecules points to some need of improvement for the data processing before Pipedream can be used as a reliable screening system. It has to be taken into account that the present screening was but an extended test run of the automated screening system and its software. The aim was to proof that the system is able to autonomously handle some externally provided protein and screen it against a large library. Another objective was the identification of weaknesses in the entire system so the overall performance could be improved and settings of the software could be adjusted. The presence of apparent ligand densities in the auto-processed files (77) that were not present when the data sets were processed manually, suggests that placement of a ligand needs additional rules in Pipedream to avoid trivial ligand detections.

Many of the questionable densities of ligands placed by Pipedream were found where usually coordinated water molecules are present in the structure. It is plausible that the NIH-molecules were able to fit into these vacant spaces, where the P domain clearly prefers something to be bound. On the other hand, it is also possible that Pipedream misinterpreted the density of water molecules by placing the ligands in densities created by water molecules in the crystal.

Concluding the automated X-ray crystallography screening is a powerful tool to assess ligand binding. It allows swift and easy screening of a given protein against a large library of potentially binding compounds. However, the test run showed that some minor adjustments are required. Still it remains a promising versatile tool for compound screenings and therefore an interesting starting point for further studies of ligand binding in various settings. Additionally, the system allows swift acquisition of numerous raw data sets for further automated or manual analysis (with and without ligand). This enables detailed analysis of the structure and possible identification of vulnerable sites (e.g. where water is regularly bound) for site-directed development of molecules.

Supplementary to the automated X-ray crystallography screening, the NIH collection was assessed for inhibitory compounds using ELISAs. It would have been interesting to correlate the ELISA results with the only data set that showed binding of a ligand after manual processing. However, this was impossible due to incomplete communication as to which exact compound the data sets referred. The ELISA results did not show evidence of inhibition by any of the NIH compounds. It has to be considered that upon pooling of the samples some compounds might have interacted with each other. However, enhancement of binding was observed with eight of the pooled samples, two of which exhibited stronger cases of enhancement. This 'negative' inhibition or enhancement of binding was concentration-dependent, as shown in an additional assay where small dilution series were tested (serial dilution, 1:4; 10–0.01 μ M). Therefore, it seemed likely that the negative inhibition values were real observations and not the result of random variation. The influence observed by the presence of DMSO in the ELISA was also interesting and might be explained by the binding of DMSO observed during the automated X-ray crystallography screening. Probably DMSO can increase the signal by attaching to one or more sites on the P domain, thereby altering the interaction with PGM or the interaction with detection antibodies. Although, upon retesting of the NIH collection at a concentration where DMSO was no longer able to shield inhibitory effects, no inhibition could be observed. However, the enhanced effects caused by several compounds were still observable. This enhanced binding or detection effect observed with some of the compounds might be of interest for further research, but seems less practical in direct application as an antiviral.

4.1.2 Synthetic Multivalent Fucose Oligomers

Nine of the twelve multivalent fucose oligomers exhibited binding to the GII.10 P domain as was observable in X-ray crystallography data. Seemingly, the oligomers allowed access of the fucose moiety to the HBGA-binding site. Yet no structure yielded evidence for the intended binding of multiple fucose moieties to a single P domain. Contradicting our results, other analysis showed binding of multiple fucose moieties per P domain dimer [10]. It is unclear, if these multiple fucose moieties came from a single fucose oligomer or from different molecules. The complete absence of the backbone of the oligomer in the X-ray crystallography structures raises the question if the backbone is either too flexible and not bound rigid enough to appear in the crystal structure, or if fucose and linker got separated from the original

molecule. Unfortunately, binding ELISA could not be conducted due to lack of a detection system for the multivalent fucose oligomers when bound to VLPs or P domain. On the other hand, there was not enough of the manually synthesized compounds to coat ELISA plates with them and detect attachment of VLPs. However, none of the fucose-oligomers showed inhibition in ELISA (at 31.25 μ M), despite the observation of a ligand in the structure. It should be taken into account that the concentration for inhibition testing of the fucose-oligomers was low (max 500 μ M) and inhibition would have only been observable if the inhibition of the oligomers was considerably better than 2'FL (250 mM). In conclusion, no inhibitory effect was observed with these synthetic compounds. Likewise, no evidence for the binding of multiple fucose moieties from one oligomer to the P domain was obtained [10].

4.1.3 GI.1-specific Nanobodies

A panel of twelve GI.1-specific Nanobodies was tested to identify their binding and inhibition potential also their cross-reactivity was assessed. Only three of the Nanobodies (58, 78 and 94), raised against GI.1 Norwalk VLPs in Alpacas, showed strong binding to GI.1 Norwalk VLPs. Two of the weaker binders (27 and 74) showed cross-reactive binding to GI.2 (Southampton), GI.3 (Kawasaki), and GI.11 (#8). Only Nanobody 58 showed strong binding to GI.1 (Norwalk), in addition to cross-reactive binding to GI.3 and GI.11 VLPs. In general, a surprisingly high number (6) of GI.1-specific Nanobodies did not bind to GI.1 VLPs compared to other VLP-specific Nanobody-libraries analyzed by our group.

Five of the Nanobodies (7, 27, 74, 78, and 94) showed good inhibition values but no cross-reactive inhibition with any of the tested genotypes could be observed. This is similar to the observations for other norovirus-specific Nanobodies [66, 69] and lab experience with other Nanobody-libraries. The binding efficiencies of VLPs and P domains were comparable with three exceptions. The highest ratio in detectable OD₄₉₀ levels (VLP (5 μ g/ml)/P domain (10 μ g/ml)) was observed with Nano-84, followed by Nano-46. The lowest ratio was observed with Nano-17. Other nanobodies ranged between 1.3 and 0.7. All Nanobodies that exhibited binding to GI.1 VLPs also bound to the GI.1 P domain. This is similar to what was observed for other Nanobodies [66]. In this study conducted in our group six GII.10-specific Nanobodies bound to GII.10 VLPs and P domain.

Three Nanobodies were selected based on their inhibition values and binding positions on the P domain for further testing and publication (Nano-7, Nano-62, and Nano-94). ITC analysis showed that Nano-7 exhibited the highest binding affinity (lowest K_d observed) among all norovirus-specific Nanobodies [66, 67]. Analysis of stoichiometry suggested binding of one Nanobody per P domain monomer. Nano-7 showed inhibition with an IC_{50} of 0.43 $\mu\text{g/ml}$ whereas Nano-62 exhibited lower inhibition of 15 % (maximal inhibition value). Interestingly X-ray crystallography structure analysis revealed that both bound on the side of the GI.1 P domain dimer. The sub-nanomolar affinity of Nano-7 seems to be reflected in the high number of contacts found in the X-ray crystallography structure of the complex [67]. As described, all three Nanobodies were able to bind to GI.1 P domain and VLPs. Interestingly, Nano-7 bound VLPs at a two-fold lower OD_{490} level compared to the other two Nanobodies. However, this striking difference in detection levels was not observed with P domain. This can be explained by the binding site of Nano-7: binding of Nano-7 at the side of the P domain might lead to sterical hindrance either in attachment of Nano-7 to the VLPs or by binding of the detection antibody to Nano-7, but direct evidence is lacking. The specific orientation of bound Nano-7 in the context of the entire particle might hinder accession of Nano-7 to its binding site or binding of the detection antibody to Nano-7. Detection of separate P domains is not marked by steric interference with other parts of the VLP particle. Nano-62 on the other hand might not be affected by this due to its slightly different orientation. Although Nano-62 also binds to the side of the P domain, it is neither the same site nor the same orientation as for Nano-7.

Modeling of the complex structure onto the GI.1 VLP particle indeed revealed clashes of Nano-7 and Nano-62 with the S domain and neighboring P domains ([97], performed by Dr. Jessica Devant). This has also been observed for Nanobodies against GII norovirus [66, 67] and a diagnostic mAb [42]. This also hints that the P domains on the particle must be more flexible than anticipated, to allow binding of the Nanobodies.

Nanobodies raised against GI.1 VLPs were highly specific for this genotype. Whereas among a set of GII.10-specific Nanobodies cross-reactivity to other genotypes has been observed [66]. The sequence alignment of Figure 3-25, showed that the binding sites for the three analyzed Nanobodies were not located in conserved regions. In comparison to GII, the GI genogroup

exhibits high genetic diversity [11, 40]. Thus, the overall high diversity among the GI genogroup might also explain the high specificity of the entire set of GI.1-specific Nanobodies.

Based on the DLS results, Nano-7 and Nano-62 did not alter the diameter of VLP particles, giving no evidence for their mode of action. A possible mode of action could be the induction of conformational changes or locking the P domain in a position that interferes with the attachment of HBGAs. Nano-94 on the other hand seemed to cause inhibition by aggregation of VLPs, as was confirmed by EM images.

Several Nanobodies raised against GI.1 VLPs did not bind GI.1 VLPs. Also, some Nanobodies binding to GI.1-VLPs did not bind well to the GI.1 P domain. This raised the question if some might bind to parts of the S domain (parts of which might be presented in the course of the immune response within the Alpaca). Therefore, binding of the GI.1-specific Nanobodies to different constructs of the GI.1 S domain was tested. All Nanobodies were able to attach to the shortest S domain construct, but at very low levels compared to P domain or VLPs. For the, longer constructs, no Nanobodies showed any binding. Hence, none of the Nanobodies were specific for the S domain.

4.2 Screening of Natural Extracts as Antivirals

All synthetic antivirals identified in chapter 3.1 were specific Nanobodies exhibiting strong inhibition, but with very limited cross reactivity. Screenings involving unspecific compounds did not yield good inhibition. Therefore, the second chapter focused on the testing of natural inhibitors with the aim of identification of strong and cross-reactive inhibition as this has been observed for citrate [70] and the HMO 2'FL [65].

4.2.1 HMO Screening

The HMO screening conducted by the National Center of Functional Glycomics (NCFG) [124] resulted some interesting candidates marked by their ability to bind to three different GII genotypes (fractions 25, 29, 34, and 67). Fraction 67 was marked by high binding signals to GII.10, GII.4 and especially GII.17 (Kawasaki and Saitama). Several HMO-fractions bound specifically to a certain genotype, whereas others exhibited broad binding activities. A structural comparison of these two types and their binding would be of great interest and help improve our understanding what defines cross-reactive epitopes. Structural and inhibition

studies are planned to further analyze this binding. Unfortunately, a mistake in numbering that occurred at NCFG was not retraceable from my side and requests to resolve this issue remained unanswered. Therefore, the HMO candidates binding to the VLPs could not be identified preventing further analysis of these preliminary results.

4.2.2 Plant Derived Syrups and Saps

In an attempt to identify a broadly reactive inhibitor for human noroviruses, a screen of plant extracts and saps in common human nutrition was performed. The aim was to identify potential inhibitors to noroviral attachment that are safe and easy to access. Plant-derived extracts that have been consumed by humans in some cases even for centuries may be regarded as safe even among different age groups and also achieve high acceptance within the population [77]. A panel of 24 different natural extracts was screened in attachment inhibition ELISAs. Currently, the only known co-factors of human noroviruses are HBGAs and bile acids [37, 78]. The interaction might be disrupted with an antiviral binding at the HBGA-binding site. This led us to the hypothesis that an inhibitor might be found among the class of glycans. Therefore, plant extracts rich in glycans and consumed as food were screened. Further, extracts of plants usually contain defensive substances to protect plants from viral, bacterial and fungal infections [90, 93]. Among this phytochemical mixture also compounds active against human norovirus might be identified.

To date, many studies have identified natural extracts as potential inhibitors for norovirus [77, 98]. However, one problem remaining with testing of these inhibitors is the appropriate screening system and comparability [77]. The complete lack of a reliable cell culture system led to utilization of a variety of different surrogate systems [27, 77, 98]. In some studies, related but culturable surrogate viruses of the *Caliciviridae* family were utilized, while other groups used VLPs of human norovirus or other surrogate viruses to address the matter of inhibition (1.11). The result is a wide variety of different screening methods and surrogate systems. Inhibiting candidates identified with these different methods are difficult to compare because testing was performed with different systems and measuring units [52, 77, 100, 126]. In the absence of a standardized testing system for human norovirus we decided to use VLPs of human noroviruses in an ELISA setup as surrogate for the original virus. Previous studies revealed high diversity among human noroviruses and caliciviruses raising the question to

what extend inhibition results obtained with one calicivirus can be transferred to human norovirus [19]. The system selected for this thesis can only be used for the identification of attachment inhibitors however the utilization of VLPs of human norovirus ensures transferability of obtained results to human norovirus disease.

In this study, date syrup was identified as a strong inhibitor, which entirely abolished VLP attachment (100 % inhibition at a concentration of 0.2 – 0.4 % depending on the genotype) and exhibited low IC_{50} values [0.11 % (GII.10), 0.056 % (GII.4), 0.14 % (GII.17), 0.15 % (GI.1), 0.49 % (GII.1)] for a diverse range of genotypes, including genotypes from two genogroups (GI and GII). Another noteworthy candidate was barley malt, it also exhibited strong inhibition (~75 % at a concentration of 1.56 %) and a low IC_{50} value (0.9 %). However, barley malt only displayed inhibition at low IC_{50} values with GII.4 VLPs and not with the other tested VLPs. This may not be a useful property for development of a broadly reactive inhibitor, but it might be useful for a general understanding of specificity. Among the tested extracts, red wines and red grape juices also exhibited complete inhibition with low IC_{50} values (1.65 -0.26 %). It was apparent, that wines and juices derived from red grapes showed considerably stronger inhibition than those derived from white grapes. Red wines showed lower IC_{50} values (0.26 - 0.43 %) than red grape juices (0.86 – 1.65 %). This could result from the different grapes and different processing methods. Red wine and grape juices are derived from red grapes, which are known to have a higher content of polyphenols than white grapes [43, 104]. Red wines are produced by letting the grape juice ferment together with the mash of the extracted grapes [14, 33]. The prolonged close contact of the juice with the grapes and their stems along with the rising concentration of ethanol in the mixture allows improved extraction of polyphenols from the grape flesh, skins, stems and seeds [14, 15, 33]. This is why red wines are rich in polyphenols such as tannins and flavonoids, while white wines have a lower content of polyphenols due to the different processing of the grapes during which no fermentation with the mash is included [14, 32, 33].

Testing of date syrups from different sources revealed great differences in inhibition (IC_{50} values and absolute inhibition). This suggested that the inhibiting compound found within date syrup is present in different quantities within syrups of different origin. One factor could be the overall purity of the syrup or its dilution in water upon the production process. Also,

usage of different date variants, dates at different ripening stages or extraction of different parts of the date (peel, flesh, stone) could alter the concentration of the inhibiting compound[39]. Further, different storage or extraction conditions and times would also be a possible reason for the variation in inhibition.

To identify the active compound, some glycans of date syrup were identified by the Metabolomics Core Technology Platform at University Heidelberg (Gernot Poschet). Due to the high concentration of eight sugars present in date syrup in ample amounts, the identification of the less concentrated sugars in date syrup was unsuccessful. Of the eight sugars defined in gas chromatography analyses, none exhibited the equivalent attachment inhibition, as observed with date syrup. In addition, an experiment in which all eight sugars were pooled together also did not yield the level of inhibition observed with date syrup. Therefore, none of the eight sugars caused the inhibition as a single compound nor did the combination of any of them cause the inhibition. Thus, other unidentified glycans or other compounds might cause inhibition. The inhibiting compound may also be a polyphenol, for date syrup like wines are rich in this compound class [14, 39, 43, 44].

Interestingly, all natural extracts exhibiting inhibition also showed peak shifts in DLS and formation of aggregates in EM. From this result, it appears that the mode of action for date syrup, coconut blossom syrup and barley malt was due to the aggregation of VLPs, thus preventing single particles to attach to the HBGAs in the inhibition assay. Of the three genotypes tested, barley malt caused aggregation in all GII.4, GII.10 and GI.1 VLPs. However, it only caused strong inhibition against GII.4 and did not exhibit any inhibition with GI.1 VLPs. Another interesting extract was the royal jelly. It inhibited poorly with all tested VLPs, yet it showed formation of massive aggregates in DLS. Remarkably, measurements of royal jelly without VLPs resulted in identification of particles of a different size than the aggregates observed with VLPs. Moreover, in EM images, long rods were observed. We speculated that the pollen in royal jelly could potentially interact with the VLPs, but only at an affinity much lower than the binding partner HBGAs. Therefore, this weak interaction might not interfere with attachment of VLPs to PGM (depending on the genotype). The correlation between the extent of inhibition, peak shift and observation of aggregates in EM fitted together forming a pattern of inhibition caused by a given extract and hinting a possible mode of action.

Unfortunately, the attempt to identify the structure of the inhibiting compounds in X-ray crystallography structure analysis of different natural extracts did also not solve the question what molecule is active. The first obtained structure of a ligand bound to the P domain was with apple sweetener, which was not a good inhibitor. This is similar to the findings with the fucose oligomers and several other examples observed in our lab (unpublished data): a compound might be well coordinated in the crystal structure but still not a good inhibitor. For date syrup and coconut blossom syrup, ligands could also be observed in the crystal structure. Strikingly, the structures exhibit high similarities. Both structures exhibited a ligand bound at the HBGA binding site. Additionally, in both structures a second ligand was found in the central channel between the P domain monomers. A third ligand was visible in the channel at the top of the P domain between the two HBGA binding sites. This site is of special interest, as this is not a regular binding site of HBGAs or sugars on the P domain, but the location were some bile salts attach [58]. Moreover, the unexplained densities in the channel between the HBGA binding sites might be of interest. Within this channel, forming a connection between the two regular HBGA binding sites, two additional HBGA binding sites have recently been identified [68]. These additional binding sites are only occupied by fucose if crystals were soaked with high concentrations of fucose solutions. The occupancy of these additional binding sites by a compound derived from dates could mark a new location for binding of inhibitors. Further structural analysis of this site will be of great interest.

None of the unexplained densities could be further refined because this would require the knowledge of the molecule. Experimentally, the density of a fucose ring was fitted into the unexplained density observed at the HBGA binding site in a crystal with date syrup. The density of fucose fitted the unidentified density, however, as this is a known binding site of a fucose ring, it is conceivable that the molecule causing the unexplained density is highly similar in shape and charge to the fucose moiety that is intended to fit. Moreover, if a molecule bound at this position would comprise flexible parts, these would protrude from the binding site. The averaging nature of X-ray crystallography would cause them to vanish during the process of structure analysis.

4.2.3 Honey

Similar to the findings obtained with the crystal structures of natural extracts, two unexplained densities were found in the structure of P domain soaked with honey. One additional density was located at the HBGA binding site, whereas the other was located in the central channel between the two P domain dimers. The location of an additional density in the central channel, in the symmetry axis of the two P domains, has to be treated with some caution because it could be a result of the symmetry and orientation. In this case, instead of a ring e.g. EDO (cryoprotectant, shaped like a 'C') might be mirrored into a ring-like structure.

Of the set of 31 different types of honey, the ten best inhibitors were selected for further analysis. None of the honeys tested were able to reach 100 % of inhibition. The IC₅₀ values of the different types of honey ranged between 3.38 - 15.26 % and 4.72 - 24.77 % with GII.10 and GII.4 VLPs, respectively. Interestingly, the maximal inhibition values observed with GII.4 VLPs were higher than with GII.10 VLPs. None of the different types of honey showed outstanding inhibition results for norovirus. However, these results are interesting because a compound appeared to be common in different types of honey. It is not present in all honey but mostly present in honey obtained from trees. This led to the theory that the bees might have collected some common ingredient to their honey.

4.2.4 Propolis

The antiviral properties observed with propolis [46, 80, 99, 103, 116] and its origin from tree resins [80] made propolis an obvious choice for further testing. All propolis extracts tested in attachment inhibition ELISAs showed inhibition against GII.10 and GII.4 VLPs. In DLS measurements, treatment of VLPs with any of the types of honey or propolis extracts caused a peak shift, indicating the formation of aggregates. Similar to propolis, treatment with most of the honeys led to the observation of aggregates in EM.

Like date syrup, the inhibition observed with propolis was broad across multiple genotypes. Also, the extend of inhibition regarding full attachment inhibition (67 – 100 %) and IC₅₀ values (GII.10: 0.57 % (96 % ethanol), 5.00 % (70 % ethanol), 4.63 % (DMSO), 3.47 % (20 % PEG200); GII.4: 0.44 % (96 % ethanol), 3.29 % (70 % ethanol), 1.82 % (DMSO), 3.66 % (20 % PEG200)) indicated that propolis and date syrup could be good candidates for norovirus inhibition. Like

date syrup, propolis also seemed to act through aggregation of VLPs. However, unlike with other inhibitions observed, no crystal structure of a ligand attached to the P domain could be obtained with the propolis extracts. Traditionally, propolis is suspended in a mixture of ethanol and water because many of the active compounds within the propolis (e.g. tannins and other polyphenols) exhibit limited solubility in water [80]. Also, water extracts of propolis showed considerably lower inhibition than ethanol or DMSO extracts. It is possible that the limited solubility of the active compound or the effects of ethanol or DMSO affected the growth of P domain crystals, limiting the possibilities to obtain a crystal structure with the bound ligand. Few crystals formed when propolis extracts were added to the crystallization setup. However, all crystals obtained proved to be of apo structures.

Several assays were performed in an attempt to rule out that the inhibition observed with propolis extracts could be the result of solvent or wax precipitation in the set up. If no VLPs were added in the ELSIA but only propolis no signal was observable excluding the possibility that either precipitation of beeswax or other compounds in propolis extracts were contributing to any signal in the assay. Also diluting propolis extracts in their respective solvent when running the inhibition assay did not abolish the inhibition observed although some of the solvents caused problems at high concentration.

All in all, the high inhibition observed with propolis seems to result from some interaction between a compound within propolis and the VLPs. Inhibition seems to arise from aggregation of VLPs by the active compound within propolis. This compound seems to have a higher solubility in ethanol or DMSO than water. As propolis is derived from raisins it also contains polyphenols in high amounts [7, 73]. Better solubility of the active compound of propolis in ethanol and DMSO than in water could also hint at some polyphenol as an active compound.

4.2.5 Polyphenolic Compounds Common to Natural Inhibitors

The identification of several natural extracts able to inhibit attachment of VLPs raised the question if there might be a common compound or compounds causing the inhibition. The extracts with the inhibition against norovirus were date syrup, wines, propolis extracts, and honey derived from trees. Common compounds of these extracts, beside sugars, are polyphenols, e.g. tannins and flavanoids. Tannic acid was suspected to be the inhibiting

compound observed with Chinese gall [21]. Also, several other studies concluded that some polyphenols within the natural extracts might be responsible for the observed inhibition [51, 108, 109, 114]. Therefore, four building blocks of tannins present in dates, namely catechin, epicatechin, procyanidin B1, procyanidin B2 [39], were purchased and tested for their ability to inhibit VLP attachment. Unfortunately, none of these compounds showed inhibition against GII.4 and GII.10 VLPs in ELISA.

After careful comparison of the compositions of dates and wine, which were the best inhibitors, the three flavonols quercetin, kaempferol and isorhamnetin were identified as common compounds of the two [14, 39]. The compounds were purchased and tested in inhibition assays. All three compounds were able to cause full inhibition with GII.4 VLPs (e.g. dissolved in DMSO: 96 % (quercetin), 86 % (kaempferol), 98 % (isorhamnetin); with IC_{50} values of 80.4 $\mu\text{g/ml}$, 136.4 $\mu\text{g/ml}$, and 25.8 $\mu\text{g/ml}$, respectively). Therefore, it is likely that these specific compounds could be the active compounds for norovirus inhibition. However, further work will need to be performed to identify if the observed inhibition with the natural extracts arises purely from these three compounds. Other potential active compounds, such as other flavonoids, could also contribute to the inhibition. On the other hand, the precise concentration of these compounds in the tested extracts remains unknown. For quercetin, for example, published mean concentrations are 0.93 mg/100 g ($\sim 9.3 \mu\text{g/ml}$) in dates, 0.53 mg/100 g ($\sim 5.3 \mu\text{g/ml}$) in red grape juice, 0.01 - 2.11 mg/100 g ($\sim 0.1 - 21 \mu\text{g/ml}$) in wines or 0.09 mg/100 g ($\sim 0.9 \mu\text{g/ml}$) in white grape juice [43]. Total flavonols in date flesh was reported as 0.85 mg/10 g ($\sim 85 \mu\text{g/ml}$) [39]. Concentration of these flavonols in wines follows the same order as the IC_{50} values observed for wines in our experiments (white grape juice < white wine < red grape juice < red wine) [43].

The physiological concentrations of these compounds are lower than the concentrations tested [43], however they range within the same magnitude. Therefore, additional other compounds or derivatives of the described compounds might exhibit a great share of the observed inhibition in the natural extracts. However, the discovery of flavonols as inhibiting compounds remains the introduction to a new class of compounds probably even including new target sites.

4.3 Combinatory Norovirus Attachment Inhibition

The identification of several promising antiviral candidates raised the question if a combinatorial approach could improve the overall inhibition and could potentially improve the cross-reactivity. Combinations of various inhibitors have been shown to improve the overall inhibition against other virus infections. In the case of HIV treatment, a combinatorial approach became the gold standard for treatment [8, 30, 71]. Could the combination of broadly reactive compounds with a highly specific inhibiting Nanobody or antibody be a possible treatment for norovirus infections? To evaluate if combinations of different inhibitors showed improved inhibition activity, a special set of ELISAs was designed.

Improvement of inhibition was assessed for a combination of a specific Nanobody and the broadly reactive HMO 2'FL. To quantify the improvement of inhibition the Bliss model of independent interaction was chosen [5, 94]. The model assumes that binding and inhibition of each of the compounds is an independent stochastic process, where no inhibitor can affect the interaction of the other. In case of the GI.1 Nanobodies and 2'FL, structural analysis proved that the binding sites of Nanobodies and 2'FL were separate, and an independent binding mechanism could therefore be assumed. The borderline between enhancement and real synergistic improvement was drawn by an increase of inhibition over the estimated expected additive inhibition of 20 % [94]. The interaction between Nano-94 and Nano-7 with 2'FL showed enhanced inhibition for combinations of the two. Synergy evaluation showed that for certain combinations of Nano-94 with 2'FL even synergistic improvement could be observed for several combinations. Of note, also combinations of 2'FL with GI.10 specific Nanobodies showed improvement of inhibition through the combination. This finding might actually further the development of antiviral agents against norovirus in the future. A possible combination could be a Nanobody specifically inhibiting the currently circulating strain, assisted by some broadly reactive compound as 2'FL or some compound derived from date syrup or propolis. The advantage would be improved inhibition of the circulating strain by synergistic inhibition of two or more compounds. In addition, in case the norovirus causing the infection does not belong to the current strain the broadly reactive compounds could still provide their antiviral effect. This joint administration of various compounds can also help to prevent formation of resistances against the antiviral as this has been described in numerous cases [24, 35, 118]. Regarding prevention of resistance, the joint administration might even

be of interest if the combination of different compounds would not show synergistic improvement of inhibition.

Unfortunately, the combinations of honey, propolis or date syrup with Nanobodies showed severe adverse effects in some cases. It is likely that the chosen Nanobodies and the natural extracts compete for a single binding site on the VLPs. This would violate the border conditions of the Bliss model. Although this is not a good result for a possible joint administration of these specific combinations, we regard this as highly important observation. Findings of adverse effects demonstrate that combinations between different antiviral compounds have to be examined carefully in order not to impair one inhibitor by another. The observation that a combination of Nano-94 with 2'FL also yielded synergistic improvement of inhibition, demonstrates that a combination of natural inhibitors and Nanobodies is not generally unfavorable. Similarly, the synergistic improvement of attachment inhibition was observed with the two best inhibitors date syrup and propolis. A combinatorial approach including several broadly reactive natural extracts with one or more specific Nanobodies (targeted to the currently circulating genotype) might indeed be the solution to the burden of consistently involving noroviruses.

5 Conclusion

In this thesis, date syrup, red wines and propolis were identified as promising broadly reactive inhibitors for the attachment of human norovirus. Three flavonols (quercetin, kaempferol, and isorhamnetin) were identified as active inhibiting compounds. Nanobodies also displayed strong inhibition, although they are specific to the genotype they were raised against. Since this would make precise evaluation of each infection before treatment necessary this seems unpracticable. Combinatorial inhibition assays revealed that certain combinations of natural extracts and Nanobodies may greatly improve the overall inhibition results. In some cases, even synergistic improvement was observed. Therefore, a combinatorial use of antivirals would be ideal to overcome the constantly evolving noroviruses. Such a combination might contain a mixture of broadly reactive natural extracts or their compounds as well as Nanobodies. The combination, might improve the overall performance of the inhibition effect. At the same time, a combination of broadly reactive and specific antivirals might minimize the risk of the development of resistant variants. However, it has to be taken into account that all presented results were obtained in *in vitro* experiments with VLPs. Therefore, further studies with the novel enteroid cell culture system [27] or clinical trials are needed to verify these findings *in vivo*. The usage of natural extracts might simplify further studies as the natural extracts are safe as they are already part of the human diet. Yet their inhibitory potential against human noroviruses remains to be proven.

Appendix I Amendments

Appendix I.1 Publications

Journal of Virology:

Structural Basis of Nanobodies Targeting the Prototype Norovirus

Kerstin Ruoff, Turgay Kilic, Jessica Devant, Anna Koromyslova, Alessa Ringel, Alexander Hempelmann, Celina Geiss, Juliane Graf, Michelle Haas, Imme Roggenbach, Grant Hansman

Journal of Virology Mar 2019, 93 (6) e02005-18; DOI: 10.1128/JVI.02005-18

Biomacromolecules:

Fucose-functionalized precision glycomacromolecules targeting human norovirus capsid protein

Katharina Susanne Bücher, Hao Yan, Robert Creutzmacher, Kerstin Ruoff, Alvaro Mallagaray, Andrea Grafmüller, Jan Sebastian Dirks, Turgay Kilic, Sabrina Weickert, Anna Rubailo, Malte Drescher, Stephan Schmidt, Grant Hansman, Thomas Peters, Charlotte Uetrecht, Laura Hartmann

Biomacromolecules August 2018, 19 (9), 3714-3724.

Appendix I.2 Contributions

GII.10-specific Nanobodies were screened and provided by Dr. Anna Koromyslova. ELISA protocols were optimized based on protocols provided by Dr. Anna Koromyslova.

VLPs used in this study were provided by Dr. Jessica Devant and Dr. Grant Hansman, several VLPs were produced by myself.

Electron microscopy experiments were performed by myself and supported by the Core Facility unit Electron Microscopy, DKFZ, Heidelberg.

Appendix I.2.1 Screening of the NIH Collection

The automated X-ray crystallography screening was performed by Jose A. Marquez and his team at ESRF, Grenoble, France.

Mother solution and template for GII.10 026 P domain crystallization were provided by Dr. Grant Hansman.

Production, purification, and optimization of the crystallization (drop ratio) was performed by myself. As were manual screening of the auto processed data and manual processing and screening of raw data obtained in the screening.

Compounds of the NIH collection for in-house screening were organized and provided by Dr. Grant Hansman.

Experiments were conducted by myself.

Appendix I.2.2 Synthetic Multivalent Fucose Oligomers

Synthetic multivalent fucose oligomers were constructed synthesized and provided by Katharina Bücher, Hartmann group, Heinrich-Heine-University, Düsseldorf.

Crystals were provided and soaked by Dr. Grant Hansman.

X-ray crystallography data collection, structure analysis and refinement were performed in cooperation by Dr. Turgay Kilic and myself.

Data collection was performed at the ESRF in Grenoble, France.

Appendix I.2.3 GI.1-specific Nanobodies

Expression and purification of the GI.1-specific Nanobodies was performed by Alexander Hempelmann, Celina Geiss, Juliane Graf, Michelle Haas, and Imme Roggenbach in the norovirus study group of Dr. Grant Hansman.

Expression of GI VLPs was performed by Dr. Jessica Devant, Alessa Riengel and myself.

Set up of crystals, data collection and initial analysis of the X-ray crystallography data of Nano-7 was performed by myself. The structures were refined and finalized by Dr. Turgay Kilic.

Analysis of the structure was performed by Dr. Turgay Kilic, Dr. Jessica Devant, and myself.

Screening of the panel of GI.1 specific Nanobodies was performed by myself.

Further ELISA experiments and their analysis were the result of the joint efforts between Dr. Jessica Devant, Alessa Ringel and myself.

EM and DLS analyses were performed by Dr. Jessica Devant and myself.

ITC analysis were performed by Dr. Anna Koromyslova and myself (Nano-7).

The manuscript was written by Dr. Grant Hansman, Dr. Jessica Devant, Alessa Ringel, Dr. Anna Koromyslova, and myself.

Appendix I.2.4 Binding of GI.1-specific Nanobodies to S Domain

S domain constructs were designed and purchased by Dr. Grant Hansman.

Cloning, expression, and ELISA experiments were conducted by myself.

Appendix I.2.5 HMO Screening

The HMO screening was developed and performed by the National Center of Functional Glycomics (NCFG) service, Boston, USA [124].

Data was analyzed and processed by myself.

Appendix I.2.6 Plant Derived Syrups and Saps

All experiments in this chapter were designed and conducted by myself except: Crystallization screening to optimize crystallization conditions of the individual co-crystals, (mixtures of GII.10 026 P domain and the four most promising natural extracts based on performance in ELISA and DLS) was performed at the Crystallization platform at the excellence cluster, University of Heidelberg.

Gas chromatography analysis to identify compounds in date syrup was performed by the Metabolomics Core Technology Platform University Heidelberg (Gernot Poschet)

Attempts to identify the ligands in the crystal structures were supported by Dr. Charles Sabin and Dr. Turgay Kilic.

Appendix I.2.7 Honey

Contributions in this chapter were similar to the precious chapter:

All experiments in this chapter were designed and conducted by myself except:

Attempts to identify the ligands in the crystal structures were supported by Dr. Charles Sabin and Dr. Turgay Kilic.

Appendix I.2.8 Honey

Contributions in this chapter were similar to the precious chapter:

All experiments in this chapter were designed and conducted by myself except:

Crystallization screening to optimize crystallization conditions of the individual co-crystals, (mixtures of GII.10 026 P domain and the four most promising natural extracts based on performance in ELISA and DLS) was performed at the Crystallization platform at the excellence cluster, University of Heidelberg.

Attempts to identify the ligands in the crystal structures were supported by Dr. Charles Sabin and Dr. Turgay Kilic.

Appendix I.2.9 Combinations of Nanobodies with 2'FL

Synergy ELISA experiments were designed and conducted jointly by Dr. Jessica Devant, Alessa Riengel, and myself.

Appendix I.2.10 Combinations of Nanobodies with Natural Extracts

All experiments in this chapter were designed and conducted by myself.

Appendix I.2.11 Combinations of Natural Extracts

All experiments in this chapter were designed and conducted by myself.

Appendix I.3 Supplemental Tables and Figures

Appendix I.3.1 Automated X-ray Crystallography Screening

Table A I-1: Summary of automated X-ray crystallography analysis results (Pipedream)
All datasets that were auto processed by Pipedream were manually evaluated

Data set	postrefine	ligand	does map additional density fit map? manually verified	density for ligand in difference map	discription
PDMN-CD022192_A03-3_pipedream	X				
PDMN-CD022192_A03-3_pipedream1	X				
PDMN-CD022192_A04-3_pipedream	✓	✓	X	X	
PDMN-CD022192_A05-1_pipedream	✓	✓	X	X	
PDMN-CD022192_A06-1_pipedream	✓	✓	?	additional density	huge blob
PDMN-CD022192_A08-3_pipedream	X				
PDMN-CD022192_A08-3_pipedream1	X				
PDMN-CD022192_A09-1_pipedream	X				
PDMN-CD022192_A09-1_pipedream1	X				
PDMN-CD022192_A10-1_pipedream	✓	✓	X	X	
PDMN-CD022192_A11-1_pipedream	✓	✓	X	X	
PDMN-CD022192_A12-1_x1_pipedream	✓	✓	X	additional density	two large blobs
PDMN-CD022192_A12-1_x2_pipedream	✓	✓	?	X	
PDMN-CD022192_B04-1_pipedream	✓	✓	?	X	
PDMN-CD022192_B05-3_pipedream	X				
PDMN-CD022192_B05-3_pipedream1	X				
PDMN-CD022192_B06-1_pipedream	✓	✓	X	X	
PDMN-CD022192_B08-3_pipedream	✓	✓	✓	additional density	two rings
PDMN-CD022192_B09-3_pipedream	✓	✓	X	X	
PDMN-CD022192_B10-3_pipedream	✓	✓	X	X	
PDMN-CD022192_B11-2_pipedream	X				
PDMN-CD022192_B11-2_pipedream1	X				

Data set	postrefine	ligand	does map additional density fit map? manually verified	density for ligand in difference map	discription
PDMN-CD022192_B12-1_pipedream	X				
PDMN-CD022192_B12-1_pipedream1	X				
PDMN-CD022192_C05-1_2_pipedream	X				
PDMN-CD022192_C05-1_2_pipedream1	X				
PDMN-CD022192_C06-1_pipedream	✓	✓	?	X	
PDMN-CD022192_C07-1_pipedream	✓	✓	✓	X	
PDMN-CD022192_C08-1_pipedream	✓	✓	X	X	
PDMN-CD022192_C11-1_pipedream	✓	✓	Different location	additional density	four large blobs
PDMN-CD022192_C12-3_pipedream	✓	✓	X	additional density	two blobs
PDMN-CD022192_D03-1_pipedream	✓	✓	✓	additional density	two blobs
PDMN-CD022192_D04-3_pipedream	✓	✓	X	additional density	one blob
PDMN-CD022192_D05-3_pipedream	✓	✓	X	additional density	one blob
PDMN-CD022192_D06-1_pipedream	✓	✓	X	X	
PDMN-CD022192_D07-1_pipedream	✓	✓	X	additional density	two large blobs
PDMN-CD022192_D08-3_pipedream	X				
PDMN-CD022192_D08-3_pipedream1	X				
PDMN-CD022192_D09-3_pipedream	✓	✓	X	X	
PDMN-CD022192_D10-1_pipedream	X				
PDMN-CD022192_D10-1_pipedream1	X				
PDMN-CD022192_D11-1_pipedream	✓	✓	?	X	
PDMN-CD022192_D12-1_x1_pipedream	✓	✓	✓	additional density	one huge blob
PDMN-CD022192_D12-1_x1_pipedream1	✓	✓	X	X	
PDMN-CD022192_D12-1_x2_pipedream	✓	✓	X	X	
PDMN-CD022192_D12-1_x2_pipedream1	✓	✓	?	X	
PDMN-CD022192_E03-1_pipedream	✓	✓	✓	additional density	two large blobs
PDMN-CD022192_E04-1_pipedream	✓	✓	?	X	
PDMN-CD022192_E05-3_pipedream	✓	✓	X	additional density	two large blobs
PDMN-CD022192_E06-2_pipedream	✓	✓	X	X	

Data set	postrefine	ligand	does map additional density fit map? manually verified	density for ligand in difference map	discription
PDMN-CD022192_E07-2_pipedream	✓	✓	X	X	
PDMN-CD022192_E08-1_pipedream	✓	✓	X	X	
PDMN-CD022192_E09-3_pipedream	✓	✓	?	additional density	two large blobs
PDMN-CD022192_E10-3_pipedream	X				
PDMN-CD022192_E10-3_pipedream1	X				
PDMN-CD022192_E11-2_pipedream	X				
PDMN-CD022192_E11-2_pipedream1	X				
PDMN-CD022192_E12-3_pipedream	✓	✓	X	X	
PDMN-CD022192_F03-2_pipedream	✓	✓	X	additional density	two large blobs
PDMN-CD022192_F05-3_pipedream	X				
PDMN-CD022192_F05-3_pipedream1	X				
PDMN-CD022192_F06-1_pipedream	X				
PDMN-CD022192_F06-1_pipedream1	X				
PDMN-CD022192_F07-3_pipedream	X				
PDMN-CD022192_F07-3_pipedream1	X				
PDMN-CD022192_F08-1_pipedream	X				
PDMN-CD022192_F08-1_pipedream1	X				
PDMN-CD022192_F09-1_pipedream	✓	✓	X	X	
PDMN-CD022192_F10-1_pipedream	✓	✓	X	X	
PDMN-CD022192_F11-1_pipedream	✓	✓	✓	X	
PDMN-CD022192_F12-3_pipedream	✓	✓	X	X	
PDMN-CD022192_G04-1_pipedream	X				
PDMN-CD022192_G04-1_pipedream1	X				
PDMN-CD022192_G04-3_pipedream	X				
PDMN-CD022192_G04-3_pipedream1	X				
PDMN-CD022192_G05-3_pipedream	✓	✓	X	X	
PDMN-CD022192_G06-3_pipedream	✓	✓	X	X	
PDMN-CD022192_G07-1_pipedream	✓	✓	?	additional density	one large blob

Data set	postrefine	ligand	does map additional density fit map? manually verified	density for ligand in difference map	discription
PDMN-CD022192_G08-3_pipedream	X				
PDMN-CD022192_G08-3_pipedream1	X				
PDMN-CD022192_G09-1_pipedream	X				
PDMN-CD022192_G09-1_pipedream1	X				
PDMN-CD022192_G10-3_pipedream	✓	✓	X	X	
PDMN-CD022192_G11-3_pipedream	✓	✓	?	additional density	one large blob
PDMN-CD022192_G12-1_pipedream	✓	✓	X	X	
PDMN-CD022192_H03-2_x1_pipedream	✓	✓	X	X	
PDMN-CD022192_H03-2_x1_pipedream1	✓	✓	X	X	
PDMN-CD022192_H03-2_x2_pipedream	✓	✓	X	X	
PDMN-CD022192_H03-2_x2_pipedream1	✓	✓	X	X	
PDMN-CD022192_H04-1_pipedream	✓	✓	X	X	
PDMN-CD022192_H04-2_pipedream	X				
PDMN-CD022192_H04-2_pipedream1	X				
PDMN-CD022192_H05-3_pipedream	✓	✓	X	X	
PDMN-CD022192_H06-2_pipedream	X				
PDMN-CD022192_H06-2_pipedream1	X				
PDMN-CD022192_H07-3_2_pipedream	X				
PDMN-CD022192_H07-3_2_pipedream1	X				
PDMN-CD022192_H07-3_pipedream	✓	✓	X	X	
PDMN-CD022192_H08-1_pipedream	X				
PDMN-CD022192_H08-1_pipedream1	X				
PDMN-CD022192_H09-1_pipedream	X				
PDMN-CD022192_H09-1_pipedream1	X				
PDMN-CD022192_H10-1_pipedream	X				
PDMN-CD022192_H10-1_pipedream1	X				
PDMN-CD022192_H11-1_pipedream	✓	✓	X	X	
PDMN-CD022192_H12-1_pipedream	✓	✓	?	additional density	one large blob

Data set	postrefine	ligand	does map additional density fit map? manually verified	density for ligand in difference map	discription
PDMN-CD022196_A03-3_pipedream	X				
PDMN-CD022196_A03-3_pipedream1	X				
PDMN-CD022196_A05-2_pipedream	✓	✓	✓	additional density	several large blobs
PDMN-CD022196_A06-3_2_pipedream	✓	✓	?	X	
PDMN-CD022196_A06-3_pipedream	X				
PDMN-CD022196_A06-3_pipedream1	X				
PDMN-CD022196_A07-2_pipedream	✓	✓	X	X	
PDMN-CD022196_A09-2_pipedream	✓	✓	X	X	
PDMN-CD022196_A10-2_pipedream	✓	✓	✓	additional density	several huge blobs
PDMN-CD022196_B02-2_pipedream	✓	✓	X	additional density	two large blobs
PDMN-CD022196_B06-3_pipedream	✓	✓	X	X	
PDMN-CD022196_B08-2_pipedream	✓	✓	X	X	
PDMN-CD022196_B09-3_pipedream	✓	✓	?	additional density	several large blobs
PDMN-CD022196_B11-2_pipedream	✓	✓	X	additional density	two large blobs
PDMN-CD022196_C02-3_pipedream	✓	✓	X	X	
PDMN-CD022196_C03-1_pipedream	✓	✓	X	X	
PDMN-CD022196_C03-2_pipedream	✓	✓	?	additional density	two large blobs
PDMN-CD022196_C04-3_pipedream	X				
PDMN-CD022196_C04-3_pipedream1	X				
PDMN-CD022196_C05-3_pipedream	X				
PDMN-CD022196_C05-3_pipedream1	X				
PDMN-CD022196_C06-1_pipedream	✓	✓	?	additional density	three large blobs
PDMN-CD022196_C07-1_pipedream	✓	✓	X	X	
PDMN-CD022196_C08-2_pipedream	✓	✓	X	X	
PDMN-CD022196_C09-2_pipedream	✓	✓	X	X	
PDMN-CD022196_D02-2_pipedream	X				
PDMN-CD022196_D02-2_pipedream1	X				
PDMN-CD022196_D03-3_2_pipedream	✓	✓	X	X	

Data set	postrefine	ligand	does map additional density fit map? manually verified	density for ligand in difference map	discription
PDMN-CD022196_D03-3_pipedream	✓	✓	X	X	
PDMN-CD022196_D06-3_pipedream	✓	✓	X	X	
PDMN-CD022196_D08-1_pipedream	✓	✓	X	X	
PDMN-CD022196_D09-1_pipedream	✓	✓	?	additional density	five large blobs
PDMN-CD022196_D10-3_pipedream	✓	✓	X	X	
PDMN-CD022196_D11-2_pipedream	✓	✓	X	X	
PDMN-CD022196_E02-3_pipedream	✓	✓	X	X	
PDMN-CD022196_E03-2_pipedream	✓	✓	X	additional density	one ring
PDMN-CD022196_E04-1_pipedream	✓	✓	X	X	
PDMN-CD022196_E05-2_pipedream	✓	✓	X	X	
PDMN-CD022196_E06-3_pipedream	✓	✓	?	additional density	three large blobs
PDMN-CD022196_E07-1_pipedream	✓	✓	X	X	
PDMN-CD022196_E08-2_pipedream	✓	✓	X	additional density	four large blobs
PDMN-CD022196_E10-2_pipedream	X				
PDMN-CD022196_E10-2_pipedream1	X				
PDMN-CD022196_E11-3_pipedream	✓	✓	X	X	
PDMN-CD022196_F02-1_pipedream	✓	✓	Different location	additional density	two huge blobs
PDMN-CD022196_F03-3_pipedream	✓	✓	?	additional density	three large blobs
PDMN-CD022196_F04-3_pipedream	✓	✓	X	X	
PDMN-CD022196_F05-3_pipedream	✓	✓	X	X	
PDMN-CD022196_F05-3_pipedream1	X				
PDMN-CD022196_F05-3_pipedream2	X				
PDMN-CD022196_F07-1_pipedream	✓	✓	X	X	
PDMN-CD022196_F08-1_pipedream	✓	✓	X	X	
PDMN-CD022196_F09-2_pipedream	✓	✓	X	X	
PDMN-CD022196_F10-2_pipedream	✓	✓	X	X	
PDMN-CD022196_F11-2_pipedream	✓	✓	?	additional density	four large blobs
PDMN-CD022196_G02-3_pipedream	✓	✓	X	X	

Data set	postrefine	ligand	does map additional density fit map? manually verified	density for ligand in difference map	discription
PDMN-CD022196_G03-1_pipedream	✓	✓	X	X	
PDMN-CD022196_G03-2_pipedream	✓	✓	X	X	
PDMN-CD022196_G06-1_pipedream	✓	✓	X	additional density	three large blobs
PDMN-CD022196_G10-1_pipedream	✓	✓	X	X	
PDMN-CD022196_G11-2_pipedream	✓	✓	?	additional density	four large blobs
PDMN-CD022196_H02-1_pipedream	X				
PDMN-CD022196_H02-1_pipedream1	X				
PDMN-CD022196_H03-3_pipedream	✓	✓	✓	additional density	one large blob
PDMN-CD022196_H04-2_pipedream	✓	✓	X	X	
PDMN-CD022196_H05-2_pipedream	✓	✓	X	X	
PDMN-CD022196_H06-1_pipedream	✓	✓	X	X	
PDMN-CD022196_H07-1_pipedream	✓	✓	X	X	
PDMN-CD022196_H08-2_pipedream	✓	✓	X	X	
PDMN-CD022196_H10-3_pipedream	✓	✓	X	X	
PDMN-CD022196_H11-1_pipedream	✓	✓	Different location	additional density	one large blob
PDMN-CD022196_H11-3_pipedream	✓	✓	✓	additional density	two large blobs
PDMN-CD022197_A02-2_pipedream	X				
PDMN-CD022197_A02-2_pipedream1	X				
PDMN-CD022197_A03-1_pipedream	X				
PDMN-CD022197_A03-1_pipedream1	X				
PDMN-CD022197_A04-1_pipedream	X				
PDMN-CD022197_A04-1_pipedream1	X				
PDMN-CD022197_A05-1_pipedream	X				
PDMN-CD022197_A05-1_pipedream1	X				
PDMN-CD022197_A05-1_pipedream2	X				
PDMN-CD022197_A05-1_pipedream3	X				
PDMN-CD022197_A06-2_pipedream	X				
PDMN-CD022197_A06-2_pipedream1	X				

Data set	postrefine	ligand	does map additional density fit map? manually verified	density for ligand in difference map	discription
PDMN-CD022197_A07-3_pipedream	X				
PDMN-CD022197_A07-3_pipedream1	X				
PDMN-CD022197_A08-1_pipedream	X				
PDMN-CD022197_A08-1_pipedream1	X				
PDMN-CD022197_A09-3_pipedream	X				
PDMN-CD022197_A09-3_pipedream1	X				
PDMN-CD022197_A10-1_pipedream	X				
PDMN-CD022197_A10-1_pipedream1	X				
PDMN-CD022197_B02-2_pipedream	X				
PDMN-CD022197_B02-2_pipedream1	X				
PDMN-CD022197_B03-1_pipedream	X				
PDMN-CD022197_B03-1_pipedream1	X				
PDMN-CD022197_B04-2_pipedream	X				
PDMN-CD022197_B04-2_pipedream1	X				
PDMN-CD022197_B05-3_pipedream	X				
PDMN-CD022197_B05-3_pipedream1	X				
PDMN-CD022197_B05-3_pipedream2	X				
PDMN-CD022197_B05-3_pipedream3	X				
PDMN-CD022197_B06-1_pipedream	X				
PDMN-CD022197_B06-1_pipedream1	X				
PDMN-CD022197_B07-3_pipedream	X				
PDMN-CD022197_B07-3_pipedream1	X				
PDMN-CD022197_B08-1_pipedream	X				
PDMN-CD022197_B08-1_pipedream1	X				
PDMN-CD022197_B09-3_pipedream	X				
PDMN-CD022197_B09-3_pipedream1	X				
PDMN-CD022197_B11-1_pipedream	X				
PDMN-CD022197_B11-1_pipedream1	X				

Data set	postrefine	ligand	does map additional density fit map? manually verified	density for ligand in difference map	discription
PDMN-CD022197_C02-2_pipedream	X				
PDMN-CD022197_C02-2_pipedream1	X				
PDMN-CD022197_C03-3_pipedream	X				
PDMN-CD022197_C03-3_pipedream1	X				
PDMN-CD022197_C04-1_pipedream	X				
PDMN-CD022197_C04-1_pipedream1	X				
PDMN-CD022197_C05-1_pipedream	X				
PDMN-CD022197_C05-1_pipedream1	X				
PDMN-CD022197_C06-3_pipedream	X				
PDMN-CD022197_C06-3_pipedream1	X				
PDMN-CD022197_C07-3_pipedream	X				
PDMN-CD022197_C07-3_pipedream1	X				
PDMN-CD022197_C08-2_pipedream	X				
PDMN-CD022197_C08-2_pipedream1	X				
PDMN-CD022197_C10-1_pipedream	X				
PDMN-CD022197_C10-1_pipedream1	X				
PDMN-CD022197_C11-3_pipedream	X				
PDMN-CD022197_C11-3_pipedream1	X				
PDMN-CD022197_D02-3_pipedream	X				
PDMN-CD022197_D02-3_pipedream1	X				
PDMN-CD022197_D03-2_pipedream	X				
PDMN-CD022197_D03-2_pipedream1	X				
PDMN-CD022197_D04-3_1_pipedream	X				
PDMN-CD022197_D04-3_1_pipedream1	X				
PDMN-CD022197_D04-3_pipedream	X				
PDMN-CD022197_D04-3_pipedream1	X				
PDMN-CD022197_D06-1_pipedream	X				
PDMN-CD022197_D06-1_pipedream1	X				

Data set	postrefine	ligand	does map additional density fit map? manually verified	density for ligand in difference map	discription
PDMN-CD022197_D07-1_pipedream	X				
PDMN-CD022197_D07-1_pipedream1	X				
PDMN-CD022197_D08-3_pipedream	X				
PDMN-CD022197_D08-3_pipedream1	X				
PDMN-CD022197_D09-2_pipedream	X				
PDMN-CD022197_D09-2_pipedream1	X				
PDMN-CD022197_D10-2_pipedream	X				
PDMN-CD022197_D10-2_pipedream1	X				
PDMN-CD022197_D11-3_pipedream	X				
PDMN-CD022197_D11-3_pipedream1	X				
PDMN-CD022197_E02-3_pipedream	X				
PDMN-CD022197_E02-3_pipedream1	X				
PDMN-CD022197_E03-1_pipedream	X				
PDMN-CD022197_E03-1_pipedream1	X				
PDMN-CD022197_E04-2_pipedream	X				
PDMN-CD022197_E04-2_pipedream1	X				
PDMN-CD022197_E05-3_x2_pipedream	X				
PDMN-CD022197_E05-3_x2_pipedream1	X				
PDMN-CD022197_E05-3_x2_pipedream2	X				
PDMN-CD022197_E05-3_x2_pipedream3	X				
PDMN-CD022197_E05-3_x4_pipedream	X				
PDMN-CD022197_E05-3_x4_pipedream1	X				
PDMN-CD022197_E05-3_x4_pipedream2	X				
PDMN-CD022197_E05-3_x4_pipedream3	X				
PDMN-CD022197_E06-2_pipedream	X				
PDMN-CD022197_E06-2_pipedream1	X				
PDMN-CD022197_E07-2_pipedream	X				
PDMN-CD022197_E07-2_pipedream1	X				

Data set	postrefine	ligand	does map additional density fit map? manually verified	density for ligand in difference map	discription
PDMN-CD022197_E08-3_pipedream	X				
PDMN-CD022197_E08-3_pipedream1	X				
PDMN-CD022197_E09-2_pipedream	X				
PDMN-CD022197_E09-2_pipedream1	X				
PDMN-CD022197_E10-1_pipedream	X				
PDMN-CD022197_E10-1_pipedream1	X				
PDMN-CD022197_E11-2_pipedream	X				
PDMN-CD022197_E11-2_pipedream1	X				
PDMN-CD022197_F02-2_pipedream	X				
PDMN-CD022197_F02-2_pipedream1	X				
PDMN-CD022197_F03-1_pipedream	X				
PDMN-CD022197_F03-1_pipedream1	X				
PDMN-CD022197_F03-3_pipedream	X				
PDMN-CD022197_F03-3_pipedream1	X				
PDMN-CD022197_F04-1_pipedream	X				
PDMN-CD022197_F04-1_pipedream1	X				
PDMN-CD022197_F05-1_pipedream	X				
PDMN-CD022197_F05-1_pipedream1	X				
PDMN-CD022197_F06-1_pipedream	X				
PDMN-CD022197_F06-1_pipedream1	X				
PDMN-CD022197_F06-2_pipedream	X				
PDMN-CD022197_F06-2_pipedream1	X				
PDMN-CD022197_F07-2_pipedream	X				
PDMN-CD022197_F07-2_pipedream1	X				
PDMN-CD022197_F09-2_pipedream	X				
PDMN-CD022197_F09-2_pipedream1	X				
PDMN-CD022197_F10-3_pipedream	X				
PDMN-CD022197_F10-3_pipedream1	X				

Data set	postrefine	ligand	does map additional density fit map? manually verified	density for ligand in difference map	discription
PDMN-CD022197_F11-3_pipedream	X				
PDMN-CD022197_F11-3_pipedream1	X				
PDMN-CD022197_G02-3_pipedream	X				
PDMN-CD022197_G02-3_pipedream1	X				
PDMN-CD022197_G03-3_pipedream	X				
PDMN-CD022197_G03-3_pipedream1	X				
PDMN-CD022197_G04-2_pipedream	X				
PDMN-CD022197_G04-2_pipedream1	X				
PDMN-CD022198_A02-2_pipedream	✓	✓	X	X	
PDMN-CD022198_A03-1_pipedream	✓	✓	X	X	
PDMN-CD022198_A04-1_pipedream	✓	✓	X	X	
PDMN-CD022198_A05-1_pipedream	✓	✓	X	X	
PDMN-CD022198_A06-1_pipedream	X				
PDMN-CD022198_A06-1_pipedream1	X				
PDMN-CD022198_A07-2_pipedream	✓	✓	?	X	
PDMN-CD022198_B02-2_pipedream	✓	✓	X	X	
PDMN-CD022198_B03-3_pipedream	✓	✓	X	X	
PDMN-CD022198_B04-3_pipedream	✓	✓	X	X	
PDMN-CD022198_B05-1_pipedream	X				
PDMN-CD022198_B05-1_pipedream1	X				
PDMN-CD022198_B06-1_pipedream	✓	✓	X	X	
PDMN-CD022198_B07-3_pipedream	✓	✓	X	X	
PDMN-CD022198_C02-2_pipedream	✓	✓	X	X	
PDMN-CD022198_C03-3_2_x1_pipedream	✓	✓	X	X	
PDMN-CD022198_C03-3_pipedream	✓	✓	X	X	
PDMN-CD022198_C04-1_pipedream	✓	✓	X	X	
PDMN-CD022198_C05-1_pipedream	✓	✓	X	X	
PDMN-CD022198_C06-1_pipedream	✓	✓	?	additional density	two large blobs

Data set	postrefine	ligand	does map additional density fit map? manually verified	density for ligand in difference map	discription
PDMN-CD022198_D02-3_pipedream	✓	✓	X	X	
PDMN-CD022198_D03-3_pipedream	✓	✓	X	X	
PDMN-CD022198_D04-2_pipedream	X				
PDMN-CD022198_D04-2_pipedream1	X				
PDMN-CD022198_D05-2_pipedream	✓	✓	X	X	
PDMN-CD022198_D06-1_pipedream	✓	✓	X	X	
PDMN-CD022198_D07-3_pipedream	✓	✓	X	X	
PDMN-CD022198_E03-2_pipedream	✓	✓	X	X	
PDMN-CD022198_E04-2_pipedream	✓	✓	X	X	
PDMN-CD022198_E05-2_pipedream	✓	✓	X	X	
PDMN-CD022198_E07-3_pipedream	✓	✓	X	X	
PDMN-CD022198_F03-2_2_x1_pipedream	✓	✓	X	X	
PDMN-CD022198_F03-2_pipedream	✓	✓	X	X	
PDMN-CD022198_F04-3_pipedream	✓	✓	X	X	
PDMN-CD022198_F05-1_pipedream	X				
PDMN-CD022198_F05-1_pipedream1	X				
PDMN-CD022198_F06-1_pipedream	✓	✓	?	X	
PDMN-CD022198_F07-3_pipedream	✓	✓	X	X	
PDMN-CD022198_G03-2_pipedream	✓	✓	X	X	
PDMN-CD022198_G04-3_pipedream	✓	✓	X	X	
PDMN-CD022198_G05-3_pipedream	X				
PDMN-CD022198_G05-3_pipedream1	X				
PDMN-CD022198_G06-3_pipedream	✓	✓	X	X	
PDMN-CD022198_H04-2_pipedream	✓	✓	X	X	
PDMN-CD022198_H05-1_pipedream	X				
PDMN-CD022198_H05-1_pipedream1	X				
PDMN-CD022198_H06-3_2_x1_pipedream	✓	✓	X	additional density	one large blob
PDMN-CD022198_H06-3_pipedream	✓	✓	?	additional density	one large blob

Data set	postrefine	ligand	does map additional density fit map? manually verified	density for ligand in difference map	discription
PDMN-CD022648_A02-3_pipedream	✓	✓	?	additional density	several blobs
PDMN-CD022648_A03-2_pipedream	✓	✓	X	X	
PDMN-CD022648_A04-3_pipedream	✓	✓	X	X	
PDMN-CD022648_A05-1_pipedream	✓	✓	✓	X	
PDMN-CD022648_A07-3_pipedream	✓	✓	X	X	
PDMN-CD022648_A08-1_pipedream	✓	✓	X	additional density	one large blob
PDMN-CD022648_A09-2_pipedream	✓	✓	✓	additional density	one large blob
PDMN-CD022648_A10-3_pipedream	✓	✓	X	X	
PDMN-CD022648_A11-2_pipedream	✓	✓	X	additional density	one large blob
PDMN-CD022648_B02-1_pipedream	✓	✓	?	X	
PDMN-CD022648_B02-2_pipedream	X				
PDMN-CD022648_B02-2_pipedream1	X				
PDMN-CD022648_B03-2_pipedream	✓	✓	X	additional density	three large blobs
PDMN-CD022648_B04-3_pipedream	✓	✓	X	X	
PDMN-CD022648_B05-2_pipedream	✓	✓	X	additional density	one large blob
PDMN-CD022648_B07-3_pipedream	✓	✓	X	X	
PDMN-CD022648_B08-3_pipedream	✓	✓	✓	X	
PDMN-CD022648_B09-1_pipedream	✓	✓	X	X	rhofit, no mtz in postrefine
PDMN-CD022648_B09-1_pipedream1	✓	✓	X	X	rhofit, no mtz in postrefine
PDMN-CD022648_B10-1_pipedream	✓	✓	✓	X	
PDMN-CD022648_B11-3_pipedream	✓	✓	X	X	
PDMN-CD022648_C02-3_pipedream	✓	✓	✓	additional density	two large blobs
PDMN-CD022648_C03-2_pipedream	✓	✓	?	X	
PDMN-CD022648_C04-2_2_pipedream	X				
PDMN-CD022648_C04-2_2_pipedream1	X				
PDMN-CD022648_C04-2_pipedream	✓	✓	X	X	
PDMN-CD022648_C05-2_pipedream	✓	✓	X	additional density	one large blob
PDMN-CD022648_C06-1_pipedream	✓	✓	X	X	

Data set	postrefine	ligand	does map additional density fit map? manually verified	density for ligand in difference map	discription
PDMN-CD022648_C07-2_pipedream	✓	✓	X	X	
PDMN-CD022648_C08-1_pipedream	✓	✓	X	X	
PDMN-CD022648_C09-1_pipedream	✓	✓	?	X	
PDMN-CD022648_C10-2_pipedream	✓	✓	?	X	
PDMN-CD022648_C11-1_pipedream	✓	✓	X	X	rhofit, no mtz in postrefine
PDMN-CD022648_C11-1_pipedream1	✓	✓	X	X	rhofit, no mtz in postrefine
PDMN-CD022648_D02-3_pipedream	✓	✓	X	X	
PDMN-CD022648_D03-1_pipedream	X				
PDMN-CD022648_D03-1_pipedream1	X				
PDMN-CD022648_D04-2_pipedream	✓	✓	X	X	
PDMN-CD022648_D05-3_2_pipedream	✓	✓	?	X	
PDMN-CD022648_D06-1_pipedream	✓	✓	✓	X	
PDMN-CD022648_D07-1_pipedream	✓	✓	?	additional density	three large blobs
PDMN-CD022648_D08-1_pipedream	✓	✓	X	X	
PDMN-CD022648_D09-2_pipedream	✓	✓	?	X	
PDMN-CD022648_D10-2_pipedream	✓	✓	X	X	
PDMN-CD022648_D11-1_pipedream	✓	✓	X	X	
PDMN-CD022648_E02-3_pipedream	✓	✓	✓	X	
PDMN-CD022648_E03-2_pipedream	✓	✓	✓	X	
PDMN-CD022648_E04-3_pipedream	✓	✓	X	X	
PDMN-CD022648_E05-1_pipedream	✓	✓	X	X	
PDMN-CD022648_E05-3_pipedream	✓	✓	?	X	
PDMN-CD022648_E06-3_pipedream	✓	X	X	X	
PDMN-CD022648_E06-3_pipedream1	✓	X	X	X	
PDMN-CD022648_E07-1_pipedream	✓	✓	X	X	
PDMN-CD022648_E08-2_pipedream	✓	✓	✓	X	
PDMN-CD022648_E09-2_pipedream	✓	✓	X	X	
PDMN-CD022648_E10-3_pipedream	✓	✓	?	additional density	two large blobs

Data set	postrefine	ligand	does map additional density fit map? manually verified	density for ligand in difference map	discription
PDMN-CD022648_E11-2_pipedream	✓	✓	?	additional density	one large blob
PDMN-CD022648_F02-2_pipedream	✓	✓	?	additional density	two large blobs
PDMN-CD022648_F04-3_pipedream	✓	✓	X	X	
PDMN-CD022648_F06-2_pipedream	✓	✓	?	additional density	three huge blobs
PDMN-CD022648_F07-3_pipedream	✓	✓	X	additional density	one large blob
PDMN-CD022648_F08-1_pipedream	✓	✓	X	X	
PDMN-CD022648_F09-2_pipedream	✓	✓	X	X	
PDMN-CD022648_F10-3_pipedream	✓	✓	?	X	
PDMN-CD022648_F11-1_pipedream	✓	✓	X	X	
PDMN-CD022648_G03-2_pipedream	✓	✓	?	additional density	two large blobs
PDMN-CD022648_G03-3_pipedream	X				
PDMN-CD022648_G03-3_pipedream1	X				
PDMN-CD022648_G04-1_pipedream	✓	✓	?	X	
PDMN-CD022648_G05-1_pipedream	✓	✓	X	X	
PDMN-CD022648_G06-1_pipedream	✓	✓	X	X	
PDMN-CD022648_G06-2_pipedream	✓	✓	X	X	
PDMN-CD022648_G07-3_pipedream	✓	✓	?	additional density	three large blobs
PDMN-CD022648_G08-1_pipedream	✓	✓	✓	X	
PDMN-CD022648_G09-2_pipedream	✓	✓	X	X	
PDMN-CD022648_G10-3_pipedream	✓	✓	?	additional density	one large blob
PDMN-CD022648_G11-3_pipedream	✓	✓	X	additional density	two large blobs
PDMN-CD022648_H02-1_pipedream	✓	✓	X	X	
PDMN-CD022648_H03-1_pipedream	✓	✓	X	X	
PDMN-CD022648_H04-1_pipedream	✓	✓	?	X	
PDMN-CD022648_H05-3_pipedream	✓	✓	?	additional density	one large blob
PDMN-CD022648_H06-3_pipedream	✓	✓	X	X	
PDMN-CD022648_H07-2_pipedream	✓	✓	X	X	
PDMN-CD022648_H08-1_pipedream	✓	✓	?	additional density	five large blobs

Data set	postrefine	ligand	does map additional density fit map? manually verified	density for ligand in difference map	discription
PDMN-CD022648_H09-3_pipedream	✓	✓	✓	X	
PDMN-CD022648_H10-2_pipedream	✓	✓	X	X	
PDMN-CD022648_H11-2_pipedream	X				
PDMN-CD022648_H11-2_pipedream1	X				
PDMN-CD022651_A02-2_pipedream	X				
PDMN-CD022651_A02-2_pipedream1	X				
PDMN-CD022651_A06-1_pipedream	✓	✓	X	additional density	four large blobs
PDMN-CD022651_A07-1_pipedream	✓	✓	X	X	
PDMN-CD022651_A07-1_pipedream1	✓	✓	X	X	
PDMN-CD022651_A08-2_pipedream	✓	✓	?	X	
PDMN-CD022651_A09-2_pipedream	✓	✓	Different location	additional density	ten large blobs
PDMN-CD022651_B04-1_pipedream	✓	✓	X	additional density	two large blobs
PDMN-CD022651_B06-3_pipedream	✓	✓	Different location	additional density	ten large blobs
PDMN-CD022651_B07-2_pipedream	✓	✓	?	X	
PDMN-CD022651_B07-2_pipedream1	✓	✓	X	additional density	two large blobs
PDMN-CD022651_B08-2_pipedream	✓	✓	X	additional density	two large blobs
PDMN-CD022651_B09-1_pipedream	✓	✓	X	X	
PDMN-CD022651_B09-3_pipedream	✓	✓	X	X	
PDMN-CD022651_C04-2_pipedream	✓	✓	✓	X	
PDMN-CD022651_C06-3_pipedream	✓	✓	X	X	
PDMN-CD022651_C07-3_pipedream	✓	✓	X	X	
PDMN-CD022651_C09-2_pipedream	✓	✓	X	X	
PDMN-CD022651_D04-3_pipedream	✓	✓	?	additional density	one large blob
PDMN-CD022651_D07-1_pipedream	✓	✓	X	additional density	one large blob
PDMN-CD022651_D09-3_pipedream	✓	✓	?	X	
PDMN-CD022651_E04-2_pipedream	✓	✓	X	X	
PDMN-CD022651_E07-3_pipedream	✓	✓	X	X	
PDMN-CD022651_E09-1_pipedream	✓	✓	?	additional density	one large blob

Data set	postrefine	ligand	does map additional density fit map? manually verified	density for ligand in difference map	discription
PDMN-CD022651_F07-2_pipedream	✓	✓	X	X	
PDMN-CD022651_F09-2_pipedream	✓	✓	X	additional density	several blobs
PDMN-CD022651_G04-1_pipedream	✓	✓	X	X	
PDMN-CD022651_G04-2_pipedream	X				
PDMN-CD022651_G04-2_pipedream1	X				
PDMN-CD022651_G07-3_pipedream	✓	✓	X	additional density	one large blob
PDMN-CD022651_G09-1_pipedream	✓	✓	X	X	
PDMN-CD022651_H04-1_pipedream	✓	✓	X	X	

Table A I-2: Summary of automated X-ray crystallography screening results (Pipedream)
All datasets were manually processed and evaluated

Data set	xds	Phaser	Phenix	Ligand	R-free mean	Resolution	completeness high. Res.
PDMN-CD022192_A06-1_pipedream	✓	✓	✓	no	0,257	1,65	99,1
PDMN-CD022192_A12-1_x1_pipedream	✓	✓	✓	no	0,2531	1,44	99,7
PDMN-CD022192_A12-1_x2_pipedream	✓	✓	✓	no	0,2366	2,15	99,4
PDMN-CD022192_B04-1_pipedream	✓	✓	✓	no	0,2591	1,89	96,6
PDMN-CD022192_B08-3_pipedream	✓	✓	✓	no	0,2518	1,7	98,8
PDMN-CD022192_C06-1_pipedream	✓	✓	✓	no	0,2576	1,8	97,3
PDMN-CD022192_C07-1_pipedream	✓	✓	✓	no	0,2468	1,68	98,9
PDMN-CD022192_C11-1_pipedream	✓	✓	✓	no	0,2749	1,56	99,3
PDMN-CD022192_C12-3_pipedream	✓	✓	✓	no	0,2557	1,81	98,3
PDMN-CD022192_D03-1_pipedream	✓	✓	✓	no	0,2533	1,55	94,9
PDMN-CD022192_D04-3_pipedream	✓	✓	✓	no	0,2684	2,49	93,4
PDMN-CD022192_D05-3_pipedream	✓	✓	✓	no	0,2688	2,2	92,9
PDMN-CD022192_D07-1_pipedream	✓	✓	✓	no	0,2705	1,48	99,5
PDMN-CD022192_D11-1_pipedream	✓	✓	✓	no	0,2586	1,61	99,2
PDMN-CD022192_D12-1_x1_pipedream	✓	✓	✓	no	0,2708	1,49	97,9
PDMN-CD022192_D12-1_x2_pipedream1	✓	✓	✓	no	0,2501	1,69	97,9
PDMN-CD022192_E03-1_pipedream	✓	✓	✓	no	0,2567	1,58	97,3
PDMN-CD022192_E04-1_pipedream	✓	✓	✓	bad fit	0,5293	3,03	74,1
PDMN-CD022192_E05-3_pipedream	✓	✓	✓	no	0,2712	1,69	99,2
PDMN-CD022192_E09-3_pipedream	✓	✓	✓	381A	0,2623	1,52	98,2
PDMN-CD022192_F03-2_pipedream	✓	✓	✓	no	0,2559	1,67	98,4
PDMN-CD022192_F11-1_pipedream	✓	✓	✓	no	0,2774	1,38	97,5
PDMN-CD022192_G07-1_pipedream	✓	✓	✓	no	0,2543	1,47	93
PDMN-CD022192_G11-3_pipedream	✓	✓	✓	no	0,2553	1,48	99,6

Data set	xds	Phaser	Phenix	Ligand	R-free mean	Resolution	completeness high. Res.
PDMN-CD022192_H12-1_pipedream	✓	✓	✓	no	0,2576	1,64	96,1
PDMN-CD022196_A05-2_pipedream	✓		✓	no	0,2504	1,87	99,4
PDMN-CD022196_A06-3_2_pipedream	✓		✓	no	0,2504	1,87	99,4
PDMN-CD022196_B02-2_pipedream	✓	✓	✓	no	0,2888	1,42	99,8
PDMN-CD022196_B09-3_pipedream	✓	✓	✓	no	0,3124	1,5	98
PDMN-CD022196_B11-2_pipedream	✓	✓	✓	no	0,2959	1,78	99,9
PDMN-CD022196_C03-2_pipedream	✓	✓	✓	no	0,2906	1,58	99
PDMN-CD022196_C06-1_pipedream	✓	✓	✓	no	0,263	1,45	99,5
PDMN-CD022196_D09-1_pipedream	✓	✓	✓	no	0,2731	1,36	93,9
PDMN-CD022196_E03-2_pipedream	✓	✓	✓	no	0,2639	1,7	99,9
PDMN-CD022196_E06-3_pipedream	✓	✓	✓	no	0,2528	1,37	99,1
PDMN-CD022196_E08-2_pipedream	✓	✓	✓	no	0,2344	1,34	55,7
PDMN-CD022196_F02-1_pipedream	✓	✓	✓	no	0,2679	1,37	99,7
PDMN-CD022196_F03-3_pipedream	✓	✓	✓	no	0,2615	1,34	99,9
PDMN-CD022196_F11-2_pipedream	✓	✓	✓	no	0,2647	1,46	99,4
PDMN-CD022196_G11-2_pipedream	✓	✓	✓	no	0,2715	1,45	98,6
PDMN-CD022196_H03-3_pipedream	✓	✓	✓	no	0,2684	1,32	99,9
PDMN-CD022196_H11-1_pipedream	✓	✓	✓	no	0,2947	1,6	97,1
PDMN-CD022198_A07-2_pipedream	✓	✓	✓				
PDMN-CD022198_C06-1_pipedream	✓	✓	✓	no	0,2731	1,57	98,4
PDMN-CD022198_F06-1_pipedream	✓	✓	✓	no	0,2595	1,87	99,3
PDMN-CD022198_H06-3_2_x1_pipedream	✓	✓	✓	no	0,27	1,59	98,3
PDMN-CD022198_H06-3_pipedream	✓	✓	✓	no	0,2759	1,6	99,8
PDMN-CD022648_A02-3_pipedream	✓	✓	✓	no	0,2431	1,71	99,1
PDMN-CD022648_A05-1_pipedream	✓	✓	✓	no	0,2622	1,47	99,2
PDMN-CD022648_A08-1_pipedream	✓	✓	✓	no	0,2621	1,72	99,3

Data set	xds	Phaser	Phenix	Ligand	R-free mean	Resolution	completeness high. Res.
PDMN-CD022648_A09-2_pipedream	✓	✓	✓	no	0,2591	1,45	97,3
PDMN-CD022648_A11-2_pipedream	✓ SG1	✓	✓	bad fit	0,4623	2,52	95,7
PDMN-CD022648_B02-1_pipedream	✓	✓	✓	no	0,255	1,68	99,8
PDMN-CD022648_B03-2_pipedream	✓	✓	✓	no	0,2616	1,39	95,5
PDMN-CD022648_B05-2_pipedream	✓	✓	✓	no	0,2677	1,46	99,6
PDMN-CD022648_B08-3_pipedream	✓	✓	✓	no	0,2659	1,62	95,4
PDMN-CD022648_B10-1_pipedream	✓	✓	✓	no	0,2606	1,62	93,9
PDMN-CD022648_C02-3_pipedream	✓	✓	✓	no	0,261	1,49	99,4
PDMN-CD022648_C03-2_pipedream	✓	✓	✓	no	0,2595	1,71	97,7
PDMN-CD022648_C05-2_pipedream	✓	✓	✓	bad fit	0,8052	2,03	97,1
PDMN-CD022648_C09-1_pipedream	✓	✓	✓	no	0,25	1,82	99,8
PDMN-CD022648_C10-2_pipedream	✓	✓	✓	no	0,2578	1,42	99,9
PDMN-CD022648_D05-3_2_pipedream	✓	✓	✓	no	0,2531	1,58	99,6
PDMN-CD022648_D06-1_pipedream	✓	✓	✓	no	0,2552	1,54	99,4
PDMN-CD022648_D07-1_pipedream	✓	✓	✓	no	0,2649	1,46	97,5
PDMN-CD022648_D09-2_pipedream	✓	✓	✓	no	0,2591	1,61	99,8
PDMN-CD022648_E02-3_pipedream	✓	✓	✓	no	0,2429	2,05	99,2
PDMN-CD022648_E03-2_pipedream	✓	✓	✓	no	0,2581	1,51	97,1
PDMN-CD022648_E05-3_pipedream	✓	✓	✓	bad fit	0,7666	1,79	98
PDMN-CD022648_E08-2_pipedream	✓	✓	✓	no	0,2588	1,53	99,9
PDMN-CD022648_E10-3_pipedream	✓	✓	✓	no	0,2606	1,53	98,3
PDMN-CD022648_E11-2_pipedream	✓	✓	✓	no	0,2586	1,26	99,4
PDMN-CD022648_F02-2_pipedream	✓	✓	✓	no	0,2567	1,46	99,1
PDMN-CD022648_F06-2_pipedream	✓	✓	✓	no	0,2501	1,44	97,1
PDMN-CD022648_F07-3_pipedream	✓	✓	✓	no	0,2703	1,28	98,9
PDMN-CD022648_F10-3_pipedream	✓	✓	✓	no	0,2574	1,33	99,7

Data set	xds	Phaser	Phenix	Ligand	R-free mean	Resolution	completeness high. Res.
PDMN-CD022648_G03-2_pipedream	✓	✓	✓	no	0,3546	1,94	98,4
PDMN-CD022648_G04-1_pipedream	✓	✓	✓	no	0,2563	1,36	99,7
PDMN-CD022648_G07-3_pipedream	✓	✓	✓	no	0,2653	1,35	99,2
PDMN-CD022648_G08-1_pipedream	✓	✓	✓	no	0,2737	1,45	96,6
PDMN-CD022648_G10-3_pipedream	✓	✓	✓	no	0,2545	1,41	98,1
PDMN-CD022648_G11-3_pipedream	✓	✓	✓	no	0,2724	1,34	99,6
PDMN-CD022648_H04-1_pipedream	✓	✓	✓	no	0,2698	1,66	94,6
PDMN-CD022648_H05-3_pipedream	✓	✓	✓	no	0,265	1,3	98,2
PDMN-CD022648_H08-1_pipedream	✓	✓	✓	no	0,2558	1,43	99,7
PDMN-CD022648_H09-3_pipedream	✓	✓	✓	no	0,2627	1,74	99
PDMN-CD022651_A06-1_pipedream	✓	✓	✓	no	0,2644	1,39	99,5
PDMN-CD022651_A08-2_pipedream	✓	✓	✓	no	0,2621	1,31	66,3
PDMN-CD022651_B07-2_pipedream	✓	✓	✓	no	0,2684	1,42	99,9
PDMN-CD022651_B07-2_pipedream1	✓	✓	✓	no	0,2624	1,49	99,9
PDMN-CD022651_B08-2_pipedream	✓	✓	✓	no	0,2658	1,44	8,4
PDMN-CD022651_D07-1_pipedream	✓	✓	✓	no	0,326	1,84	99,4
PDMN-CD022651_D09-3_pipedream	✓	✓	✓	no	0,2665	1,5	99,9
PDMN-CD022651_E09-1_pipedream	✓	✓	✓	no	0,2607	1,32	99,6
PDMN-CD022651_G07-3_pipedream	✓	✓	✓	no	0,2718	1,53	99,4

Appendix I.3.2 HBGA-Mimetic Compounds /Synthetic Multivalent Fucose Oligomers

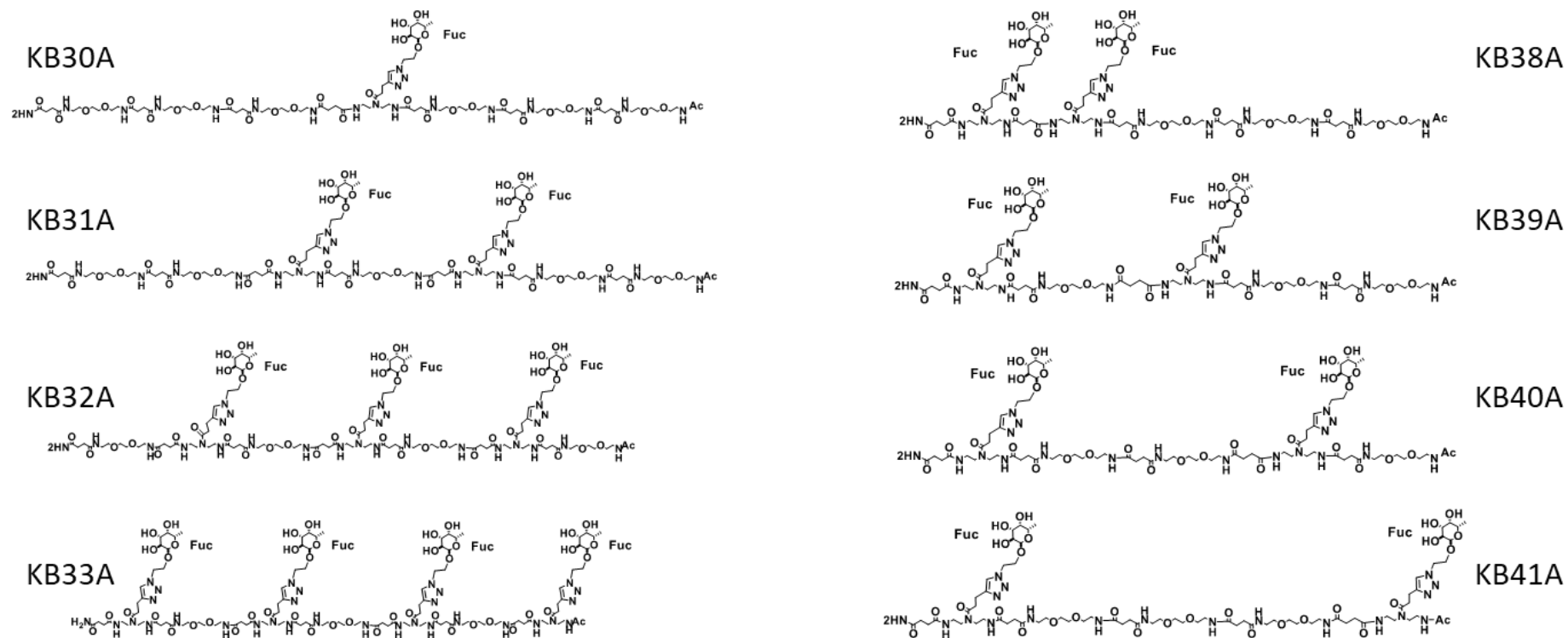


Figure A I.3-1: Chemical notation of HBGA-mimetic synthetic fucose oligomers A

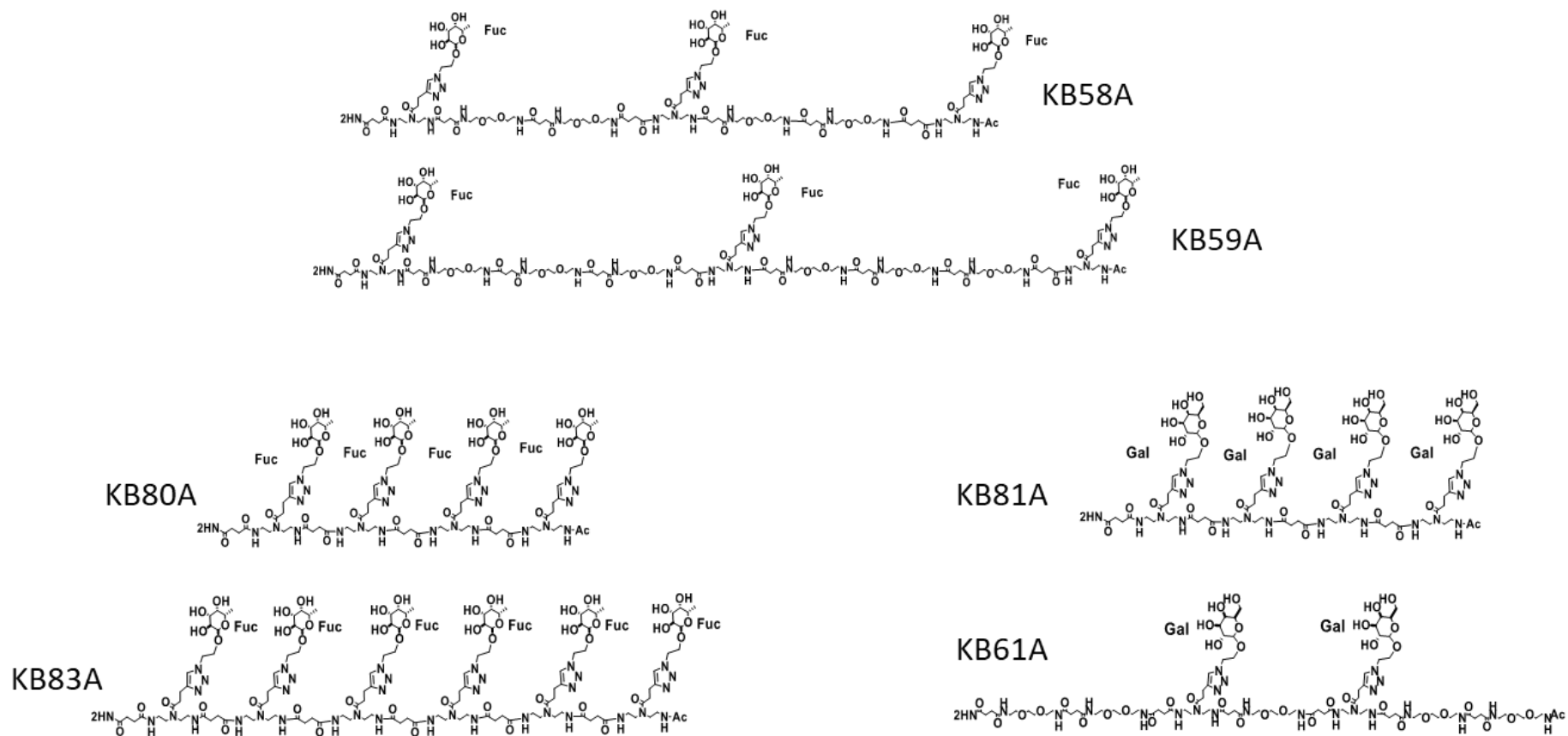


Figure A 1.3-2: Chemical notation of HBGA-mimetic synthetic fucose oligomers B

Appendix I.3.3 HMO Screening

Table A I-3: Top twenty binders of HMO screening against GII.10, GII.4, GII.17, and GII.17 VLPs
 GII.10, GII.4, GII.17 Kawasaki, and GII.17 Saitama VLPs (50 µg/ml). Criterion: sum of % of maximal detection of respective VLP

Top twenty of HMO screening			Absolute RFU values				% of maximal detection of respective VLP			
ChartID	Glycan ID	Name	GI.10	GI.4- Sydney	GI.17- Kawasaki	GI.17- Saitama	GI.10	GI.4- Sydney	GI.17- Kawasaki	GI.17- Saitama
67	HMG-087	H7N5	9853	1375	34706	715	40,93	52,70	100,00	100,00
25	HMG-034	H4N2F2	14023	379	31080	337	58,25	14,53	89,55	47,13
29	HMG-040	H4N2F3	15464	1466	28079	43	64,23	56,19	80,90	6,02
34	HMG-046	H4N2F3	14148	1122	32713	71	58,77	43,03	94,26	9,87
53	HMG-071	H5N3F3	21842	623	276	22	90,73	23,90	0,80	3,08
64	HMG-084	H5N3F4_H6N4F3	5347	352	25457	21	22,21	13,50	73,35	2,94
31	HMG-043	H4N2F3	24074	23	70	30	100,00	0,88	0,20	4,13
16	HMG-022	H4N2F1	58	2608	25	18	0,24	100,00	0,07	2,55
42	HMG-057	H5N3F2	13757	200	263	173	57,14	7,66	0,76	24,14
18	HMG-026	H4N2F2	16778	158	38	28	69,69	6,04	0,11	3,88
217	HMG-261	LNFP III	30	1832	26	37	0,13	70,24	0,07	5,14
65	HMG-085	H6N4F3	668	114	17184	33	2,77	4,37	49,51	4,55
212	HMG-252	LeY pentaose (GLY052)	11694	196	18	19	48,57	7,50	0,05	2,69
96	HMG-121	H4N2S1	107	801	61	140	0,44	30,70	0,17	19,56
46	HMG-061	H5N3F2	8625	60	50	23	35,83	2,31	0,14	3,17
44	HMG-059	H5N3F2	8658	29	22	21	35,96	1,12	0,06	2,97
147	HMG-178	H5N3F2S1	8259	28	16	16	34,31	1,05	0,05	2,24
146	HMG-177	H5N3F2S1	7111	34	69	33	29,54	1,28	0,20	4,55
9	HMG-009	H3N1F2	4757	37	2226	38	19,76	1,42	6,41	5,35
168	HMG-202	H5N3F2S1	69	50	58	218	0,29	1,93	0,17	30,51

Appendix I.3.4 Plant Derived Syrups and Saps

Table A I-4: Summary table structure screening natural extracts, propolis and honey

Data collection was performed at ESRF, Grenoble at beamline ID 23-1. Summary of disordered loops and additional densities observed in the structures; density for loop not defined (disordered), density for protein backbone but no density for side chains (no side chains), wrong space group identified during refinement (wrong sg), crystal was either product of a soaking experiment (soaking) or of co-crystallization (co), observation of additional unexplained densities in the density map (- not observed, + observed, +(EDO?) possibly EDO), bad or low resolution not allowing to address the question of additional densities or disordered loops (bad/low res). For examples of the 'ring'/half ring' structures observed with apple sweetener see Figure 3-34.

Compound	Crystal	Disordered Loops									Additional Densities close to Position								
		517A-521A	344A-351A	296A-300A	296B-300B	488-492A	488-492B	518B-520B	382-384A	382-384B	385A	385B	381A/B	280A/B	470A	447B	287A	468A/B	415B
15EtOH-1	co	disordered	disordered	disordered	disordered	no side chains	no side chains	-	-	-	-	-	+(EDO?)	+	-	-	-	-	-
15EtOH-2	co	no side chains	disordered	disordered	disordered	no side chains	no side chains	-	-	-	-	-	+(EDO?)	+	-	+	-	-	-
15EtOH-3	co	-	disordered	disordered	disordered	no side chains	no side chains	disordered	-	-	-	-	+(EDO?)	+	-	+	-	-	-
15EtOH-4	co	-	disordered	disordered	disordered	no side chains	no side chains	-	-	-	-	-	+(EDO?)	+	-	+	-	-	-
15EtOH-5	co	-	disordered	disordered	disordered	no side chains	no side chains	-	-	-	-	-	+(EDO?)	+	*	+	-	-	-
70EtOH-1	co	-	disordered	-	disordered	no side chains	no side chains	-	-	-	-	-	+(EDO?)	+	-	-	-	-	-
70EtOH-2	co	-	disordered	disordered	disordered	no side chains	no side chains	-	-	-	-	-	+(EDO?)	+	-	+	-	-	-
70EtOH-3	co	-	disordered	no side chains	disordered	no side chains	no side chains	-	-	-	-	-	+(EDO?)	+	-	+	-	-	-
70EtOH-4	co	-	disordered	no side chains	disordered	no side chains	no side chains	-	-	-	-	-	+(EDO?)	-	-	+	-	-	-
70EtOH-5	co	-	disordered	disordered	disordered	no side chains	no side chains	-	-	-	-	-	+(EDO?)	-	-	+	-	-	-
95EtOH-1	co	-	disordered	disordered	disordered	no side chains	no side chains	-	-	-	-	-	+(EDO?)	+	-	+	-	-	-
95EtOH-3	co	-	disordered	disordered	disordered	no side chains	no side chains	-	-	-	-	-	+(EDO?)	+	-	+	-	-	-
95EtOH-4	co	-	disordered	disordered	disordered	disordered	no side chains	-	disordered	-	-	-	-	-	-	-	-	-	-
DMSO-1	co	-	disordered	-	disordered	no side chains	no side chains	-	-	-	-	-	+(EDO?)	+	-	-	-	-	-
DMSO-2	co	-	disordered	no side chains	disordered	no side chains	no side chains	-	-	-	-	-	-	-	-	-	-	-	-
DMSO-4	co	-	disordered	no side chains	disordered	no side chains	no side chains	-	-	-	-	-	-	-	-	-	-	-	-
DMSO-5	co	-	disordered	no side chains	disordered	no side chains	no side chains	-	-	-	-	-	-	-	-	-	-	-	-
Gly-1	co	-	disordered	-	disordered	no side chains	no side chains	-	-	-	-	-	+(EDO?)	-	-	+	-	-	-
Gly-2	co	-	disordered	disordered	disordered	no side chains	no side chains	-	-	-	-	-	+(EDO?)	+	-	+	-	-	-
Gly-3	co	-	disordered	-	disordered	no side chains	no side chains	-	-	-	-	-	+(EDO?)	+	-	-	-	-	-
Gly-4	co	-	disordered	disordered	disordered	no side chains	no side chains	-	-	-	-	-	+(EDO?)	+	-	+	-	-	-
H2O-1	co	-	disordered	disordered	disordered	no side chains	no side chains	disordered	-	-	-	-	+(EDO?)	+	-	+	-	-	-
H2O-2	co	-	disordered	disordered	disordered	no side chains	no side chains	disordered	-	-	-	-	+(EDO?)	+	-	+	-	-	-
H2O-3	co	-	disordered	-	disordered	no side chains	no side chains	-	-	-	-	-	+(EDO?)	-	-	-	-	-	-
H2O-4	co	-	disordered	no side chains	disordered	no side chains	no side chains	disordered	-	-	-	-	+(EDO?)	+	-	+	-	-	-
H2O-5	co	-	disordered	no side chains	disordered	no side chains	no side chains	-	-	-	-	-	+(EDO?)	+	-	+	-	-	-
PEG-1	co	-	disordered	-	disordered	no side chains	no side chains	-	-	-	-	-	+(EDO?)	-	+	-	-	-	-
PEG-2	co	-	disordered	no side chains	disordered	no side chains	no side chains	-	-	-	-	-	+(EDO?)	+	-	+	-	-	-
PEG-3	co	-	disordered	no side chains	disordered	no side chains	no side chains	-	-	-	-	-	+(EDO?)	+	-	-	-	-	-
PEG-4	co	-	disordered	-	disordered	no side chains	no side chains	-	-	-	-	-	+(EDO?)	+	-	-	+	-	-
PEG-5	co	-	disordered	no side chains	disordered	no side chains	no side chains	-	-	-	-	-	+(EDO?)	+	-	-	+	-	-
Prop-1	co	-	disordered	-	no side chains	no side chains	-	-	-	-	-	-	+	*	+	-	-	-	-

Compound	Crystal	Disordered Loops									Additional Densities close to Position											
		517A-521A	344A-351A	296A-300A	296B-300B	488-492A	488-492B	518B-520B	382-384A	382-384B	385A	385B	381A/B	280A/B	470A	447B	287A	468A/B	415B			
Prop-2	co	-	disordered	disordered	disordered	no side chains	-	-	-	-	-	-	+	+	-	-	-	-	-			
Prop-3	co	-	disordered	disordered	disordered	no side chains	-	-	-	-	-	-	+	+	-	+	-	-	-			
Prop-4	co	-	disordered	disordered	disordered	no side chains	-	-	-	-	-	-	-	+	-	-	+	-	-			
Prop-5	co	-	disordered	disordered	disordered	-	-	-	-	-	-	-	-	+	-	+	+	-	-			
Apple-2	co	-	-	disordered	disordered	no side chains	no side chains	-	-	-	-	-	half ring	+	+	(EDO?)	+	-	-	Ring	-	
Apple-3	co	-	disordered	disordered	disordered	no side chains	no side chains	-	-	-	-	-	half ring	-	+	(EDO?)	+	-	-	Ring	-	
Apple-4	co	-	disordered	disordered	disordered	no side chains	no side chains	-	-	-	-	-	half ring	-	+	+	+	-	-	Ring	-	
Apple-5	co	-	disordered	disordered	disordered	no side chains	no side chains	-	-	-	-	-	half ring*	-	+	+	+	-	-	Ring*	-	
Apple-A	soaking	-	disordered	no side chains	disordered	no side chains	no side chains	disordered	-	-	-	-	half ring	-	+	-	-	-	-	+	-	
Apple-B	soaking	-	disordered	disordered	disordered	no side chains	disordered	-	-	-	-	-	half ring	-	+	+	-	-	-	-	-	
Apple-C	soaking	-	disordered	disordered	disordered	no side chains	disordered	-	-	-	-	-	half ring	-	+	+	-	-	-	-	-	
Coco-1	co	-	disordered	disordered	disordered	no side chains	-	-	-	-	-	-	+	+	-	+	+	-	-	-	-	
Coco-2	co	-	disordered	disordered	disordered	no side chains	-	-	-	-	-	-	+	+	+	(EDO?)	+	-	-	-	+	-
Coco-3	wrong sg	-	-	-	-	-	-	-	-	-	-	-	-	-	-	-	-	-	-	-	-	-
Coco-5	co	-	disordered	disordered	disordered	no side chains	no side chains	-	-	-	-	disordered	+	+	+	(EDO?)	+	*	-	-	-	-
Coco-B	wrong sg	-	-	-	-	-	-	-	-	-	-	-	-	-	-	-	-	-	-	-	-	-
Coco-C	soaking	-	disordered	disordered	disordered	no side chains	disordered	-	-	-	-	-	-	-	+	(EDO?)	-	-	-	-	-	-
Date-1	co	-	disordered	no side chains	disordered	no side chains	no side chains	-	-	-	-	-	-	-	-	+	(EDO?)	+	-	-	-	-
Date-2	co	-	disordered	no side chains	disordered*	no side chains	no side chains	-	-	-	-	-	-	-	-	+	(EDO?)	+	-	-	-	-
Date-3	bad res	-	disordered	no side chains	disordered	no side chains	-	-	-	-	-	-	-	-	-	+	(EDO?)	-	+	-	-	-
Date-4	bad res	-	disordered	disordered	disordered	no side chains	no side chains	-	-	-	-	-	-	-	-	+	(EDO?)	-	-	-	-	-
Date-5	co	-	disordered	disordered	disordered	no side chains	no side chains	-	-	-	-	-	+	-	+	*	+	-	-	-	+	-
Date-A	soaking	-	disordered	disordered	disordered	no side chains	-	-	-	-	-	-	-	-	+	+	-	-	-	-	-	-
Date-B	soaking	disordered	disordered	no side chains	disordered	no side chains	no side chains	disordered	-	-	-	-	-	-	+	+	+	-	-	-	-	-
Date-C	soaking	-	disordered	disordered	disordered	no side chains	no side chains	disordered	-	-	-	-	-	-	+	+	+	-	-	-	-	+
Date-D	soaking	disordered	disordered	disordered	disordered	no side chains	no side chains	disordered	-	-	-	-	-	-	+	+	+	-	-	-	-	+
Flower-A	soaking	disordered	disordered	disordered	disordered	no side chains	no side chains	disordered	-	-	-	-	+	+	+	+	+	-	-	-	-	+
Flower-B	soaking	-	disordered	disordered	disordered	no side chains	no side chains	disordered	-	-	-	-	+	-	+	-	-	-	-	-	-	+
Maile-A	soaking	-	disordered	disordered	disordered	no side chains	no side chains	disordered	-	-	-	-	-	+	+	+	+	-	-	-	-	-
Maile-C	soaking	disordered	disordered	disordered	disordered	no side chains	no side chains	disordered	-	-	-	-	-	+	+	+	+	-	-	-	+	+
Pine-1	co	-	disordered	-	disordered	no side chains	no side chains	-	-	-	-	-	+	-	-	+	-	-	-	-	-	-
Pine-B	soaking	-	disordered	-	disordered	no side chains	no side chains	-	-	-	-	-	-	+	+	+	+	-	-	-	-	-
Pine-C	soaking	-	-	-	disordered	no side chains	no side chains	-	-	-	-	-	-	+	+	+	+	-	-	-	-	-
Pine-D	bad res	-	disordered	-	disordered	no side chains	no side chains	-	-	-	-	-	-	-	+	-	-	-	-	-	-	-
Honey-1-a	soaking	disordered	disordered	-	no side chains	no side chains	disordered	disordered	-	-	-	-	-	-	+	+	-	-	-	-	-	-
Honey-1-b	soaking	-	disordered	-	no side chains	no side chains	-	-	-	-	-	-	+	-	+	-	-	-	-	-	-	-
Honey-1-c	soaking	-	disordered	-	no side chains	no side chains	no side chains	disordered	-	-	-	-	-	-	+	+	-	-	-	-	-	-
Honey-2-b	bad res	-	disordered	-	no side chains	no side chains	no side chains	-	-	-	-	-	-	-	+	+	-	-	-	-	-	-
Honey-2-c	low res	-	disordered	-	disordered	no side chains	no side chains	-	-	-	-	-	-	+	+	+	-	-	-	-	-	-
Honey-3-a	soaking	disordered	disordered	-	no side chains	no side chains	-	disordered	-	-	-	-	-	-	+	+	-	-	-	-	-	-
Honey-3-b	soaking	disordered	disordered	-	no side chains	disordered	disordered	-	-	-	-	-	-	-	+	+	+	+	-	-	-	-

Compound	Crystal	Disordered Loops									Additional Densities close to Position								
		517A-521A	344A-351A	296A-300A	296B-300B	488-492A	488-492B	518B-520B	382-384A	382-384B	385A	385B	381A/B	280A/B	470A	447B	287A	468A/B	415B
Honey-3-c	soaking	disordered	disordered	-	no side chains	disordered	no side chains	-	-	-	+	-	+		+	-	-	-	-
Honey-3-d	soaking	disordered	disordered	-	no side chains	no side chains	no side chains	-	-	-	-	-	+		-	-	-	-	-

Table A I-5: Summary of JCSG-condition screening for co-crystals of GII.10 P domain + natural extract
Crystallization conditions of a JCSG screen were tested at the crystallization platform, excellence cluster, Universität Heidelberg.
The amount of crystals formed in a given condition was evaluated (success), compounds of the respective mother solution are listed (A, B, C, D).

	Success	Mother Solution A	Mother Solution B	Mother Solution C	Mother Solution D
Coconut blossom syrup					
JCSG-1 A8	cubes	0	0,2M sodium citrate	20 m/v PEG3350	
JCSG-1 A11	plates	0	0,2M potassium acetate	20m/v PEG3350	
JCSG-1 A12	Plates, needles	+	0,2M magnesium acetate	20 m/v PEG 3350	
JCSG-1 B1	needles	+	0,2M sodium chloride	20m/v PEG 3000	0,1M HEPES
JCSG-1 B2	plates, platelets	++		20w/v PEG 8000	0,1M HEPES
JCSG-1 B3	plates	0		10w/v PEG 8000	0,1M HEPES
JCSG-1 B5	cubes, plates, needles	++		20 w/v PEG 4000	0,1 M HEPES 10 v/v 2 propanol
JCSG-1 B7	plate0		0,2 M di-sodium tartrate	20w/v propylene glycol 3350	
JCSG-1 B8	Plates, needles	++	0,2 M calcium acetate	20 w/v PEG 3350	
JCSG-1 B9	cubes, plates, needles	++	0,2 M potassium formate	20 w/v PEG 3350	
JCSG-1 B11	platelets, needles	++	0,2 M sodium formate	20 w/v PEG 3350	
JCSG-1 B12	plates	0	0,2 M potassium fluoride	20 m/v PEG 3350	
JCSG-1 C1	plates, platelets, needles	+	0,2 M ammonium acetate	20 w/v PEG 3350	
JCSG-1 C2	plates, needles	+	0,2 M lithium nitrate	20 w/v PEG 3350	
JCSG-1 C7	needles	++		20 w/v PEG ether 2000	0,1 M Tris
JCSG-1 C8	needles	++	0,2 M sodium acetate	20 w/v PEG 3350	
JCSG-1 C10	plates	+		20 w/v PEG 6000	0,1 M HEPES
JCSG-1 D3	Plates, needles	+	0,2M sodium chloride	20 w/v PEG 3350	
JCSG-1 D5	cube, needles	+	0,2 M lithium chloride	20 w/v PEG 3350	
JCSG-1 D9	needles	++	0,2 M ammonium formate	20 w/v PEG 3350	
JCSG-1 D12	plates	+	0,2 M magnesium acetate	20 w/v PEG 8000	0,1 M sodium cacodylate
JCSG-1 E1	plates, platelets, needles	++	0,2 M ammonium nitrate	20 w/v PEG 3350	
JCSG-1 E2	Plates, needles	+	0,2 M ammonium chloride	20 w/v PEG 3350	
JCSG-1 E3	cubes, needles	0	0,2M sodium chloride	10 w/v PEG 8000	0,1 M Na K phosphate
JCSG-1 E4	platelets, needles	+	0,2 M ammonium iodide	20 w/v PEG 3350	
JCSG-1 E5	Plates, needles	++	0,2 M ammonium fluoride	20 w/v PEG 3350	
JCSG-1 E7	small cubes	+	0,2 M calcium acetate	20 w/v PEG 8000	0,1 M MES
JCSG-1 E8	platelets	+	0,2 M ammonium sulfate	20 w/v PEG 3350	
JCSG-1 E12	plates, platelets	++		20 w/v PEG 6000	0,1 M MES
JCSG-1 F1	cube, plates	+		10 w/v PEG 6000	0,1 M MES

		Success	Mother Solution A	Mother Solution B	Mother Solution C	Mother Solution D
JCSG-1 F2	plates, platelets	0	0,2 M magnesium formate	20 w/v PEG 3350		
JCSG-1 F8	cube, needles	+		20 w/v PEG 3000	0,1 M sodium citrate	
JCSG-1 G4	plates, platelets	++		20 w/v PEG 6000	0,1 M citric acid	
JCSG-1 G5	plates	+		10 w/v PEG 6000	0,1 M citric acid	
JCSG-1 G7	cubes	+	0,2 M potassium dihydrogen phosphate	20 w/v PEG 3350		
JCSG-1 G8	cubes	+	0,2 M ammonium dihydrogen phosphate	20 w/v PEG 3350		
JCSG-1 G11	plates	+	0,2 M ammonium sulfate	25 w/v PEG 4000	0,1 M sodium acetate	
JCSG-1 H2	plates	+		20 w/v PEG 3000	0,1 M sodium acetate	
JCSG-1 H3	plates	+	0,2 sodium dihydrogen phosphate	20 w/v PEG 3350		
JCSG-1 H4	plates	+	0,05 M potassium dihydrogen phosphate	20 w/v PEG 8000		
JCSG-2 A1	plates, platelets	++	0,2 M sodium chloride	20 w/v PEG 8000	0,1 M CAPS	
JCSG-2 A2	plates, platelets	++	0,2 M sodium chloride	1,26 M ammonium sulfate	0,1 M CHES	
JCSG-2 B3	cubes	0	0,2 M calcium acetate	10 w/v PEG 8000	0,1 imidazole	
JCSG-2 B6	plates, platelets	0	20 w/v PEG 6000	0,1 M Tris		
JCSG-2 B7	plates, platelets	+	0,2 M lithium acetate	20 w/v PEG 3350		
JCSG-2 C5	platelets	+	0,2 M sodium flouride	20 w/v PEG 3350		
JCSG-2 C10	cubes0	0	10 w/v PEG 6000	0,1 M HEPES		
JCSG-2 D2	platelets, needles	0	0,2 M sodium nitrate	20 w/v PEG 3350		
JCSG-2 D11	plates	+	12 w/v PEG 20,000	0,1 M MES		
JCSG-2 D12	cubes	0	0,2 M zinc acetate	40 v/v PEG 600	0,1 imidazole	
JCSG-2 G11	cubes, plates	+	0,2 M zinc acetate	10 w/v PEG 3000	0,1 M sodium acetate	
JCSG-2 H5	plates	++	0,1 M phosphate- citrate	0,2 M sodium chloride	20 w/v PEG 8000	
JCSG-3 A12	plates	++	1 M di-ammonium hydrogen phosphate	0,1 M Tris		
JCSG-3 B1	plates	++	0,2 M magnesium cholride	20 w/v PEG 8000	0,1 M Tris	
JCSG-3 E1	plates	+	1,26 M ammonium sulfate	0,1 M sodium cacodylate		
JCSG-3 E8	plates, platelets	+	0,2 M calcium acetate	18 w/v PEG 8000	0,1 M sodium cacodylate	
JCSG-3 E9	plates, platelets	+	0,2 M sodium acetate	30 w/v PEG 8000	0,1 M sodium cacodylate	
JCSG-3 G5	platelets	+	0,2 M calcium chloride	20 w/v PEG 3350		
JCSG-3 G8	cubes	0	0,1 M citric acid	30 w/v PEG 6000		
JCSG-4 B3	plates	+		30 w/v PEG 6000	0,1 M bicine	
JCSG-4 C8	plates, platelets	0	0,2 M sodium chloride	1 M di- ammonium hydrogen phosphate	0,1 imidazole	
JCSG-4 G2	plates	+	1 M potassium sodium tartrate	0,1 M MES		
JCSG-4 H5	platelets	0	1 M di-ammonium hydrogen phosphate	0,1 M sodium acetate		
Date syrup						
JCSG-1 A1	sand	+++		20 w/v PEG 8000	0,1 M CHES	
JCSG-1 A8	cubes	0	0,2 M sodium citrate	20 w/v PEG 3350		
JCSG-1 A9	cubes	0	0,2 M lithium citrate	20 w/v PEG 3350		
JCSG-1 A11	plates, platelets, sand	+++	0,2 M potassium acetate	20 w/v PEG 3350		
JCSG-1 A12	needles, sand	+++	0,2 M magnesium acetate	20 w/v PEG 3350		
JCSG-1 B1	cubes, plates, sand	+++	0,2 M sodium chloride	20 w/v PEG 3000	0,1 M HEPES	
JCSG-1 B2	needles, sand	+++		20 w/v PEG 8000	0,1 M HEPES	
JCSG-1 B3	bad shape	++		10 w/v PEG 8000	0,1 M HEPES	

		Success	Mother Solution A	Mother Solution B	Mother Solution C	Mother Solution D
JCSG-1 B5	plates, Needles	+++		20 w/v PEG 4000	0,1 M HEPES	10 v/v 2-propanol
JCSG-1 B7	cubes, plates, sand	+++	0,2 M di-sodium tartrate	20 w/v PEG 3350		
JCSG-1 B8	?	+++	0,2 M calcium acetate	20 w/v PEG 3350		
JCSG-1 B9	plates, sand	+++	0,2 M potassium formate	20 w/v PEG 3350		
JCSG-1 B10	cubes, sand	+++	0,2 M potassium sodium tartrate	20 w/v PEG 3350		
JCSG-1 C1	sand	'+++	0,2 M ammonium acetate	20 w/v PEG 3350		
JCSG-1 C2	sand	'+++	0,2 M lithium nitrate	20 w/v PEG 3350		
JCSG-1 C5	sand	'+++	0,2 M calcium acetate	20 w/v PEG 3000	0,1 M Tris	
JCSG-1 C7	plates, sand	+++		20 w/v PEG monomethyl ether 2000	0,1 M Tris	
JCSG-1 C8	sand	+++	0,2 M sodium acetate	20 w/v PEG 3350		
JCSG-1 C9	cubes	+	0,2 M potassium thiocyanate	20 w/v PEG 3350		
JCSG-1 C11	cubes, needles, sand	+++	0,2 potassium nitrate	20 w/v PEG 3350		
JCSG-1 C12	cubes sand	++	0,2 M sodium thiocyanate	20 w/v PEG 3350		
JCSG-1 D1	cubes sand	+++	0,2 sodium iodine	20 w/v PEG 3350		
JCSG-1 D2	cubes sand	+++	0,2 potassoim chloride	20 w/v PEG 3350		
JCSG-1 D3	cubes sand	+++	0,2 M sodium chloride	20 w/v PEG 3350		
JCSG-1 D4	cubes sand	++	0,2 M potassium iodine	20 w/v PEG 3350		
JCSG-1 D5	cubes sand	++	0,2 M lithium chloride	20 w/v PEG 3350		
JCSG-1 D7	sand	+++	0,2 M di-ammonium tartrate	20 w/v PEG 3350		
JCSG-1 D9	sand	+++	0,2 M ammonium formate	20 w/v PEG 3350		
JCSG-1 D10	sand	++		10 w/v PEG 6000	0,1 M HEPES	5 v/v 2-methyl-2,4-pentandiol
JCSG-1 E3	cubes, sand	+++	0,2 M sodium chloride	10 w/v PEG 8000	0,1 M Na K phosphate	
JCSG-1 E4	cubes, sand	+++	0,2 M ammonium iodine	20 w/v PEG 3350		
JCSG-1 E5	cubes, sand	+++	0,2 M ammonium flouride	20 w/v PEG 3350		
JCSG-1 E7	sand	+++	0,2 M calcium acetate	20 w/v PEG 8000	0,1 M MES	
JCSG-1 E9	cubes, sand	+++	0,2 M ammonium sulfate	20 w/v PEG 3350		
JCSG-1 F1	cubes, sand	+++		10 w/v PEG 6000	0,1 M MES	
JCSG-1 F2	cubes, sand	+++	0,2 M magnesium sulfate	20 w/v PEG 3350		
JCSG-1 F3	cubes, sand	+++	0,2 M magnesium formate	20 w/v PEG 3350		
JCSG-1 F4	cubes, sand	++	0,2 M magnesium nitrate	20 w/v PEG 3350		
JCSG-1 F5	cubes, sand	++	0,2 M magnesium chloride	20 w/v PEG 3350		
JCSG-1 F6	cubes, sand	+	0,95 M sodium citrate	19 w/v PEG 4000	5 v/v glycerol	19 v/v 2-propanol
JCSG-1 F7	cubes	0	0,1 M sodium citrate	20 w/v PEG 4000	20 v/v 2-propanol	
JCSG-1 F8	cubes, needles, sand	+++	0,1 M sodium citrate	20 w/v PEG 3000		
JCSG-1 G1	sand	++	0,18 M tri-ammonium citrate	20 w/v PEG 3350		
JCSG-1 G3	cubes, needles, sand	+++	1 M lithium chloride	10 w/v PEG 6000	0,1 M citric acid	
JCSG-1 G5	cubes, needles, sand	+++		10 w/v PEG 6000	0,1 M citric acid	
JCSG-1 G6	cubes	++		5 w/v PEG 6000	0,1 M citric acid	
JCSG-1 G7	cubes, sand	+++	0,2 M potassium dihydrogen phosphate	20 w/v PEG 3350		
JCSG-1 G8	cubes, sand	+++	0,2 ammonium dihydrogen phosphate	20 w/v PEG 3350		
JCSG-1 G10	Needles	+++		8w/v PEG 4000	0,1 M sodium acetate	
JCSG-1 G11	cubes, sand	+++	0,2 M ammonium sulfate	25 w/v PEG 4000	0,1 M sodium acetate	
JCSG-1 H2	sand	+++		20 w/v PEG 3000	0,1 M sodium acetate	

		Success	Mother Solution A	Mother Solution B	Mother Solution C	Mother Solution D
JCSG-1 H3	cubes, sand	+++	0,2 M sodium dihydrogen phosphate	20 w/v PEG 3350		
JCSG-1 H5	cubes, sand	+++	0,1 M phosphate-citrate	0,2 M sodium chloride	10 w/v PEG 3000	
JCSG-1 H11	cubes, sand	++	1 M lithium chloride	10 w/v PEG 6000	0,1 M citric acid	
JCSG-1 H12	cubes	+	0,1 M citric acid	5 w/v PEG 6000		
JCSG-2 A1	plates, needles	++	0,2 M sodium chloride	20 w/v PEG 8000	0,1 M CAPS	
JCSG-2 B3	plates, platelets	++	0,2 M calcium acetate	10 w/v PEG 8000	0,1 M imidazole	
JCSG-2 B6	cubes, needles, sand	+++		20 w/v PEG 6000	0,1 M Tris	
JCSG-2 B7	plates, needles	+++	0,2 M lithium acetate	20 w/v PEG 3350		
JCSG-2 C5	plates, needles	+++	0,2 M sodium flourite	20 w/v PEG 3350		
JCSG-2 C10	plates, platelets	++		10 w/v PEG 6000	0,1 M HEPES	
JCSG-2 D11	plates, platelets, sand	+++		12 w/v PEG 20,000	0,1 M MES	
JCSG-2 H5	needles	+++	0,1 M phosphate-citrate	0,2 M sodium chloride	20 w/v PEG 8000	
JCSG-2 H12	plates	++		20 w/v PEG 6000	0,1 M citric acid	
JCSG-3 B1	sand	+++	0,2 M magnesium chloride	20 w/v PEG 8000	0,1 M Tris	
JCSG-3 E8	cubes, sand	+++	0,2 M calcium acetate	18 w/v PEG 8000	0,1M sodium cacodylate	
JCSG-3 G5	cubes, sand	+++	0,2 M calcium chloride	20 w/v PEG 3350		
JCSG-4 A11	cube	0	0,8 M ammonium sulfate	0,1 M bicine		
JCSG-4 C7	cubes, needles	++		10 w/v PEG 8000	0,1 M imidazole	
JCSG-4 C10	cubes	0		5 w/v PEG 6000	0,1 M Tris	
JCSG-4 D4	cubes	0		50 w/v PEG 200	0,1 M HEPES	
JCSG-4 E12	sand	+++		30 w/v PEG 6000	0,1 M HEPES	
Propolis extract 95 % EtOH						
JCSG-1 A1	cubes	0		20 w/v PEG 8000	0,1 M CHES	
JCSG-1 A2	plates	0		20 w/v PEG 6000	0,1 M bicine	
JCSG-1 A11	platelets	+	0,2 M potassium acetate	20 w/v PEG 3350		
JCSG-1 B2	cubes, plates	+++		20 w/v PEG 8000	0,1 M HEPES	
JCSG-1 B5	cubes	++		20 w/v PEG 4000	0,1 M HEPES	10 v/v 2-propanol
JCSG-1 B8	cubes	0	0,2 M calcium acetate	20 w/v PEG 3350		
JCSG-1 B9	plates	+	0,2 M potassium formate	20 w/v PEG 3350		
JCSG-1 B11	cubes, plates	+	0,2 M sodium formate	20 w/v PEG 3350		
JCSG-1 C1	Plates, platelets	+	0,2 M ammonium acetate	20 w/v PEG 3350		
JCSG-1 C2	Plates, platelets	0	0,2 M lithium nitrate	20 w/v PEG 3350		
JCSG-1 C7	plates	0		20 w/v PEG 2000	0,1 M Tris	
JCSG-1 C8	cubes, plates	0	0,2 M sodium acetate	20 w/v PEG 3350		
JCSG-1 C10	plates	++		20 w/v PEG 6000	0,1 M HEPES	
JCSG-1 D3	plates	0	0,2 M sodium chloride	20 w/v PEG 3350		
JCSG-1 D5	cubes	+	0,2 M lithium chloride	20 w/v PEG 3350		
JCSG-1 D9	cubes, plates	0	0,2 M sodium formate	20 w/v PEG 3350		
JCSG-1 D12	needles	+++	0,2 M magnesium acetate	20 w/v PEG 8000	0,1 M sodium cacodylate	
JCSG-1 E1	cubes, plates	+	0,2 M ammonium nitrate	20 w/v PEG 3350		
JCSG-1 E2	cubes, plates	+	0,2 M ammonium chloride	20 w/v PEG 3350		
JCSG-1 E3	cubes, plates	+	0,2 M sodium chloride	10 w/v PEG 8000	0,1 M Na K phosphate	

		Success	Mother Solution A	Mother Solution B	Mother Solution C	Mother Solution D
JCSG-1 E4	sand	+++	0,2 M ammonium iodide	20 w/v PEG 3350		
JCSG-1 E5	plates	0	0,2 M ammonium flouride	20 w/v PEG 3350		
JCSG-1 E7	cubes	+++	0,2 M calcium acetate	20 w/v PEG 8000	0,1 M MES	
JCSG-1 E12	plates	++		20 w/v PEG 6000	0,1 M MES	
JCSG-1 F1	plates	0		10 w/v PEG 6000	0,1 M MES	
JCSG-1 F6	plate	0	0,095 M sodium citrate	19 w/v PEG 4000	5 v/v glycerol	19 v/v 2-propanol
JCSG-1 F8	plates	0		20 w/v PEG 3000	0,1 M sodium citrate	
JCSG-1 G4	plates	0		20 w/v PEG 6000	0,1 M citric acid	
JCSG-1 G5	plates	0		10 w/v PEG 6000	0,1 M citric acid	
JCSG-1 G7	plates	0	0,2 M potassium dihydrogen phosphate	20 w/v PEG 3350		
JCSG-1 G11	cubes, plates	0	0,2 M ammonium sulfate	25 w/v PEG 4000	0,1 M sodium acetate	
JCSG-2 A1	cubes, plates	0	0,2 M sodium chloride	20 w/v PEG 8000	0,1 M CAPS	
JCSG-2 B6	plates	++		20 w/v PEG 6000	0,1 M Tris	
JCSG-2 B7	plates	0	0,2 M lithium acetate	20 w/v PEG 3350		
JCSG-2 C5	plates	0	0,2 M sodium flouride	20 w/v PEG 3350		
JCSG-2 D11	cubes, plates, platelets	+		12 w/v PEG 20,000	0,1 M MES	
JCSG-2 F10	plates	0	0,8 M smmonium sulfate	0,1 M citric acid		
JCSG-2 F11	cubes	+++	1 M lithium chloride	20w/v PEG 6000	0,1 M citric acid	
JCSG-3 E78	plate	0	0,2 M calcium acetate	18 w/v PEG 8000	0,1 M sodium cacodylate	
JCSG-4 E12	plate	0		30 w/v PEG 6000	0,1 M HEPES	
JCSG-4 H2	cubes	++	0,2 M ammonium acetate	30 w/v PEG 4000	0,1 M sodium acetate	
JCSG-4 H5	plate	0	1 M di-ammonium hydrogen phosphate	0,1 M sodium acetate		
Propolis extract DMSO						
JCSG-1 A11	platelets	0	0,2 M potassium avetate	20 w/v PEG 3350		
JCSG-1 A12	plates	0	0,2 M magnesium acetate	20 w/v PEG 3350		
JCSG-1 B2	plates	+		20 w/v PEG 8000	0,1 M HEPES	
JCSG-1 B11	platelets	0	0,2 M sodium formate	20 w/v PEG 3350		
JCSG-1 B12	plates	0	0,2 M potassium flouride	20 w/v PEG 3350		
JCSG-1 C1	plate	0	0,2 M ammoniumacetate	20 w/v PEG 3350		
JCSG-1 C4	cube	0	0,2 M magnesium chloride	10 w/v PEG 8000	0,1 M Tris	
JCSG-1 C10	platelets	+		20 w/v PEG 6000	0,1 M HEPES	
JCSG-1 D9	cubes, plates	+	0,2 M ammonium formate	20 w/v PEG 3350		
JCSG-1 D12	cubes, plates	+	0,2 M magnesium acetate	20 w/v PEG 8000	0,1 M sodium cacodylate	
JCSG-1 E1	plates, platelets	+	0,2 M ammonium nitrate	20 w/v PEG 3350		
JCSG-1 E2	platelets	+	0,2 M ammonium chloride	20 w/v PEG 3350		
JCSG-1 E4	plates	+	0,2 M ammonium iodide	20 w/v PEG 3350		
JCSG-1 E5	plates	+	0,2 M ammonium flouride	20 w/v PEG 3350		
JCSG-1 E7	plates	++	0,2 M calium acetate	20 w/v PEG 8000	0,1 M MES	
JCSG-1 E12	cubes, plates	++		20 w/v PEG 6000	0,1 M MES	
JCSG-1 F1	plate	0		10 w/v PEG 6000	0,1 M MES	
JCSG-1 G4	cubes, plates	+		20 w/v PEG 6000	0,1M citric acid	
JCSG-1 G7	cubes, plates	+	0,2 M potassium dihydrogen phsphate	20 w/v PEG 3350		

		Success	Mother Solution A	Mother Solution B	Mother Solution C	Mother Solution D
JCSG-1 G11	cubes, plates	+	0,2 M ammonium sulfate	25 w/v PEG 4000	0,1 M sodium acetate	
JCSG-1 H3	plates, needles	+	0,2 M sodium dihydrogen phosphate	20 w/v PEG 3350		
JCSG-2 A1	plates, platelets	+	0,2 M sodium chloride	20 w/v PEG 8000	0,1 M CAPS	
JCSG-2 A2	platelets	0	0,2 M sodium chloride	1,26 M ammonium sulfate	0,1 M CHES	
JCSG-2 B6	plates, platelets	+		20 w/v PEG 6000	0,1 M Tris	
JCSG-2 B7	cubes, plates, platelets	+	0,2 M lithium acetate	20 w/v PEG 3350		
JCSG-2 D11	cubes, plates	+		12 w/v PEG 20,000	0,1 M MES	
JCSG-2 E10	cubes, plates	+	0,1 M sodium citrate	0,2 M ammonium acetate	30 w/v PEG 4000	
JCSG-2 H5	plates	+	0,1 M phosphate-citrate	0,2 M sodium chloride	20 w/v PEG 8000	
JCSG-3 A12	cubes, plates	0	1 M di-ammonium hydrogen phosphate	0,1 M Tris		
JCSG-3 B1	cubes, plates	0	0,2 M magnesium chloride	20 w/v PEG 8000	0,1 M Tris	
JCSG-3 E1	plates	0	1,26 ammonium sulfate	0,1 M sodium cacodylate		
JCSG-3 E2	platelets	0	0,16 M magnesium acetate	16 w/v PEG 8000	0,08 M sodium cacodylate	20 v/v glycerol
JCSG-3 E8	cubes, plates	+	0,2 M calcium acetate	18 w/v PEG 8000	0,1 M sodium cacodylate	
JCSG-4 B3	platelets	0		30 w/v PEG 6000	0,1 M bicine	
JCSG-4 C8	cube	0	0,2 M sodium chloride	1 M di-ammonium hydrogen phosphate	0,1 M imidazole	

Table A I-6: Summary table structure screening natural extracts, optimized JCSG-crystallization conditions

Data collection was performed at ESRF, Grenoble at beamline ID 30B. Summary of disordered loops and additional densities observed in the structures; density for loop not defined (disordered), density for protein backbone but no density for side chains (no side chains), wrong space group identified during refinement (wrong sg), crystals were product of co-crystallization optimized condition for crystal see condition, observation of additional unexplained densities in the density map (- not observed, + observed, bad or low resolution not allowing to address the question of additional densities or disordered loops (bad/low res). For examples of the 'ring'/'half ring' structures observed with apple sweetener see Figure 3-34.

Compound	JCSG	Quality of Dataset	Disordered Loops									Additional Densities close to Position								
			517A-521A	344A-351A	296A-300A	296B-300B	488-492A	488-492B	518B-520B	382-384A	382-384B	385A	385B	381A/B	280A/B	470A	447B	287A	468A/B	415B
95EtOH	JCSG-1 A8		-	-	disordered	disordered	no side chains	not perfect	-	-	-	-	-	+	+	-	-	-	-	-
95EtOH	JCSG-1 B7		-	disordered	disordered	disordered	no side chains	no side chains	-	-	-	-	-	+	+	-	+	-	-	-
95EtOH	JCSG-1 C12		-	disordered	not perfect	disordered	no side chains	no side chains	-	-	-	-	-	+	+	-	+	-	-	-
95EtOH	JCSG-1 G3	bad map	-																	
95EtOH	JCSG-2 C5		not perfect	disordered	disordered	disordered	no side chains	no side chains	-	-	-	-	-	+	+	+	-	-	-	-
95EtOH	JCSG-1 F2		-	disordered	disordered	disordered	no side chains	no side chains	-	-	-	-	-	+	+	-	-	-	+	-
Coco	JCSG-1 A8		-	disordered	no side chains	disordered	no side chains	no side chains	-	-	-	+	-	+	+	-	-	-	-	-
Coco	JCSG-1 B5		-	disordered	no side chains	disordered	-	-	-	-	-	+	-	+	-	-	-	-	-	-
Coco	JCSG-1 B7		-	disordered	disordered	disordered	no side chains	no side chains	-	-	-	+	-	+	+	-	-	-	+	-
Coco	JCSG-1 C12	bad map	-																	
Coco	JCSG-1 F1		-	disordered	disordered	disordered	no side chains	no side chains	-	-	-	?	-	+	+	-	+	-	-	+
Coco	JCSG-1 F2		-	disordered	disordered	disordered	no side chains	no side chains	-	-	-	+	-	-	+	-	+	-	ring	-
Coco	JCSG-1 G3	wrong packing	-	disordered	disordered	disordered	-	-	-	not perfect	-	?	-	-	-	-	-	-	-	-
Coco	JCSG-2 C5		-	disordered	disordered	disordered	no side chains	no side chains	-	-	-	+	-	+	+	-	-	-	-	+
Date	JCSG-1 A8		-	disordered	no side chains	disordered	no side chains	no side chains	-	-	-	-	-	+	-	-	-	-	-	-
Date	JCSG-1 F2		-	disordered	disordered	disordered	no side chains	no side chains	-	-	-	+	-	+	-	-	-	-	+	-
Date	JCSG-1 G3	wrong packing	-	disordered	disordered	disordered	not perfect	no side chains	-	-	-	-	+	-	-	-	-	-	-	-
Date	JCSG-2 C5		-	disordered	disordered	disordered	no side chains	no side chains	-	-	-	+	-	+	+	-	-	-	+	+

Appendix I.3.5 Honey

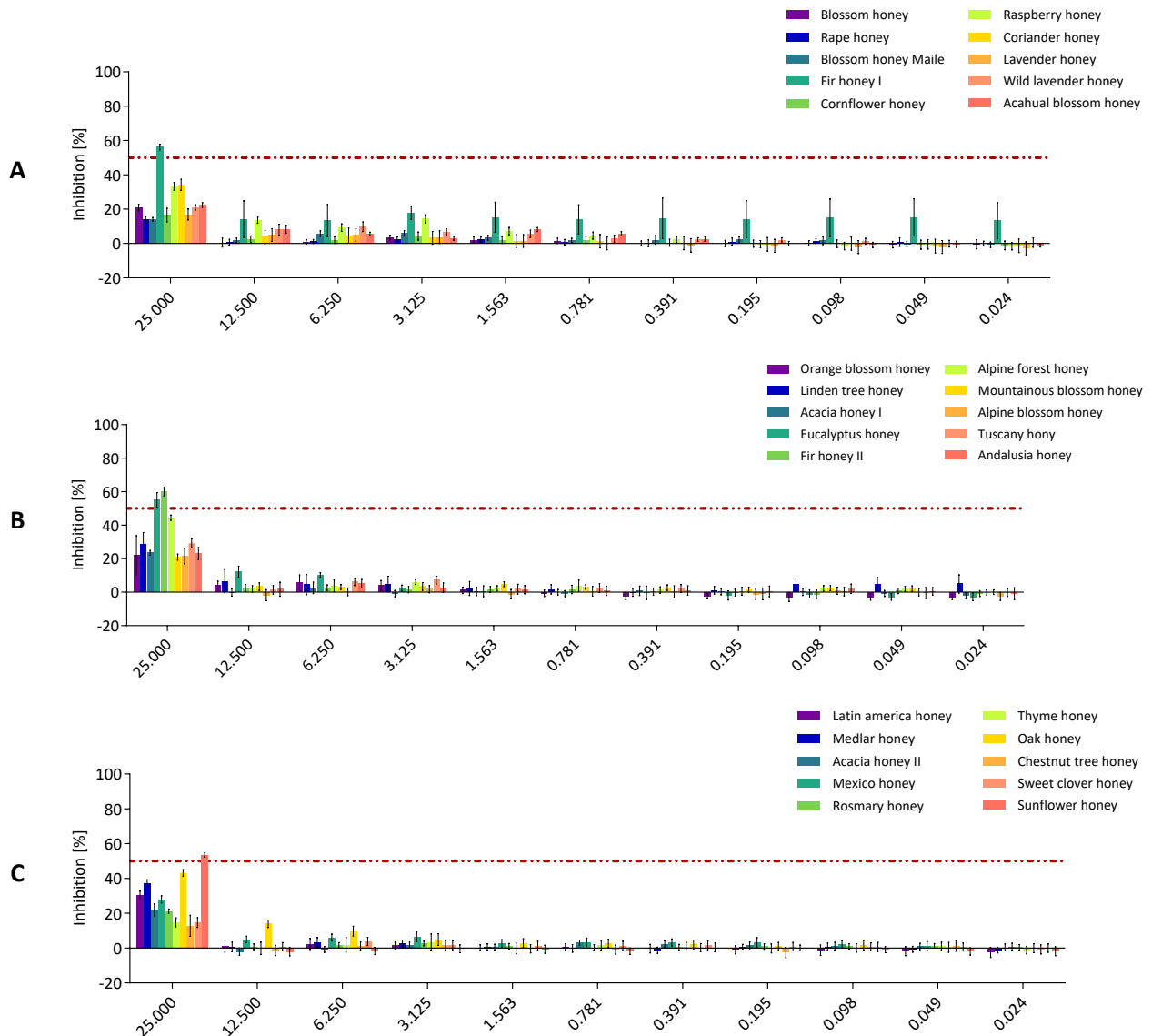


Figure A I-3: Attachment inhibition of GII.10 VLPs by 30 different types of honey
 Attachment inhibition by different types of honey A: 1 – 10. B: 11 – 20. C: 21 – 30. Alpine forest, coriander, eucalyptus, fir I, fir II, Mexico, oak, orange blossom, and raspberry honey (the six best and three with low inhibition) were chosen for further analysis. After this selection robinia honey was added to the panel Single experiment; measurements were performed in triplicate wells, error bars shown.

Appendix II Acknowledgements

I would like to seize this opportunity to express my gratitude to some people without whom it would not have been possible to reach the point where this thesis was printed.

First, I would like to thank Dr. Grant Hansman for the great opportunity to work in his Lab. Thanks for having me as a PhD student and for letting me develop my work within your lab. Thanks for being supportive and always ready to give advice when needed. It was a great chance to work in your very well-organized lab and without pressure regarding financing my ideas.

I also want to thank the further members of my TAC Prof. Dr. Martin Müller and Prof. Dr. Dr. Henri-Jacques Delecluse. Thank you for the time you gave to guide my work and carefully examine the directions I was heading. Especially the interesting discussions we had after TAC meetings where inspiring and did a great deal to set me on the right track and revise my own work.

Thank you Prof. Dr. Frauke Gräter for being my fourth examiner and chair at my defense on short notice.

I cannot over emphasize the importance of and the gratitude to my further lab members and colleges (past and present).

Thank you, Jessica, and Thank you Jen. You were amazing friends during this time. Thank you so much for carefully reviewing my thesis – I think you really helped me to improve and structure it. Thanks for many inspiring talks and scientific coffee breaks.

Also, thanks to Anna for always giving help in the lab when needed. No matter what time, no matter if you were busy and no matter if it was about a protocol, location of an antibody, support for EM or discussing results.

I want to thank Virginie Malak for her enthusiastic work in our lab. You kept our lab structured and tidy. You were always helpful especially during my beginning in the lab when you introduced me to

Acknowledgements

protocols and showed me the organization of the lab. Your style in organization and structure in our lab will always guide my lab work.

Thank you Turgay for introducing me to the field of x-ray crystallography. You explained me the more practical parts of the technique regarding setting up and optimization of crystals. You also patiently explained me how to use the various programs involved in structure processing and helped me to clear one error after the other on my way to solving structures.

Many thanks to Charles who never got tired to teach detailed matters of the background of structure analysis. Also, thanks for trying very hard to forward my attempts to solve the riddle of the inhibiting compound in date syrup. You were a great support in the lab and a real friend.

My very special thanks to Angelika. From before my first day in the Lab you were a true pearl always offering help in plenty regarding any field of administrative work. I don't know how many times we ran into trouble with some official admin stuff and you always knew how to solve any problem. Thank you also for being a great and supportive friend during these past years. Thanks for countless shared lunches and dinners and for showing the bright side even when I had trouble seeing it.

I also want to take this opportunity to thank my family. You have been incredibly supportive during my entire time of studies including the time it took me to finish this thesis. Thank you so much for all the support I always felt on the path I took.

Appendix III References

1. **Adams, P.D., P.V. Afonine, G. Bunkoczi, V.B. Chen, I.W. Davis, N. Echols, J.J. Headd, L.-W. Hung, G.J. Kapral, R.W. Grosse-Kunstleve, A.J. McCoy, N.W. Moriarty, R. Oeffner, R.J. Read, D.C. Richardson, J.S. Richardson, T.C. Terwilliger, and P.H. Zwart**, *PHENIX: a comprehensive Python-based system for macromolecular structure solution*. Acta Crystallographica Section D, 2010. **66**(2): p. 213-221.
2. **Alvarado, G., K. Ettayebi, R.L. Atmar, R.G. Bombardi, N. Kose, M.K. Estes, and J.E. Crowe Jr**, *Human monoclonal antibodies that neutralize pandemic GII. 4 noroviruses*. Gastroenterology, 2018. **155**(6): p. 1898-1907.
3. **Anstee, D.J.**, *The relationship between blood groups and disease*. Blood, 2010. **115**(23): p. 4635-43.
4. **Bartsch, S.M., B.A. Lopman, S. Ozawa, A.J. Hall, and B.Y. Lee**, *Global Economic Burden of Norovirus Gastroenteritis*. PLoS One, 2016. **11**(4): p. e0151219-e0151219.
5. **Bliss, C.I.**, *The toxicity of poisons applied jointly 1*. Annals of applied biology, 1939. **26**(3): p. 585-615.
6. **Bok, K., G.I. Parra, T. Mitra, E. Abente, C.K. Shaver, D. Boon, R. Engle, C. Yu, A.Z. Kapikian, S.V. Sosnovtsev, R.H. Purcell, and K.Y. Green**, *Chimpanzees as an animal model for human norovirus infection and vaccine development*. Proceedings of the National Academy of Sciences, 2011. **108**(1): p. 325-330.
7. **Bonvehí, J.S. and F.V. Coll**, *Study on propolis quality from China and Uruguay*. Zeitschrift für Naturforschung c, 2000. **55**(9-10): p. 778-784.
8. **Borroto-Esoda, K., J.E. Vela, F. Myrick, A.S. Ray, and M.D. Miller**, *In vitro evaluation of the anti-HIV activity and metabolic interactions of tenofovir and emtricitabine*. Antiviral therapy, 2006. **11**(3): p. 377.
9. **Bu, W., A. Mamedova, M. Tan, M. Xia, X. Jiang, and R.S. Hegde**, *Structural basis for the receptor binding specificity of Norwalk virus*. J Virol, 2008. **82**(11): p. 5340-7.
10. **Bücher, K.S., H. Yan, R. Creutzmacher, K. Ruoff, A. Mallagaray, A. Grafmüller, J.S. Dirks, T. Kilic, S. Weickert, and A. Rubailo**, *Fucose-functionalized precision glycomacromolecules targeting human norovirus capsid protein*. Biomacromolecules, 2018. **19**(9): p. 3714-3724.
11. **Chakravarty, S., A.M. Hutson, M.K. Estes, and B.V. Prasad**, *Evolutionary trace residues in noroviruses: importance in receptor binding, antigenicity, virion assembly, and strain diversity*. J Virol, 2005. **79**(1): p. 554-568.
12. **Chapman, A.S., C.T. Witkop, J.D. Escobar, C.A. Schlorman, L.S. DeMarcus, L.M. Marmer, and M.E. Crum**, *Norovirus outbreak associated with person-to-person transmission, U.S. Air Force Academy, July 2011*. MSMR, 2011. **18**(11): p. 2-5.
13. **Chen, V.B., W.B. Arendall, J.J. Headd, D.A. Keedy, R.M. Immormino, G.J. Kapral, L.W. Murray, J.S. Richardson, and D.C. Richardson**, *MolProbity: all-atom structure validation for macromolecular crystallography*. Acta Crystallographica Section D: Biological Crystallography, 2010. **66**(1): p. 12-21.
14. **Cheynier, V., M. Duenas-Paton, E. Salas, C. Maury, J.-M. Souquet, P. Sarni-Manchado, and H. Fulcrand**, *Structure and properties of wine pigments and tannins*. American Journal of Enology and Viticulture, 2006. **57**(3): p. 298-305.
15. **Cheynier, V., C. Prieur, S. Guyot, J. Rigaud, and M. Moutounet**, *The structures of tannins in grapes and wines and their interactions with proteins*. 1997, ACS Publications.
16. **Chhabra, P., M. de Graaf, G.I. Parra, M.C. Chan, K. Green, V. Martella, Q. Wang, P.A. White, K. Katayama, H. Vennema, M.P.G. Koopmans, and J. Vinjé**, *Updated classification of norovirus genogroups and genotypes*. J Gen Virol, 2019. **100**(10): p. 1393-1406.

References

17. **Choi, J.-M., A.M. Hutson, M.K. Estes, and B.V. Prasad**, *Atomic resolution structural characterization of recognition of histo-blood group antigens by Norwalk virus*. Proceedings of the National Academy of Sciences, 2008. **105**(27): p. 9175-9180.
18. **Cooling, L.**, *Blood Groups in Infection and Host Susceptibility*. Clinical microbiology reviews, 2015. **28**(3): p. 801-870.
19. **Cromeans, T., G.W. Park, V. Costantini, D. Lee, Q. Wang, T. Farkas, A. Lee, and J. Vinjé**, *Comprehensive comparison of cultivable norovirus surrogates in response to different inactivation and disinfection treatments*. Appl Environ Microbiol, 2014. **80**(18): p. 5743-5751.
20. **Daniels, G.**, *Human blood groups*. 2008: John Wiley & Sons.
21. **Daudt, C.E. and A.d.O. Fogaça**, *Phenolic compounds in Merlot wines from two wine regions of Rio Grande do Sul, Brazil*. Food Science and Technology, 2013. **33**(2): p. 355-361.
22. **Davis, R., S. Zivanovic, D.H. D'Souza, and P.M. Davidson**, *Effectiveness of chitosan on the inactivation of enteric viral surrogates*. Food microbiology, 2012. **32**(1): p. 57-62.
23. **Dolin, R., N.R. Blacklow, H. DuPont, R.F. Buscho, R.G. Wyatt, J.A. Kasel, R. Hornick, and R.M. Chanock**, *Biological Properties of Norwalk Agent of Acute Infectious Nonbacterial Gastroenteritis*. Proceedings of the Society for Experimental Biology and Medicine, 1972. **140**(2): p. 578-583.
24. **Drlica, K.**, *The mutant selection window and antimicrobial resistance*. Journal of Antimicrobial Chemotherapy, 2003. **52**(1): p. 11-17.
25. **Elizaquível, P., M. Azizkhani, R. Aznar, and G. Sánchez**, *The effect of essential oils on norovirus surrogates*. Food Control, 2013. **32**(1): p. 275-278.
26. **Emsley P, L.B., Scott WG, Cowtan K.**, *Features and development of Coot*. Acta Crystallographica Section D: Biological Crystallography. , 2010. **66**(4): p. 486-501.
27. **Ettayebi, K., S.E. Crawford, K. Murakami, J.R. Broughman, U. Karandikar, V.R. Tenge, F.H. Neill, S.E. Blutt, X.L. Zeng, L. Qu, B. Kou, A.R. Opekun, D. Burrin, D.Y. Graham, S. Ramani, R.L. Atmar, and M.K. Estes**, *Replication of human noroviruses in stem cell-derived human enteroids*. Science, 2016. **353**(6306): p. 1387-1393.
28. **Etzold, S. and L. Bode**, *Glycan-dependent viral infection in infants and the role of human milk oligosaccharides*. Current Opinion in Virology, 2014. **7**: p. 101-107.
29. **Feld, J.J., K.V. Kowdley, E. Coakley, S. Sigal, D.R. Nelson, D. Crawford, O. Weiland, H. Aguilar, J. Xiong, T. Pilot-Matias, B. DaSilva-Tillmann, L. Larsen, T. Podsadecki, and B. Bernstein**, *Treatment of HCV with ABT-450/r-Ombitasvir and Dasabuvir with Ribavirin*. New England Journal of Medicine, 2014. **370**(17): p. 1594-1603.
30. **Feng, J.Y., J.K. Ly, F. Myrick, D. Goodman, K.L. White, E.S. Svarovskaia, K. Borroto-Esoda, and M.D. Miller**, *The triple combination of tenofovir, emtricitabine and efavirenz shows synergistic anti-HIV-1 activity in vitro: a mechanism of action study*. Retrovirology, 2009. **6**(1): p. 44.
31. **Flamini, R., F. Mattivi, M.D. Rosso, P. Arapitsas, and L. Bavaresco**, *Advanced knowledge of three important classes of grape phenolics: anthocyanins, stilbenes and flavonols*. International journal of molecular sciences, 2013. **14**(10): p. 19651-19669.
32. **Frankel, E.N., A.L. Waterhouse, and P.L. Teissedre**, *Principal phenolic phytochemicals in selected California wines and their antioxidant activity in inhibiting oxidation of human low-density lipoproteins*. Journal of agricultural and food chemistry, 1995. **43**(4): p. 890-894.
33. **Fuhrman, B., N. Volkova, A. Suraski, and M. Aviram**, *White wine with red wine-like properties: increased extraction of grape skin polyphenols improves the antioxidant capacity of the derived white wine*. Journal of agricultural and food chemistry, 2001. **49**(7): p. 3164-3168.
34. **Gallimore, C.I., D. Cubitt, N. du Plessis, and J.J. Gray**, *Asymptomatic and symptomatic excretion of noroviruses during a hospital outbreak of gastroenteritis*. J Clin Microbiol, 2004. **42**(5): p. 2271-2274.

References

35. **Ghany, M.G. and E.C. Doo**, *Antiviral resistance and hepatitis B therapy*. *Hepatology*, 2009. **49**(S5): p. S174-S184.
36. **Gilling, D.H., M. Kitajima, J. Torrey, and K.R. Bright**, *Antiviral efficacy and mechanisms of action of oregano essential oil and its primary component carvacrol against murine norovirus*. *Journal of applied microbiology*, 2014. **116**(5): p. 1149-1163.
37. **Graziano, V.R., J. Wei, and C.B. Wilen**, *Norovirus attachment and entry*. *Viruses*, 2019. **11**(6): p. 495.
38. **Haga, K., A. Fujimoto, R. Takai-Todaka, M. Miki, Y.H. Doan, K. Murakami, M. Yokoyama, K. Murata, A. Nakanishi, and K. Katayama**, *Functional receptor molecules CD300lf and CD300ld within the CD300 family enable murine noroviruses to infect cells*. *Proceedings of the National Academy of Sciences*, 2016. **113**(41): p. E6248-E6255.
39. **Hammouda, H.d., J.K. Chérif, M. Trabelsi-Ayadi, A. Baron, and S. Guyot**, *Detailed polyphenol and tannin composition and its variability in Tunisian dates (Phoenix dactylifera L.) at different maturity stages*. *Journal of agricultural and food chemistry*, 2013. **61**(13): p. 3252-3263.
40. **Hansman, G.S., K. Natori, H. Shirato-Horikoshi, S. Ogawa, T. Oka, K. Katayama, T. Tanaka, T. Miyoshi, K. Sakae, S. Kobayashi, M. Shinohara, K. Uchida, N. Sakurai, K. Shinozaki, M. Okada, Y. Seto, K. Kamata, N. Nagata, K. Tanaka, T. Miyamura, and N. Takeda**, *Genetic and antigenic diversity among noroviruses*. *J Gen Virol*, 2006. **87**(Pt 4): p. 909-19.
41. **Hansman, G.S., S. Shahzad-ul-Hussan, J.S. McLellan, G.-Y. Chuang, I. Georgiev, T. Shimoike, K. Katayama, C.A. Bewley, and P.D. Kwong**, *Structural basis for norovirus inhibition and fucose mimicry by citrate*. *J Virol*, 2012. **86**(1): p. 284-292.
42. **Hansman, G.S., D.W. Taylor, J.S. McLellan, T.J. Smith, I. Georgiev, J.R. Tame, S.Y. Park, M. Yamazaki, F. Gondaira, M. Miki, K. Katayama, K. Murata, and P.D. Kwong**, *Structural basis for broad detection of genogroup II noroviruses by a monoclonal antibody that binds to a site occluded in the viral particle*. *J Virol*, 2012. **86**(7): p. 3635-46.
43. **Haytowitz, D.B., X. Wu, and S. Bhagwat**, *USDA Database for the Flavonoid Content of Selected Foods, Release 3.3*. US Department of Agriculture, Agricultural Research Service. Nutrient Data Labrotatory. Available online: <https://www.ars.usda.gov/nutrientdata/flav> (accessed on 17 August 2019), 2018.
44. **Hong, Y.J., F. Tomas-Barberan, A.A. Kader, and A.E. Mitchell**, *The flavonoid glycosides and procyanidin composition of Deglet Noor dates (Phoenix dactylifera)*. *Journal of agricultural and food chemistry*, 2006. **54**(6): p. 2405-2411.
45. **Huang, P., T. Farkas, S. Marionneau, W. Zhong, N. Ruvoën-Clouet, A.L. Morrow, M. Altaye, L.K. Pickering, D.S. Newburg, and J. LePendou**, *Noroviruses bind to human ABO, Lewis, and secretor histo-blood group antigens: identification of 4 distinct strain-specific patterns*. *J Infect Dis*, 2003. **188**(1): p. 19-31.
46. **Huleihel, M. and V. Isanu**, *Anti-herpes simplex virus effect of an aqueous extract of propolis*. *The Israel Medical Association Journal: IMAJ*, 2002. **4**(11 Suppl): p. 923-927.
47. **Hutson, A.M., R.L. Atmar, D.Y. Graham, and M.K. Estes**, *Norwalk virus infection and disease is associated with ABO histo-blood group type*. *J Infect Dis*, 2002. **185**(9): p. 1335-7.
48. **Jan Vinjé, M.K.E., Pedro Esteves, Kim Y. Green, Kazuhiko Katayama, Nick J. Knowles, Yvan L'Homme, Vito Martella, Harry Vennema, Peter A. White**, *Caliciviridae*, in *Virus Taxonomy, The ICTV Report on Virus Classification and Taxon Nomenclature*. 2019.
49. **Johnson, P.C., J.J. Mathewson, H.L. DuPont, and H.B. Greenberg**, *Multiple-challenge study of host susceptibility to Norwalk gastroenteritis in US adults*. *Journal of Infectious Diseases*, 1990. **161**(1): p. 18-21.
50. **Jones, M.K., M. Watanabe, S. Zhu, C.L. Graves, L.R. Keyes, K.R. Grau, M.B. Gonzalez-Hernandez, N.M. Iovine, C.E. Wobus, J. Vinjé, S.A. Tibbetts, S.M. Wallet, and S.M. Karst**, *Enteric bacteria promote human and mouse norovirus infection of B cells*. *Science*, 2014. **346**(6210): p. 755-759.

References

51. **Joshi, S.S., A.B. Howell, and D.H. D'Souza**, *Reduction of enteric viruses by blueberry juice and blueberry proanthocyanidins*. *Food Environ Virol*, 2016. **8**(4): p. 235-243.
52. **Joshi, S.S., X. Su, and D.H. D'Souza**, *Antiviral effects of grape seed extract against feline calicivirus, murine norovirus, and hepatitis A virus in model food systems and under gastric conditions*. *Food microbiology*, 2015. **52**: p. 1-10.
53. **Kabsch, W.**, *XDS*. *Acta Cryst.*, 2010. **D66**: p. 125-132.
54. **Kamimoto, M., Y. Nakai, T. Tsuji, T. Shimamoto, and T. Shimamoto**, *Antiviral effects of persimmon extract on human norovirus and its surrogate, bacteriophage MS2*. *Journal of food science*, 2014. **79**(5): p. M941-M946.
55. **Kapikian, A.Z., R.G. Wyatt, R. Dolin, T.S. Thornhill, A.R. Kalica, and R.M. Chanock**, *Visualization by immune electron microscopy of a 27-nm particle associated with acute infectious nonbacterial gastroenteritis*. *J Virol*, 1972. **10**(5): p. 1075-1081.
56. **Karst, S.M., C.E. Wobus, I.G. Goodfellow, K.Y. Green, and H.W. Virgin**, *Advances in norovirus biology*. *Cell host & microbe*, 2014. **15**(6): p. 668-680.
57. **Khodabakhsh, F., M. Behdani, A. Rami, and F. Kazemi-Lomedasht**, *Single-domain antibodies or nanobodies: a class of next-generation antibodies*. *International reviews of immunology*, 2018. **37**(6): p. 316-322.
58. **Kilic, T., A. Koromyslova, and G.S. Hansman**, *Structural Basis for Human Norovirus Capsid Binding to Bile Acids*. *J Virol*, 2019. **93**(2).
59. **Kilic, T., A. Koromyslova, V. Malak, and G.S. Hansman**, *Atomic structure of the murine norovirus protruding domain and soluble CD300lf receptor complex*. *J Virol*, 2018. **92**(11).
60. **King, A.M., E. Lefkowitz, M.J. Adams, and E.B. Carstens**, *Virus taxonomy: ninth report of the International Committee on Taxonomy of Viruses*. 2011: Elsevier.
61. **Kirby, A.E., J. Shi, J. Montes, M. Lichtenstein, and C.L. Moe**, *Disease course and viral shedding in experimental Norwalk virus and Snow Mountain virus infection*. *J Med Virol*, 2014. **86**(12): p. 2055-2064.
62. **Kirk, M.D., S.M. Pires, R.E. Black, M. Caipo, J.A. Crump, B. Devleeschauwer, D. Döpfer, A. Fazil, C.L. Fischer-Walker, T. Hald, A.J. Hall, K.H. Keddy, R.J. Lake, C.F. Lanata, P.R. Torgerson, A.H. Havelaar, and F.J. Angulo**, *World Health Organization Estimates of the Global and Regional Disease Burden of 22 Foodborne Bacterial, Protozoal, and Viral Diseases, 2010: A Data Synthesis*. *PLoS Med*, 2015. **12**(12): p. e1001921-e1001921.
63. **Knipe, D.M.**, *Fields Virology*. 2013: Wolters Kluwer Health.
64. **Koho, T., L. Huhti, V. Blazevic, K. Nurminen, S.J. Butcher, P. Laurinmäki, N. Kalkkinen, G. Rönholm, T. Vesikari, and V.P. Hytönen**, *Production and characterization of virus-like particles and the P domain protein of GII. 4 norovirus*. *Journal of virological methods*, 2012. **179**(1): p. 1-7.
65. **Koromyslova, A., S. Tripathi, V. Morozov, H. Schrotten, and G.S. Hansman**, *Human norovirus inhibition by a human milk oligosaccharide*. *Virology*, 2017. **508**: p. 81-89.
66. **Koromyslova, A.D. and G.S. Hansman**, *Nanobodies targeting norovirus capsid reveal functional epitopes and potential mechanisms of neutralization*. *PLoS Pathog*, 2017. **13**(11): p. e1006636.
67. **Koromyslova, A.D. and G.S. Hansman**, *Nanobody Binding to a Conserved Epitope Promotes Norovirus Particle Disassembly*. *Journal of Virology*, 2015. **89**(5): p. 2718-2730.
68. **Koromyslova, A.D., M.M. Leuthold, M.W. Bowler, and G.S. Hansman**, *The sweet quartet: binding of fucose to the norovirus capsid*. *Virology*, 2015. **483**: p. 203-208.
69. **Koromyslova, A.D., V.A. Morozov, L. Hefele, and G.S. Hansman**, *Human norovirus neutralized by a monoclonal antibody targeting the histo-blood group antigen pocket*. *J Virol*, 2019. **93**(5).

References

70. **Koromyslova, A.D., P.A. White, and G.S. Hansman**, *Treatment of norovirus particles with citrate*. *Virology*, 2015. **485**: p. 199-204.
71. **Kulkarni, R., R. Hluhanich, D.M. McColl, M.D. Miller, and K.L. White**, *The combined anti-HIV-1 activities of emtricitabine and tenofovir plus the integrase inhibitor elvitegravir or raltegravir show high levels of synergy in vitro*. *Antimicrob Agents Chemother*, 2014. **58**(10): p. 6145-6150.
72. **Kunz, C., S. Rudloff, W. Baier, N. Klein, and S. Strobel**, *Oligosaccharides in Human Milk: Structural, Functional, and Metabolic Aspects*. *Annual Review of Nutrition*, 2000. **20**(1): p. 699-722.
73. **Kurek-Gorecka, A., A. Rzepecka-Stojko, M. Gorecki, J. Stojko, M. Sosada, and G. Swierczek-Zieba**, *Structure and antioxidant activity of polyphenols derived from propolis*. *Molecules (Basel, Switzerland)*, 2013. **19**(1): p. 78-101.
74. **Lai, C.-C., Y.-H. Wang, C.-Y. Wu, C.-H. Hung, D.D.-S. Jiang, and F.-T. Wu**, *A norovirus outbreak in a nursing home: Norovirus shedding time associated with age*. *Journal of Clinical Virology*, 2013. **56**(2): p. 96-101.
75. **Lee, J.-H., S.Y. Bae, M. Oh, K.H. Kim, and M.S. Chung**, *Antiviral effects of mulberry (*Morus alba*) juice and its fractions on foodborne viral surrogates*. *Foodborne pathogens and disease*, 2014. **11**(3): p. 224-229.
76. **Lee, M.H., B.-H. Lee, J.-Y. Jung, D.-S. Cheon, K.-T. Kim, and C. Choi**, *Antiviral effect of Korean red ginseng extract and ginsenosides on murine norovirus and feline calicivirus as surrogates for human norovirus*. *Journal of ginseng research*, 2011. **35**(4): p. 429.
77. **Li, D., L. Baert, and M. Uyttendaele**, *Inactivation of food-borne viruses using natural biochemical substances*. *Food microbiology*, 2013. **35**(1): p. 1-9.
78. **Lindesmith, L., C. Moe, S. Marionneau, N. Ruvoen, X. Jiang, L. Lindblad, P. Stewart, J. LePendou, and R. Baric**, *Human susceptibility and resistance to Norwalk virus infection*. *Nature medicine*, 2003. **9**(5): p. 548-553.
79. **Lopman, B.A., D. Steele, C.D. Kirkwood, and U.D. Parashar**, *The Vast and Varied Global Burden of Norovirus: Prospects for Prevention and Control*. *PLoS Med*, 2016. **13**(4): p. e1001999-e1001999.
80. **Marcucci, M.**, *Propolis: chemical composition, biological properties and therapeutic activity*. 1995.
81. **Marionneau, S., A. Cailleau-Thomas, J. Rocher, B. Le Moullac-Vaidye, N. Ruvoën, M. Clément, and J. Le Pendu**, *ABH and Lewis histo-blood group antigens, a model for the meaning of oligosaccharide diversity in the face of a changing world*. *Biochimie*, 2001. **83**(7): p. 565-573.
82. **Marionneau, S., N. Ruvoën, B. Le Moullac-Vaidye, M. Clement, A. Cailleau-Thomas, G. Ruiz-Palacois, P. Huang, X. Jiang, and J. Le Pendu**, *Norwalk virus binds to histo-blood group antigens present on gastroduodenal epithelial cells of secretor individuals*. *Gastroenterology*, 2002. **122**(7): p. 1967-1977.
83. **Marsh, M. and A. Helenius**, *Virus entry: open sesame*. *Cell*, 2006. **124**(4): p. 729-740.
84. **McCoy AJ, G.-K.R., Adams PD, Winn MD, Storoni LC, Read RJ.** , *Phaser crystallographic software*. *Journal of Applied Crystallography.*, 2007. **40**(4): p. 658-674.
85. **Muyldermans, S., T. Baral, V.C. Retamozzo, P. De Baetselier, E. De Genst, J. Kinne, H. Leonhardt, S. Magez, V. Nguyen, and H. Revets**, *Camelid immunoglobulins and nanobody technology*. *Veterinary immunology and immunopathology*, 2009. **128**(1-3): p. 178-183.
86. **Nordgren, J., E. Kindberg, P.E. Lindgren, A. Matussek, and L. Svensson**, *Norovirus gastroenteritis outbreak with a secretor-independent susceptibility pattern, Sweden*. *Emerg Infect Dis*, 2010. **16**(1): p. 81-87.
87. **Oh, E.-G., K.-L. Kim, S.B. Shin, K.-T. Son, H.-J. Lee, T.H. Kim, Y.-M. Kim, E.-J. Cho, D.-K. Kim, and E.-W. Lee**, *Antiviral activity of green tea catechins against feline calicivirus as a surrogate for norovirus*. *Food science and biotechnology*, 2013. **22**(2): p. 593-598.

References

88. **Oh, M., S.Y. Bae, J.-H. Lee, K.J. Cho, K.H. Kim, and M.S. Chung**, *Antiviral effects of black raspberry (Rubus coreanus) juice on foodborne viral surrogates*. Foodborne pathogens and disease, 2012. **9**(10): p. 915-921.
89. **Orchard, R.C., C.B. Wilen, J.G. Doench, M.T. Baldrige, B.T. McCune, Y.-C.J. Lee, S. Lee, S.M. Pruett-Miller, C.A. Nelson, and D.H. Fremont**, *Discovery of a proteinaceous cellular receptor for a norovirus*. Science, 2016. **353**(6302): p. 933-936.
90. **Pandey, A. and S. Kumar**, *Perspective on plant products as antimicrobial agents: A review*. Pharmacologia, 2013. **4**(7): p. 469-480.
91. **Parrino, T.A., D.S. Schreiber, J.S. Trier, A.Z. Kapikian, and N.R. Blacklow**, *Clinical immunity in acute gastroenteritis caused by Norwalk agent*. New England Journal of Medicine, 1977. **297**(2): p. 86-89.
92. **Pelliccia, S., Y.-H. Wu, A. Coluccia, G. La Regina, C.-K. Tseng, V. Famiglioni, D. Masci, J. Hiscott, J.-C. Lee, and R. Silvestri**, *Inhibition of dengue virus replication by novel inhibitors of RNA-dependent RNA polymerase and protease activities*. Journal of Enzyme Inhibition and Medicinal Chemistry, 2017. **32**(1): p. 1091-1101.
93. **Perumal Samy, R. and P. Gopalakrishnakone**, *Therapeutic potential of plants as anti-microbials for drug discovery*. Evidence-based complementary and alternative medicine, 2010. **7**.
94. **Pöch, G., P. Dittrich, R. Reiffenstein, W. Lenk, and A. Schuster**, *Evaluation of experimental combined toxicity by use of dose–frequency curves: comparison with theoretical additivity as well as independence*. Canadian journal of physiology and pharmacology, 1990. **68**(10): p. 1338-1345.
95. **Pomeroy, J.J., G.L. Drusano, J.L. Rodriguez, and A.N. Brown**, *Searching for synergy: Identifying optimal antiviral combination therapy using Hepatitis C virus (HCV) agents in a replicon system*. Antiviral Research, 2017. **146**(Supplement C): p. 149-152.
96. **Prasad, B.V., M.E. Hardy, T. Dokland, J. Bella, M.G. Rossmann, and M.K. Estes**, *X-ray crystallographic structure of the Norwalk virus capsid*. Science, 1999. **286**(5438): p. 287-290.
97. **Ruoff, K., T. Kilic, J. Devant, A. Koromyslova, A. Ringel, A. Hempelmann, C. Geiss, J. Graf, M. Haas, I. Roggenbach, and G. Hansman**, *Structural Basis of Nanobodies Targeting the Prototype Norovirus*. J Virol, 2019. **93**(6).
98. **Ryu, S., H.J. You, Y.W. Kim, A. Lee, G.P. Ko, S.J. Lee, and M.J. Song**, *Inactivation of norovirus and surrogates by natural phytochemicals and bioactive substances*. Molecular nutrition & food research, 2015. **59**(1): p. 65-74.
99. **Schnitzler, P., A. Neuner, S. Nolkemper, C. Zundel, H. Nowack, K.H. Sensch, and J. Reichling**, *Antiviral activity and mode of action of propolis extracts and selected compounds*. Phytotherapy Research, 2010. **24**(S1): p. S20-S28.
100. **Seo, D.J. and C. Choi**, *Inhibition of murine norovirus and feline calicivirus by edible herbal extracts*. Food Environ Virol, 2017. **9**(1): p. 35-44.
101. **Shanker, S., R. Czakó, G. Sapparapu, G. Alvarado, M. Viskovska, B. Sankaran, R.L. Atmar, J.E. Crowe, M.K. Estes, and B.V. Prasad**, *Structural basis for norovirus neutralization by an HBGA blocking human IgA antibody*. Proceedings of the National Academy of Sciences, 2016. **113**(40): p. E5830-E5837.
102. **Sharia M Ahmed, A.J.H., Anne E Robinson, Linda Verhoef, Prasanna Premkumar, Umesh D Parashar, Marion Koopmans, Benjamin A Lopman**, *Global prevalence of norovirus in cases of gastroenteritis: a systematic review and meta-analysis*. The Lancet infectious diseases, 2014. **14**(8): p. 725-730.
103. **Silva-Beltrán, N.P., A.P. Balderrama-Carmona, M.A. Umsza-Guez, and B.A.S. Machado**, *Antiviral effects of Brazilian green and red propolis extracts on Enterovirus surrogates*. Environmental Science and Pollution Research, 2019: p. 1-8.

References

104. **Simonetti, P., P. Pietta, and G. Testolin**, *Polyphenol content and total antioxidant potential of selected Italian wines*. *Journal of agricultural and food chemistry*, 1997. **45**(4): p. 1152-1155.
105. **Singh, B.K., M.M. Leuthold, and G.S. Hansman**, *Structural constraints on human norovirus binding to histo-blood group antigens*. *MSphere*, 2016. **1**(2).
106. **Sosnovtsev, S. and K.Y. Green**, *RNA transcripts derived from a cloned full-length copy of the feline calicivirus genome do not require VpG for infectivity*. *Virology*, 1995. **210**(2): p. 383-390.
107. **Su, X., A.B. Howell, and D.H. D'Souza**, *The effect of cranberry juice and cranberry proanthocyanidins on the infectivity of human enteric viral surrogates*. *Food microbiology*, 2010. **27**(4): p. 535-540.
108. **Su, X., A.B. Howell, and D.H. D'Souza**, *Antiviral effects of cranberry juice and cranberry proanthocyanidins on foodborne viral surrogates—a time dependence study in vitro*. *Food microbiology*, 2010. **27**(8): p. 985-991.
109. **Su, X., M.Y. Sangster, and D.H. D'Souza**, *In vitro effects of pomegranate juice and pomegranate polyphenols on foodborne viral surrogates*. *Foodborne pathogens and disease*, 2010. **7**(12): p. 1473-1479.
110. **Tam, C.C., L.C. Rodrigues, L. Viviani, J.P. Dodds, M.R. Evans, P.R. Hunter, J.J. Gray, L.H. Letley, G. Rait, D.S. Tompkins, S.J. O'Brien, and I.I.D.S.E. Committee**, *Longitudinal study of infectious intestinal disease in the UK (IID2 study): incidence in the community and presenting to general practice*. *Gut*, 2012. **61**(1): p. 69-77.
111. **Tan, M., P. Huang, J. Meller, W. Zhong, T. Farkas, and X. Jiang**, *Mutations within the P2 domain of norovirus capsid affect binding to human histo-blood group antigens: evidence for a binding pocket*. *J Virol*, 2003. **77**(23): p. 12562-71.
112. **Tan, M. and X. Jiang**, *The p domain of norovirus capsid protein forms a subviral particle that binds to histo-blood group antigen receptors*. *J Virol*, 2005. **79**(22): p. 14017-30.
113. **Thorven, M., A. Grahn, K.-O. Hedlund, H. Johansson, C. Wahlfrid, G. Larson, and L. Svensson**, *A homozygous nonsense mutation (428G-->A) in the human secretor (FUT2) gene provides resistance to symptomatic norovirus (GGII) infections*. *J Virol*, 2005. **79**(24): p. 15351-15355.
114. **Ueda, K., R. Kawabata, T. Irie, Y. Nakai, Y. Tohya, and T. Sakaguchi**, *Inactivation of pathogenic viruses by plant-derived tannins: strong effects of extracts from persimmon (Diospyros kaki) on a broad range of viruses*. *PLoS One*, 2013. **8**(1).
115. **Van Dycke, J., A. Ny, N. Conceição-Neto, J. Maes, M. Hosmillo, A. Cuvry, I. Goodfellow, T.C. Nogueira, E. Verbeken, and J. Matthijnsens**, *A robust human norovirus replication model in zebrafish larvae*. *PLoS Pathog*, 2019. **15**(9): p. e1008009.
116. **Vynograd, N., I. Vynograd, and Z. Sosnowski**, *A comparative multi-centre study of the efficacy of propolis, acyclovir and placebo in the treatment of genital herpes (HSV)*. *Phytomedicine*, 2000. **7**(1): p. 1-6.
117. **Weichert, S., A. Koromyslova, B.K. Singh, S. Hansman, S. Jennewein, H. Schroten, and G.S. Hansman**, *Structural Basis for Norovirus Inhibition by Human Milk Oligosaccharides*. *J Virol*, 2016. **90**(9): p. 4843-8.
118. **White, N.**, *Antimalarial drug resistance and combination chemotherapy*. *Philosophical Transactions of the Royal Society of London. Series B: Biological Sciences*, 1999. **354**(1384): p. 739-749.
119. **Wikswø, M.E., J. Cortes, A.J. Hall, G. Vaughan, C. Howard, N. Gregoricus, and E.H. Cramer**, *Disease Transmission and Passenger Behaviors during a High Morbidity Norovirus Outbreak on a Cruise Ship, January 2009*. *Clinical Infectious Diseases*, 2011. **52**(9): p. 1116-1122.
120. **Wobus, C.E., S.M. Karst, L.B. Thackray, K.-O. Chang, S.V. Sosnovtsev, G. Belliot, A. Krug, J.M. Mackenzie, K.Y. Green, and H.W. Virgin IV**, *Replication of Norovirus in cell culture reveals a tropism for dendritic cells and macrophages*. *PLoS Biol*, 2004. **2**(12): p. e432.

References

121. **Wyatt, R.G., R. Dolin, N.R. Blacklow, H.L. DuPont, R.F. Buscho, T.S. Thornhill, A.Z. Kapikian, and R.M. Chanock**, *Comparison of three agents of acute infectious nonbacterial gastroenteritis by cross-challenge in volunteers*. *Journal of Infectious Diseases*, 1974. **129**(6): p. 709-714.
122. **Yao, L., Y. Jiang, B. D'Arcy, R. Singanusong, N. Datta, N. Caffin, and K. Raymont**, *Quantitative high-performance liquid chromatography analyses of flavonoids in Australian Eucalyptus honeys*. *Journal of agricultural and food chemistry*, 2004. **52**(2): p. 210-214.
123. **Yu, Y., Y. Lasanajak, X. Song, L. Hu, S. Ramani, M.L. Mickum, D.J. Ashline, B.V.V. Prasad, M.K. Estes, V.N. Reinhold, R.D. Cummings, and D.F. Smith**, *Human Milk Contains Novel Glycans That Are Potential Decoy Receptors for Neonatal Rotaviruses*. *Molecular & Cellular Proteomics : MCP*, 2014. **13**(11): p. 2944-2960.
124. **Yu, Y., S. Mishra, X. Song, Y. Lasanajak, K.C. Bradley, M.M. Tappert, G.M. Air, D.A. Steinhauer, S. Halder, and S. Cotmore**, *Functional glycomic analysis of human milk glycans reveals the presence of virus receptors and embryonic stem cell biomarkers*. *Journal of Biological Chemistry*, 2012. **287**(53): p. 44784-44799.
125. **Yunus, M.A., L.M.W. Chung, Y. Chaudhry, D. Bailey, and I. Goodfellow**, *Development of an optimized RNA-based murine norovirus reverse genetics system*. *J Virol Methods*, 2010. **169**(1): p. 112-118.
126. **Zhang, X.-F., Y.-C. Dai, W. Zhong, M. Tan, Z.-P. Lv, Y.-C. Zhou, and X. Jiang**, *Tannic acid inhibited norovirus binding to HBGA receptors, a study of 50 Chinese medicinal herbs*. *Bioorganic & medicinal chemistry*, 2012. **20**(4): p. 1616-1623.
127. **Zhang, X.-F., Q. Huang, Y. Long, X. Jiang, T. Zhang, M. Tan, Q.-L. Zhang, Z.-Y. Huang, Y.-H. Li, and Y.-Q. Ding**, *An outbreak caused by GII. 17 norovirus with a wide spectrum of HBGA-associated susceptibility*. *Sci Rep*, 2015. **5**: p. 17687.